Final Technical Report

For:

Measurements of HNO_3, SO_2, High Resolution Aerosol SO_4^{2-}, and Selected Aerosol Species Aboard the NASA DC-8 Aircraft

During the Transport and Chemical Evolution Over the Pacific Airborne Mission (TRACE-P)

Prepared by:

Robert W. Talbot, Principal Investigator
Jack E. Dibb, Principal Investigator

Institute for the Study of Earth, Oceans, and Space
University of New Hampshire
Morse Hall
Durham, NH 03824

NASA Grant # NCC-1-410

Performance Period: July 1, 2000 – June 30, 2004

Project Summary:

The UNH investigation during TRACE-P provided measurements of selected acidic gases and aerosol species aboard the NASA DC-8 research aircraft. Our investigation focused on measuring HNO_3, SO_2, and fine (<2 μm) aerosol SO_4^{2-} with two minute time resolution in near-real-time. We also quantified mixing ratios of aerosol ionic species, and aerosol ^{210}Pb and ^{7}Be collected onto bulk filters at better than 10 minute resolution. This suite of measurements contributed extensively to achieving the principal objectives of TRACE-P. In the context of the full data set collected by experimental teams on the DC-8, our observations provide a solid basis for assessing decadal changes in the chemical composition and source strength of Asian continental outflow. This region of the Pacific should be impacted profoundly by Asian emissions at this time with significant degradation of air quality over the next few decades. Atmospheric measurements in the western Pacific region will provide a valuable time series to help quantify the impact of Asian anthropogenic activities. Our data also provide important insight into the chemical and physical processes transforming Asian outflow during transport over the Pacific, particularly uptake and reactions of soluble gases on aerosol particles. In addition, the TRACE-P data set provide strong constraints for assessing and improving the chemical fields simulated by chemical transport models.

Objectives

This investigation pursued the following specific objectives through measurements on the DC-8 and subsequent analysis:

1. To conduct measurements of HNO_3, SO_2, fine (< 2.5 μm) aerosol SO_4^{2-}, and selected additional aerosol species to provide concentration and compositional information on Asian continental outflow over the western North Pacific;

2. To investigate the fate (e.g., scavenging, dilution, production/regeneration) of soluble gases and aerosols in continental outflow air parcels as they evolve and age during transport across the western/central North Pacific;

3. To use our high resolution measurements of fine aerosol SO_4^{2-} to gain new insight on inter-relationships of aerosols and trace gases (e.g., SO_2, CO, CO_2, and hydrocarbons) in "fresh" to more "aged" continental outflow; and

4. To use the distributions of the naturally occurring radionuclides ^{210}Pb and ^{7}Be to serve as tracers of continental and stratospheric air parcels respectively, especially for air parcels sampled 1-3 days since leaving the Asian continent.

UNH Contributions to TRACE-P

We provided all proposed data products (preliminary and final) on time, and actively participated in all science team meetings. Members of our group took the lead on five different manuscripts which have been published in JGR. Four of these papers focused on establishing the distribution of Asian outflow in the study region, using

different approaches. The fifth primarily examined the interaction between airborne Asian dust and anthropogenic pollution.

Dibb et al., 2003 focused on the distribution of aerosol-associated ions and specifically compared geographic regions that had been sampled previously in the PEM West B campaign. Mixing ratios of ions associated with dust and anthropogenic pollutants were much higher near Asia during TRACE-P than they had been during PEM West B. This finding was unique in the TRACE-P data set since most gaseous pollutants showed small changes between the two campaigns. Increasing emissions of dust due to land use changes in China accounted for the enhancements observed over the downwind Pacific ocean, but it is not clear why pollution tracers like sulfate, nitrate and ammonium associated with aerosols showed much larger increases than most gaseous pollutants. Jordan et al., 2003a, Russo et al., 2003 and Talbot et al., 2003 all used the transport history of sampled airmasses (derived from backwards trajectories provided by H. Fuelberg's group) to bin the TRACE-P data into several regions of origin. Russo et al., 2003 presented a large scale picture of the distribution of most compounds measured from the DC-8 while Jordan et al., 2003a, and Talbot et al., 2003 focused on aerosols and reactive nitrogen oxides respectively. Companion papers by Blake et al., 2004 and Browell et al., 2003 also described large scale characteristics of the airmasses east of Asia, using different analytical and statistical approaches. All of these papers agreed on one fundamental issue; Asian outflow encountered during TRACE-P generally reflected a complex mixture from a variety of natural and anthropogenic sources.

Jordan et al., 2003b addressed the interaction between anthropogenic acids and continental dust, and the impact of this interaction on the composition of aerosols and the gas phase in heavily polluted airmasses just a few days downwind of China. This analysis confirmed that models will need to adequately capture such heterogeneous processing if the evolution of continental outflow or megacity plumes is to be accurately simulated. Tang et al., 2004 used the TRACE-P data set to test one such model, which has a relatively detailed aerosol module, with encouraging results.

Dibb et al., 2003 also presented the distributions of the radionuclide tracers, and used these to provide insight into the impact that stratosphere/troposphere exchange and deep convection with precipitation scavenging had on the distributions of soluble aerosol-associated ions. Liu et al., 2004 used these tracers in a chemical transport model to assess the relative importance of photochemical production versus injection from the stratosphere as a source of tropospheric ozone.

Manuscripts Resulting from this Investigation

UNH lead author:

Dibb, J. E., R. W. Talbot, E. Scheuer, G. Seid, M. A, Avery, and H. B. Singh, Aerosol chemical composition in Asian continental outflow during TRACE-P: Comparison to PEM-West B, *Journal of Geophysical Research, 108 (D21)*, 8815, doi:10.1029/2002JD003111, 2003.

Jordan, C. E., B. E. Anderson, **R. W. Talbot, J. E. Dibb**, H. E. Fuelberg, C. H. Hudgins, C. M. Kiley, R. Russo, **E. Scheuer, G. Seid**, K. L. Thornhill, and E. Winstead, Chemical and physical properties of bulk aerosols within four sectors observed during TRACE-P, *Journal of Geophysical Research, 108 (D21)*, 8813, doi:10.1029/2002JD003337, 2003a.

Jordan, C. E., J. E. Dibb, B. E. Anderson, and H. E. Fuelberg, Uptake of nitrate and sulfate on dust aerosols during TRACE-P, *Journal of Geophysical Research, 108 (D21)*, 8817, doi:10.1029/2002JD003101, 2003b.

Russo, R. Talbot, J. Dibb, E. Scheuer, G. Seid, S. Sandholm, D. Tan, H. Singh, D. Blake, N. Blake, E. Atlas, C. Jordan, G. Sachse, M. Avery, S. Vay, J. Snow, and B. Heikes, Chemical composition of Asian outflow over the western Pacific: Results from TRACE P, *Journal of Geophysical Research, 108 (D20)*, 8804, doi:10.1029/2002JD003184, 2003.

Talbot, R., J. Dibb, E. Scheuer, G. Seid, R. Russo, S. Sandholm, D. Tan, H. Singh, D. Blake, N. Blake, E. Atlas, G. Sachse, and M. Avery, Reactive nitrogen in Asian continental outflow over the western Pacific: Results from the NASA TRACE-P airborne mission, *Journal of Geophysical Research, 108 (D20)*, 8803, 10.1029/2002JD003129, 2003.

Collaborative papers:

Blake, N. J., D. G. Streets, J.-H. Woo, I. J. Simpson, J. Green, S. Meinardi, K. Kita, E. Atlas, H. E. Fuelberg, G. Sachse, M. A. Avery, S. A. Vay, **R. W. Talbot, J. E. Dibb**, A. R. Bandy, D. C. Thornton, F. S. Rowland, and D. R. Blake, Carbonyl-sulfide (OCS) and carbon disulfide (CS2): Large scale distribution over the Western Pacific and emissions from Asia during TRACE-P, *Journal of Geophysical Research 109*, D15S05, doi:10.1029/2003JD004259, 2004.

Browell, E. V., M. A. Fenn, C. F. Butler, W. B. Grant, V. G. Brackett, J. W. Hair, M. A. Avery, R. E. Newell, Y. Hu, H. E. Fuelberg, D. J. Jacob, B. E. Anderson, E. L. Atlas, D. R. Blake, W. H. Brune, **J. E. Dibb**, A. Fried, B. J. Heikes, G. W. Sachse, S. T. Sandholm, H. B. Singh, **R. W. Talbot**, S. A. Vay, and R. J. Weber, Large-scale ozone and aerosol distributions, air mass characteristics, and ozone fluxes over the western Pacific ocean in late-winter/early spring, *Journal of Geophysical Research, 108 (D20)*, 8805, doi:10.1029/2002JD003290, 2003.

Eisele, F. L., L. Mauldin, C. Cantrell, M. Zondlo, E. Apel, A. Fried, J. Walega, R. Shetter, B. Lefer, F. Flocke, A. Weinheimer, M. Avery, S. Vay, G. Sachse, H. B. Singh, W. Brune, H. Harder, M. Martinez, A. Bandy, D. Thornton, B. Heikes, Y. Kondo, D. Reimer, S. Sandholm, D. Tan, **R. Talbot** and **J. Dibb**, Summary of measurement intercomparisons during TRACE-P, *Journal of Geophysical Research, 108 (D20)*, 8791, doi:10.1029/2002JD3167, 2003.

Liu, H., D. J. Jacob, **J. E. Dibb**, A. M. Fiore, and R. M. Yantosca, Constraints on the sources of tropospheric ozone from ^{210}Pb-^{7}Be-O_3 correlations, *Journal of Geophysical Research 109*, D7, D07306, 10.1029/2003JD003988, 2004.

Ma, Y., R. J. Weber, K. Meier, D. A. Orsini, Y.-N. Lee, B. J. Huebert, S. G. Howell, T. Bertram, **R. W. Talbot, J. E. Dibb**, and **E. Scheuer**, Intercomparisons of airborne measurements of aerosol ionic chemical composition during TRACE-P and ACE-

Asia, *Journal of Geophysical Research, 109*, D15S06, doi:10.1029/2003JD003673, 2004.

Moore, K. G., II, A. D. Clarke, V. N. Kapustin, C. McNaughton, B. E. Anderson, E. L. Winstead, R. Weber, Y. Ma, Y.-N. Lee, **R. Talbot, J. Dibb**, T. Anderson, S. Doherty, D. Covert, and D. Rogers, A comparison of similar aerosol measurements made on the NASA P-3B, DC-8 and NSF C-130 aircraft during TRACE-P and ACE-Asia, *Journal of Geophysical Research, 109*, D15S15, doi:10.1029/2003JD003543, 2004.

Tang, Y., G. R. Carmichael, J. H. Seinfeld, D. Dabdub, R. J. Weber, B. Huebert, A. D. Clarke, S. A. Guazzotti, D. A. Sodeman, K. A. Prather, I. Uno, J.-H. Woo, J. J. Yienger, D. G. Streets, P. K. Quinn, J. E. Johnson, C.-H. Song, V. H. Grassian, A. Sandu, **R. W. Talbot**, and **J. E. Dibb**, Three-dimensional studies of aerosol ions and their size distribution in East Asia during Spring 2001, *Journal of Geophysical Research, 109*, D19S23, doi:10.1029/2003JD004201, 2004.

APPENDIX I

JOURNAL OF GEOPHYSICAL RESEARCH, VOL. 108, NO. D21, 8815, doi:10.1029/2002JD003111, 2003

Aerosol chemical composition in Asian continental outflow during the TRACE-P campaign: Comparison with PEM-West B

Jack E. Dibb, Robert W. Talbot, Eric M. Scheuer, and Garry Seid

Climate Change Research Center, Institute for the Study of Earth, Oceans, and Space, University of New Hampshire, Durham, New Hampshire, USA

Melody A. Avery

NASA Langley Research Center, Hampton, Virginia, USA

Hanwant B. Singh

NASA Ames Research Center, Moffett Field, California, USA

Received 31 October 2002; revised 19 February 2003; accepted 24 March 2003; published 11 November 2003.

[1] Aerosol associated soluble ions and the radionuclide tracers ^{7}Be and ^{210}Pb were quantified in 414 filter samples collected in spring 2001 from the DC-8 during the Transport and Chemical Evolution over the Pacific (TRACE-P) campaign. Binning the data into near Asia (flights from Hong Kong and Japan) and remote Pacific (all other flights) revealed large enhancements of NO_3^-, $SO_4^=$, $C_2O_4^=$, NH_4^+, K^+, Mg^{2+}, and Ca^{2+} near Asia. The boundary layer and lower troposphere were most strongly influenced by continental outflow, and the largest enhancements were seen in Ca^{2+} (a dust tracer) and NO_3^- (reflecting uptake of HNO_3 onto the dust). Comparing the TRACE P near Asia bin with earlier results from the same region during PEM-West B (in 1994) shows at least twofold enhancements during TRACE P in most of the ions listed above. Calcium and NO_3^- were most enhanced in this comparison as well (more than sevenfold higher in the boundary layer and threefold higher in the lower troposphere). Independent estimation of Asian emissions of gaseous precursors of the aerosol-associated ions suggest only small changes between the two missions, and precipitation fields do not suggest any significant difference in the efficiency of the primary sink, precipitation scavenging. It thus appears that with the possible exception of dust, the enhancements of aerosol-associated species during TRACE P cannot be explained by stronger sources or weaker sinks. We argue that the enhancements largely reflect the fact that TRACE P focused on characterizing Asian outflow, and thus the DC-8 was more frequently flown into regions that were influenced by well-organized flow off the continent. *INDEX TERMS:* 0305 Atmospheric Composition and Structure: Aerosols and particles (0345, 4801); 0365 Atmospheric Composition and Structure: Troposphere—composition and chemistry; 0368 Atmospheric Composition and Structure: Troposphere—constituent transport and chemistry; *KEYWORDS:* Asian outflow, TRACE-P, aerosol-associated soluble ions, beryllium-7, lead-210

Citation: Dibb, J. E., R. W. Talbot, E. M. Scheuer, G. Seid, M. A. Avery, and H. B. Singh, Aerosol chemical composition in Asian continental outflow during the TRACE-P campaign: Comparison with PEM-West B, *J. Geophys. Res.*, *108*(D21), 8815, doi:10.1029/2002JD003111, 2003.

1. Introduction

[2] The Transport and Chemical Evolution over the Pacific (TRACE-P) aircraft mission was the third time NASA's Global Tropospheric Experiment has targeted the western north Pacific. TRACE-P deployed two aircraft to conduct intensive sampling flights out of Hong Kong and Yakota Air Force Base in February–April 2001. These operation bases were also used during the Pacific Exploratory Mission (PEM) West A (in 1991) and B (in 1994) campaigns. TRACE-P flights used the combined capabilities of the Dryden DC-8 and the Wallops P3 to characterize the composition of Asian outflow and assess changes in that composition during transport [*Jacob et al.*, 2003]. The PEM-West campaigns used just the DC-8 in more of a survey mode, addressing several competing objectives.

[3] As the population of Asia grows and industrialization in the region proceeds at an increasing pace, it is expected that export of pollution to the Pacific Ocean and regions even further downwind will increase [*Houghton et al.*, 2001]. Concern over intercontinental transport of materials introduced into the atmosphere by anthropogenic activities has led IGPB's International Global Atmospheric Chemistry

0148-0227/03/2002JD003111$09.00

project to coordinate a new initiative focused on quantifying such long-range impacts. Transport of particles, including relatively coarse dust aerosol mixed with pollution, across the Pacific to western north America has been documented frequently in the past few years [e.g., *Gregory et al.*, 1997; *Xiao et al.*, 1997; *Jaffe et al.*, 1999, 2003; *Newell and Evans*, 2000; *Wilkening et al.*, 2000; *Husar et al.*, 2001; *McKendry et al.*, 2001; *Tratt et al.*, 2001; *Uno et al.*, 2001; *Vaughan et al.*, 2001; *Thulasiraman et al.*, 2002].

[4] The UNH group made in situ measurements of soluble acidic gases [*Talbot et al.*, 2003] and of aerosol-associated species collected onto filters from the DC-8 as part of TRACE-P. This paper focuses on the filter sampling, which provide distributions of ten water-soluble ionic species and the natural radionuclides ^{7}Be and ^{210}Pb, in the troposphere above the western north Pacific. The suite of ions includes several that are dominantly derived from anthropogenic emissions in much of the Northern Hemisphere (e.g., NO_3^-, $SO_4^=$, and NH_4^+), others that have been used to trace biomass burning emissions (e.g., K^+, $PO_4^=$, and $C_2O_4^=$), and a suite dominated by emissions of soil dust and sea salt into the atmosphere (e.g., Ca^{2+}, Mg^{2+}, Na^+, and Cl^-). We note that airborne dust can have both natural and anthropogenic sources, while generation of sea-salt aerosols is still largely a natural process. Beryllium-7 is a cosmogenic isotope produced in the atmosphere. Maximum production is near 15 km altitude; thus ^{7}Be is a tracer of stratospheric and upper tropospheric air masses mixing downward into the troposphere. Lead-210 is a daughter of ^{222}Rn, which is released from soils and rocks on continents. Therefore ^{210}Pb can be useful as a tracer of air masses that have been impacted by the continental boundary relatively recently.

[5] Most of the aerosol-associated ions that we measured on filters were also quantified with Particle into Liquid Sampler techniques employed on both the Wallops P3 and the NCAR C-130 (as part of the ACE-Asia campaign) [*Ma et al.*, 2003, Y. Ma et al., Intercomparisons of airborne measurements of fine particle ionic chemical composition during TRACE-P and ACE-Asia, submitted to *Journal of Geophysical Research*, 2003, hereinafter referred to as Ma et al., submitted manuscript, 2003]. Several additional techniques to characterize the chemical composition of aerosols were also used on the C-130. As part of TRACE-P, three instrument intercomparison flight legs were conducted where the DC-8 and P3 endeavored to fly in close formation for up to 1.5 hours [*Eisele et al.*, 2003]. In addition, the P3 conducted similar coordinated sampling for intercomparison with the C-130 during part of two flights. K. Moore et al. (Intercomparison of aerosol physical, optical and chemical characteristics measured from 3 platforms during TRACE-P and ACE-Asia, submitted to *Journal of Geophysical Research*, 2003) and Ma et al. (submitted manuscript, 2003) discuss the results of these intercomparisons for the range of aerosol measurements that were made on the different platforms. A primary conclusion was that inlet and operational details made it difficult to compare the composition measurements, since most, if not all, of the instruments were measuring different size fractions. Because of this complication, we restrict our attention to the DC-8 filter sampling. However, the bulk aerosol sampling system we used on the DC-8 has not changed since 1991, and our analysis has been by ion chromatography throughout the GTE program. Thus our TRACE P results should be comparable to all previous missions where we measured bulk aerosol composition from the DC-8. In particular, we will compare TRACE-P results to those from PEM-West B, which was conducted in the same general region during the same season in 1994.

2. Methods

2.1. Sampling

[6] We collected aerosols from the DC-8 using the UNH dual sampling probe that we have employed for all GTE missions on the DC-8 (all missions since 1991 except for TRACE A). This system was reproduced and also flown on the P3 during PEM Tropics B and is described in detail by *Dibb et al.* [2002] and references therein. These probes employ curved leading edge nozzles, isoaxially mounted inside cylindrical shrouds, and have adjustable sampling flow rates to maintain isokinetic sampling (within 10%). *Dibb et al.* [2002] discuss evidence we have obtained over several past missions which indicates that the way we operate these probes allows us to sample ambient aerosol particles with diameters up to at least 6 microns without significant losses in the sampling probe.

[7] As in past missions, sampling during TRACE-P was generally restricted to level flight legs. One of the sampling probes was used to collect aerosol-associated soluble ion samples onto 90 mm diameter 2 micron Millipore Fluoropore filters. The other probe was used to collect aerosol-associated ^{7}Be and ^{210}Pb on 90 mm diameter Whatman GF/A glass fiber filters. Continual improvement in the sensitivity of our analytical system, low and stable blank values from the Fluoropore filters, and relatively heavy aerosol loading over the western Pacific allowed us to reduce filter exposure time compared with all previous missions. A total of 414 filter pairs were exposed on the 17 science (transit and intensive) flights the DC-8 conducted during TRACE-P. Sampling intervals ranged from 1 to 40 min but averaged just over 6 min at altitudes below 1 km, 9 minutes from 1 to 6 km, 14 min between 6 and 9 km, and 17 min at altitudes above 9 km. Median sample exposure times in these altitude bins were slightly shorter than the means but not by more than 10%.

2.2. Analysis

[8] Exposed filters were stored in zero-air-purged clean room bags in a cooler [see *Dibb et al.*, 2002] until they were extracted immediately after each flight. Because our acidic gas sampling system [*Talbot et al.*, 2003] includes two custom ion chromatographs configured for anion analyses, it has been our practice to quantify anions in the aerosol filter extracts on the next nonflight day (usually the next day) and to preserve the remaining solution with chloroform. Cations are quantified in our laboratories in New Hampshire as soon as the samples have been returned at the end of the campaign. We began TRACE-P in this fashion, but the large number of aerosol samples collected made it impossible to keep up with the anion analyses. All extracts from flights 4 through 10 were analyzed in the field, for flights 11–20 the preserved extracts were returned to New Hampshire for quantification of both anions and cations. We

Table 1. Summary of the 37 Blank Filters Generated During TRACE-P

Bin, km	Mean Volume, SCM	Cl^-	NO_3^-	$PO_4^=$	$SO_4^=$	$C_2O_4^=$	Na^+	NH_4^+	K^+	Mg^{2+}	Ca^{2+}
		Loading on Blanks, nmol filter^{-1}									
Mean		7.2	1.5	0.1	1.8	0.4	14.6	3.5	1.9	0.7	7.3
Std. Dev.		2.6	0.3	0.2	0.3	0.5	2.1	0.7	1.0	0.4	3.6
		Uncertainty in Mixing Ratios Due to Blanks, ppt									
<1	2.18	26.5	2.8	2.3	2.6	5.1	21.1	6.7	10.0	4.4	37.2
1–6	2.88	20.0	2.1	1.8	1.9	3.9	15.9	5.1	7.6	3.3	28.2
6–9	3.10	18.6	2.0	1.6	1.8	3.6	14.8	4.7	7.0	3.1	26.2
>9	2.58	22.4	2.4	2.0	2.2	4.3	17.8	5.6	8.5	3.7	31.5

also reanalyzed anions in the samples from the first seven flights and found no significant changes due to storage (for up to 6 weeks).

[9] Blank Fluoropore filters were generated (2–3 per flight) by placing a filter into a cassette, inserting it into the sampling probe, and opening all valves to allow airflow for less than 5 s. These blanks were then stored in purged clean room bags and extracted along with the exposed filters. We have found that variability in the loading of analyte ions on blank filters often constitutes the largest source of uncertainty in determining the mixing ratios of aerosol-associated ions. *Dibb et al.* [2002] noted that Fluoropore blanks during PEM Tropics B were much lower and less variable than we had ever obtained with Zefluor filters, reducing uncertainty and leading to lower detection limits. Mean values of the ion loadings on TRACE-P blank filters (Table 1) were similar (often slightly higher) than those for PEM Tropics B, but the variability was less by 50–100%. The more stable blanks yield lower uncertainty, but this is partly negated by the smaller sample volumes during TRACE-P. Table 1 shows the contribution variability in the blanks makes to uncertainty in calculated mixing ratios for samples with volumes equal to the mean in each of 4 altitude bins. (Note that we report mixing ratios of aerosol-associated ions in units of parts per trillion (ppt = (picomoles of analyte) (mole of air)$^{-1}$) to facilitate comparison to gaseous precursors.) Samples with larger (smaller) volumes of air filtered will have proportionately smaller (larger) uncertainty. During TRACE-P the range of sample volumes was 0.9–4.0, 1.4–6.8, 1.2–7.0, and 1.2–5.8 standard cubic meters (SCM) in the boundary layer, 1–6 km, 6–9 km, and >9 km altitude bins, respectively. Therefore the uncertainty in mixing ratios reported for any sample rarely differ from those listed in Table 1 by more than a factor of two.

[10] Glass fiber filters were returned to UNH by express mail in several groups during the deployment, so that ^7Be (half-life = 53 days) could be quantified by nondestructive gamma spectroscopy as quickly as possible. We quantify ^{210}Pb through alpha spectroscopic determination of ^{210}Po, after allowing at least 11 months for the daughter to "grow in" [*Dibb et al.*, 1996].

2.3. Binning and Averaging

[11] One focus of the following discussion is comparing the distribution of aerosol-associated species between TRACE P and PEM West B. *Dibb et al.* [1996, 1997] found it convenient to divide the study region sampled during PEM West A and B into two broad subregions: near Asia and remote north Pacific. We will follow this lead and consider that all of the TRACE-P flights out of Hong Kong and Yakota (except the transit from Japan to Kona) sampled the near-Asia region (Figure 1). We consider the westbound transit flights (Dryden to Kona, Kona to Guam, and the first half of Guam to Hong Kong) and the return (Japan to Kona to Dryden, including the local flight out of Kona), to have sampled the remote Pacific. This division is based on the operational bases of the DC-8, which guided the scientific objectives of each flight [*Jacob et al.*, 2003], rather than any strict geographic consideration. However, the vast majority of near Asia samples were collected west of 150 E, with nearly all remote samples east of this longitude (Figure 1).

[12] The near-Asia region substantially overlaps the comparable region considered during both PEM West campaigns, with some potentially significant differences that will be discussed more fully later. The TRACE-P remote Pacific data set has a much greater emphasis on the eastern Pacific and correspondingly less sampling in the tropical and subtropical western north Pacific, than either PEM West campaign. TRACE-P sampling was also restricted to latitudes south of 47 N, contrasting the transit flights through Anchorage on both PEM West campaigns. It should also be emphasized that the number of samples in both regions was much higher during TRACE-P (284 versus 72 near Asia samples, 130 versus 44 remote samples in PEM West B, with even fewer samples in PEM West A).

[13] We have used the altitude bins defined by *Dibb et al.* [1997]; <1 km to represent the boundary layer, 1–6 km as a lower troposphere bin, and 6–9 and >9 km to represent the middle and upper troposphere, respectively. A disproportionate fraction of our filter samples (approximately 40% in each of the geographic regions) fall into the boundary layer bins, largely due to the shorter sample times we used at low altitude. To further highlight the larger size of the TRACE-P data set, we note that more samples were collected in the near Asia boundary layer during TRACE-P than the total at all altitudes in both regions during PEM West B.

[14] We also compare the distributions of selected gaseous species (O_3, HNO_3, and PAN) to the aerosol-associated species which are the primary focus. All of these gases were

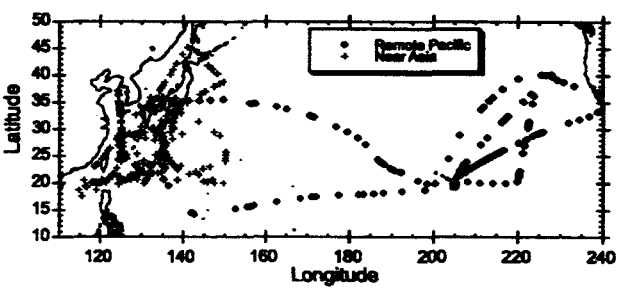

Figure 1. Geographic distribution of bulk aerosol filter samples collected from the DC-8 during TRACE-P. Samples shown with crosses are considered to be near Asia; those indicated by diamonds are considered to be over the remote Pacific in this paper.

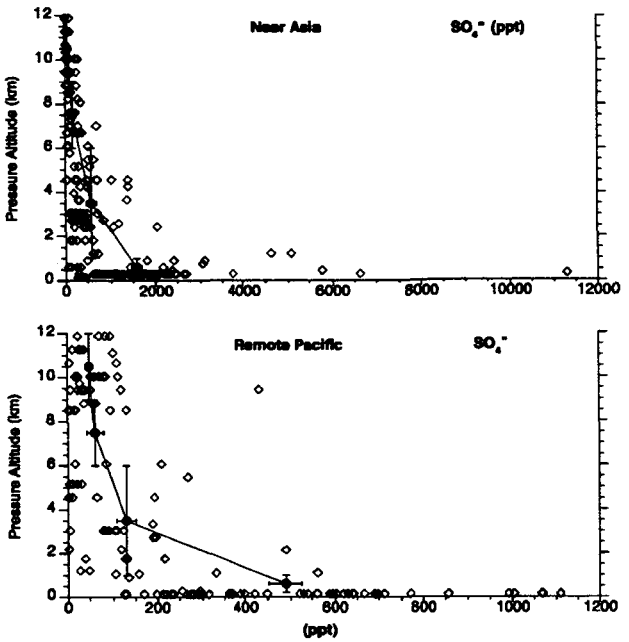

Figure 2. Mixing ratios of aerosol-associated $SO_4^=$ as a function of altitude in the two geographic bins. The solid diamonds (connected by the lines) show the means in four altitude bins (<1, 1–6, 6–9, and >9 km). Vertical error bars on the solid diamonds indicate the depth of the altitude bins, while the horizontal bars show the standard error of the bin means.

measured at higher frequency than we collected aerosol filters, and detailed discussions of their high-resolution data sets are presented in companion papers in this issue. In this paper we exclusively use a merged data set, generated by the GTE project office, wherein all fast response measurements were averaged to the varying integration time of the individual aerosol filter samples.

3. Results

[15] The distribution of $SO_4^=$ as a function of altitude in the two geographic bins illustrates our sampling density, and highlights two features that are common to the distributions of many of the aerosol-associated species (Figure 2). In the boundary layer mixing ratios vary over more than an order of magnitude, but even the lowest values tend to be enhanced compared with those in the free troposphere. As a result, the boundary layer means exceed those in the lower troposphere by more than a factor of 2.5 and are at least 15-fold higher than upper troposphere means. Similarly rapid decreases with altitude characterize the distributions of Cl^-, NO_3^-, Na^+, NH_4^+, K^+, Mg^{2+}, and Ca^{2+}, with the trend more striking near Asia for Ca^{2+} and K^+ (Table 2). It should be noted that the summary statistics tabulated in Table 2 consider only those samples for which the individual ion was above detection limit and thus may considerably overestimate the mean and median in some of the higher altitude bins (e.g., $PO_4^=$ and Cl^- above 9 km near Asia, $PO_4^=$, Cl^-, Na^+, Mg^{2+}, Ca^{2+} in the highest remote bin). (*Dibb et al.* [1997] also omitted below detection limit samples when calculating summary statistics for the PEM West B data set.) However, it must also be pointed out that despite the smaller sample volumes for TRACE P samples, a smaller proportion of samples were reported as below detection limit than in all previous GTE campaigns. Below 6 km, all aerosol-associated species except ^7Be and $PO_4^=$ were quantified in more than 90% of the near Asia samples and in more than 65% of the remote Pacific samples. At higher altitudes all species (except for $PO_4^=$ far from Asia) were quantified in more than 27% of all samples, while those species usually dominating the accumulation mode (NH_4^+ and $SO_4^=$) were too low to quantify in just two and

Table 2. Concentrations of Aerosol-Associated Species in Eight Geographic/Altitude Bins Over the North Pacific During TRACE-P[a]

	Cl^-	NO_3^-	$PO_4^=$	$SO_4^=$	$C_2O_4^=$	Na^+	NH_4^+	K^+	Mg^{2+}	Ca^{2+}	^7Be	^{210}Pb
Near Asia												
<1 km (118 Samples)												
n[b]	118	118	46	118	114	118	118	115	118	112	78	118
Mean	2022	839	33	1574	67	2238	1613	276	366	1366	368	20.3
Serr[c]	150	136	3	121	5	163	147	29	30	243	37	1.2
Med.	1839	508	32	1497	56	1878	1332	210	281	407	289	16.9
1–6 km (67 Samples)												
n[b]	47	66	57	67	67	61	67	67	63	58	47	67
Mean	214	220	8	587	39	422	528	98	156	969	500	10.7
Serr[c]	64	72	2	103	5	152	82	25	53	345	68	0.6
Med.	45	73	5	346	28	61	371	42	25	135	442	10.2
6–9 km (44 Samples)												
n[b]	15	39	19	44	44	24	44	33	25	24	31	44
Mean	66	42	4	158	12	73	148	17	23	118	847	7.5
Serr[c]	21	10	0.6	21	1.5	29	20	3	7	35	213	0.6
Med.	21	25	3	115	12	8	115	10	8	52	562	6.5
>9 km (55 Samples)												
n[b]	12	35	11	52	46	18	53	24	16	22	45	55
Mean	100	12	4	54	7	72	58	15	28	81	1057	4.9
Serr[c]	30	3	0.5	9	0.9	23	10	6	11	25	240	0.3
Med.	34	5	4	27	6	27	37	4	11	28	504	4.8
Remote Pacific												
<1 km (51 Samples)												
n[b]	51	51	3	51	49	51	49	51	51	42	19	51
Mean	2608	139	12	490	26	2523	522	79	261	93	381	7.0
Serr[c]	242	11	4	37	2	211	37	6	23	10	61	0.4
Med.	1659	129	16	422	23	1637	466	65	167	85	450	6.8
1–6 km (34 Samples)												
n[b]	24	27	5	34	33	22	32	28	20	13	12	34
Mean	491	29	5	130	11	506	137	23	65	87	425	6.9
Serr[c]	168	6	3	22	1	163	24	5	21	33	81	0.9
Med.	55	18	5	105	9	114	129	15	22	25	367	7.0
6–9 km (12 Samples)												
n[b]	2	10	3	12	11	4	12	8	5	3	5	12
Mean	11	9	1	61	21	15	86	15	1	11	657	6.9
Serr[c]	6	2	2	18	5	8	221	6	0.7	6	312	1.0
Med.	11	9	1	47	18	15	82	5	0.5	15	400	6.4
>9 km (33 Samples)												
n[b]	12	21	3	33	29	12	33	14	13	11	24	33
Mean	99	7	3	49	18	125	60	17	4	33	1838	6.5
Serr[c]	32	1	2	6	2	43	9	9	1	7	578	0.6
Med.	49	5	2	37	18	62	52	5	0.8	22	691	6.1

[a]Ions are reported in mixing ratios as parts per trillion (ppt) while the two radionuclide tracers are given in fCi scm^{-1}.
[b]Here n is the number of samples above detection limit.
[c]Serr is the standard error (=standard deviation/square root of n).

three samples, respectively (Table 2). Oxalate and ^{210}Pb also decrease with altitude, but their gradients are less steep than the ions listed above. The distribution of ^{7}Be is unique among all the aerosol-associated species, increasing strongly with altitude (Table 2). This is not unexpected, given the production profile (maximum near 15 km) and the much higher concentrations of ^{7}Be in the stratosphere.

[16] The distribution of $SO_4^=$ also illustrates the enhancement of several aerosol-associated species near Asia. Peak mixing ratios in the boundary layer and lower troposphere were roughly an order of magnitude higher in this region (Figure 2), and the average was more than 2.6-fold higher in all near Asia bins below 9 km (Table 2). Nitrate and Ca^{2+} showed even larger enhancements (>4.7- and >10.7-fold, respectively) near Asia than did $SO_4^=$. Oxalate, NH_4^+, K^+, and ^{210}Pb enhancements near Asia were comparable to those in $SO_4^=$ but only in the boundary layer and lower troposphere, while the Mg^{2+} enhancement near Asia increased with altitude. In contrast, mean mixing ratios of Cl^- and Na^+ were higher in the remote low-altitude bins, and ^{7}Be mean concentrations did not differ by more than 30% below 9 km.

[17] Calcium shows the largest enhancements near Asia of all aerosol-associated species (Table 2). Soluble Ca^{2+} is often considered to be the best tracer of continental dust among the ionic species, though sea salt is also a significant source of Ca^{2+} which can dominate in the marine boundary layer far from land [e.g., *Dibb et al.*, 1999a]. During TRACE-P it is clear that outflow of Asian dust was the overwhelmingly dominant source of Ca^{2+}, as it was greatly in excess of the sea-salt ratio in all near Asia free troposphere samples, most of the remote tropospheric samples, and in many boundary layer samples from both regions. The abundance of Asian dust in the near Asia region also impacted the distribution of Mg^{2+}, particularly below 9 km. However, the larger contribution that sea salt makes to Mg^{2+} mixing ratios (Mg^{2+} is more than fivefold more abundant than Ca^{2+} in sea salt, on a molar basis) masked the enhancement of dust-derived Mg^{2+} in the near Asia region. The dust fraction of Mg^{2+} was likely 10–15 times higher near Asia than over the remote Pacific, but the lower sea-salt mixing ratios near Asia resulted in total Mg^{2+} enhancements that were roughly a factor of 2 below 6 km, (Table 2). In the remote Pacific the relationships between Na^+ and Mg^{2+} are consistent with sea salt being the dominant source of Mg^{2+}. It should be noted that the abundance of dust near Asia is so high in some samples that a significant fraction of the measured Na^+ may also be derived from this source [e.g., *Song and Carmichael*, 2001]. In a later section, we will use Na^+ to estimate the non-sea-salt (nss) fraction of several ions but recognize that these will be underestimates to the extent that Asian dust is a source of the measured Na^+. *Jordan et al.* [2003a] base much of their discussion on similarly estimated nss fractions and argue that dust-derived Na^+ is only likely to be significant in a small number of samples originating from a limited region.

[18] As noted above, NO_3^- shows the second highest enhancements near Asia, followed by $SO_4^=$ and NH_4^+ (Table 2). The precursors of all three of these ions are emitted by a range of anthropogenic activities; hence they are often considered to be pollution tracers. *Jordan et al.* [2003a] demonstrate that uptake of HNO_3 onto Asian dust

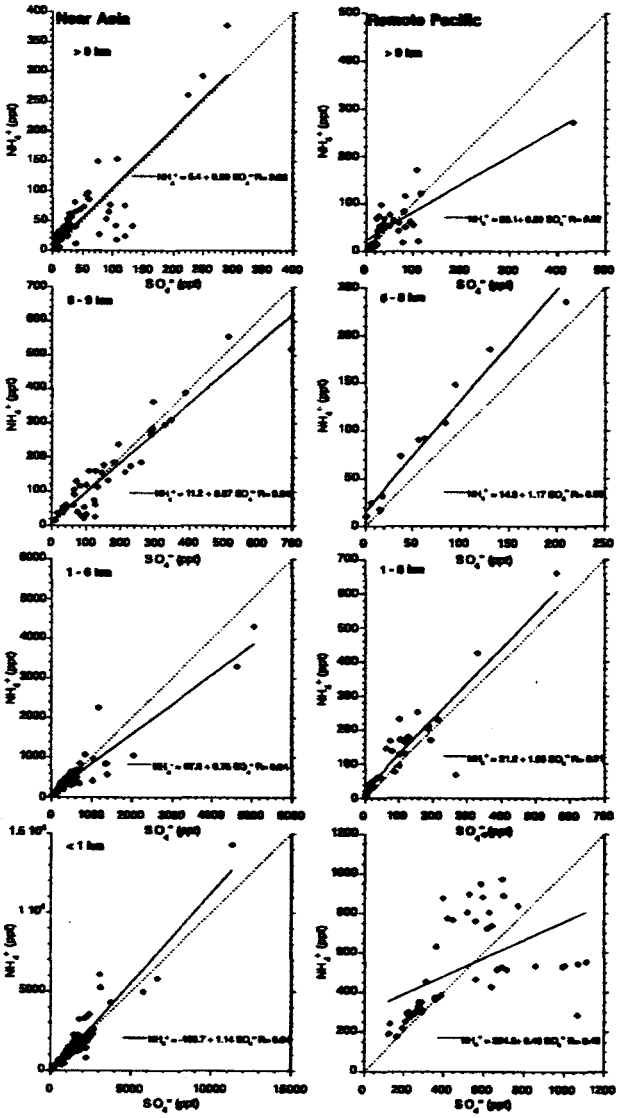

Figure 3. Scatter plots of NH_4^+ against $SO_4^=$ in the same eight bins. The dotted lines have slopes of unity, corresponding to NH_4HSO_4. Solid lines are least squares fits of the data.

can account for many of the highest mixing ratios of aerosol-associated NO_3^-, while uptake of HNO_3 onto sea-salt aerosol contributes to elevated NO_3^- in boundary layer regions with smaller dust loading [*Talbot et al.*, 2003]. Sulfur dioxide and H_2SO_4 can react with sea salt, dust, and NH_3 to form aerosol $SO_4^=$. It is likely that all three processes contributed to the aerosol-associated $SO_4^=$ we measured during TRACE-P, though the strong relationships between $SO_4^=$ and NH_4^+ suggest that formation of NH_4HSO_4 may have been extensive near Asia (Figure 3). If most of the $SO_4^=$ exported from Asia is associated with NH_4^+ in accumulation mode particles rather than on coarse sea salt and dust, the potential for very long-range transport across the Pacific will be increased. Scatter plots of $SO_4^=$ versus Ca^{2+} (not shown) show essentially no relationship except that

samples with very strong dust signals (4–15 ppb Ca^{2+}) also have elevated $SO_4^=$ (2–5 ppb). Similarly, $SO_4^=$ shows no clear relationship to Na^+ (plots not shown). Unfortunately, size-resolved measurements, which could confirm that $SO_4^=$ is dominantly associated with fine particles, were not made on the DC-8. However, measurements made from the NCAR C-130 during ACE Asia did find that $SO_4^=$ was predominantly in the accumulation mode (B. Huebert, personal communication, November 2001). On the other hand, $SO_4^=$ does show general correlation with $PO_4^=$ and $C_2O_4^=$, particularly near Asia (not shown). Their relationships to $SO_4^=$, and their enhancements in the two low-altitude near-Asia bins (Table 2), suggest that $PO_4^=$ and $C_2O_4^=$ are also anthropogenically impacted components of the Asian outflow sampled during TRACE-P.

4. Discussion

[19] *Jordan et al.* [2003b], *Russo et al.* [2003], and *Talbot et al.* [2003] all use the same binning scheme based on air mass origin (from trajectories) to characterize the composition of Asian outflow sampled from the DC-8 during TRACE-P. *Blake et al.* [2003], combined the extensive data sets on hydrocarbons and halocarbons collected from the DC-8 and P3 and searched for signatures of specific types of emissions (e.g., regional differences in urban/industrial sources, biogenic emissions, biomass burning, etc.). All of these authors conclude that the continental outflow generally contained a mixture of emissions that made it difficult to pinpoint the influence of specific sources or regions. *Bartlett et al.* [2003] focused on CH_4 measurements from both aircraft and used spatial binning to address similar issues. They also found that the distribution of CH_4 and its relations to selected NMHC reflected the influence of a complex mixture of sources but show that biomass burning and biofuel combustion emissions from Southeast Asia had a dominant influence on upper tropospheric air in the central Pacific. Simulations with the global three-dimensional model, GEOS-CHEM, indicate that biomass burning emissions in south east Asia had to be lifted to the middle and upper troposphere before they could be advected into the TRACE P study region [*Liu et al.*, 2003]. *Carmichael et al.* [2003] find that their regional-scale three-dimensional chemical transport model (STEM 2K1) reproduced this feature as well, and *Ma et al.* [2003] present fine K^+ measurements on the P3 which show biomass burning plumes from Southeast Asia above polluted boundary layer outflow. Simulations with STEM 2K1 also suggested that near Asia the processes exporting dust and pollution into the Pacific generally caused layering, with dust overlying urban/industrial pollution (G. Carmichael, personal communication, June 2002). M. Chin et al. (An assessment of regional Pacific Rim sulfur chemistry based on observations from TRACE-P and ACE-Asia, submitted to *Journal of Geophysical Research*, 2003) found similar vertical separation of dust and pollution in their global model, consistent with observations from previous airborne sampling [*Clarke and Kapustin*, 2002].

[20] We examined the vertical distributions of aerosol-associated ions in the near-Asia bin to see if they provide evidence that outflowing pollution (from urban/industrial sources and from combustion of biomass) and dust are transported at different altitudes. Non-sea-salt Ca^{2+} was selected as the dust tracer, using Na^+ to estimate the sea-salt fraction. Non-sea-salt $SO_4^=$ represents urban/industrial pollution, while nss K^+ and $C_2O_4^=$ where included as the best tracers of biomass or biofuel combustion among the aerosol-associated ions ($C_2O_4^=$ and its precursor $H_2C_2O_4$ is a product of combustion generally but has been shown to be greatly enhanced in boreal wild fires [*Lefer et al.*, 1994; *Gorzelska et al.*, 1994]). Simply dividing the 1–9 km altitude band into four bins of 2 km thickness reveals that nss $SO_4^=$ (and also NH_4^+) is greatly elevated below 1 km, while the highest mean nss Ca^{2+} (also nss Mg^{2+}) mixing ratios are found in the 1–3 km range. In order to show all four tracers on a comparable scale, we divided the mixing ratios of tracer ions in each sample by their means above 9 km and then calculated summary statistics for the normalized values in six altitude bins (<1, 1–3, 3–5, 5–7, 7–9, and >9 km) (Figure 4). Enhanced transport of dust between 1 and 3 km occurs in well-organized plumes with very elevated concentrations [*Jordan et al.*, 2003a, 2003b], as demonstrated by the fact that the mean for this bin but not the median is the highest in the near-Asia region. It should be noted that there is substantial dust in the boundary layer bin, mixing with the pollution and also that nss $SO_4^=$ is present in abundance in the 1–3 km bin where dust is highest (Figure 4). One result of mixing dust with the

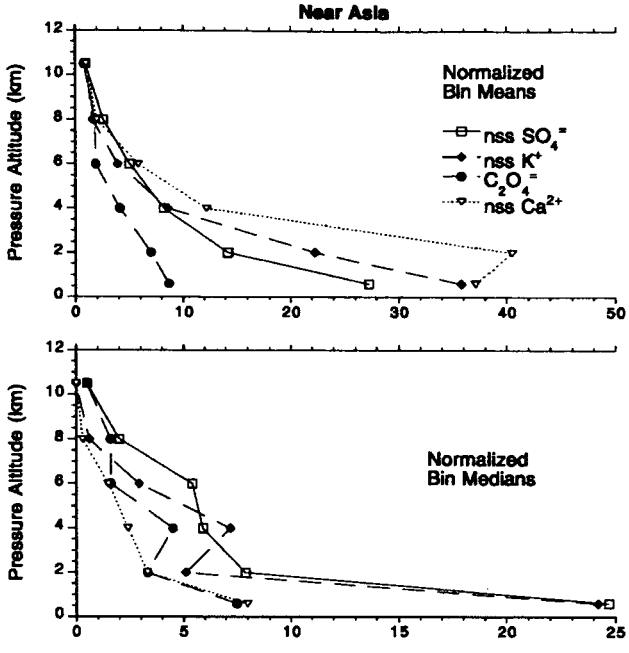

Figure 4. Altitude distributions of nss $SO_4^=$ (considered to represent urban/industrial emissions), nss K^+, and $C_2O_4^=$ (often tracers of biomass burning) and nss Ca^{2+} in the TRACE-P near-Asia region. Sea-salt corrections use Na^+ as the tracer. The points are plotted at the mean (upper panel) and median (lower panel) values of normalized mixing ratios in <1, 1–3, 3–5, 5–7, 7–9, and >9 km altitude bins. The normalization process consisted simply of dividing mixing ratios in each sample by the mean in the >9 km bin.

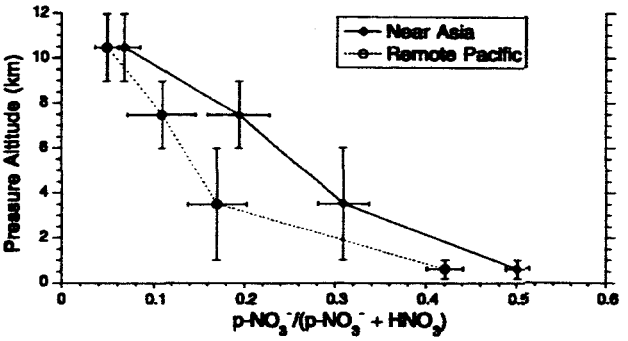

Figure 5. Mean partitioning of inorganic nitrate between the gas and particulate phases in the eight bins defined in Table 2. Error bars as defined for Figure 2.

pollutant emissions during transport over the Pacific is that HNO_3 is taken up by the dust [*Jordan et al.*, 2003a], causing a larger fraction of inorganic NO_3^- to be found in the particulate phase in the near-Asia region in all altitude bins up to 9 km (Figure 5). The mean mixing ratios of nss K^+ and $C_2O_4^=$ smoothly decrease with altitude, like nss $SO_4^=$ (Figure 4), suggesting that their sources are mixed with urban/industrial emissions before reaching the TRACE-P study region. It does not appear that the large-scale distributions of aerosol-associated ions provide any evidence for an influence from biomass/biofuel combustion that can be separated from the general urban/industrial emissions in the regions sampled by the DC-8.

4.1. Insights From the Radionuclide Tracers

[21] Relatively strong correlations between ^{210}Pb and O_3, and weak or no relationships between ^7Be and O_3 during both of the PEM West campaigns suggested that tropospheric production was a much more significant O_3 source than injection from the stratosphere for the Pacific region during the campaigns [*Dibb et al.*, 1996, 1997]. In the fall of 1991 (PEM West A), ^{210}Pb and O_3 were correlated throughout the troposphere in both regions; during the spring of 1994 (PEM West B) this relationship was only apparent over the remote Pacific.

[22] The relationship between ^7Be and O_3 during TRACE-P argues for a minor contribution from the stratosphere in this region during spring 2001 as well (Figure 6). A small number of samples with very high values result in relatively high correlation coefficients (>0.78) in the top two near-Asia bins and above 9 km over the remote Pacific, but the bulk of the data in these bins show essentially no relationship. At lower altitudes in both regions the relationships are weak, with O_3 tending to be anticorrelated with ^7Be below 6 km far from Asia. There was also little correlation between ^{210}Pb and O_3 in the near-Asia region (Figure 7). Above 9 km there is a reasonably strong relationship ($O_3 = 28.0 + 5.2$ (^{210}Pb), R = 0.58) if the four stratospheric samples (O_3 > 200 ppb) are omitted. Over the remote Pacific the relationship between ^{210}Pb and O_3 was strongest in the two bins above 6 km, though the slopes were just over half as large as in the highest near Asia altitude bin (Figure 7). We have previously argued that strong correlations between these species reflect advection (vertical and horizontal) of ^{222}Rn and O_3 precursors from the polluted continental boundary layer, with ^{210}Pb and O_3 building up over time during subsequent transport [*Dibb et al.*, 1996, 1997, 1999b].

4.2. Comparison With PEM West B

[23] As noted earlier, the TRACE-P remote Pacific data set is based on three flights between Hawaii and the west coast of North America plus the westbound transits through Guam to Hong Kong and the eastbound flight from Japan to Hawaii (Figure 1). In contrast, the remote Pacific data set from PEM West B was based on flights out of Guam which targeted tropical and subtropical air masses near 150 E. In both campaigns the remote regions provide a sharp contrast to near Asia air masses, but the TRACE-P data set could be more influenced by aged Asian outflow that had transited the Pacific and recirculated in the "river of pollution" [*Renner*, 2000; *Staudt et al.*, 2001; *Martin et al.*, 2003]. This region

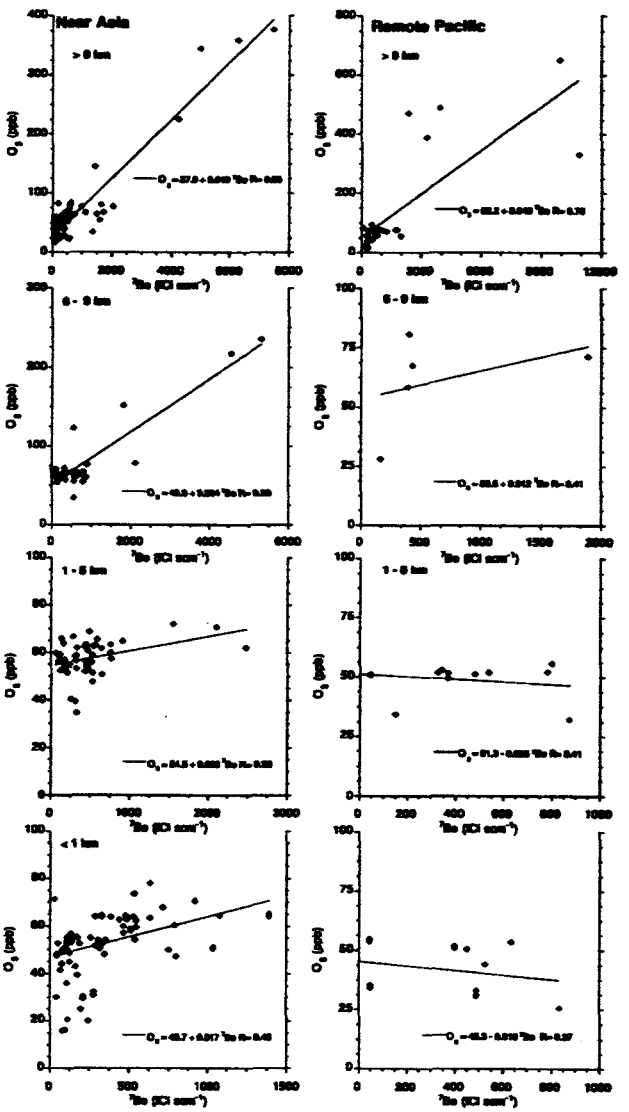

Figure 6. Scatter plots of O_3 against ^7Be in the eight bins defined in Table 2. Lines are least squares fits of the data.

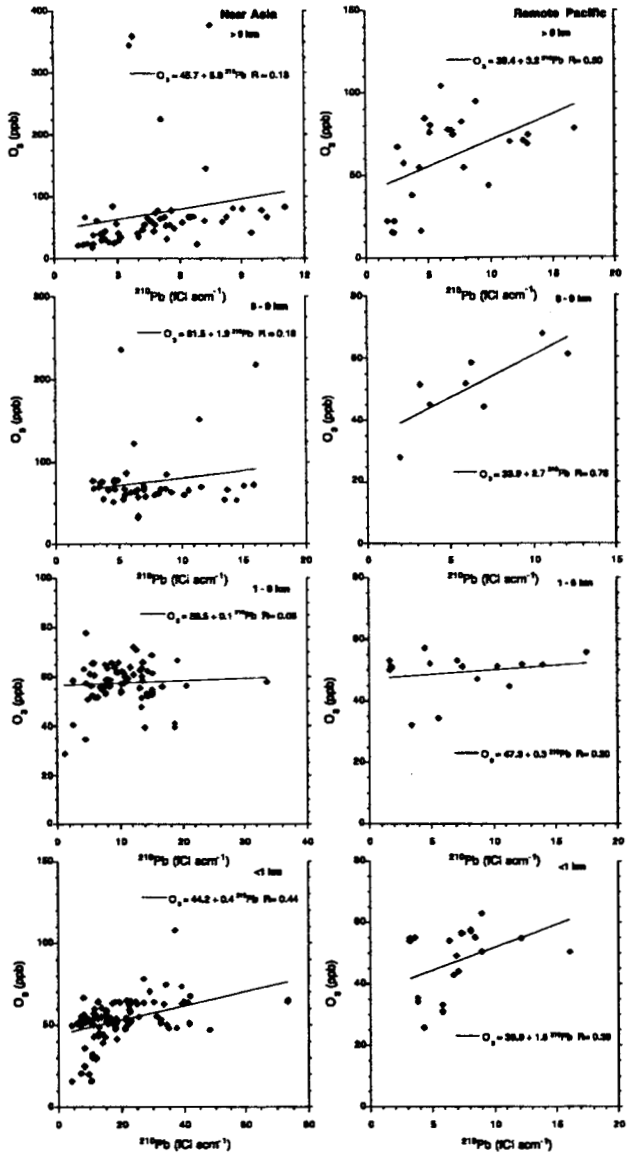

Figure 7. Scatter plots of O_3 against ^{210}Pb in the four near-Asia altitude bins. Lines are least squares fits of the data.

may also be influenced by North American outflow to some extent. The near-Asia region data sets would appear to be more directly comparable, since they are based on similar flights by the DC-8 from the same operational bases in Hong Kong and Yakota, Japan. However, we must point out that no sampling was conducted in the region bounded approximately by 27–37 N, 120–135 E during PEM West B. Several TRACE-P flights specifically targeted this near China region (Figure 1) and encountered very strong outflow.

[24] The aerosol-associated tracers of dust and pollution were all higher in TRACE-P than PEM West B (Figure 8). Calcium near Asia was more than 16 times higher in the boundary layer, nearly 6 times higher in the 1–6 km bin, and showed more than twofold enhancement at higher altitudes. At low altitudes over the remote Pacific, Ca^{2+} was likewise roughly twofold higher during TRACE-P. Nitrate showed the second largest enhancements in the near Asia low-altitude bins (factors of 3 and 7 in the lower troposphere and boundary layer) but only increased (a factor of 2) in the boundary layer over the remote Pacific. Enhancements of $SO_4^=$ and NH_4^+ (TRACE-P >2.5 and >1.7 times higher, respectively) were larger in the remote region and extended through the full DC-8 altitude range (Figure 8). Near Asia the average $SO_4^=$ mixing ratios were 2.4–3.4 times higher during TRACE-P from 9 km to the surface, contrasting small (10–30 %) NH_4^+ enhancements in all bins except the boundary layer where TRACE-P was 2.5 times higher than PEM West B. It is important to point out that ions with major contributions from sea salt, and the

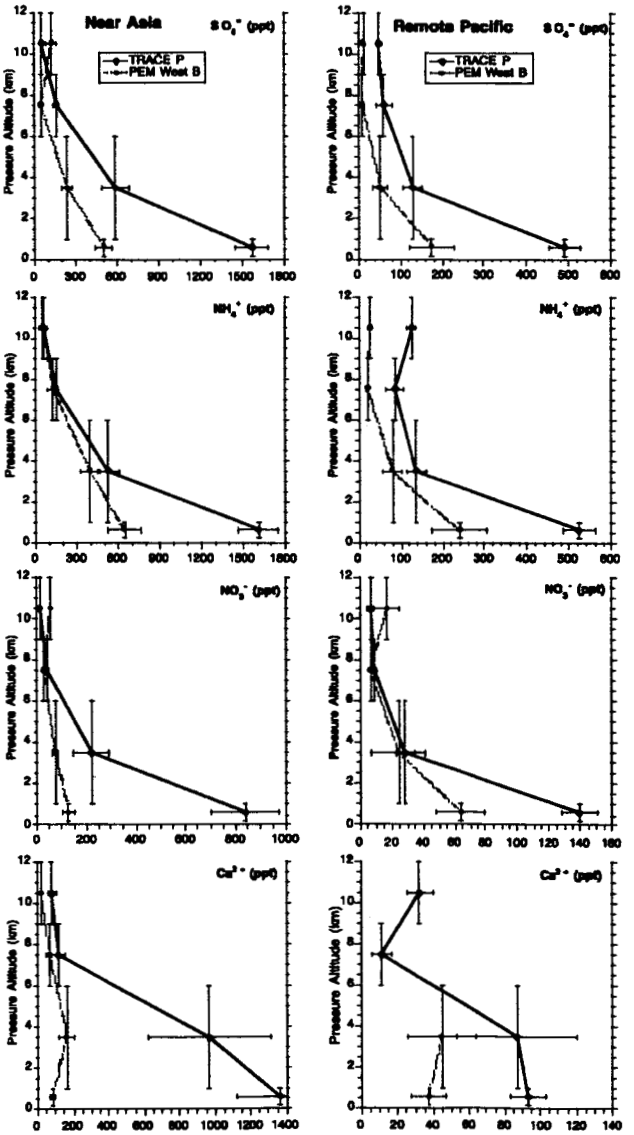

Figure 8. Comparison of mean mixing ratios of $SO_4^=$, NH_4^+, NO_3^-, and Ca^{2+} in four altitude bins in regions near to, and far from, Asia between TRACE-P and PEM West B. Error bars as defined in Figure 2.

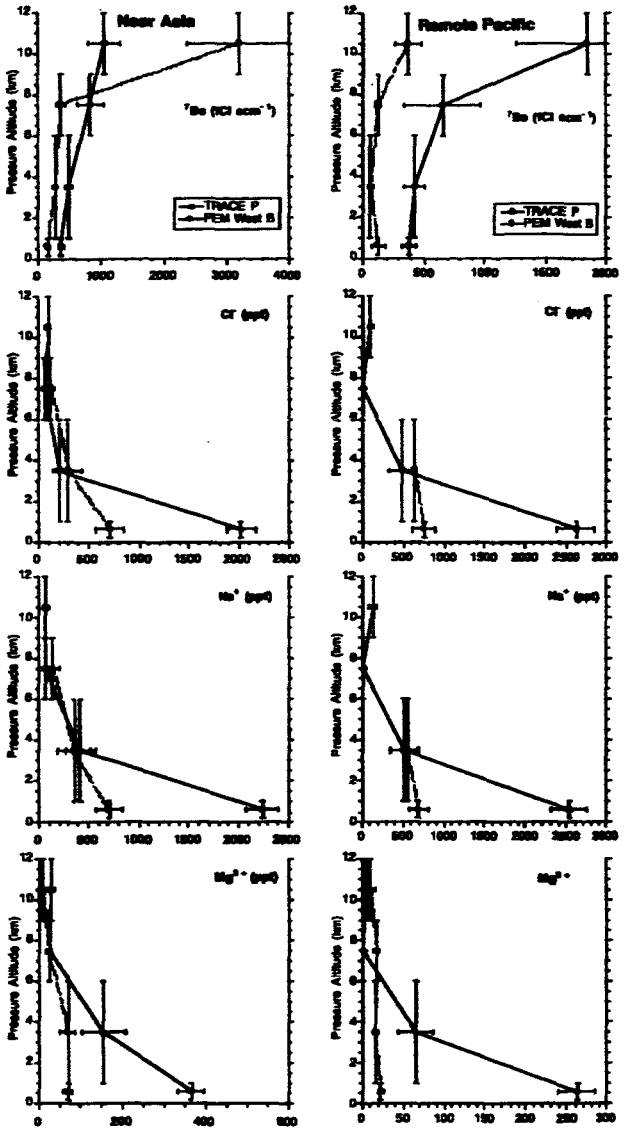

Figure 9. As in Figure 8 but for ^{7}Be, Cl^{-}, Na^{+}, and Mg^{2+}.

cosmogenic radionuclide ^{7}Be, were also higher during TRACE-P in some of the bins (Figure 9). Sodium, Cl^{-}, and Mg^{2+} were all enhanced by at least a factor of 2.8 in the boundary layer in both regions. It is likely that the enhancements of Mg^{2+} in both lower troposphere bins, which are not seen in the other sea-salt species (Figure 9), reflect contributions from dust, as suggested by the Ca^{2+} distributions (Figure 8). Beryllium-7 was higher during TRACE-P in all bins except near Asia above 9 km (the high concentrations in this bin during PEM West B reflect extended sampling in and near a tropopause fold [*Dibb et al.*, 1997]). Enhancements of ^{7}Be were larger (3.1 to 6.4 times higher during TRACE-P) over the remote Pacific than near Asia (1.8–2.3 below 9 km).

[25] Sharply higher concentrations of many aerosol-associated species over the Pacific are to some extent an anomaly in the TRACE-P data set. Most comparisons of the distributions of trace gases between TRACE-P and PEM West B found small differences or changes that appear to reflect seasonal (e.g., O_3) or global trends (e.g., CH_4) [*Bartlett et al.*, 2003; *Blake et al.*, 2003; *Russo et al.*, 2003; *Talbot et al.*, 2003; D. D. Davis et al., A comparison of photochemical environments in the NW Pacific as observed during NASA's PEM-West B [1994] and TRACE-P [2001] airborne field studies, submitted to *Journal of Geophysical Research*, 2003]. Several different scenarios may have contributed to the changes in distributions of aerosol-associated species depicted in Figures 8 and 9. Our comparison may have generated large apparent differences that are not "real." The issue of whether an airborne campaign captures a regionally representative data set is always an important question. On the large scale, the meteorolgical conditions and sampling regions were very similar between PEM West B and TRACE-P [*Fuelberg et al.*, 2003], though *Liu et al.* [2003] suggest that more frequent cold surges enhanced boundary layer outflow of Asian air to the Pacific during TRACE-P. We will examine the impact of differences in sampling between the two missions shortly but first consider potential causes for much higher levels of dust and aerosol-associated pollutants in 2001 versus 1994. Clearly, increased emissions in Asia are expected to impact much of the troposphere above the Pacific and further downwind. However, greater export from Asia during TRACE-P than PEM West B should be apparent as increases in many gaseous pollutants as well. Assuming that emissions from Asia have not greatly increased, higher mixing ratios of aerosols exported from Asia could be explained by a weaker sink, i.e., less efficient removal of particles by precipitation scavenging. In the following, we present available evidence on differences in scavenging, Asian emissions, and possible transport/sampling bias between TRACE-P and PEM West B.

4.2.1. Scavenging

[26] Concentrations of ^{7}Be above the northern Pacific during both PEM West campaigns were very low compared with expectations and our observations over the south Pacific during PEM Tropics A [*Dibb et al.*, 1996, 1997, 1999a]. We interpreted these low values as evidence of extensive removal by scavenging; hence the higher concentrations observed during TRACE-P (Figure 9) may reflect reduced removal of aerosols over the northern Pacific. We have also found that ^{210}Pb and its relationship to sparingly soluble gaseous pollutants (specifically precursors to PAN [*Dibb et al.*, 1996, 1997] and NMHC emitted in wild fires [*Dibb et al.*, 1999b]) can provide insight into scavenging during deep wet convection. During the PEM West campaigns we found that ^{210}Pb tended to be strongly correlated with PAN, but not aerosol NO_3^-, HNO_3, or their sum (termed t-NO_3^-), and argued that HNO_3 had been scavenged in the wet convective pumping that lifted ^{222}Rn and pollutants out of the Asian boundary layer. Interestingly, ^{210}Pb and PAN were correlated in the near Asia and remote regions during PEM West A, but only in the remote region during PEM West B.

[27] Nitric acid and PAN were clearly enhanced in Asian outflow during TRACE-P (mean mixing ratios were 2.6–3.9 and 5.1–11.5 times higher, respectively, in our near Asia bins below 6 km) (see also *Talbot et al.* [2003]). However, like ^{210}Pb, there were very small differences in

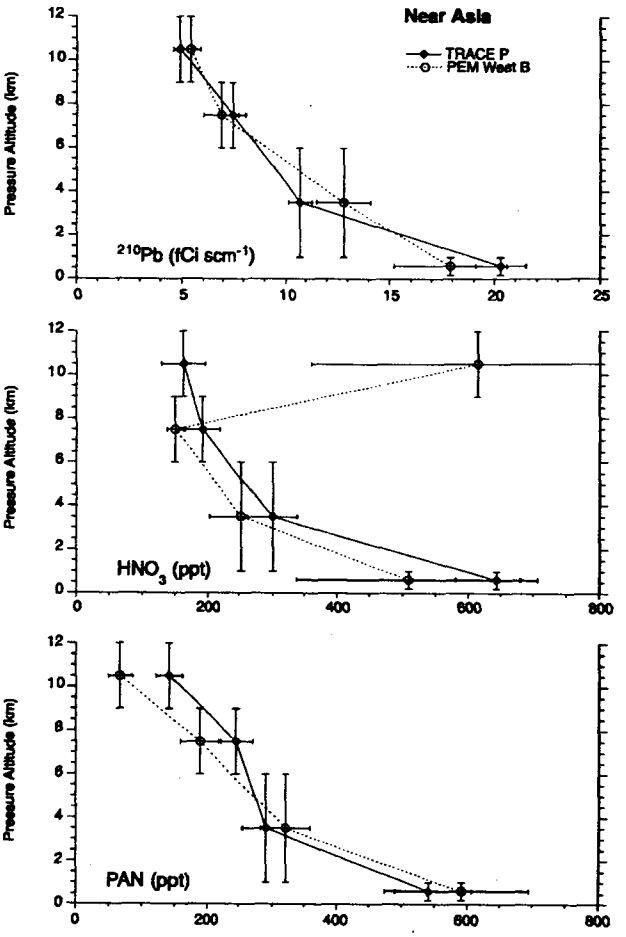

Figure 10. Comparison of mean mixing ratios of ^{210}Pb, HNO_3, and PAN in the four near-Asia altitude bins between TRACE-P and PEM West B. Error bars as defined in Figure 2.

their distributions near Asia between PEM West B and TRACE-P (Figure 10). We note that if export of HNO_3 did not change much between the two campaigns, the close similarity in HNO_3 distributions over the western Pacific would argue that precipitation scavenging was not significantly more efficient during PEM West B. TRACE-P also resembled PEM West B in the weak relationships between ^{210}Pb and PAN near Asia (Figure 11). More importantly, the relationships between ^{210}Pb and t-NO_3^- were also quite weak (Figure 12) (the same is true for HNO_3 and NO_3^- considered separately (not shown)). If removal of HNO_3 in precipitation explains the poor correlations during PEM West B, similarly weak relationships during TRACE P argue against significantly reduced scavenging as an explanation for the higher concentrations of aerosol-associated species in the latter campaign.

[28] We also note that *Fuelberg et al.* [2003] found no differences in the large-scale precipitation fields between TRACE-P and PEM West B. Examination of SSMI rainfall products and GPCP precipitation anomaly fields likewise failed to reveal any persistent differences in precipitation anywhere in eastern Asia or over the western Pacific that would indicate greater efficiency of scavenging during the PEM West study period. *Liu et al.* [2003] find that deep convective activity was enhanced over south east Asia during TRACE-P compared with PEM West B, but its impact was largely to lift biomass burning emissions into the upper troposphere. In summary, we do not think the higher concentrations of aerosol-associated ions during TRACE P can be attributed to a weaker sink.

4.2.2. Emissions

[29] Advection of Asian dust over the Pacific has long been recognized as an important feature of the northern hemisphere. A particularly large event just after the TRACE-P deployment ended attracted much public attention when the plume was tracked all the way across North America [e.g., *Thulasiraman et al.*, 2002]. It also appears that the frequency and severity of Chinese dust storms extending to eastern China and the western Pacific is increasing [*Menon et al.*, 2002]. Unpublished Chinese data indicates that Beijing experienced more dusty days in 2001 than in any year since 1966, with more than twice as many reports in 2001 than in 1994 (R. Arimoto, personal communication, June 2002). As noted above, no striking differ-

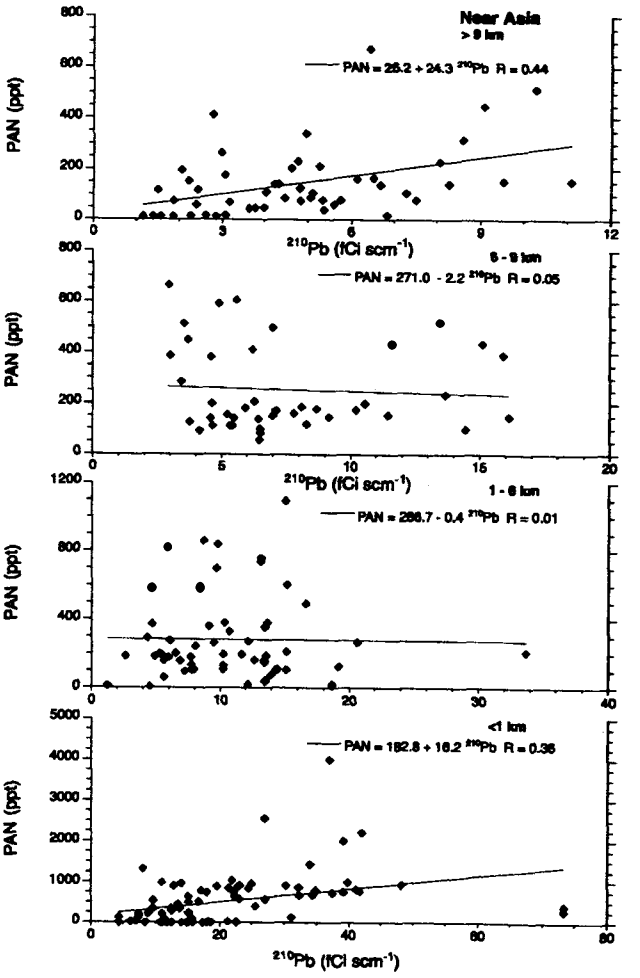

Figure 11. Scatter plots of PAN against ^{210}Pb in the four near-Asia altitude bins. Lines are least squares fits to the data.

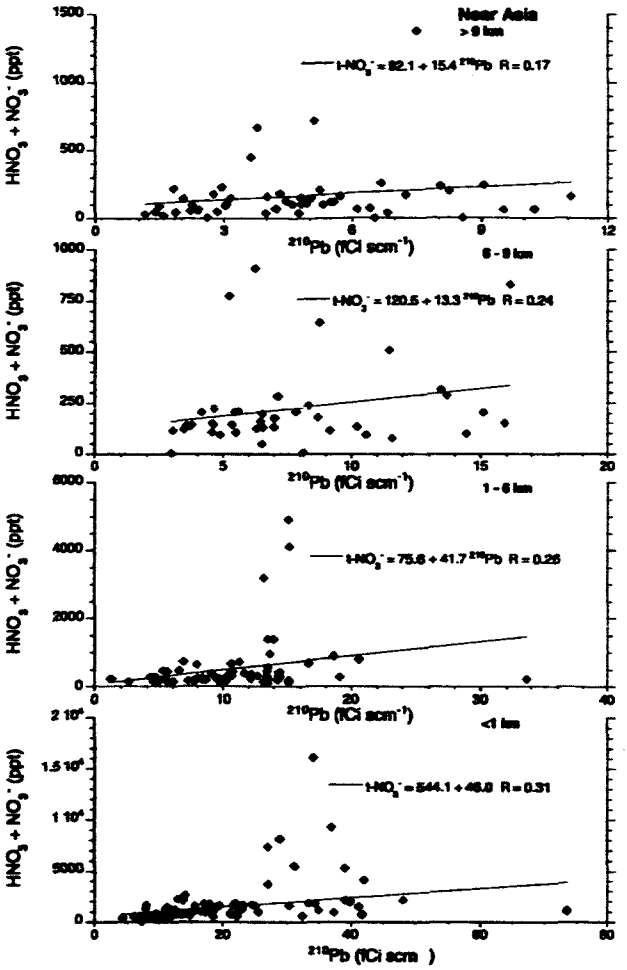

Figure 12. As in Figure 11 but for (NO_3^- + HNO_3) against ^{210}Pb.

ences in synoptic scale meteorology or precipitation that would be likely to cause more dust outbreaks have been found between the PEM West B and TRACE-P study periods. We also examined the satellite precipitation products for several months before the DC-8 deployments in 1994 and 2001 and found no regions that were unusually arid which could have provided unusually strong dust emissions. Thus it appears that increased dust emissions from China reflect, in part, changing land use and anthropogenic activities [*Menon et al.*, 2002]. Regardless of the detailed source(s) of the dust, evidence suggests that the increase in Ca^{2+} observed in TRACE-P could reflect greater dust export from Asia.

[30] On the other hand, *Streets et al.* [2003] estimate that Asian emissions of SO_2 decreased by 17%, while NO_x and NH_3 emissions increased by 12 and 16%, respectively, between PEM West B and TRACE-P. The increased emissions of NO_x and NH_3 are about an order of magnitude lower than the changes we observed in NO_3^- and NH_4^+ (Figure 8), while decreasing SO_2 emissions oppose significantly higher $SO_4^=$. Having largely ruled out changes in the strength of both sources and sinks of pollution-derived aerosols requires that we reexamine the validity of the comparisons we have presented.

4.2.3. Are the TRACE-P and PEM West B Data Sets Truly Comparable?

[31] We readily grant that the remote Pacific bins defined in this paper are far from those defined in our earlier work on the PEM West data sets and in different flow regimes. However, the near Asian regions overlap considerably. The most obvious difference between near-Asia sampling in PEM West B and TRACE-P are the approximately 100 filters collected near the Yellow Sea and Chinese coast, in a region we noted was not sampled at all in PEM West B. This region includes all of the boundary layer heavily dust-impacted samples that originated in the Channel region identified by *Jordan et al.* [2003a]. These authors point out that many Channel samples also had elevated levels of aerosol-associated and gas phase pollutants. The Shanghai plume discussed in many of the companion papers in this issue (with mission maximum values of many species) was also encountered in this area, as were all of the CO_2 plumes identified by *Vay et al.* [2003]. One might expect that adding a very polluted region to the TRACE P near-Asia bins could elevate mean mixing ratios and create artifact enhancements when compared to the PEM West B near Asia data set.

[32] Excluding all samples collected in the region bounded by 27–37 N, 120–135 E (see Figure 1) causes the mean Ca^{2+} mixing ratio in the boundary layer to decrease nearly 70%, with a reduction just less than 50% in the lower troposphere bin (Figure 13). However, threefold enhancements over PEM West B averages are still apparent in the low-altitude TRACE-P bins. Considering the association of NO_3^- and dust near Asia, it is not surprising that average NO_3^- mixing ratios also decrease significantly (48 and 43% in the boundary layer and 1–6 km bins, respectively) when samples from the dustiest part of the TRACE P study area are excluded. Here too, we note that the filtered TRACE-P low-altitude bins still exceed those in PEM West B by at least a factor of two. In contrast to the marked decreases in Ca^{2+} and NO_3^-, average mixing ratios of NH_4^+ are reduced by no more than 28% and those of $SO_4^=$ by no more than 20% in all modified TRACE-P bins below 9 km. As a result, TRACE-P still shows greater than twofold enhancements of $SO_4^=$ through much of the troposphere, with boundary layer NH_4^+ similarly enhanced (Figure 13).

[33] Even after removing an obvious sampling bias, we find that aerosol-associated tracers of pollution show large enhancements near Asia during TRACE-P that can not readily be attributed to increased source strength, or decreased sinks, when compared with PEM West B. Dust also increased between the two missions, though this may reflect previously documented increases in emissions from China. It seems that the enhancements of NO_3^- and particularly $SO_4^=$ and NH_4^+ can only be explained as a consequence of sampling just a tiny fraction of a huge volume of atmosphere, when making in situ measurements from an airborne platform. TRACE-P demonstrated that the troposphere over the western Pacific is highly structured, such that very small changes in flight tracks could yield significantly different impressions of the composition of the region. A major focus of TRACE-P was to characterize continental

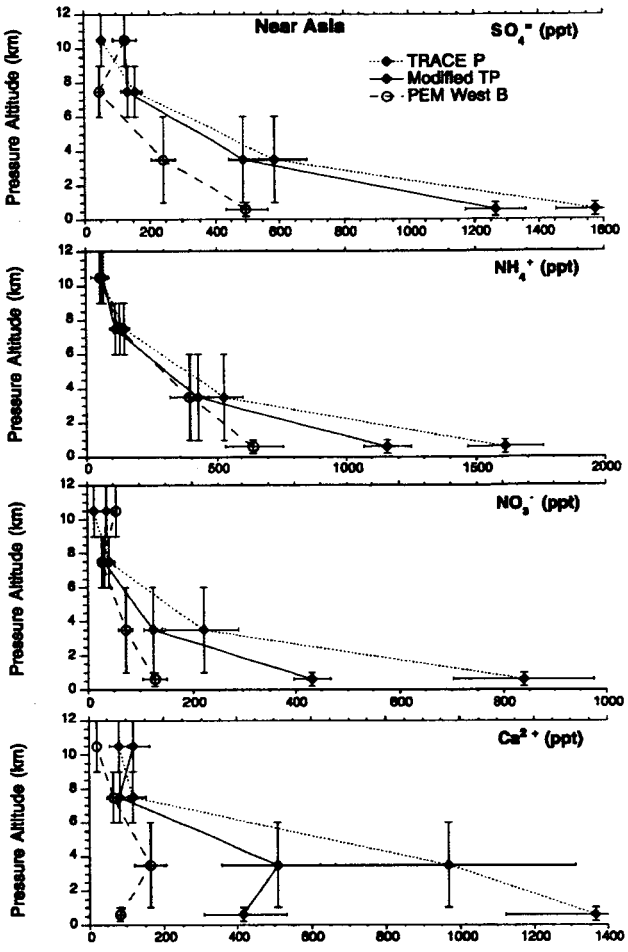

Figure 13. Comparison of the mean mixing ratios of $SO_4^=$, NH_4^+, NO_3^-, and Ca^{2+} in four near-Asia altitude bins. A modified TRACE-P data set, excluding about 100 samples collected over the Yellow Sea, is compared to the full TRACE-P data set and PEM West B data shown in Figure 8.

outflow, while PEM West B was an exploratory mission with multiple objectives. Our otherwise unexplained enhancements in aerosol-associated species suggest that TRACE-P flight paths succeeded in sampling continental outflow more extensively than was the case in PEM West B.

[34] We also find that different binning of the same data set can impact the impression one is left with. A perfect example is seen in HNO_3; in this paper we find very small increases near Asia between PEM West B and TRACE-P, yet *Talbot et al.* [2003] compare the heavily impacted Channel and Coastal air mass classes to fresh continental North air masses sampled in PEM West B and find TRACE-P to be fivefold higher. Similarly, *Blake et al.* [2003] find no systematic differences in a suite of NMHC binned to 2.5 degree patches, while *Bartlett et al.* [2003] find significant decreases in several of the same species when binned into different geographic regions. It may be that artifacts created by binning contribute to the contrast between the aerosol-associated pollutants (which are significantly higher in the TRACE-P data set) and the range of gaseous pollutants (which tend to show small differences compared to PEM West B). Perhaps the extreme heterogeneity of particle distributions in the atmosphere helps to make the observed distribution of aerosol-associated species more sensitive to small differences in sampling and data binning than is the case for trace gases.

5. Conclusions

[35] We have shown that the mixing ratios of soluble ions derived from soil dust and anthropogenic emissions were substantially higher in the near-Asia regions sampled by the DC-8 during TRACE-P compared with PEM West B. The enhancements in Ca^{2+}, NO_3^-, $SO_4^=$, and NH_4^+ sharply contrast the distributions of many trace gases that are also derived from anthropogenic activities, yet were quite similar between the two missions. Asian emissions of the precursor gases that yield the aerosol-associated pollution tracers were estimated to have changed by less than 17% between 1994 and 2001. Likewise, we could find no evidence to support a hypothesis that aerosols were higher in 2001 due to less efficient scavenging by precipitation.

[36] It must be stressed that the enhancements we found were strongly dependent on the exact locations that were probed by the DC-8 on each flight. TRACE-P objectives lead to many more flights specifically targeting continental outflow than was the case in PEM West B. Thus while the sampling regions overlapped a broad geographic area, TRACE-P flights often included repeated transects through small areas that were predicted to have strong continental outflow. On the larger scale, nearly 1/3 of the filter samples we collected near Asia during TRACE-P were above the Yellow Sea and other coastal Chinese waters and hence frequently influenced by outflow events. No sampling was conducted in this region during PEM West B. When these near China samples are filtered out of the TRACE-P data set, enhancements of the ions associated with dust (Ca^{2+} and NO_3^-) decrease, from factors as high as 16, to about 2–3 times higher than PEM West B. Mean mixing ratios of NH_4^+ and $SO_4^=$ also decrease when the TRACE-P data set does not include sampling very near China but by less than 28%.

[37] Our observations do not necessarily imply that the troposphere over the western Pacific was more influenced by Asian emissions in 2001 than 1994. Rather, we feel that the enhancements we found largely confirm that TRACE-P DC-8 flights succeeded in sampling continental outflow more often than did those in PEM West B. However, it is not clear why more focused sampling in the regions of strong outflow did not also result in enhancements of trace gases emitted in Asia. We speculate that this may be further evidence of the extreme heterogeneity in the distribution of aerosols in the troposphere, especially close to major sources.

[38] **Acknowledgments.** As always, the flight and ground crews for the DC-8 provided outstanding service during TRACE-P. Support provided by "locals" in Kona, Guam, Hong Kong, Okinawa, and Yakota is also deeply appreciated. We also thank the many officials at various levels (that we rarely ever even met) throughout the Pacific that permitted and assisted DC-8 flights in and near their airspace. This research was supported by NASA's Global Tropospheric Chemistry Program.

References

Bartlett, K. B., G. W. Sachse, T. Slate, C. Harward, D. R. Blake, and N. J. Blake, Large-scale distribution of CH_4 in the western Pacific: Sources

and transport from the Asian continent, *J. Geophys. Res.*, *108*(D20), 8807, doi:10.1029/2002JD003076, in press, 2003.

Blake, N. J., D. R. Blake, I. Simpson, S. Meinarde, G. Sachse, M. Avery, S. Vay, and H. Fuelberg, NMHC and halocarbons in Asian continental outflow during TRACE P, *J. Geophys. Res.*, *108*(D20), 8806, doi:10.1029/2002JD003367, in press, 2003.

Carmichael, G. R., et al., Regional-scale chemical transport modeling in support of intensive field experiments: Overview and analysis of the TRACE-P observations, *J. Geophys. Res.*, *108*(D21), 8823, doi:10.1029/2002JD003117, in press, 2003.

Clarke, A. D., and V. N. Kapustin, A Pacific aerosol survey, part 1: A decade of data on particle formation, transport, evolution, and mixing in the troposphere, *J. Atmos. Sci.*, *59*, 363–382, 2002.

Dibb, J. E., R. W. Talbot, K. I. Klemm, G. L. Gregory, H. B. Singh, J. D. Bradshaw, and S. T. Sandholm, Asian influence over the western north Pacific during the fall season: Inferences from lead 210, soluble ionic species, and ozone, *J. Geophys. Res.*, *101*, 1779–1792, 1996.

Dibb, J. E., R. W. Talbot, B. L. Lefer, E. Scheuer, G. L. Gregory, E. V. Browell, J. D. Bradshaw, S. T. Sandholm, and H. B. Singh, Distributions of beryllium 7 and lead 210, and soluble aerosol-associated ionic species over the western Pacific: PEM West B, February–March 1994, *J. Geophys. Res.*, *102*, 28,287–28,302, 1997.

Dibb, J. E., R. W. Talbot, E. M. Scheuer, D. R. Blake, N. J. Blake, G. L. Gregory, G. W. Sachse, and D. C. Thornton, Aerosol chemical composition and distribution during the Pacific Exploratory Mission (PEM) Tropics, *J. Geophys. Res.*, *104*, 5785–5800, 1999a.

Dibb, J. E., R. W. Talbot, L. D. Meeker, E. M. Scheuer, N. J. Blake, D. R. Blake, G. L. Gregory, and G. W. Sachse, Constraints on the age and dilution of Pacific Exploratory Mission-Tropics biomass burning plumes from the natural radionuclide tracer ^{210}Pb, *J. Geophys. Res.*, *104*, 16,233–16,241, 1999b.

Dibb, J. E., R. W. Talbot, G. Seid, C. Jordan, E. Scheuer, E. Atlas, N. J. Blake, and D. R. Blake, Airborne sampling of aerosol particles: Comparison between surface sampling at Christmas Island and P-3 sampling during PEM Tropics B, *J. Geophys. Res.*, 107, 8230, doi:10.1029/2001JD000408, 2002. [printed *108*(D2), 2003]

Eisele, F. L., et al., Informal instrument intercomparison summary, *J. Geophys. Res.*, *108*(D20), 8791, doi:10.1029/2002JD003167, in press, 2003.

Fuelberg, H. E., C. M. Kiley, J. R. Hannan, D. J. Westberg, M. A. Avery, and R. E. Newell, Atmospheric transport during the Transport and Chemical Evolution over the Pacific (TRACE-P) experiment, *J. Geophys. Res.*, *108*(D20), 8782, doi:10.1029/2002JD003092, in press, 2003.

Gorzelska, K., R. W. Talbot, K. Klemm, B. Lefer, O. Klemm, G. L. Gregory, B. Anderson, and L. A. Barrie, Chemical composition of the atmospheric aerosol in the troposphere over the Hudson Bay lowlands and Quebec-Labrador regions of Canada, *J. Geophys. Res.*, *99*, 1763–1779, 1994.

Gregory, G. L., J. T. Merrill, M. C. Shipham, D. R. Blake, G. W. Sachse, and H. B. Singh, Chemical characteristics of tropospheric air over the Pacific ocean as measured during PEM-West B: Relationship to Asian outflow and trajectory history, *J. Geophys. Res.*, *102*, 28,275–28,285, 1997.

Houghton, J. T., et al. (Eds.), *Climate Change 2001: The Scientific Basis*, Cambridge Univ. Press, New York, 2001.

Husar, R. B., et al., Asian dust events of 1998, *J. Geophys. Res.*, *106*, 18,317–18,330, 2001.

Jacob, D. J., J. H. Crawford, M. M. Kleb, V. S. Connors, R. J. Bendura, J. L. Raper, G. W. Sachse, J. Gille, L. Emmons, and J. C. Heald, The Transport and Chemical Evolution over the Pacific (TRACE-P) mission: Design, execution, and first results, *J. Geophys. Res.*, *108*(D20), 8781, doi:10.1029/2002JD003276, in press, 2003.

Jaffe, D., T. Anderson, D. Covert, R. Kotchenruther, B. Trost, J. Danielson, W. Simpson, T. Berntsen, S. Karlsdottir, D. Blake, J. Harris, G. Carmichael, and I. Uno, Transport of Asian air pollution to North America, *Geophys. Res. Lett.*, *26*, 711–714, 1999.

Jaffe, D., I. McKendry, T. Anderson, and H. Price, Six "new" episodes of trans-Pacific transport of air pollutants, *Atmos. Environ.*, *37*, 391–404, 2003.

Jordan, C. E., J. E. Dibb, B. E. Anderson, and H. Fuelberg, Uptake of nitrate and sulfate on dust aerosols during TRACE-P, *J. Geophys. Res.*, *108*(D21), 8817, doi:10.1029/2002JD3101, in press, 2003a.

Jordan, C. E., et al., Chemical and physical properties of bulk aerosols within four sectors observed during TRACE-P, *J. Geophys. Res.*, *108*(D21), 8813, doi:10.1029/2002JD003337, in press, 2003b.

Lefer, B. L., et al., Enhancement of acidic gases in biomass burning impacted air masses over Canada, *J. Geophys. Res.*, *99*, 1721–1737, 1994.

Liu, H., D. J. Jacob, I. Bey, R. M. Yantosca, B. N. Duncan, and G. W. Sachse, Transport pathways for Asian combustion outflow over the Pacific: Interannual and seasonal variations, *J. Geophys. Res.*, *108*(D20), 8786, doi:10.1029/2002JD003102, in press, 2003.

Ma, Y., et al., The characteristics and influence of biomass burning aerosols on fine particle ionic composition measured in Asian outflow during TRACE-P, *J. Geophys. Res.*, *108*(D21), 8816, doi:10.1029/2002JD003128, in press, 2003.

Martin, B. D., H. E. Fuelberg, N. J. Blake, J. H. Crawford, J. A. Logan, D. R. Blake, and G. W. Saschse, Long-range transport of Asian outflow to the Equatorial Pacific, *J. Geophys. Res.*, *108*(D2), 8233, doi:10.1029/2001JD001418, 2003.

McKendry, I. G., J. P. Hacker, R. Stull, S. Sakiyama, D. Mignacca, and K. Reid, Long-range transport of Asian dust to the lower Fraser Valley, British Columbia, Canada, *J. Geophys. Res.*, *106*, 18,361–18,370, 2001.

Menon, S., J. Hansen, L. Nazarenko, and Y. Luo, Climate effects of black carbon aerosols in China and India, *Science*, *297*, 2250–2253, 2002.

Newell, R. E., and M. J. Evans, Seasonal changes in pollutant transport to the north Pacific: The relative importance of Asian and European sources, *Geophys. Res. Lett.*, *27*, 2509–2512, 2000.

Renner, R., A river of pollution, *Env. Sci Technol.*, *34*, 330A–331A, 2000.

Russo, R., et al., Chemical composition of Asian outflow over the western Pacific: Results from TRACE P, *J. Geophys. Res.*, *108*(D20), 8804, doi:10.1029/2002JD003184, in press, 2003.

Song, C. H., and G. R. Carmichael, Gas-particle partitioning of nitric acid modulated by alkaline aerosol, *J. Atmos. Chem.*, *40*, 1–22, 2001.

Staudt, A. C., D. J. Jacob, J. A. Logan, D. Bachiochi, T. N. Krishnamurti, and G. W. Sachse, Continental sources, transoceanic transport, and interhemispheric exchange of carbon monoxide over the Pacific, *J. Geophys. Res.*, *106*, 32,571–32,589, 2001.

Streets, D. G., et al., An inventory of gaseous and primary aerosol emissions in Asia in the year 2000, *J. Geophys. Res.*, *108*(D21), 8809, doi:10.1029/2002JD003093, in press, 2003.

Talbot, R., et al., Reactive nitrogen in Asian continental outflow over the western Pacific: Results from the NASA TRACE-P airborne mission, *J. Geophys. Res.*, *108*(D20), 8803, doi:10.1029/2002JD003129, in press, 2003.

Thulasiraman, S., N. T. O'Neill, A. Royer, B. N. Holben, D. L. Westphal, and L. J. B. McArthur, Sunphotometric observations of the 2001 Asian dust storm over Canada and the U. S., *Geophys. Res. Lett.*, *29*(8), 1255, doi:10.1029/2001GL014188, 2002.

Tratt, D. M., R. J. Frouin, and D. L. Westphal, April 1998 Asian dust event: A southern California perspective, *J. Geophys. Res.*, *106*, 18,371–18,379, 2001.

Uno, I., H. Amano, S. Emori, K. Kinoshita, I. Matsui, and N. Sugimoto, Trans-Pacific yellow sand transport observed in April 1998: A numerical simulation, *J. Geophys. Res.*, *106*, 18,331–18,344, 2001.

Vaughan, J. K., C. Claiborn, and D. Finn, April 1998 Asian dust event over the Columbia Plateau, *J. Geophys. Res.*, *106*, 18,381–18,402, 2001.

Vay, S., et al., The influence of regional-scale anthropogenic activity on CO2 distributions over the western Pacific, *J. Geophys. Res.*, *108*(D20), 8801, doi:10.1029/2002JD003094, in press, 2003.

Wilkening, K. E., L. A. Barrie, and M. Engle, Trans-Pacific air pollution, *Science*, *290*, 65–67, 2000.

Xiao, H., G. R. Carmichael, J. Durchenwald, D. Thornton, and A. Bandy, Long-range transport of SO_x and dust in east Asia during the PEM B experiment, *J. Geophys. Res.*, *102*, 28,589–28,612, 1997.

M. A. Avery, NASA Langley Research Center, Hampton, VA 23665, USA. (m.a.avery@larc.nasa.gov)

J. E. Dibb, R. W. Talbot, E. M. Scheuer, and G. Seid, Climate Change Research Center, Institute for the Study of Earth, Oceans, and Space, Morse Hall, University of New Hampshire, Durham, NH 03825, USA. (jack.dibb@unh.edu)

H. B. Singh, NASA Ames Research Center, Moffett Field, CA 94035, USA.

JOURNAL OF GEOPHYSICAL RESEARCH, VOL. 108, NO. D21, 8813, doi:10.1029/2002JD003337, 2003

Chemical and physical properties of bulk aerosols within four sectors observed during TRACE-P

C. E. Jordan,[1] B. E. Anderson,[2] R. W. Talbot,[3] J. E. Dibb,[4] H. E. Fuelberg,[5]
C. H. Hudgins,[2] C. M. Kiley,[5] R. Russo,[4] E. Scheuer,[3] G. Seid,[3]
K. L. Thornhill,[6] and E. Winstead[7]

Received 20 December 2002; revised 12 May 2003; accepted 27 May 2003; published 15 November 2003.

[1] Chemical and physical aerosol data collected on the DC-8 during TRACE-P were grouped into four sectors based on back trajectories. The four sectors represent long-range transport from the west (WSW), regional circulation over the western Pacific and Southeast Asia (SE Asia), polluted transport from northern Asia with substantial sea salt at low altitudes (NNW) and a substantial amount of dust (Channel). WSW has generally low mixing ratios at both middle and high altitudes, with the bulk of the aerosol mass due to non-sea-salt water-soluble inorganic species. Low altitude SE Asia also has low mean mixing ratios in general, with the majority of the aerosol mass comprised of non-sea-salts, however, soot is also relatively important in this region. NNW had the highest mean sea salt mixing ratios, with the aerosol mass at low altitudes (<2 km) evenly divided between sea salts, non-sea-salts, and dust. The highest mean mixing ratios of water-soluble ions and soot were observed at the lowest altitudes (<2 km) in the Channel sector. The bulk of the aerosol mass exported from Asia emanates from Channel at both low and midaltitudes, due to the prevalence of dust compared to other sectors. Number densities show enhanced fine particles for Channel and NNW, while their volume distributions are enhanced due to sea salt and dust. Low-altitude Channel exhibits the highest condensation nuclei (CN) number densities along with enhanced scattering coefficients, compared to the other sectors. At midaltitudes (2–7 km), low mean CN number densities coupled with a high proportion of nonvolatile particles (≥65%) observed in polluted sectors (Channel and NNW) are attributed to wet scavenging which removes hygroscopic CN particles. Low single scatter albedo in SE Asia reflects enhanced soot. *INDEX TERMS:* 0305 Atmospheric Composition and Structure: Aerosols and particles (0345, 4801); 0345 Atmospheric Composition and Structure: Pollution—urban and regional (0305); 0365 Atmospheric Composition and Structure: Troposphere—composition and chemistry; 0368 Atmospheric Composition and Structure: Troposphere—constituent transport and chemistry; *KEYWORDS:* aerosols, TRACE-P, Asia

Citation: Jordan, C. E., et al., Chemical and physical properties of bulk aerosols within four sectors observed during TRACE-P, *J. Geophys. Res.*, *108*(D21), 8813, doi:10.1029/2002JD003337, 2003.

1. Introduction

[2] TRACE-P (Transport and Chemical Evolution Over the Pacific was conducted over the western Pacific), just off the coast of Asia, from February to April of 2001. Two aircraft were used to investigate the chemical composition of Asian outflow over the western Pacific and its chemical evolution [*Jacob et al.*, 2003]. Aerosols are an important component of Asian continental outflow. Throughout this special section, aerosols are shown to be important not just in their own right, but also for the interactions which influence gas phase processes as well [*Crawford et al.*, 2003; *Jordan et al.*, 2003; *Lefer et al.*, 2003; *Price et al.*, 2003; *Tang et al.*, 2003a, 2003b].

[3] TRACE-P was conducted in spring for several reasons [*Jacob et al.*, 2003]. This is the season when Asian export to the Pacific is at its maximum, biomass burning peaks during this time in Southeast Asia, photochemistry is already active, and stratospheric intrusions are also at their

[1]National Research Council, NASA Langley Research Center, Hampton, Virginia, USA.
[2]Atmospheric Sciences Competency, NASA Langley Research Center, Hampton, Virginia, USA.
[3]Complex Systems Research Center, Institute for the Study of Earth, Oceans, and Space, University of New Hampshire, Durham, New Hampshire, USA.
[4]Climate Change Research Center, Institute for the Study of Earth, Oceans, and Space, University of New Hampshire, Durham, New Hampshire, USA.
[5]Department of Meteorology, Florida State University, Tallahassee, Florida, USA.
[6]SAIC, NASA Langley Research Center, Hampton, Virginia, USA.
[7]GATS, NASA Langley Research Center, Hampton, Virginia, USA.

0148-0227/03/2002JD003337$09.00

maximum. Further, the cold fronts which are responsible for the strong seasonal outflow to the Pacific also give rise to dust storms, making spring the season of maximum dust export as well [*Sun et al.*, 2001; *Jacob et al.*, 2003]. Hence, natural and anthropogenic aerosol emissions, which include dust, biomass-burning particulates, and anthropogenic pollutant aerosols, are anticipated to be at a maximum at this time of year.

[4] A better understanding of aerosols and the processes in which they are involved is needed for a variety of reasons. As discussed by *Streets et al.* [2003], black carbon and organic carbon emissions are the most poorly constrained species in their Asian emission inventories. *Crawford et al.* [2003] report statistically significant differences in trace gas concentrations between clear-sky and cloudy conditions. This has implications for whether satellite retrievals adequately represent the export and evolution of various species in outflow associated with cloudy frontal regions. *Lefer et al.* [2003] and *Tang et al.* [2003a, 2003b] both discuss the influence of clouds and aerosols on photolysis frequencies and hence photochemistry. Better knowledge of aerosol optical properties is needed (e.g., aerosol optical depth and single scatter albedo) to improve measurement/model agreement [*Lefer et al.*, 2003]. Meanwhile, Asian aerosols are found on average to have a greater photochemical influence than clouds during TRACE-P, reducing photolysis rates throughout the column [*Tang et al.*, 2003a].

[5] *Price et al.* [2003] report observations in North America of Asian dust, mixed with pollution, where O_3 and aerosol scatter were anti-correlated. The authors suggest that this may be attributed to either reduced O_3 formation on account of the large amount of dust reducing UV reaching the surface, or the loss of O_3 to the surface of the dust particles. *Jordan et al.* [2003] report evidence of the uptake of NO_3^- and $SO_4^=$ on dust particles, resulting in a change in the phase partitioning of these species with implications for both deposition to the western Pacific coastal waters and chemical evolution of the air mass downwind.

[6] Companion papers in this special section each address specific questions pertaining to the role of aerosols in the chemical composition and evolution of Asian outflow. In this paper we present an overview of the aerosol physical and chemical properties as measured on the DC-8, flights 8–18 (19°–45°N, 115°–198°E). Back trajectories are used to divide the aerosol data into four sectors reflecting the general geographic origins of the particles. The chemical and physical properties of these bulk aerosols are evaluated together to yield a comprehensive picture of the particulates in this region. As is discussed elsewhere, aerosols in this area are highly heterogeneous in their distribution [*Dibb et al.*, 2003; *Ma et al.*, 2003]. However, given the incomplete descriptions of particles presently incorporated into regional and global atmospheric models, and the need for validation of satellite aerosol observations on fairly large geographic scales, we believe this broad description may be useful.

2. Methods

2.1. Aerosol Physical Properties

[7] The suite of instruments flown aboard the DC-8 included: three condensation nuclei counters (CNC) to obtain the number densities and volatility of submicron aerosols; a Passive Cavity Aerosol Spectrometer Probe (PCASP) to measure the dry size of 0.1–3.0 μm diameter particles, a Forward Scattering Spectrometer Probe (FSSP-300) to obtain size spectra of 0.3–20 μm particles under ambient conditions; a 3-wavelength nephelometer (TSI 3560) to measure aerosol scattering coefficients at wavelengths of 450, 550, and 700 nm; and a Particle Soot Absorption Photometer (PSAP) to measure total aerosol absorption, from which the mass of soot particles was determined.

[8] The CNCs drew samples from a common manifold maintained at a constant pressure of either 213 or 267 hPa, depending on flight level, to eliminate altitude-related fluctuations in sensitivity and performance. The CN data have been corrected for the pressure dependent sensitivities of the counters (typically 30 to 40%) and are presented in units of number per cubic centimeter at sea level conditions (20°C and 1013 hPa, STP). These number densities are estimated to have ±20% precision, due primarily to uncertainies in particle loss through the sample inlet and imprecision in the instrument flow rate measurements.

[9] The PCASP and FSSP-300 probes were mounted on a pylon extending 0.5 m below the aircraft's left wing-tip, a location calculated to be minimally affected by aircraft-induced flow distortion. The FSSP-300 has an open sample cavity that provides size distribution measurements at ambient temperature and humidity conditions. PCASP dehydrates aerosols to <30% RH prior to measurement due to sample air being drawn through a heated capillary tube to the resonance cavity, combined with the sample air being surrounded by a concentric flow of dry filtered air to maintain laminar flow through the cavity. The probes' size sensitivities were determined using non-absorbing latex spheres with real and imaginary refractive indices, n_r and n_i, of 1.59 and 0.0, respectively. These data were then used in conjunction with output from a Mie scattering model to set the PCASP and FSSP size-channel thresholds for aerosols with real refractive indices of 1.55 (sulfate) and 1.44 (hydrated sea salt), respectively. Number densities provided by the two instruments are estimated to have a ±25% precision due largely to the difficulty in defining the instruments' effective sample volumes.

[10] Aerosol scattering coefficients (σ_{sp}) were measured at 450, 550, and 700 nm using a TSI model 3563 Integrating Nephelometer [i.e., *Bodhaine et al.*, 1991; *Anderson et al.*, 1996]. This instrument would ideally collect light scattered from its sample volume over a 180° viewing angle, but practical considerations limit its integrating volume to between 7° and 170°. *Anderson et al.* [1996] discuss this truncation problem and calculate that it may cause the instrument to significantly underestimate σ_{sp} for aerosol populations dominated by supermicron sized particles. Because, as discussed below, our sample inlet did not efficiently transmit particles >1 μm in diameter, we have simply applied a truncation error correction factor of 1.07 to the entire scattering coefficient data set.

[11] Aerosol absorption coefficients (σ_{ap}) at 565 nm were measured with a Radiance Research Particle Soot Absorption Photometer (PSAP). These data were corrected for aerosol scattering using the technique proposed by *Bond et al.* [1999] and were filtered to remove time periods when the instrument performed poorly due to rapid changes in

sample pressure and humidity. Even so, this particular instrument was exceptionally noisy when operated at reduced pressures. Thus its data use is limited to establishing a mean single scattering albedo value (ω_o) and inferring soot mass (assuming an absorption efficiency of 10 m^2g^{-1}) in polluted air masses where σ_{ap} exceeded 1 Mm^{-1}.

[12] Sample air for the nephelometer and PSAP were drawn in through a forward facing, knife-edge type inlet probe mounted on a window plate adjacent to the aerosol instrument rack. This probe extended ~30 cm out from the aircraft skin, had a tip diameter of 0.3 cm and a 7° conical expansion region downstream of the tip which gradually expanded the flow out into a 2.5-cm i.d. stainless steel pipe. The pipe was bent at a 60° angle and brought through the window plate where it was connected to the nephelometer using a short length (~0.5 m) of conductive tubing of approximately the same inside diameter. A "tee" was placed in this tubing and used to supply ~2 LPM of flow to the PSAP. The exhaust of the nephelometer was connected to a window-mounted venturi pump across a large diameter ball valve that was adjusted to maintain isokinetic flow at the probe tip. This typically resulted in a volumetric flow of ~100 LPM through the nephelometer. In order to evaluate inlet losses for this probe, we compared σ_{sp} measured by the nephelometer with values calculated from PCASP size distributions truncated at various upper size-diameters. Data collected in the marine boundary layer (MBL), where 50–75% of the overall scattering was due to coarse particles, showed the nephelometer data had the best overall fit with scattering parameters calculated from PCASP size distributions cut off at 1 μm diameter.

[13] To relate "dry" aerosol optical parameters back to ambient conditions we applied humidity corrections using the formula $\sigma_{sp}(RH) = \sigma_{sp}(dry)\ (1 - RH/100)^{-g}$ [*Kasten*, 1969] We selected a value of 0.43 for g to yield a $\sigma_{sp}(80\%)/\sigma_{sp}(30\%)$ ratio of ~1.7, the value recommended by *Charlson et al.* [1992] for polluted air masses. This approach produces infinitely large values of $\sigma_{sp}(RH)$ as RH approaches 100%, which frequently occurs in the vicinity of clouds. We thus restricted our data set to points with corresponding RH values of ≤95%, which corresponds to a maximum $\sigma_{sp}(RH)/\sigma_{sp}(30\%)$ ratio of ~3.6.

2.2. Aerosol Chemical Properties

[14] The aerosol water-soluble inorganic chemical measurements are described in greater detail elsewhere [*Dibb et al.*, 1999, 2000, 2002, 2003], so only a brief synopsis appears here. Air enters an anodized aluminum curved leading edge nozzle centered in a shroud that extends 20 cm forward of the nozzle. This allows for nearly isoaxial sampling throughout the flight [*Dibb et al.*, 2002, references therein]. Once inside the aircraft, air then flows through a Delrin ball valve, followed by a Delrin diffuser, to a 9 cm, 2 micron Millipore Fluoropore Teflon filter in a Delrin holder [*Dibb et al.*, 2002]. Behind the filter is another valve, a mass flowmeter, and a venturi pump. Sampling flow rates were manually adjusted to be isokinetic within 10% along each flight leg [*Dibb et al.*, 2002]. Filters were processed according to procedures described by *Dibb et al.* [1999, 2000]. Inorganic anion and cation mixing ratios were obtained from ion chromatography. Samples were collected only during level flight legs with sampling times ranging from 3–36 minutes with mean and median times of 10 and 8 minutes, respectively. For a complete discussion of the chemical measurements and error analysis, see *Dibb et al.* [2003]. Note that mixing ratios (pptv) were converted to moles or mass per unit volume using standard cubic meters rather than volumetric cubic meters (e.g., μg m^{-3} STP or μmol SCM^{-1}).

2.3. Back Trajectories

[15] The back trajectories are also discussed in greater detail elsewhere [*Fuelberg et al.*, 1996, 1999, 2000, 2003], so again only an overview is given here. Five day back trajectories were calculated using a kinematic model based on global meteorological analyses from the European Centre for Medium-Range Weather Forecasts (ECMWF) [*Fuelberg et al.*, 2003]. ECMWF data were available for 0000, 0600, 1200, and 1800 UTC, at 60 vertical levels with a T319 spherical harmonic triangular truncation, interpolated to a 1° × 1° latitude-longitude horizontal grid [*Fuelberg et al.*, 2003]. For a thorough description of the trajectory model, see *Fuelberg et al.* [1996, 1999, 2000].

2.4. Group Determinations

[16] Of the three data sets used here, the aerosol chemical data had the coarsest resolution, with sample times ranging from 3–36 minutes. Five day back trajectories were calculated every 5 minutes along level flight legs during TRACE-P. Aerosol physical properties had the highest resolution, with 1 minute averages available for most parameters. We wanted to determine whether aerosols from various source regions had characteristic bulk properties, e.g., a strong biomass-burning signal from Southeast Asia with enhanced absorption, or enhanced pollution from northern Asia with enhanced scattering, etc. In order to properly compare data from these disparate sources, all physical data were averaged to the time intervals of the chemical data. The first step was to assess the back trajectory information to sort the chemical data into groups. While there are limitations to the usefulness of back trajectories [*Kahl*, 1993; *Fuelberg et al.*, 2000; *Maloney et al.*, 2001; *Stohl et al.*, 1995; *Stohl*, 1998], they are suitable for classifying this relatively high-resolution data set into broad categories.

[17] Given the length of chemical sample times, there were potentially 1–7 back trajectories available per sample (typically, 2–3 for most samples). Looking at the trajectories, four distinct groups emerged (Figure 1). Trajectories for samples collected above 7 km altitude are shown in the top left panel of Figure 1. Trajectories are shown from northern Asia (NNW) in red, from the west (WSW) in gold, and from Southeast Asia (SE Asia) in blue. In general, these trajectories for samples collected at high altitudes show relatively long range transport, with altitudes generally well above the height of the Tibetan Plateau (Figure 1, bottom left panel). However, the altitude bins are determined by where the sample was collected, not the altitude of the trajectories themselves during their 5 day histories, so some of these trajectories suggest transport from lower altitudes to the measurement height on the aircraft. In contrast to the high altitude trajectories, low altitude trajectories (those for samples collected below 2 km altitude) are shown in the right panels of Figure 1. The top right panel shows the trajectories from above, while the bottom right panel shows

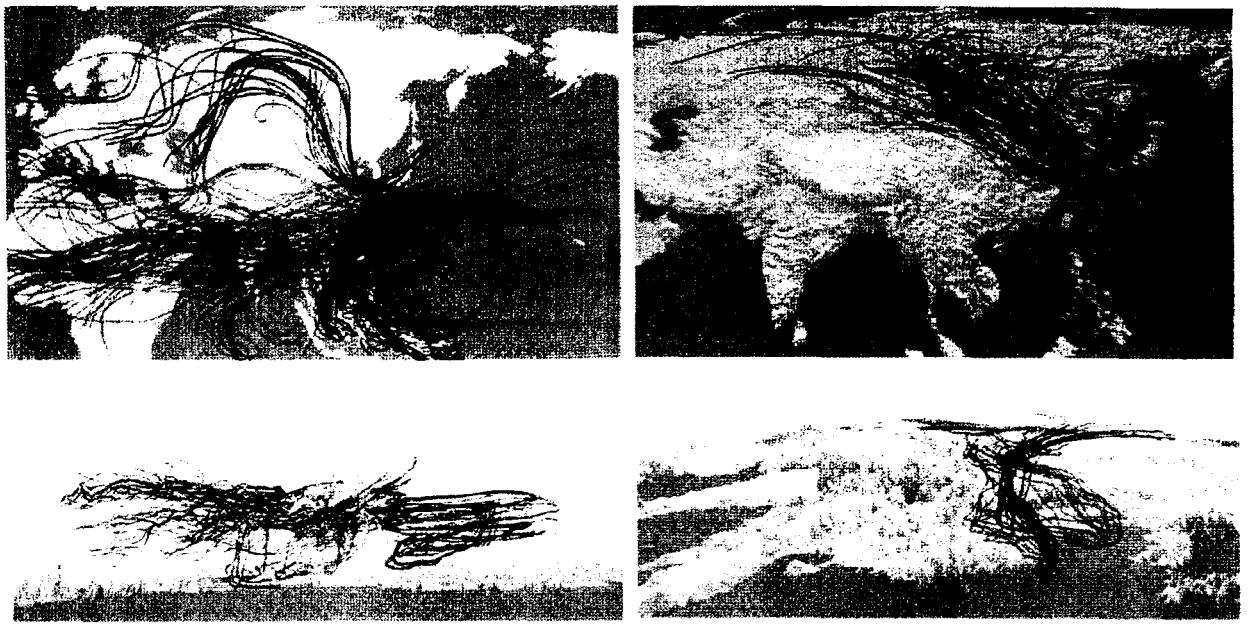

Figure 1. Back trajectories for the aerosol samples divided into four sectors. The top left panel shows trajectories for samples collected at altitudes >7 km. Only three sectors are represented at those altitudes, NNW (red), WSW (gold), and SE Asia (blue). The bottom left panel is a side view from the Pacific Ocean looking toward the Tibetan Plateau. This view shows these trajectories typically represent high altitude long distance transport. The top right panel shows trajectories for samples collected at altitudes <2 km. Only three sectors are represented at these altitudes, NNW (red), Channel (green), and SE Asia (blue). The bottom right panel shows only the low altitude Channel trajectories, angled to show that these trajectories flow along the surface and are confined by the surface topography. See color version of this figure at back of this issue.

an angled view to better show that these low altitude trajectories flow close to the surface and are constrained by its topography. For the low altitude trajectories, red again represents the northern Asia group NNW and blue again represents SE Asia, however, there is an additional group in green called Channel. This can almost be thought of as a subset of the NNW group. However, the chemical data showed greatly enhanced Ca^{2+} in this region, which is what set it apart in this analysis. Midaltitude trajectories (2–7 km, not shown in Figure 1) include all 4 groups, NNW, Channel, WSW, and SE Asia.

[18] Samples with multiple back trajectories were considered "mixed" if the trajectories came from different groups (e.g., a trajectory from SE Asia and another from NNW). Mixed trajectories are due to horizontal and vertical wind shear across the sampling period (distance). Samples were classified as belonging to a particular group only if all trajectories for that sample emanated from the same group. In this way, we evaluated the bulk aerosol properties for each of these four regions with minimal influence from mixed samples. Our deletion of mixed samples insures that geographical partitioning is based only on those trajectory groups with the greatest reliability. Initially, there were 415 chemical samples from 17 flights. Since we are interested in Asian outflow, only samples collected near Asia were included in this analysis (flights 8–18, 19°–45°N, 115°–198°E). Note that only 8 samples (from flight 18) were east of 163°E; the rest were west of 150°E. This left 282 samples. Of these, 70 were mixed, and 19 could not be classified due to missing trajectory data. Mixed trajectories were common during TRACE-P due to numerous middle latitude circulation features that produced shear in the TRACE-P area [*Fuelberg et al.*, 2003]. The remaining samples could be classified into the four groups as follows, 77 NNW, 38 Channel, 47 WSW, and 31 SE Asia.

3. Discussion

3.1. Water-Soluble Ions and Dust

[19] The highest mean water-soluble ion mixing ratios are seen at the lowest altitudes, below 2 km (Figure 2, top panel; Table 1). *Jacob et al.* [2003] attribute this to capping by subsidence inversions at 1–2 km altitude. Channel has the highest concentrations of NH_4^+, $SO_4^=$, and NO_3^- observed (mean mixing ratios of 148, 129, and 108 nmol/m^3, respectively), indicating the highest pollution emanates from this sector. This is not surprising, as the trajectories for this sector pass over many Chinese cities, including Shanghai (Figure 1, top right panel). These elevated aerosol mixing ratios are also consistent with expectations given that Chinese emissions of anthropogenic species dominate those of other Asian regions, contributing 59% of SO_2, 42% of NO_x, 49% of NH_3, 42% of CO, and 41% of black carbon to the total [*Streets et al.*, 2003]. Further, some gas phase species also show enhancements in the Channel sector (Table 2). The highest mean mixing ratios of HNO_3 (1406 pptv), SO_2 (4302 pptv), CO (321 ppbv), and C_2Cl_4 (16 pptv) are found in the low altitude Channel sector

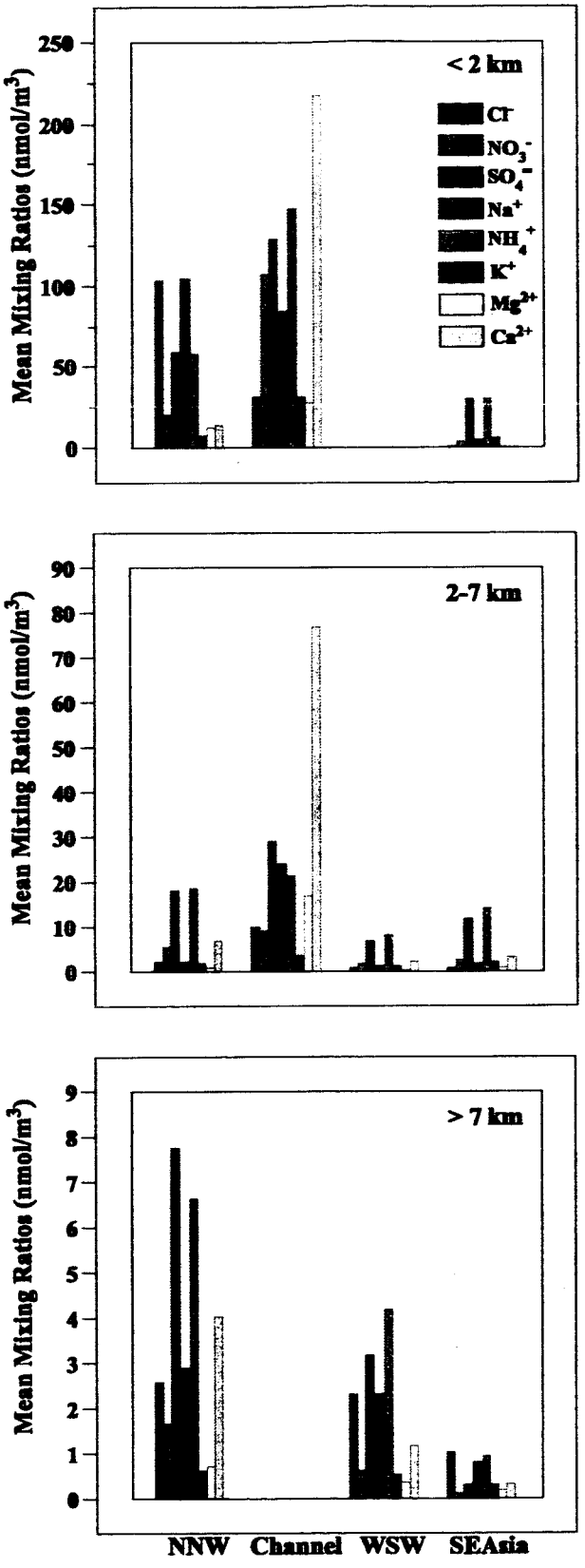

Figure 2. Aerosol mean chemical signatures for each group, split by altitude. See color version of this figure at back of this issue.

(Table 2). This is consistent with the results of *Russo et al.* [2003] and *Talbot et al.* [2003], both of whom used the same sector classification scheme employed here to evaluate trace gas measurements. However, the distinctions observed between aerosols from these sectors are more pronounced than those of the gas phase species [*Russo et al.*, 2003; *Talbot et al.*, 2003]. Note that these enhanced mixing ratios may be compared to background values of 15 pptv (SO_2), 70 ppbv (CO), and 2 pptv (C_2Cl_4) reported by *Russo et al.* [2003]. At midaltitudes, Channel's dominance of mixing ratios does not hold for these gases. This is due to factors other than proximity to sources which control their mixing ratios in the atmosphere, e.g., transport and mixing, photochemical processing, scavenging in clouds, etc.

[20] The striking feature of the Channel group, however, is the dominance of Ca^{2+}, a tracer of dust. The Ca^{2+} mixing ratio is an order of magnitude higher in this group than any other group (e.g., 217 nmol/m^3 versus 14 nmol/m^3 for NNW), which is the case both at low and midaltitudes (Table 1). The Channel trajectories are typical of the transport pathways which carry dust out of the major Asian deserts over the western Pacific [*Sun et al.*, 2001; *Jordan et al.*, 2003]. It is because of the presence of Ca^{2+} in these samples that the Channel group was treated separately from the NNW group. Both NNW and Channel show large amounts of sea salts at low altitudes (Na^+ = 105 and 85 nmol/m^3; Cl^- = 104 and 32 nmol/m^3, respectively). The Cl^- deficit (relative to the sea salt ratio) in low altitude Channel samples probably reflects some loss of Cl^- from sea salt due to reaction with acidic gases, but may also be partly an artifact to the extent that some of the measured Na^+ is associated with abundant dust. At these altitudes (<2 km), only two samples had back trajectories classified as SE Asia, and none from WSW. The SE Asia group is much cleaner than the other two groups, nonetheless NH_4^+ and $SO_4^=$ are the dominant water-soluble ions here (31 and 30 nmol/m^3, respectively).

[21] At midaltitudes, NH_4^+ and $SO_4^=$ are the dominant water-soluble ions in aerosols in all groups, except Channel, where dust is still the dominant component as indicated by the dominant Ca^{2+} (77 nmol/m^3), and enhanced Na^+ (24 nmol/m^3) and Mg^{2+} (17 nmol/m^3; Table 1, Figure 2, middle panel). As was the case at low altitude, the highest mixing ratios of the pollution species, NH_4^+ (21 nmol/m^3) and $SO_4^=$ (29 nmol/m^3), are found in the Channel group, followed by NNW (19 and 18 nmol/m^3), SE Asia (14 and 12 nmol/m^3), and WSW (8 and 7 nmol/m^3). High altitude samples (>7 km) have the lowest mixing ratios observed (Figure 2, bottom panel), as expected. NNW shows higher mixing ratios of NH_4^+ (7 nmol/m^3) and $SO_4^=$ (8 nmol/m^3) than the other two groups. Sea salts, Na^+ ($\approx$2 nmol/m^3) and Cl^- ($\approx$2 nmol/m^3) are comparable between the three groups (Table 1). Ca^{2+} (4 nmol/m^3) is an important component in the NNW group, but not so much in WSW and SE Asia. Channel is not classified at the highest altitudes, because the high altitude trajectories are sufficiently high as to not be greatly influenced by the defining topography of the Channel group (bounded by the Tibetan Plateau to the south and west, and by mountains to the north). At high altitudes, the Channel and NNW trajectories are combined into the NNW group. While there is dust present in these high altitude samples, it is not dominant, as it is in low and midaltitude

Table 1. Water-Soluble Ion Mixing Ratios and Soot Mass Means, Standard Deviations, Medians, Minima, and Maxima[a]

	Cl^-, nmol/m^3	NO_3^-, nmol/m^3	$SO_4^=$, nmol/m^3	Na^+, nmol/m^3	NH_4^+, nmol/m^3	K^+, nmol/m^3	Mg^{2+}, nmol/m^3	Ca^{2+}, nmol/m^3	Soot, ng/m^3
				NNW Sector at <2 km Altitude					
Mean ± SD	103.8 ± 67.0	20.8 ± 13.0	58.9 ± 23.6	105.4 ± 64.4	57.9 ± 22.5	7.8 ± 3.8	12.9 ± 7.2	14.4 ± 12.6	513 ± 224
Median (min.–max.)	102.4 (5.2–252.2)	19.7 (2.1–9.8)	57.1 (11.2–108.5)	105.7 (7.9–255.1)	57.1 (11.6–100.5)	8.2 (0.8–14.0)	12.8 (1.5–27.9)	11.2 (0.6–49.8)	552 (76–897)
No. of samples	41	41	41	41	41	41	41	41	41
				NNW Sector at 2–7 km Altitude					
Mean ± SD	2.3 ± 4.4	5.5 ± 17.2	18.3 ± 14.4	2.3 ± 4.1	18.5 ± 17.9	1.8 ± 3.5	1.0 ± 2.0	6.8 ± 11.9	136 ± 164
Median (min.–max.)	1.1 (0.5–22.2)	2.0 (0.4–89.7)	14.5 (2.9–62.1)	0.9 (0.4–16.1)	14.4 (2.7–101.0)	1.1 (0.04–18.5)	0.4 (0.04–9.9)	3.3 (0.04–59.8)	94 (7–837)
No. of samples	26	26	26	26	26	26	26	26	25
				NNW Sector at >7 km Altitude					
Mean ± SD	2.6 ± 2.7	1.7 ± 1.1	7.8 ± 3.4	2.9 ± 3.5	6.6 ± 3.5	0.7 ± 0.6	0.7 ± 0.8	4.0 ± 4.9	22 ± 12
Median (min.–max.)	1.4 (0.7–9.1)	1.7 (0.1–3.4)	7.0 (4.0–15.4)	1.2 (0.5–10.4)	7.0 (1.1–13.8)	0.4 (0.2–2.0)	0.3 (0.1–2.1)	1.9 (0.1–13.1)	22 (6–42)
No. of samples	10	10	10	10	10	10	10	10	8
				Channel Sector at <2 km Altitude					
Mean ± SD	32.2 ± 24.2	107.7 ± 123.0	129.0 ± 101.1	85.0 ± 101.3	147.5 ± 120.7	31.1 ± 22.8	27.6 ± 26.9	216.9 ± 193.4	2201 ± 1874
Median (min.–max.)	23.5 (11.0–89.5)	45.0 (29.1–602.4)	81.4 (51.7–504.8)	33.0 (16.1–313.7)	96.9 (27.2–639.0)	18.2 (10.4–111.1)	14.3 (1.9–92.8)	138.8 (57.5–629.2)	1199 (1024–9487)
No. of samples	25	25	25	25	25	25	25	25	25
				Channel Sector at 2–7 km Altitude					
Mean ± SD	9.9 ± 16.9	8.9 ± 6.7	29.2 ± 26.1	23.9 ± 45.8	21.3 ± 14.7	3.5 ± 3.2	17.0 ± 29.0	76.7 ± 97.9	254 ± 158
Median (min.–max.)	4.4 (0.7–63.5)	7.2 (0.7–23.3)	21.9 (5.5–91.7)	9.5 (0.6–171.6)	14.6 (5.6–47.2)	2.0 (0.1–10.0)	6.9 (0.2–110.0)	34.2 (1.8–329.3)	249 (11–496)
No. of samples	13	13	13	13	13	13	13	13	12
				WSW Sector at 2–7 km Altitude					
Mean ± SD	1.1 ± 0.8	1.7 ± 1.7	6.8 ± 4.9	1.6 ± 2.0	8.0 ± 5.1	1.3 ± 0.7	0.5 ± 0.7	2.3 ± 3.5	70 ± 55
Median (min.–max.)	0.8 (0.4–2.8)	1.3 (0.1–5.3)	4.4 (1.5–13.5)	0.7 (0.3–5.9)	5.3 (2.4–16.3)	1.3 (0.3–2.1)	0.2 (0.1–1.8)	0.7 (0.1–10.0)	42 (30–168)
No. of samples	7	7	7	7	7	7	7	7	6
				WSW Sector at >7 km Altitude					
Mean ± SD	2.3 ± 3.0	0.6 ± 0.8	3.2 ± 3.4	2.3 ± 3.6	4.2 ± 3.9	0.5 ± 0.5	0.4 ± 0.4	1.2 ± 2.0	38 ± 30
Median (min.–max.)	1.2 (0.8–12.9)	0.3 (0.1–3.5)	2.3 (0.1–13.1)	1.0 (0.6–14.9)	2.6 (0.8–16.9)	0.4 (0.04–2.5)	0.2 (0.1–1.8)	0.3 (0.1–11.1)	31 (1–103)
No. of samples	40	40	40	40	40	40	40	40	31
				SE Asia Sector at <2 km Altitude					
Mean ± SD	0.75 ± 0.02	4.3 ± 0.4	29.8 ± 3.1	5.6 ± 1.5	30.8 ± 0.6	6.3 ± 0.3	0.6 ± 0.1	0.5 ± 0.6	638 ± 28
Median (min.–max.)	0.75 (0.73–0.76)	4.3 (4.1–4.6)	29.8 (27.6–31.9)	5.6 (4.5–6.6)	30.8 (30.4–31.3)	6.3 (6.1–6.5)	0.6 (0.5–0.7)	0.5 (0.1–0.9)	638 (618–657)
No. of samples	2	2	2	2	2	2	2	2	2
				SE Asia Sector at 2–7 km Altitude					
Mean ± SD	0.9 ± 0.3	2.6 ± 4.1	12.0 ± 9.6	1.9 ± 2.3	14.2 ± 11.5	2.2 ± 1.8	0.9 ± 1.3	3.2 ± 4.5	219 ± 174
Median (min.–max.)	0.9 (0.4–1.4)	1.0 (0.04–13.4)	11.5 (1.7–32.1)	0.8 (0.3–7.0)	14.0 (1.8–38.0)	2.1 (0.2–5.4)	0.3 (0.1–4.1)	1.5 (0.1–13.3)	210 (17–535)
No. of samples	10	10	10	10	10	10	10	10	10
				SE Asia Sector at >7 km Altitude					
Mean ± SD	1.0 ± 0.4	0.1 ± 0.1	0.3 ± 1.0	0.8 ± 0.3	0.9 ± 0.7	0.3 ± 0.2	0.2 ± 0.1	0.3 ± 0.4	17 ± 13
Median (min.–max.)	0.9 (0.5–1.8)	0.1 (0.05–0.4)	0.1 (0.04–4.2)	0.7 (0.4–1.4)	0.9 (0.1–2.5)	0.3 (0.04–0.7)	0.2 (0.1–0.3)	0.2 (0.1–1.9)	16 (3–36)
No. of samples	19	19	19	19	19	19	19	19	8

[a]No samples from the Channel sector at >7 km altitude or the WSW sector at <2 km altitude.

Table 2. Mixing Ratios of Various Gases, Means, Standard Deviations, Medians, Minima, Maxima, and Number of Samples[a]

	O_3, ppbv	CO, ppbv	HNO_3, pptv	SO_2, pptv	C_2Cl_4, pptv	HCN, pptv	CH_3Cl, pptv	CH_3CN, pptv
NNW Sector at <2 km Altitude								
Mean ± SD	56 ± 7	204 ± 23	481 ± 213	568 ± 575	12 ± 3	210 ± 40	556 ± 17	99 ± 47
Median (min.–max.)	54 (36–67)	209 (139–249)	434 (78–1010)	321 (38–2300)	11 (6–22)	205 (107–294)	554 (524–589)	84 (69–317)
No. of samples	41	41	41	35	39	27	39	27
NNW Sector at 2–7 km Altitude								
Mean ± SD	58 ± 5	149 ± 50	184 ± 218	600 ± 1158	8 ± 3	229 ± 70	554 ± 19	108 ± 24
Median (min.–max.)	58 (52–66)	126 (109–266)	121 (80–1184)	47 (18–3890)	6 (4–15)	215 (124–354)	548 (528–598)	107 (69–149)
No. of samples	26	26	25	21	26	22	26	22
NNW Sector at >7 km Altitude								
Mean ± SD	131 ± 107	128 ± 49	407 ± 446	103 ± 96	6 ± 4	229 ± 37	542 ± 26	143 ± 43
Median (min.–max.)	75 (54–377)	133 (43–199)	141 (64–1376)	65 (19–257)	6 (1–10)	236 (180–264)	545 (489–578)	126 (95–209)
No. of samples	10	10	10	6	10	4	10	10
Channel Sector at <2 km Altitude								
Mean ± SD	67 ± 10	321 ± 129	1406 ± 1155	4302 ± 3950	16 ± 14	517 ± 340	637 ± 188	144 ± 70
Median (min.–max.)	64 (55–108)	267 (177–830)	910 (597–5914)	2649 (876–20861)	12 (9–79)	319 (259–1612)	559 (540–1458)	106 (80–317)
No. of samples	25	25	25	25	25	21	25	17
Channel Sector at 2–7 km Altitude								
Mean ± SD	59 ± 6	136 ± 25	206 ± 68	137 ± 172	6 ± 2	177 ± 7	562 ± 17	141 ± 45
Median (min.–max.)	57 (48–71)	130 (109–178)	180 (140–346)	94 (19–541)	6 (5–11)	177 (172–188)	555 (543–595)	144 (84–223)
No. of samples	13	13	13	8	13	5	13	11
WSW Sector at 2–7 km Altitude								
Mean ± SD	62 ± 4	118 ± 23	175 ± 47		4 ± 2	271 ± 18	574 ± 26	169 ● 21
Median (min.–max.)	63 (54–66)	112 (95–158)	159 (128–254)		4 (2–8)	270 (241–301)	570 (550–623)	172 (134–199)
No. of samples	7	7	6	0	7	7	7	7
WSW Sector at >7 km Altitude								
Mean ± SD	88 ± 63	134 ± 54	137 ± 114	59	3 ± 2	220 ± 18	589 ± 39	208 ± 57
Median (min.–max.)	76 (35–359)	121 (41–239)	111 (47–670)	59	3 (0.2–7)	213 (205–258)	588 (486–658)	207 (115–305)
No. of samples	40	40	37	1	40	11	40	35
SE Asia Sector at <2 km Altitude								
Mean ± SD	40 ± 1	212 ± 10	793 ± 25		5 ± 0.03	358	634 ± 15	251
Median (min.–max.)	40 (40–41)	212 (205–219)	793 (776–811)		5 (5–5)	358	634 (624–645)	251
No. of samples	2	2	2	0	2	1	2	1
SE Asia Sector at 2–7 km Altitude								
Mean ± SD	51 ± 13	156 ± 81	397 ± 390	154 ± 226	5 ± 4	235 ± 67	591 ± 45	148 ± 35
Median (min.–max.)	54 (29–67)	129 (75–302)	250 (191–1352)	24 (22–415)	4 (2–13)	237 (154–312)	574 (538–674)	135 (126–227)
No. of samples	10	10	8	3	10	6	10	7
SE Asia Sector at >7 km Altitude								
Mean ± SD	34 ± 12	103 ± 32	60 ± 34		3 ± 1	207 ± 76	571 ± 37	152 ± 37
Median (min.–max.)	32 (21–62)	97 (71–191)	50 (26–153)		2 (2–5)	187 (131–344)	556 (531–636)	158 (106–214)
No. of samples	19	19	16	0	19	6	19	16

[a]No samples from the Channel sector at >7 km altitude or the WSW sector at <2 km altitude.

Channel. SE Asia shows the lowest mixing ratios among the high altitude groups (Figure 2, bottom panel). This is not surprising, since these trajectories generally start (5 days earlier) over the Pacific, then carry air over Southeast Asia (Figure 1, top panels).

3.2. Soot

[22] The highest mean soot mass is found in the Channel sector at both low and midaltitudes (2201 and 254 ng/m^3, respectively), followed by SE Asia (638 and 219 ng/m^3, respectively; Figure 3, Table 1). Given the water-soluble chemical data, where NH_4^+ and $SO_4^=$ were much lower in SE Asia than in both Channel and NNW, these soot averages suggest the source of the soot in SE Asia is biomass burning, whereas that in Channel is likely related to residential (biofuel) and industrial sources. HCN, CH_3CN, and CH_3Cl have all been discussed as tracers for biomass burning in other papers in this special section [*Blake et al.*, 2003; *Crawford et al.*, 2003; *Heald et al.*, 2003; *Li et al.*, 2003; *Singh et al.*, 2003]. Here we see that all three of these tracers are elevated in the low altitude Channel samples compared to those from NNW (Table 2). They are also elevated in SE Asia compared to NNW (Table 2). This is consistent with the elevated soot observed here. It seems reasonable to expect that the soot in Channel is due to industrial and residential (biofuels) combustion, while that from SE Asia is due to open biomass burning. However, there does not appear to be a tracer which clearly distinguishes between biofuel and biomass combustion from this analysis.

[23] The high soot observed in Channel and SE Asia is consistent with expected emissions. *Streets et al.* [2003]

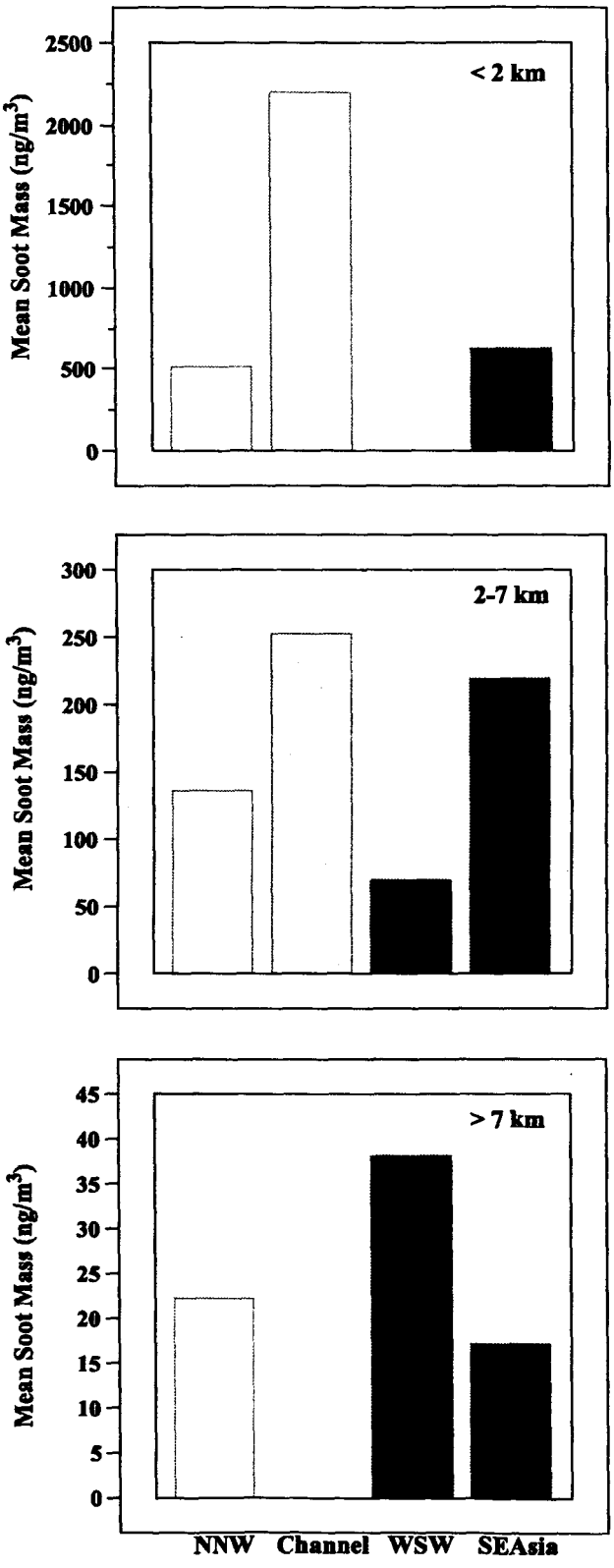

Figure 3. Mean soot mass (ng/m^3) for each group, split by altitude.

estimate that 64% of black carbon emissions are residential and related to the combustion of coal, kerosene, and biofuels in stoves, cookers, and heaters. Most of the rest (18%) is expected to be from biomass burning (which they distinguish from biofuel combustion as open biomass burning, i.e., forest burning, savanna/grassland burning, and crop residues burned in field after harvest). They note that the 18% contribution from biomass burning is primarily due to contributions from Southeast Asia. Further, other studies in this special section also report significant biomass burning from this region [*Heald et al.*, 2003; *Ma et al.*, 2003; *Russo et al.*, 2003; *Tang et al.*, 2003b]. *Liu et al.* [2003] note that deep convection is the most important transport mechanism exporting biomass-burning effluents from Southeast Asia. This is consistent with most of our samples in this sector being collected above 7 km (19 samples) with only 2 samples below 2 km, and the remainder (10 samples) obtained between 2 and 7 km (Table 1). However, it should also be noted, that soot was found in only 8 of the highest altitude samples from SE Asia, and on average these samples generally had an order of magnitude less soot than that found at lower altitudes (Table 1).

[24] Note, even though the water-soluble ion mixing ratios and soot mass were measured with very different techniques, by two different groups, the measurements are consistent with each other as shown in Figure 4. There are very good correlations between soot and both NH_4^+ (R^2 = 0.92) and $SO_4^=$ (R^2 = 0.91), which likely represents similar pollution sources (since SO_2 is typically released by fossil fuel rather than biomass combustion [*Ma et al.*, 2003]). There is no correlation between Na^+ and soot (R^2 = 0.29), which is expected since sea salt and soot aerosols are generated by very different mechanisms. There is a moderate correlation between nss-Ca^{2+} and soot (R^2 = 0.63). However, this is probably coincidental due to the co-location of dust and pollution sources, and hence does not represent a real relationship between processes which emit dust and soot. Finally, the best correlation is found with K^+ (R^2 = 0.96, Figure 4). This is particularly encouraging, since K^+ is predominantly produced by biomass combustion (both open biomass-burning and biofuel combustion) and since K^+ primarily resides in fine mode particles, as does soot [*Ma et al.*, 2003; *Hasegawa and Ohta*, 2002]. This gives us some confidence that the soot mass and water-soluble ion mixing ratios can reasonably be compared.

3.3. Partitioning Between Aerosol Types

[25] To get a better understanding of the partitioning between various aerosol types, the measured constituent masses were calculated and added up for each sample. Then the contribution of each type of aerosol to the total was determined (Table 3). Na^+ was used as the reference species to determine the proportion of sea salts present (Ca^{2+}, Mg^{2+}, K^+, Cl^-, and $SO_4^=$ all have sea salt components). The difference between the total measured water-soluble ions and their sea salt contributions, was used to determine the non-sea-salt fractions (dominated by anthropogenic ammonium sulfate). Using Na^+ as the reference species requires all of the Na^+ to be assigned to the sea salt fraction, even though some is actually due to dust. This results in an overestimate of the sea salt fraction, and an underestimate of

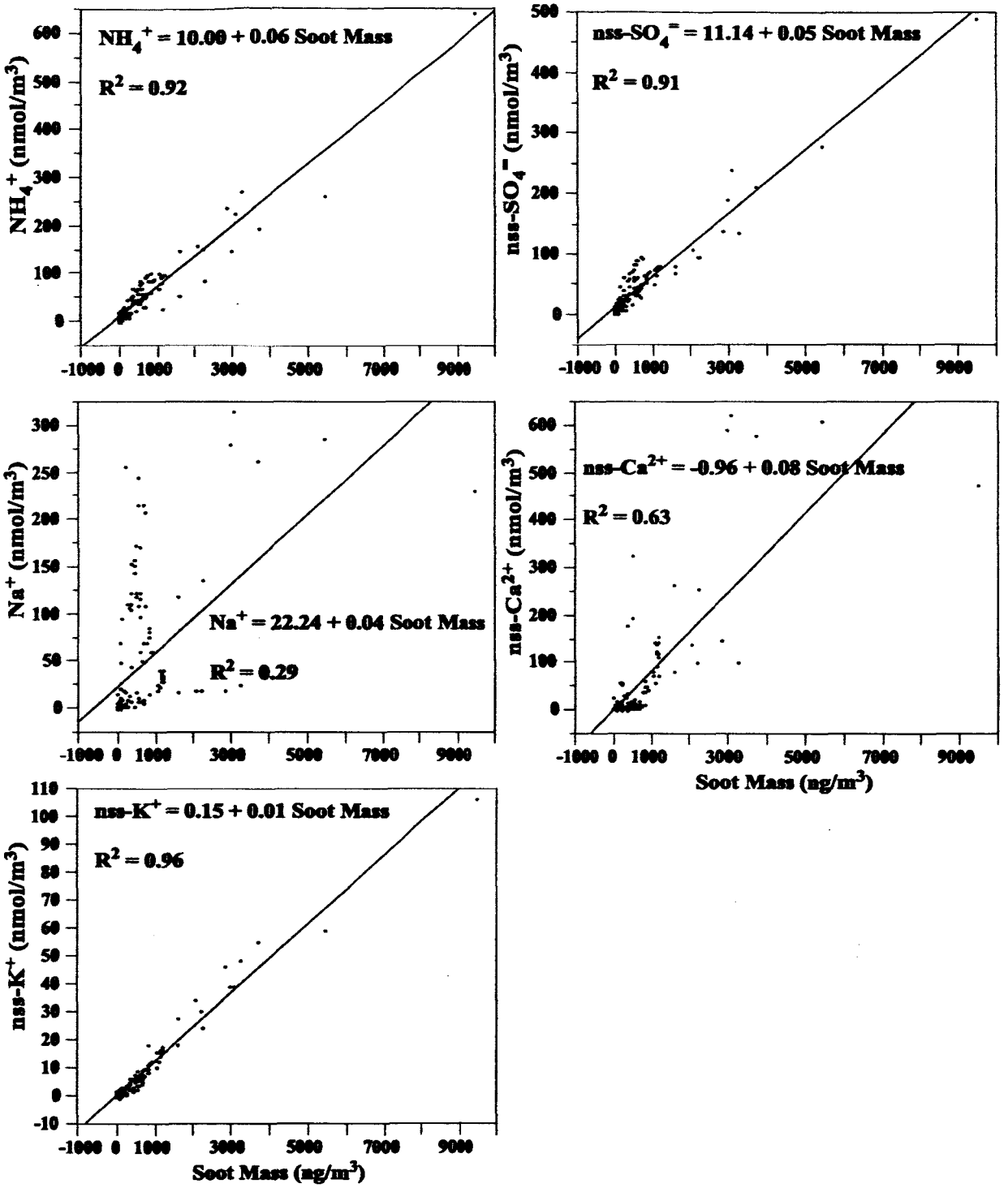

Figure 4. Various water-soluble aerosol species plotted versus soot.

the non-sea-salt fraction. Non-sea-salt-Ca^{2+} (nss-Ca^{2+}) was used to calculate the dust mass, assuming it represents 6.80% of the dust mass by weight [*Song and Carmichael*, 2001]. Since nss-Ca^{2+} is underestimated somewhat due to the problems with using Na^+ as a reference species, the dust fraction is underestimated here somewhat. Note, dust fractions (which include both nss-Ca^{2+} and nss-Mg^{2+}) were not included in the non-sea-salt (NSS) fraction (i.e., NSS = NO_3^- + nss-$SO_4^=$ + NH_4^+ + nss-K^+). Nss-K^+ is primarily produced by combustion processes as discussed in the previous section, however it is also a constituent of Asian dust (0.91% by weight [*Song and Carmichael*, 2001]). Hence, the NSS fraction does represent some dust, particularly in Channel, via the inclusion of all of the nss-K^+.

Table 3. Calculated Aerosol Mass and Percentages Contributing to the Total, Means, Standard Deviations, Medians, Minima, and Maxima[a]

	Total Mass	Soot	SS	NSS	Dust
		NNW Sector at <2 km Altitude			
Mean ± SD	22.6 ± 10.8	2.5 ± 1.5	33.2 ± 19.2	36.4 ± 10.1	27.8 ± 19.0
Median (min.–max.)	20.7 (4.8–46.4)	2.0 (0.5–7.0)	34.9 (4.1–77.1)	35.1 (19.3–63.8)	27.7 (0–63.9)
No. of samples	41	41	41	41	41
		NNW Sector at 2–7 km Altitude			
Mean ± SD	6.9 ± 9.7	2.2 ± 1.8	2.4 ± 2.0	50.7 ± 23.2	44.7 ± 24.3
Median (min.–max.)	3.9 (0.4–50.5)	1.6 (0–8.2)	1.6 (0.4–7.3)	46.0 (16.6–90.8)	50.9 (2.0–79.8)
No. of samples	26	26	26	26	26
		NNW Sector at >7 km Altitude			
Mean ± SD	3.6 ± 3.4	0.8 ± 0.7	5.5 ± 3.1	49.6 ± 27.9	44.1 ± 29.6
Median (min.–max.)	2.1 (0.7–10.4)	0.6 (0–1.8)	5.1 (1.5–11.7)	46.6 (15.9–85.3)	50.3 (7.7–78.6)
No. of samples	10	10	10	10	10
		Channel Sector at <2 km Altitude			
Mean ± SD	133.8 ± 112.1	1.7 ± 0.7	2.3 ± 0.7	17.4 ± 7.3	78.6 ± 7.5
Median (min.–max.)	97.3 (46.1–422.1)	1.5 (0.7–3.2)	2.4 (0.9–3.5)	15.8 (6.9–36.4)	80.4 (58.7–89.1)
No. of samples	23	23	23	23	23
		Channel Sector at 2–7 km Altitude			
Mean ± SD	50.1 ± 62.0	0.8 ± 0.7	2.1 ± 1.1	15.2 ± 11.7	81.9 ± 11.8
Median (min.–max.)	25.1 (1.8–210.2)	0.6 (0–2.4)	1.9 (0.6–3.8)	9.2 (4.7–38.4)	87.3 (58.7–92.4)
No. of samples	13	13	13	13	13
		WSW Sector at 2–7 km Altitude			
Mean ± SD	2.5 ± 2.7	4.3 ± 3.9	6.4 ± 7.7	53.4 ± 18.9	35.9 ± 24.4
Median (min.–max.)	1.9 (0.5–8.1)	5.0 (0–9.1)	3.7 (1.1–2.3)	57.3 (23.5–75.7)	33.9 (10.1–72.4)
No. of samples	7	7	7	7	7
		WSW Sector at >7 km Altitude			
Mean ± SD	1.3 ± 1.4	3.9 ± 4.4	14.0 ± 12.3	45.6 ± 25.0	36.5 ± 28.2
Median (min.–max.)	0.8 (0.2–7.9)	2.3 (0–15.1)	11.3 (1.8–54.8)	49.7 (5.2–88.0)	25.0 (0–90.3)
No. of samples	40	40	40	40	40
		SE Asia Sector at <2 km Altitude			
Mean ± SD	5.3 ± 0.6	12.2 ± 2.0	3.9 ± 0.5	79.8 ± 4.2	4.1 ± 5.7
Median (min.–max.)	5.3 (4.8–5.7)	12.2 (10.8–13.6)	3.9 (3.6–4.3)	79.8 (76.8–82.8)	4.1 (0.04–8.1)
No. of samples	2	2	2	2	2
		SE Asia Sector at 2–7 km Altitude			
Mean ± SD	3.9 ● 4.2	7.4 ± 4.8	3.3 ± 1.8	53.8 ± 20.4	35.5 ± 24.4
Median (min.–max.)	2.5 (0.4–13.6)	7.0 (1.4–16.2)	2.7 (1.3–7.5)	52.6 (19.1–80.5)	36.0 (4.4–76.6)
No. of samples	10	10	10	10	10
		SE Asia Sector at >7 km Altitude			
Mean ± SD	0.3 ± 0.3	4.1 ± 6.9	23.4 ± 10.3	27.1 ± 16.1	45.5 ± 22.3
Median (min.–max.)	0.2 (0.1–1.2)	0 (0–20.4)	26.7 (4.3–35.5)	26.6 (3.9–76.3)	39.4 (12.7–91.7)
No. of samples	17	17	17	17	17

[a]Total mass is in units of $\mu g/m^3$. All other numbers are percentages. No samples from the Channel sector at >7 km altitude or the WSW sector at <2 km altitude.

Also note, organic species are not included in this discussion. This may be a significant factor, especially for SE Asia where biomass-burning sources may result in organic particulates which constitute a substantial fraction of the mass (e.g., *Mayol-Bracero et al.* [2002] reported that particulate organic matter constituted 35% of the fine aerosol mass during the Indian Ocean Experiment (INDOEX)).

[26] The bulk of the aerosol mass exported from Asia is carried in the Channel sector, 134 $\mu g/m^3$ on average below 2 km (Table 3). This is almost a factor of 6 higher than that from the NNW sector at the same altitudes. At midaltitudes Channel still carries the most material, 50 $\mu g/m^3$ on average between 2 and 7 km, about a factor of 7 higher than that of NNW. At midaltitudes, SE Asia and WSW contain only about half the material present in NNW. At high altitudes, NNW contains only about half the material that was present there at midaltitudes, 3.6 $\mu g/m^3$ on average, which is about 3 times that in WSW and 10 times that in SE Asia.

[27] At low altitudes, only about 2% of the aerosol mass in Channel is due to either soot or sea salt. 17% is NSS, while the remaining 79% of the mass in Channel is dust (Table 3). The percentages are similar for midaltitude Channel samples with dust increasing to 82%, NSS dropping to 15%, and soot dropping to 1%. NNW also has a low percentage of soot (3%), but the sea salt, NSS, and dust fractions are all comparable at low altitudes, at 33%, 36%, and 28%, respectively. At midaltitudes, the sea salts are far less important, contributing only 2% to the total mass in NNW, resulting in NSS constituting 51% and dust 45% of

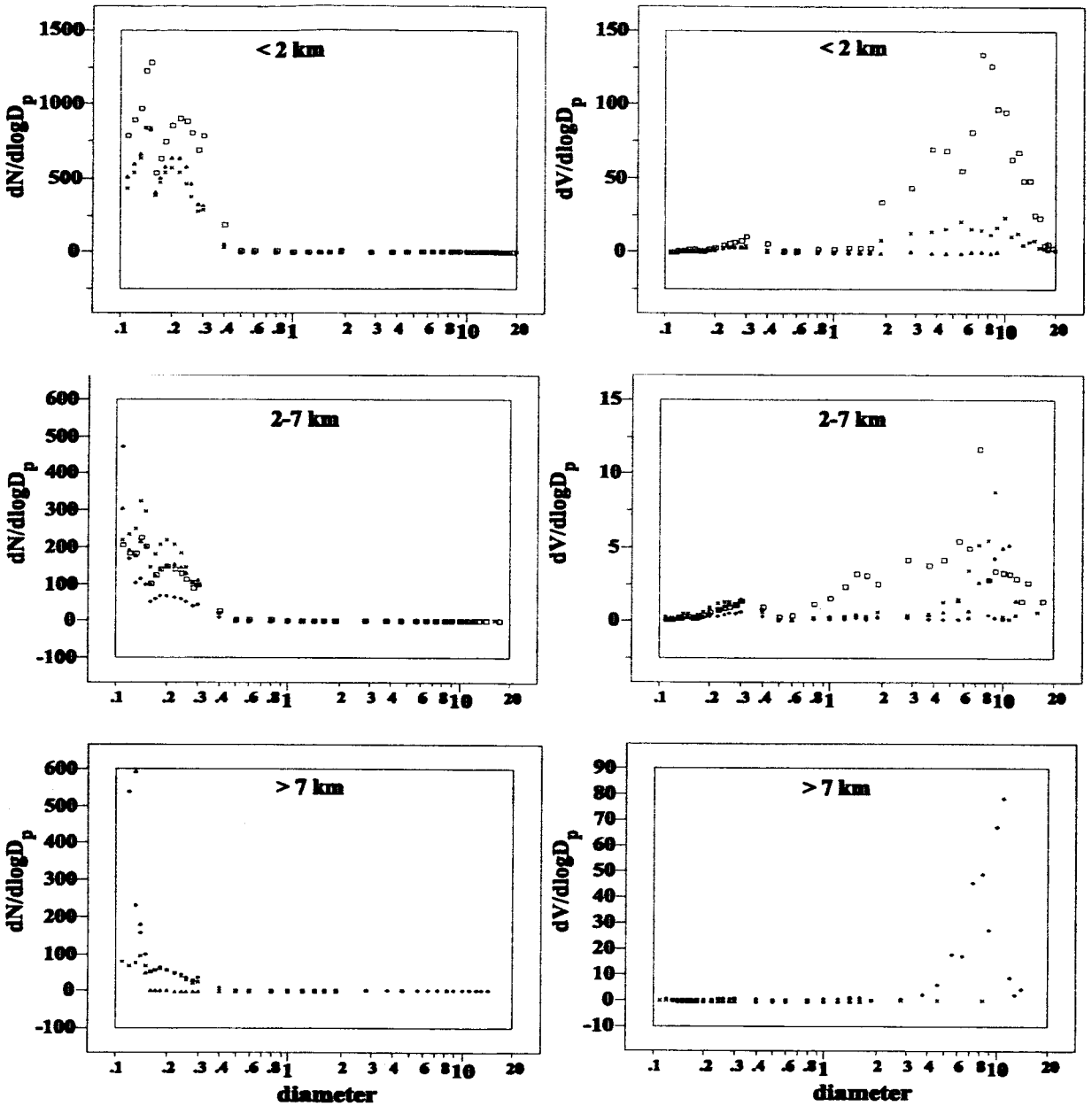

Figure 5. Size distributions of particle number (left panels) and dry particle volume (right panels) are shown for particle sizes ranging from 0.11–20 μm diameter. These distributions are binned according to altitude (separate panels) and groups (NNW (x's), Channel (squares), WSW (circles), and SE Asia (triangles)).

the mass, while soot remains at 2%. These percentages remain nearly the same for high altitude NNW.

[28] SE Asia particulate mass, on the other hand, is about 12% soot, with sea salts and dust each only adding 4%, while the bulk of material, 80% is NSS at low altitude. At midaltitude, soot comprises 7% of the mass, while sea salt remains low at about 3%, and NSS drops to 54% due to the relative increase in dust to 36%. At high altitudes, soot comprises 4%, while sea salt and NSS are comparable at 23% and 27%, respectively, and dust increases to 46%. Note, there is very little mass here, compared with the other altitudes and groups, and there is wide variability in these high altitude SE Asia fractions.

[29] WSW has about 4% soot and 36% dust at both middle and high altitudes, while sea salt contributes 6% and 14%, respectively, and NSS makes up the rest at 53% and 46%.

[30] As pointed out by *Jacob et al.* [2003], only minor dust plumes were sampled during TRACE-P. The largest dust plumes in 2001 appeared after TRACE-P and were sampled by ACE-Asia and PHOBEA-II [*Jacob et al.*, 2003; *Huebert et al.*, 2003; *Price et al.*, 2003]. This suggests that

dust export from a major storm event, and any associated pollution, may substantially exceed the mass presented here.

3.4. Size Distributions

[31] Number densities (Figure 5, left panels) show the highest concentrations in the fine mode occur in the low altitude Channel samples. Note that the instrument response drops off for the smallest sizes. It is expected, that rather than peaking at about 0.14 μm, the number densities should increase all the way down to 0.11 μm, the smallest particle diameter shown here. There is a secondary peak around 0.22 μm diameter present at all altitudes. The high values seen in the Channel number densities support the chemical data in that pollution is highest in this sector. However, at midaltitudes, the highest number densities are generally in the NNW sector, except for the high values seen in WSW and SE Asia. This also supports the chemical data, where the highest pollution species mixing ratios were seen in Channel and NNW. For the most part, number densities decrease with altitude. However, some high values are in SE Asia and WSW in the highest altitude samples.

[32] Volume distributions (Figure 5, right panels) show the highest volumes in the Channel sector at low altitudes. The high volumes seen in the supermicron sizes for both Channel and NNW are due to both dust and sea salts. This is still the case at midaltitudes, but the volumes are about an order of magnitude smaller. Note, a small enhancement in volume is seen at all altitudes around 0.3 μm, which is likely due to the high number of accumulation mode particles. Some fraction of these are likely the $(NH_4)_2SO_4$ (or NH_4HSO_4) seen in the chemical data. These size distributions, both number and volume, have excluded samples collected when the DC-8 flew through a cloud. This led to the exclusion of 11 NNW (5 low, 2 middle, 4 high altitude), 0 Channel, 6 WSW (1 middle, 5 high altitude), and 5 SE Asia (2 middle, 3 high altitude) samples. Had the cloud data remained, the volume curves were seen to increase dramatically from 5–20 μm. For the most part, the influence of cloud data has been removed. However, at high altitudes, the high volumes seen in WSW supermicron volumes is likely due to passage near a cloud, with some residual enhanced particle volumes (Figure 5, bottom right panel).

[33] The low altitude size distributions here are consistent with those from various marine boundary layer locations reported by *Bates et al.* [2002]. They showed number distributions had a peak at 0.2 μm from many source regions measured during INDOEX, Aerosols99, ACE-1, and ACE-2. Some of these locations also exhibited number density peaks at sub-0.1 μm diameters, while others did not. A volume distribution curve from the Atlantic Ocean of African mineral dust exhibited the highest volume in their comparison with a peak $dV/d\log D_p$ value of about 70 for 2.5 μm particles, compared to about 125 for 8 μm particles here.

3.5. Condensation Nuclei

[34] Mean condensation nuclei measurements (Figure 6 and Table 4) are again highest in the low altitude Channel sector (17084 cm^{-3} CN > 4 nm, 12182 cm^{-3} CN > 14 nm). Number densities of mean condensation nuclei >4 nm (#/cm^3 at STP) are shown along with unheated and heated measurements of CN > 14 nm (Figure 6 and Table 4). The

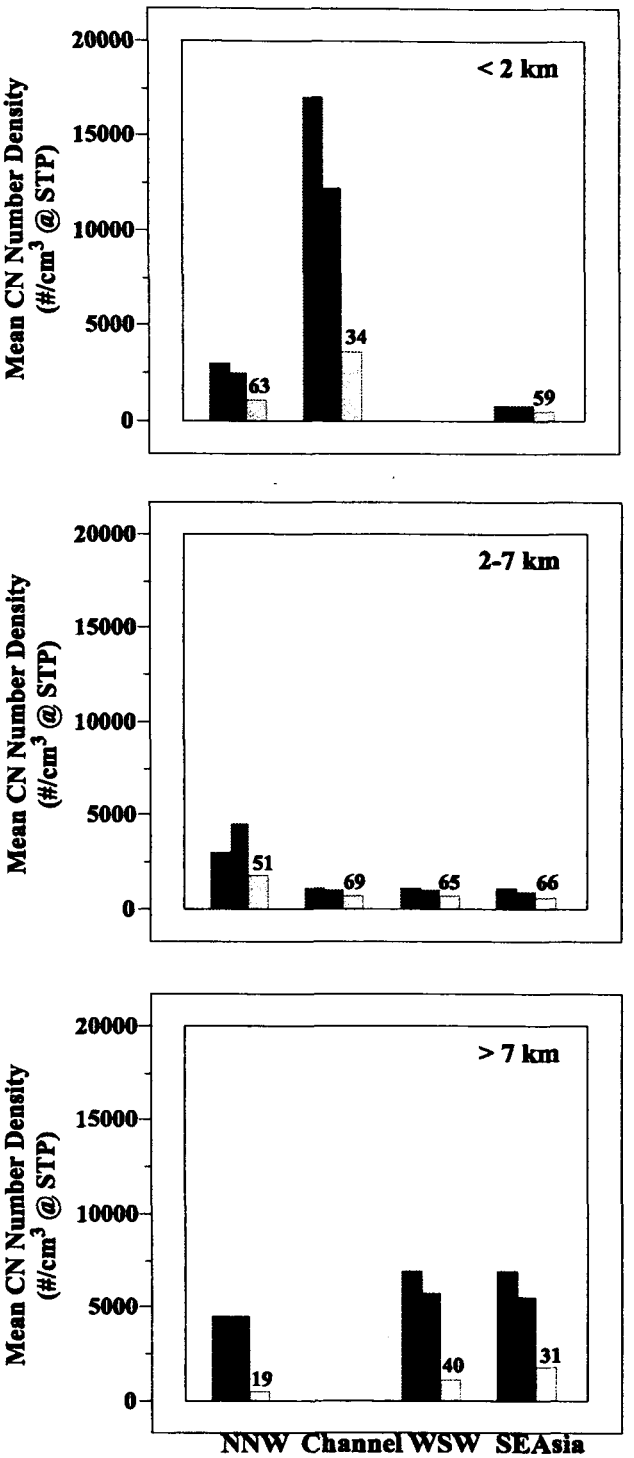

Figure 6. Mean condensation nuclei (CN) > 4 nm (black), unheated CN > 14 nm (medium gray), and heated CN > 14 nm (light gray), split by group and altitude. The numbers above the heated CN columns are the percentages of the total for each group represented by nonvolatile CN > 14 nm.

Table 4. Condensation Nuclei and Volatility, Means, Standard Deviations, Medians, Minima, Maxima, and Number of Samples[a]

		CN > 14 nm		
	CN > 4 nm	Unheated	Heated	Ratio (Heated/Unheated)
		NNW Sector at <2 km Altitude		
Mean ± SD	2988 ± 4901	2520 ± 3495	1107 ± 919	0.63 ± 0.27
Median (min.–max.)	1111 (36–23274)	1068 (38–16611)	686 (16–3765)	0.70 (0.04–0.99)
No. of samples	38	41	39	39
		NNW Sector at 2–7 km Altitude		
Mean ± SD	3073 ± 3327	4553 ± 11084	1851 ± 1356	0.51 ± 0.32
Median (min.–max.)	1202 (371–9625)	767 (433–49923)	1661 (289–4537)	0.41 (0.10–0.97)
No. of samples	26	20	8	8
		NNW Sector at >7 km Altitude		
Mean ± SD	4595 ± 8685	4508 ± 7898	457 ± 311	0.19 ± 0.19
Median (min.–max.)	1654 (686–29120)	1479 (547–26096)	363 (8–915)	0.13 (0.004–0.43)
No. of samples	10	10	7	7
		Channel Sector at <2 km Altitude		
Mean ± SD	17084 ± 18087	12182 ± 12604	3645 ± 3313	0.34 ± 0.27
Median (min.–max.)	10683 (1018–70675)	4811 (1062–40746)	2445 (765–11718)	0.26 (0.03–0.82)
No. of samples	23	20	10	10
		Channel Sector at 2–7 km Altitude		
Mean ± SD	1100 ± 873	1041 ± 814	696 ± 444	0.69 ± 0.18
Median (min.–max.)	675 (405–3418)	631 (378–3132)	512 (321–1871)	0.61 (0.50–1.03)
No. of samples	13	13	13	13
		WSW Sector at 2–7 km Altitude		
Mean ± SD	1132 ± 366	1023 ± 311	666 ± 106	0.65 ± 0.21
Median (min.–max.)	1064 (730–1762)	998 (685–1563)	672 (481–796)	0.63 (0.31–0.92)
No. of samples	7	7	7	7
		WSW Sector at >7 km Altitude		
Mean ± SD	6963 ± 12334	5778 ± 9906	1104 ± 932	0.40 ± 0.21
Median (min.–max.)	2150 (594–50592)	1993 (583–42289)	913 (214–4678)	0.37 (0.02–0.89)
No. of samples	40	40	38	38
		SE Asia Sector at <2 km Altitude		
Mean ± SD	815 ± 30	829 ± 34	513 ± 30	0.59 ± 0.06
Median (min.–max.)	815 (794–837)	829 (805–853)	513 (492–535)	0.59 (0.55–0.63)
No. of samples	2	2	2	2
		SE Asia Sector at 2–7 km Altitude		
Mean ± SD	1127 ± 1017	928 ± 621	560 ± 316	0.66 ± 0.27
Median (min.–max.)	715 (431–3805)	647 (353–2353)	524 (61–1146)	0.70 (0.09–0.98)
No. of samples	10	10	10	10
		SE Asia Sector >7 km Altitude		
Mean ± SD	7000 ± 4586	5510 ± 3651	1815 ± 1914	0.31 ± 0.19
Median (min.–max.)	5041 (931–14802)	4196 (804–12245)	1129 (300–7689)	0.27 (0.07–0.68)
No. of samples	17	17	17	17

[a]Condensation nuclei units are #/cm^3 @ STP. No samples from the Channel sector at >7 km altitude or the WSW sector at <2 km altitude.

numbers above the heated CN columns are the mean percentages of nonvolatile (at 300°C) particles. What is striking here, is both the low mean values of total particles (≈1000 cm^{-3}, along with the high percentage (≥65%) of nonvolatile particles observed at midaltitudes (Figure 6) for all groups except NNW. This likely reflects the influence of cloud processing on these condensation nuclei. Clouds predominantly reside in this midaltitude (2–7 km) layer. Particles in this size range readily grow in clouds and volatile particles are scavenged. This has apparently led to preferential removal of these particles at midaltitudes.

3.6. Optical Properties

[35] Asian aerosols exert a great influence on the photochemistry of this region [*Lefer et al.*, 2003; *Tang et al.*, 2003a]. Aerosols influence photochemistry directly via their own scattering properties, and indirectly via their role in cloud formation, with cloud radiative properties also affecting photolysis rates. Photolysis frequencies are enhanced/reduced depending on whether the observation is above/below clouds and depending on whether the ambient aerosol population is highly scattering/absorbing [*Lefer et al.*, 2003]. While clouds have a greater instantaneous effect on photolysis frequencies [*Lefer et al.*, 2003], on average aerosols have a greater impact on O_3 production [*Tang et al.*, 2003a]. The net photochemical effect of clouds and aerosols during TRACE-P was a large decrease in photochemical O_3 in the boundary layer [*Lefer et al.*, 2003].

[36] The particulates in Asian megacity plumes can reduce NO_x photolysis such that the mixing ratio increases

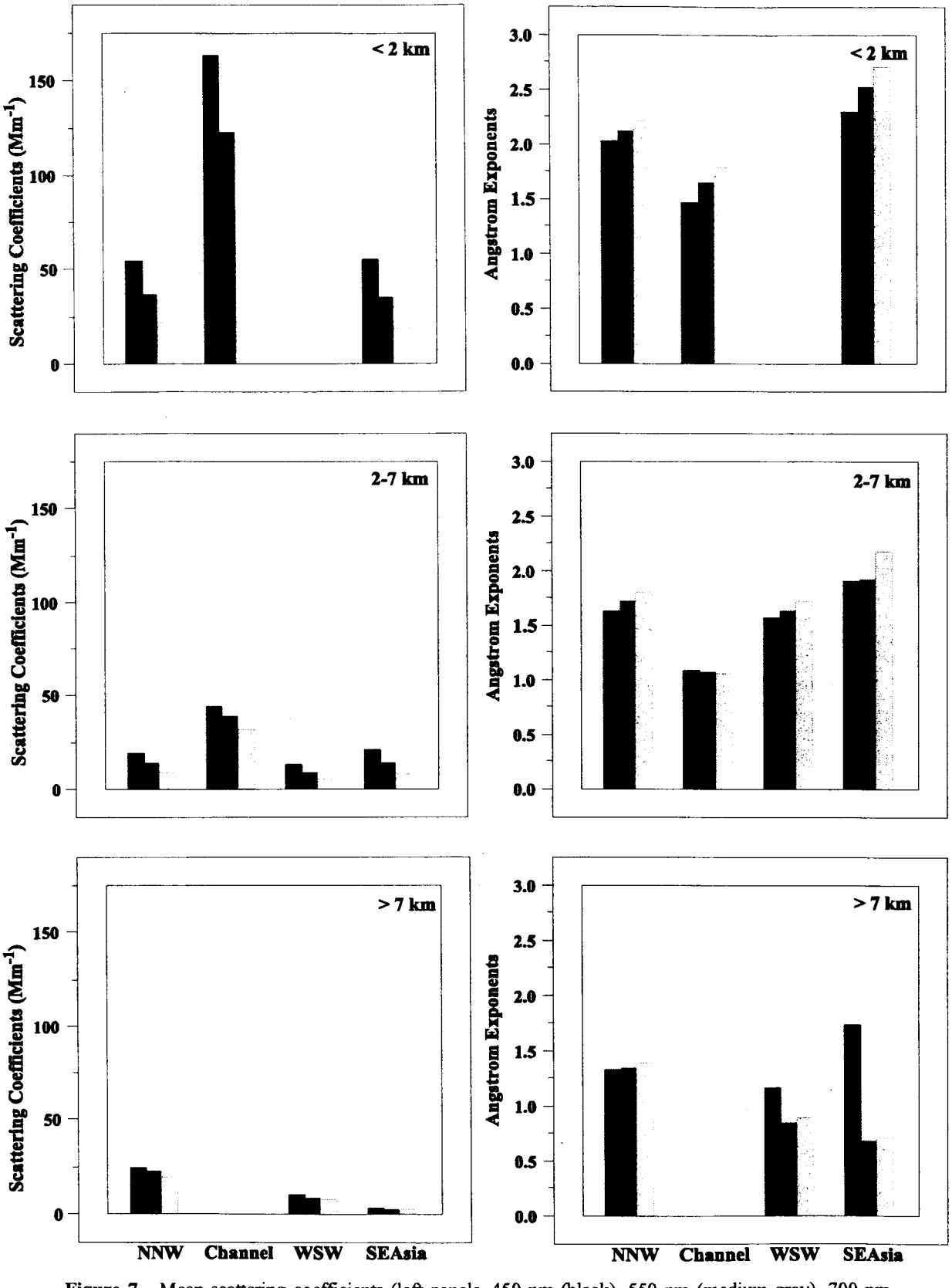

Figure 7. Mean scattering coefficients (left panels, 450 nm (black), 550 nm (medium gray), 700 nm (light gray)) and angstrom exponents (right panels, 450–700 nm (black), 450–550 nm (medium gray), 550–700 nm (light gray)) split by group and altitude.

Table 5. Single Scatter Albedo, Scattering Coefficients and Angstrom Exponent Means, Standard Deviations, Medians, Minima, and Maxima[a]

	ω_o	σ_{sp} 450 nm $\times 10^{-6}$ (m^{-1})	σ_{sp} 550 nm $\times 10^{-6}$ (m^{-1})	σ_{sp} 700 nm $\times 10^{-6}$ (m^{-1})	å 450–700	å 450–550	å 550–700
			NNW Sector at <2 km Altitude				
Mean ± SD	0.87 ± 0.02	55 ± 21	37 ± 17	22 ± 13	2.03 ± 0.31	2.13 ± 0.26	2.21 ± 0.27
Median (min.–max.)	0.86 (0.81–0.93)	56 (10–123)	37 (7–112)	21 (4–90)	2.10 (0.77–2.40)	2.19 (1.31–2.48)	2.28 (1.27–2.54)
No. of samples	41	41	41	41	41	41	41
			NNW Sector at 2–7 km Altitude				
Mean ± SD	0.84 ± 0.08	20 ± 23	14 ± 16	9 ± 10	1.64 ± 0.40	1.73 ± 0.46	1.80 ± 0.54
Median (min.–max.)	0.87 (0.65–0.94)	14 (4–121)	10 (3–82)	6 (3–48)	1.72 (0.81–2.37)	1.86 (0.34–2.35)	1.77 (0.31–2.69)
No. of samples	26	26	26	26	26	26	26
			NNW Sector at >7 km Altitude				
Mean ± SD	0.93 ± 0.04	25 ± 24	23 ± 25	19 ± 23	1.33 ± 1.20	1.34 ± 0.74	1.40 ± 0.62
Median (min.–max.)	0.92 (0.88–0.98)	13 (6–70)	9 (3–67)	7 (2–59)	0.76 (0.0001–3.23)	1.43 (0.11–2.53)	1.24 (0.40–2.35)
No. of samples	8	10	10	10	10	10	10
			Channel Sector at <2 km Altitude				
Mean ± SD	0.86 ± 0.02	163 ± 114	123 ± 86	82 ± 59	1.47 ± 0.48	1.65 ± 0.47	1.79 ± 0.47
Median (min.–max.)	0.85 (0.83–0.90)	97 (88–586)	71 (62–429)	45 (38–267)	1.63 (0.25–1.87)	1.80 (0.44–2.09)	1.94 (0.60–2.27)
No. of samples	25	23	23	23	23	23	23
			Channel Sector at 2–7 km Altitude				
Mean ± SD	0.88 ± 0.05	44 ± 38	39 ± 36	31 ± 31	1.10 ± 0.54	1.08 ± 0.43	1.07 ± 0.37
Median (min.–max.)	0.87 (0.79–0.95)	31 (6–130)	26 (4–123)	21 (2–105)	1.01 (0.32–2.26)	0.97 (0.48–1.78)	1.01 (0.57–1.74)
No. of samples	13	13	13	13	13	13	13
			WSW Sector at 2–7 km Altitude				
Mean ± SD	0.81 ± 0.08	13 ± 11	9 ± 7	6 ± 4	1.58 ± 1.07	1.64 ± 1.00	1.73 ± 0.83
Median (min.–max.)	0.82 (0.67–0.91)	11 (1–29)	7 (2–19)	5 (2–12)	1.98 (0.02–2.90)	2.02 (0.002–2.77)	1.77 (0.42–2.59)
No. of samples	7	7	7	7	7	7	7
			WSW Sector at >7 km Altitude				
Mean ± SD	0.84 ± 0.08	10 ± 11	9 ± 9	8 ± 8	1.17 ± 0.95	0.85 ± 0.72	0.89 ± 0.60
Median (min.–max.)	0.86 (0.60–0.96)	6 (1–45)	5 (2–43)	5 (2–40)	1.19 (0.06–3.26)	0.59 (0.0001–2.37)	0.68 (0.06–2.36)
No. of samples	36	40	40	40	40	40	40
			SE Asia Sector at <2 km Altitude				
Mean ± SD	0.82 ± 0.00	55 ± 4	35 ± 2	18 ± 1	2.30 ± 0.01	2.53 ± 0.002	2.72 ± 0.005
Median (min.–max.)	0.82 (0.82–0.82)	55 (53–58)	35 (33–37)	18 (17–19)	2.30 (2.29–2.31)	2.53 (2.53–2.53)	2.72 (2.72–2.72)
No. of samples	2	2	2	2	2	2	2
			SE Asia Sector at 2–7 km Altitude				
Mean ± SD	0.78 ± 0.05	21 ± 16	14 ± 10	8 ± 6	1.91 ± 0.73	1.92 ± 0.76	2.17 ± 0.51
Median (min.–max.)	0.81 (0.71–0.84)	23 (1–43)	15 (1–30)	8 (1–19)	2.06 (0.05–2.58)	1.94 (0.11–2.79)	2.07 (1.54–2.94)
No. of samples	10	10	10	10	10	10	10
			SE Asia Sector at >7 km Altitude				
Mean ± SD	0.80 ± 0.06	3 ± 1	2 ± 1	3 ± 1	1.75 ± 0.97	0.68 ± 0.59	0.70 ± 0.35
Median (min.–max.)	0.80 (0.71–0.90)	3 (0.5–6)	2 (2–4)	3 (1–4)	1.80 (0.0002–3.80)	0.47 (0.0001–2.06)	0.61 (0.27–1.49)
No. of samples	16	17	17	17	17	17	17

[a]No samples from the Channel sector at >7 km altitude or the WSW sector at <2 km altitude.

by 40% [*Tang et al.*, 2003a]. This is supported by the finding that HNO_3 and PAN dominate NO_y (NO_x < 100 pptv), except in plumes, where NO_x can be >1000 pptv [*Talbot et al.*, 2003]. O_3 is produced by the photolysis of NO_2. Hence, reducing NO_x photolysis, reduces O_3 production. Since the photolysis of O_3 produces OH and OH is the primary sink of CO, it is also expected that the aerosol influence on photolysis will reduce O_3 and increase CO in plumes [*Tang et al.*, 2003a]. This is supported by observations made during PHOBEA-II (flight 8, April 14, 2001), where an Asian dust plume transported to North America was found to have O_3 anti-correlated with aerosol scattering [*Price et al.*, 2003]. Further, the highest CO observed during PHOBEA-II was associated with this plume [*Price et al.*, 2003].

[37] To accurately model photochemistry then, a good understanding of aerosol optical properties is needed for any given region. In the next three sub-sections, we will discuss the scattering coefficients, angstrom exponents, and single scatter albedo measurements in the same context as we did for the chemical and size distribution data.

3.6.1. Scattering

[38] The scattering coefficients (σ_{sp}) obtained from an integrating nephelometer as a function of group and altitude, show Channel enhanced compared to the other groups both at low and midaltitudes (left panels Figure 7; Table 5). Otherwise, at each altitude level, mean σ_{sp} is not statistically significantly different between the groups. Submicron particles are the most efficient scatterers, particularly in the 0.2–1.0 μm diameter range [*Quinn et al.*, 2002a]. Further,

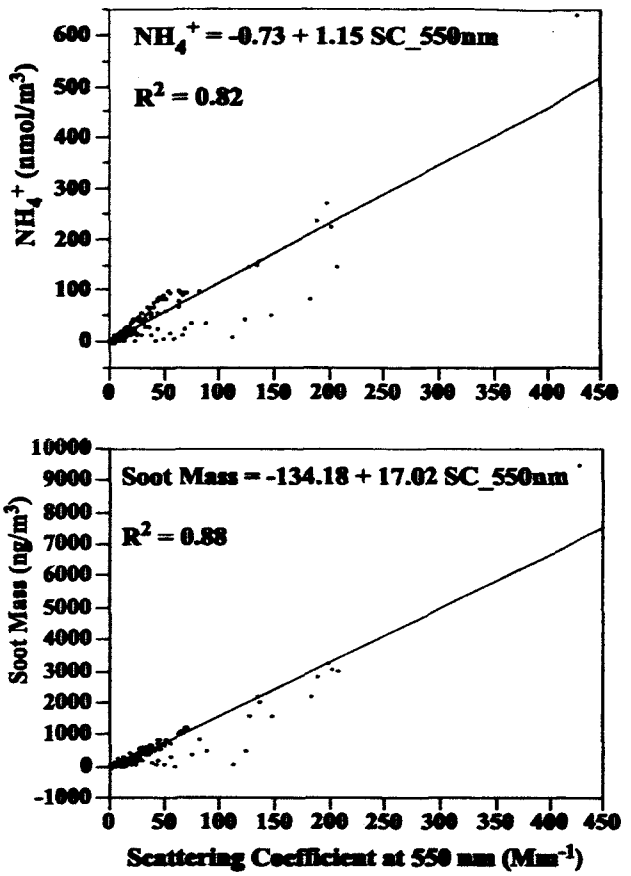

Figure 8. NH_4^+ mixing ratio and soot mass plotted versus the scattering coefficient for 550 nm.

σ_{sp} is mostly strongly dependent upon the amount of particulate matter present, as opposed to its size distribution or composition [*Delene and Ogren*, 2002]. Note that good correlations are found for both NH_4^+ (R^2 = 0.82) and soot (R^2 = 0.88) versus σ_{sp}(550 nm) (Figure 8). These overall correlations are driven primarily by the Channel and SE Asia sectors, with R^2 = 0.83 and 0.94, respectively for NH_4^+ and R^2 = 0.90 and 0.93 for soot. The other two sectors have much poorer correlations of 0.40 (NNW NH_4^+), 0.25 (WSW NH_4^+), 0.42 (NNW soot), and 0.20 (WSW soot). It seems likely the good correlations observed for the Channel and SE Asia sectors are due to the prevalence of fine mode particulates in these regions.

[39] Channel, with the most fine mode particles (see section 3.3, Figure 5), exhibits the highest values of σ_{sp} (e.g., 123 and 39 Mm^{-1} at 550 nm for low and midaltitude samples, respectively). Comparable values of σ_{sp} observed in NNW and SE Asia at low altitudes (≈35 Mm^{-1} at 550 nm) reflect the comparable numbers of particles present (Figure 5 top left panel). Lower σ_{sp} observed, <10 Mm^{-1} at 550 nm, for WSW and high altitude SE Asia is consistent with the lower number densities observed in these sectors at their respective altitudes, compared to the other groups (Figures 5 and 7; Table 5). These values are consistent with those reported by *Quinn et al.* [2002b] for their eight source regions during INDOEX, with median values ranging from about 15–135 Mm^{-1} at 550 nm. Similarly, *Sheridan et al.* [2002] reported a mean value of 53 Mm^{-1} at 550 nm observed on the C-130 during INDOEX.

3.6.2. Angstrom Exponent

[40] Although, we measured size distributions directly (see section 3.3) with PCASP and FSSP probes, an underlying goal of the Global Troposphere Experiments has been to link in situ measurements with satellite observations [*Crawford et al.*, 2003]. The angstrom exponent is a measure of the wavelength dependence of scattering which can be used to describe aerosol size information based on a remotely sensed measurement [*Price et al.*, 2003]. Hence, in this section, we describe the angstrom exponents measured by the DC-8 in comparison with the measured size distributions, although this is somewhat redundant with the information presented in section 3.3. In principle, space-based observations of angstrom exponents may eventually provide regional- and global-scale inputs of aerosol size distributions for regional and global models.

[41] The angstrom exponent (å) decreases with increasing particle size, from values of 3 to 1 between 10 and 1000 nm. For particle distributions dominated by supermicron particles, å approaches 0 [*Price et al.*, 2003]. Comparing the mean å shown in Figure 7 (right panels) to the volume distributions shown in Figure 5 (right panels), å clearly reflects the presence of larger particles. The greatest influence of the larger particles is seen in low altitude Channel (due to the presence of dust), followed by NNW (due to sea salt), with the highest values observed in SE Asia at these altitudes.

[42] Note, å is calculated from the scattering coefficients [*Delene and Ogren*, 2002], which most strongly respond to particles in the 0.2–1.0 μm diameter range [*Quinn et al.*, 2002a]. So the shifting size distributions indicated by å most strongly reflect this submicron mode rather than the supermicron sizes where the bulk of the dust and sea salt mass resides. Due to inefficiencies with the nephelometer inlet on the DC-8, supermicron particles were not passed efficiently through to the instrument. This is a greater problem for the sea salt particles than the dust particles. However, since the submicron fraction dominates the scattering, it is not expected that the scattering coefficients and angstrom exponents reported here are greatly affected by the inlet problems.

[43] Observations of Asian dust transported to the eastern Pacific/western United States made during PHOBEA-II flight 8 showed å of 0.6 (450/550) and 0.8 (550/700) in the heaviest dust layers [*Price et al.*, 2003]. These values are comparable to the lowest values measured in Channel by the DC-8 during TRACE-P of ≈0.5 (450/550, Table 5) and ≈0.6 (550/700, Table 5). The nephelometer used during PHOBEA-II also did not pass supermicron particles efficiently [*Price et al.*, 2003], so the different values here probably reflect a somewhat larger size distribution near Asia.

[44] Mean angstrom exponents reported by *Quinn et al.* [2002b] during INDOEX range from <0.25 to about 1.7 (for 450–700 nm) for the 8 sources regions they observed. These values are lower than the mean values reported here for SE Asia and WSW (1.17–2.30, 450–700 nm). This reflects the larger particles included in their measurement (up to 10 μm) compared to those here (up to 1 μm). *Sheridan et al.* [2002] report a mean value of 2.02 (550–

700 nm) measured on the C-130 during INDOEX, with mean values from their most polluted region ranging from 1.37 (>5 km) to about 2.0 at lower altitudes. These values are for submicron particles only, so are more comparable to those measured here in SE Asia and WSW. However, they span a narrower range of values than these two groups, 0.70–2.72 (550–700 nm) for SE Asia and 0.89–1.73 (550–700 nm) for WSW.

3.6.3. Single Scatter Albedo

[45] Single scatter albedo (ω_o) indicates the relative proportion of scattering and absorbing coefficients [$\sigma_{sp}/(\sigma_{sp} + \sigma_{ap})$] such that a greater relative presence of absorbing soot compared to sulfate will result in a lower ω_o [*Delene and Ogren*, 2002]. While the greatest amount of soot was observed in Channel, the greatest amount of sulfate was observed there as well. Thus, the mean ω_o in Channel is not the lowest observed (Table 5). The lowest mean ω_o is seen in SE Asia (Table 5), where the relative proportion of soot particulates is much higher than in any other group (see Table 3). Most of the SE Asia means ($\approx$0.80) are statistically significantly lower than those of the other groups ($\approx$0.84–0.93), while the means of the other groups are not significantly different from each other. The lowest values measured were in the WSW group ($\approx$0.60, Table 5). These observations for WSW and SE Asia are consistent with those of *Sheridan et al.* [2002], who found mean values of $\omega_o \approx 0.80$ for their most polluted sector at altitudes above 3 km during INDOEX.

[46] If the soot and sulfate present in SE Asia and WSW are externally mixed, the mean ω_o indicates ammonium sulfate dominates the mixture (constituting about 80% of the mass [*Seinfeld and Pandis*, 1998]). If however, these constituents are internally mixed, e.g., a soot core, with a sulfate coating, then these materials each contribute about 50% by mass to the mixture on average. An aerosol population for these regions consisting of approximately 80% sulfate and 20% soot is consistent with the findings of *Bush and Valero* [2002], who found during INDOEX that an aerosol mixture with 83% from highly scattering sulfate-type aerosols and 17% from absorptive soot-type aerosols could best explain the total aerosol optical depth at 500 nm. Further, they found similar contributions whether the observation was made on days with relatively low or high aerosol concentrations, suggesting the composition remains consistent, despite differences in total aerosol concentrations. In the NNW and Channel sectors, which exhibit larger mean ω_o, sulfate dominates the mixture whether it is internally or externally mixed.

4. Summary

[47] We have presented the chemical and physical aerosol data obtained on the DC-8 platform during TRACE-P, grouped based on back trajectories into four sectors and divided into three altitude levels. The four sectors represent long range transport from the west (WSW), regional circulation over the western Pacific and Southeast Asia (SE Asia), polluted transport from northern Asia with substantial sea salt at low altitudes (NNW) and a substantial amount of dust (Channel).

[48] The highest mean mixing ratios of water-soluble ions and soot were observed at the lowest altitudes (<2 km) in the Channel sector, with 217 nmol/m^3 Ca^{2+}, 148 nmol/m^3 NH_4^+, 129 nmol/m^3 $SO_4^=$, 108 nmol/m^3 NO_3^-, and 2201 ng/m^3 soot. NNW had the highest mean sea salt mixing ratios, 105 nmol/m^3 Na^+ and 104 nmol/m^3 Cl^-, while NH_4^+ and $SO_4^=$ were about a factor of 2 lower than those in low altitude Channel and Ca^{2+} was an order of magnitude lower (14 nmol/m^3). Low altitude SE Asia had lower mixing ratios in general, with Na^+, Cl^-, and Ca^{2+} < 10 nmol/m^3 and NH_4^+ and $SO_4^=$ about 30 nmol/m^3. However, soot is relatively important in this region, contributing 638 ng/m^3 in the low altitude samples and 219 ng/m^3 in the midaltitude samples on average. WSW has generally low mixing ratios at both middle and high altitudes, with no species >10 nmol/m^3 and <100 ng/m^3 of soot.

[49] The bulk of the aerosol mass (determined from soot, sea salt, dust, and water-soluble inorganic ions, no organic species included here) exported from Asia emanates from Channel below 2 km altitude, 134 μg/m^3 on average, compared with 50 μg/m^3 at these altitudes from NNW. Between 2 and 7 km, Channel still exports the most particulate material, averaging 50 μg/m^3 compared with 7, 4, and 3 μg/m^3 from NNW, SE Asia, and WSW, respectively. At high altitudes <4 μg/m^3 is exported on average, from all sectors.

[50] Dust contributes 79% of the mass in the Channel sector, followed by non-sea-salt water-soluble inorganic species (17%) below 2 km. At these altitudes, NNW aerosol has comparable amounts of sea salt, dust, and non-sea-salts, 33%, 28%, and 36%, respectively. The bulk of the mass for both SE Asia and WSW is due to non-sea-salt water-soluble inorganic species, although SE Asia also contains a relatively high proportion of soot, 12% at low altitudes, 7% between 2 and 7 km.

[51] The aerosol physical data is consistent with the chemical data. Number density and volume distributions support the chemical data showing enhanced fine particles in Channel and NNW as well as enhanced supermicron volumes for these sectors due to sea salt and dust. The highest condensation nuclei number densities are in the Channel sector at low altitudes, with ultrafine particles >4 nm exceeding 17,000 particles/cm^3 on average. At midaltitudes (2–7 km) mean condensation nuclei number densities are at their lowest ($\approx$1000 particles cm^{-3}), while the nonvolatile fraction is at its highest (51% NNW, $\geq$65% for the other groups). This is attributed to wet scavenging which removes hygroscopic CN particles.

[52] Enhanced scattering (>80 Mm^{-1}) in the Channel sector is attributed to the high densities of fine particles compared to other groups. Angstrom exponents show good agreement with the volume measurements, yielding the lowest mean values in the dusty Channel sector. The single scatter albedo reflects the enhanced soot in the SE Asia sector, with mean values of about 0.80. The polluted sectors, NNW and Channel have means ranging from 0.84–0.93.

[53] The industrialization of Asia is expected to continue, leading to an increase in emissions of both gases and particulates. Throughout this TRACE-P special section, aerosols are shown to play various important roles in the composition and evolution of Asian outflow. Aerosols exhibit extreme spatial and temporal heterogeneity complicating their representation in regional and global models.

This overview has tried to provide a context for better understanding the composition, physical properties, and distribution of aerosols measured during TRACE-P, and their role in the export and evolution of Asian continental outflow.

[54] **Acknowledgments.** The authors are grateful for the extensive assistance provided by John Holdzkom and Sarah Bittenbender for the 3-D visualization of the back trajectories in vGeo. The authors also wish to thank the NASA Global Tropospheric Chemistry Program and the National Research Council for their support of this work.

References

Anderson, T. L., et al., Performance characteristics of a high-sensitivity, three wavelength, total scatter/backscatter nephelometers, *J. Atmos. Oceanic Technol.*, *13*, 967–986, 1996.

Bates, T. S., D. J. Coffman, D. S. Covert, and P. K. Quinn, Regional marine boundary layer aerosol size distributions in the Indian, Atlantic, and Pacific Oceans: A comparison of INDOEX measurements with ACE-1, ACE-2, and Aerosols99, *J. Geophys. Res.*, *107*(D19), 8026, doi:10.1029/2001JD001174, 2002.

Blake, N., et al., NMHCs and halocarbons in Asian continental outflow during Transport and Chemical Evolution Over the Pacific (TRACE-P): Comparison With PEM-West B, *J. Geophys. Res.*, *108*(D20), 8806, doi:10.1029/2002JD003367, 2003.

Bodhaine, B. A., et al., Three-wavelength nephelometer suitable for aircraft measurement of background aerosol scattering coefficient, *Atmos. Environ.*, *25A*, 2267–2276, 1991.

Bond, C. T., et al., Calibration and intercomparison of filter-based measurements of visible light absorption by aerosols, *Aerosol Sci. Technol.*, *30*, 582–600, 1999.

Bush, B. C., and F. P. J. Valero, Spectral aerosol radiative forcing at the surface during the Indian Ocean Experiment (INDOEX), *J. Geophys. Res.*, *107*(D19), 8003, doi:10.1029/2000JD000020, 2002.

Charlson, R. J., et al., Climate forcing by anthropogenic aerosols, *Science*, *255*, 423–430, 1992.

Crawford, J., et al., Clouds and trace gas distributions during TRACE-P, *J. Geophys. Res.*, *108*(D21), 8818, doi:10.1029/2002JD003177, in press, 2003.

Delene, D. J., and J. A. Ogren, Variability of aerosol optical properties at four North American surface monitoring sites, *J. Atmos. Sci.*, *59*, 1135–1150, 2002.

Dibb, J. E., R. W. Talbot, E. M. Scheuer, D. R. Blake, N. J. Blake, G. L. Gregory, G. W. Sachse, and D. C. Thornton, Aerosol chemical composition and distribution during the Pacific Exploratory Mission, Tropics, *J. Geophys. Res.*, *104*, 5785–5800, 1999.

Dibb, J. E., R. W. Talbot, and E. M. Scheuer, Composition and distribution of aerosols over the North Atlantic during the Subsonic Assessment Ozone and Nitrogen Oxide Experiment (SONEX), *J. Geophys. Res.*, *105*, 3709–3717, 2000.

Dibb, J. E., R. W. Talbot, G. Seid, C. Jordan, E. Scheuer, E. Atlas, N. J. Blake, and D. R. Blake, Airborne sampling of aerosol particles: Comparison between surface sampling at Christmas Island and P-3 sampling during PEM-Tropics B, *J. Geophys. Res.*, *107*, 8230, doi:10.1029/2001JD000408, 2002. [printed *108*(D2), 2003]

Dibb, J. E., R. W. Talbot, E. Scheuer, G. Seid, M. Avery, and H. Singh, Aerosol chemical composition in Asian continental outflow during the Transport and Chemical Evolution Over the Pacific (TRACE-P): Comparison with PEM-West B, *J. Geophys. Res.*, *108*(D21), 8815, doi:10.1029/2002JD003111, in press, 2003.

Fuelberg, H. E., R. O. Loring Jr., M. V. Watson, M. C. Sinha, K. E. Pickering, A. M. Thompson, G. W. Sachse, D. R. Blake, and M. R. Schoeberl, TRACE-A Trajectory Intercomparison: 2. Isentropic and kinematic methods, *J. Geophys. Res.*, *101*, 23,927–23,939, 1996.

Fuelberg, H. E., R. E. Newell, S. P. Longmore, W. Zhu, D. J. Westberg, E. V. Browell, D. R. Blake, G. L. Gregory, and G. W. Sachse, A meteorological overview of the PEM-Tropics period, *J. Geophys. Res.*, *104*, 5585–5622, 1999.

Fuelberg, H. E., J. R. Hannan, P. F. J. van Velthoven, E. V. Browell, G. Bieberbach Jr., R. D. Knabb, G. L. Gregory, K. E. Pickering, and H. B. Selkirk, A meteorological overview of the SONEX period, *J. Geophys. Res.*, *105*, 3633–3651, 2000.

Fuelberg, H. E., C. M. Kiley, J. R. Hannan, D. J. Westberg, M. A. Avery, and R. E. Newell, Meteorological conditions and transport pathways during the Transport and Chemical Evolution over the Pacific (TRACE-P) experiment, *J. Geophys. Res.*, *108*(D20), 8782, doi:10.1029/2002JD003092, 2003.

Hasegawa, S., and S. Ohta, Some measurements of the mixing state of soot containing particles at urban and non-urban sites, *Atmos. Environ.*, *36*, 3899–3908, 2002.

Heald, C., D. J. Jacob, P. I. Palmer, M. J. Evans, G. W. Sachse, H. B. Singh, and D. R. Blake, Biomass burning emission inventory with daily resolution: Application to aircraft observations of Asian outflow, *J. Geophys. Res.*, *108*(D21), 8811, doi:10.1029/2002JD003082, in press, 2003.

Huebert, B. J., T. Bates, P. B. Russell, G. Shi, Y. J. Kim, K. Kawamura, G. Carmichael, and T. Nakajima, An overview of ACE-Asia: Strategies for quantifying the relationships between Asian aerosols and their climatic impacts, *J. Geophys. Res.*, *108*(DXX), doi:10.1029/2003JD003550, in press, 2003.

Jacob, D. J., J. H. Crawford, M. M. Kleb, V. S. Connors, R. J. Bendura, J. L. Raper, G. W. Sachse, J. C. Gille, L. Emmons, and C. L. Heald, Transport and Chemical Evolution Over the Pacific (TRACE-P) mission: Design, execution, and first results, *J. Geophys. Res.*, *108*(D20), 9000, doi:10.1029/2002JD003276, 2003.

Jordan, C. E., J. E. Dibb, B. E. Anderson, and H. E. Fuelberg, Uptake of nitrate and sulfate on dust aerosols during TRACE-P, *J. Geophys. Res.*, *108*(D21), 8817, doi:10.1029/2002JD003101, 2003.

Kahl, J. D., A cautionary note on the use of air trajectories in interpreting atmospheric chemistry measurements, *Atmos. Environ.*, *27A*, 3037–3038, 1993.

Kasten, F., Visibility forecast in the phase of pre-condensation, *Tellus*, *21*(5), 631–635, 1969.

Lefer, B., R. E. Shetter, S. R. Hall, J. H. Crawford, and J. R. Olson, Impact of clouds and aerosols on photolysis frequencies and photochemistry during TRACE-P: 1. Analysis using radiative transfer and photochemical box models, *J. Geophys. Res.*, *108*(D21), 8821, doi:10.1029/2002JD003171, in press, 2003.

Li, Q., D. J. Jacob, R. M. Yantosca, C. L. Heald, H. Singh, M. Koike, Y. Zhao, G. W. Sachse, and D. Streets, A global three-dimensional model analysis of the atmospheric budgets of HCN and CH_3CN: Constraints from aircraft and ground measurements, *J. Geophys. Res.*, *108*(D21), 8827, doi:10.1029/2002JD003075, 2003.

Liu, H., D. J. Jacob, I. Bey, R. M. Yantosca, B. N. Duncan, and G. W. Sachse, Transport pathways for Asian combustion outflow over the Pacific: Interannual and seasonal variations, *J. Geophys. Res.*, *108*(D20), 8786, doi:10.1029/2002JD003102, 2003.

Ma, Y., et al., Characteristics and influence of biosmoke on the fine-particle ionic composition measured in Asian outflow during the Transport and Chemical Evolution Over the Pacific (TRACE-P) experiment, *J. Geophys. Res.*, *108*(D21), 8816, doi:10.1029/2002JD003128, in press, 2003.

Maloney, J. C., H. E. Fuelberg, M. A. Avery, J. H. Crawford, D. R. Blake, B. G. Heikes, G. W. Sachse, S. T. Sandholm, H. Singh, and R. W. Talbot, Chemical characteristics of air from different source regions during the second Pacific Exploratory Mission in the Tropics (PEM-Tropics B), *J. Geophys. Res.*, *106*, 32,609–32,625, 2001.

Mayol-Bracero, O. L., R. Gabriel, M. O. Andreae, T. W. Kirchstetter, T. Novakov, J. Ogren, P. Sheridan, and D. G. Streets, Carbonaceous aerosols over the Indian Ocean during the Indian Ocean Experiment (INDOEX): Chemical characterization, optical properties, and probable sources, *J. Geophys. Res.*, *107*(D19), 8030, doi:10.1029/2000JD000039, 2002.

Price, H. U., D. A. Jaffe, P. V. Doskey, I. McKendry, and T. Anderson, Vertical profiles of O_3, aerosols, CO and NMHCs in the northeast Pacific during the TRACE-P and ACE-ASIA experiments, *J. Geophys. Res.*, *108*(D20), 8799, doi:10.1029/2002JD002930, 2003.

Quinn, P. K., T. L. Miller, T. S. Bates, J. A. Ogren, E. Andrews, and G. E. Shaw, A 3-year record of simultaneously measured aerosol chemical and optical properties at Barrow, Alaska, *J. Geophys. Res.*, *107*(D11), 4130, doi:10.1029/2001JD001248, 2002a.

Quinn, P. K., D. J. Coffman, T. S. Bates, T. L. Miller, J. E. Johnson, E. J. Welton, C. Neusüss, M. Miller, and P. J. Sheridan, Aerosol optical properties during INDOEX 1999: Means, variability, and controlling factors, *J. Geophys. Res.*, *107*(D19), 8020, doi:10.1029/2000JD000037, 2002b.

Russo, R., et al., Chemical composition of Asian continental outflow over the western Pacific: Results from Transport and Chemical Evolution over the Pacific (TRACE-P), *J. Geophys. Res.*, *108*(D20), 8804, doi:10.1029/2002JD003184, 2003.

Seinfeld, J. H., and S. N. Pandis, *Atmospheric Chemistry and Physics: From Air Pollution to Climate Change*, John Wiley, Hoboken, N. J., 1998.

Sheridan, P. J., A. Jefferson, and J. A. Ogren, Spatial variability of submicrometer aerosol radiative properties over the Indian Ocean during INDOEX, *J. Geophys. Res.*, *107*(D19), 8011, doi:10.1029/2000JD000166, 2002.

Singh, H. B., et al., In situ measurements of HCN and CH_3CN over the Pacific Ocean: Sources, sinks, and budgets, *J. Geophys. Res.*, *108*(D20), 8795, doi:10.1029/2002JD003006, 2003.

Song, C. H., and G. R. Carmichael, Gas-particle partitioning of nitric acid modulated by alkaline aerosol, *J. Atmos. Chem.*, *40*, 1–22, 2001.

Stohl, A., Computation, accuracy, and applications of trajectories—A review and bibliography, *Atmos. Environ.*, *32*, 947–966, 1998.

Stohl, A., G. Wotawa, P. Seibert, and H. Kromp-Kolb, Interpolation errors in wind fields as a function of spatial and temporal resolution and their impact on different types of kinematic trajectories, *J. Appl. Meteorol.*, *34*, 2149–2165, 1995.

Streets, D., et al., An inventory of gaseous and primary aerosol emissions in Asia in the year 2000, *J. Geophys. Res.*, *108*(D21), 8809, doi:10.1029/2002JD003093, in press, 2003.

Sun, J., M. Zhang, and L. Tungsheng, Spatial and temporal characteristics of dust storms in China and its surrounding regions, 1960–1999: Relations to source area and climate, *J. Geophys. Res.*, *106*, 10,325–10,333, 2001.

Talbot, R., et al., Reactive nitrogen in Asian continental outflow over the western Pacific: Results from the NASA TRACE-P airborne mission, *J. Geophys. Res.*, *108*(D20), 8803, doi:10.1029/2002JD003129, 2003.

Tang, Y., et al., Impacts of aerosols and clouds on photolysis frequencies and photochemistry during TRACE-P: 2. Three-dimensional study using a regional chemical transport model, *J. Geophys. Res.*, *108*(D21), 8822, doi:10.1029/2002JD003100, in press, 2003a.

Tang, Y., et al., Influences of biomass burning during the Transport and Chemical Evolution Over the Pacific (TRACE-P) experiment identified by the regional chemical transport model, *J. Geophys. Res.*, *108*(D21), 8824, doi:10.1029/2002JD003110, in press, 2003b.

B. E. Anderson and C. H. Hudgins, Atmospheric Sciences Competency, NASA Langley Research Center, MS 483, Hampton, VA 23681, USA. (b.e.anderson@larc.nasa.gov)

J. E. Dibb and R. Russo, Climate Change Research Center, Institute for the Study of Earth, Oceans, and Space, University of New Hampshire, Durham, NH 03824, USA.

H. E. Fuelberg and C. M. Kiley, Department of Meteorology, Florida State University, Tallahassee, FL 32306, USA.

C. E. Jordan, National Research Council, NASA Langley Research Center, MS 483, Hampton, VA 23681, USA. (c.e.jordan@larc.nasa.gov)

E. Scheuer, G. Seid, and R. W. Talbot, Complex Systems Research Center, Institute for the Study of Earth, Oceans, and Space, University of New Hampshire, Durham, NH 03824, USA.

K. L. Thornhill, SAIC, NASA Langley Research Center, MS 483, Hampton, VA 23681, USA.

E. Winstead, GATS, NASA Langley Research Center, MS 483, Hampton, VA 23681, USA.

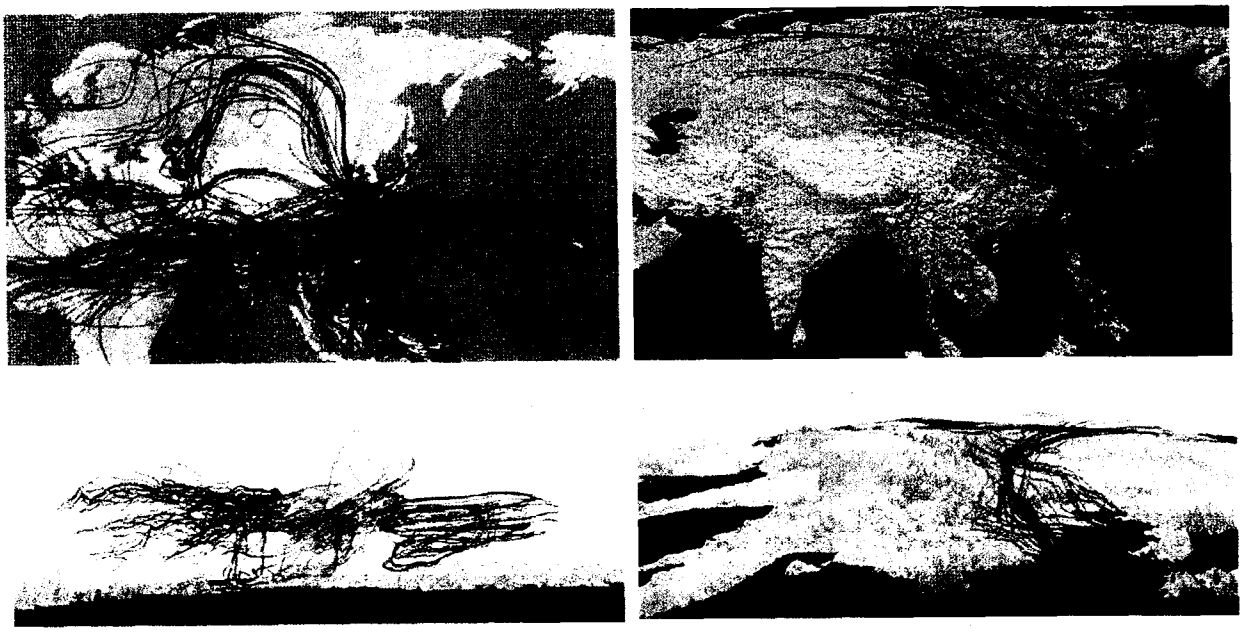

Figure 1. Back trajectories for the aerosol samples divided into four sectors. The top left panel shows trajectories for samples collected at altitudes >7 km. Only three sectors are represented at those altitudes, NNW (red), WSW (gold), and SE Asia (blue). The bottom left panel is a side view from the Pacific Ocean looking toward the Tibetan Plateau. This view shows these trajectories typically represent high altitude long distance transport. The top right panel shows trajectories for samples collected at altitudes <2 km. Only three sectors are represented at these altitudes, NNW (red), Channel (green), and SE Asia (blue). The bottom right panel shows only the low altitude Channel trajectories, angled to show that these trajectories flow along the surface and are confined by the surface topography.

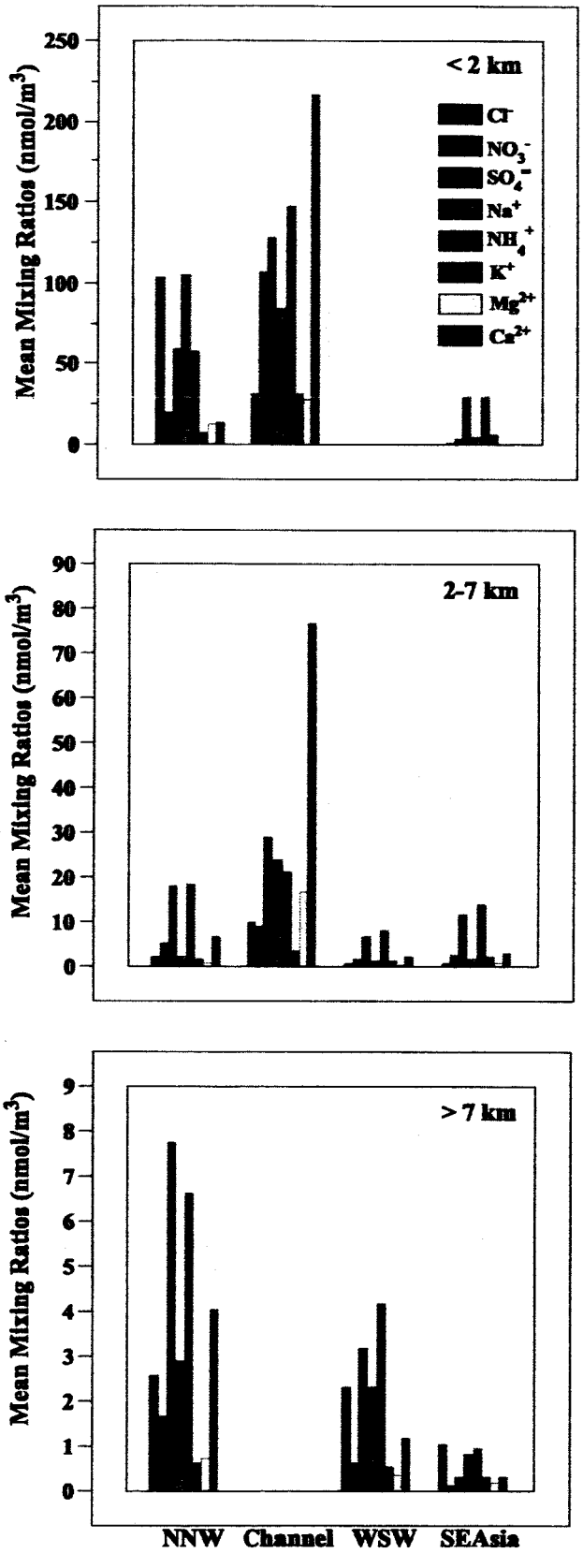

Figure 2. Aerosol mean chemical signatures for each group, split by altitude.

Uptake of nitrate and sulfate on dust aerosols during TRACE-P

C. E. Jordan,[1] J. E. Dibb,[2] B. E. Anderson,[1] and H. E. Fuelberg[3]

Received 30 October 2002; accepted 22 May 2003; published 24 September 2003.

[1] Aerosol data collected near Asia on the DC-8 aircraft platform during TRACE-P has been examined for evidence of uptake of NO_3^- and $SO_4^=$ on dust surfaces. Data is compared between a sector where dust was predominant and a sector where dust was less of an influence. Coincident with dust were higher mixing ratios of anthropogenic pollutants. HNO_3, SO_2, and CO were higher in the dust sector than the nondust sector by factors of 2.7, 6.2, and 1.5, respectively. The colocation of dust and pollution sources allowed for the uptake of NO_3^- and nss-$SO_4^=$ on the coarse dust aerosols, increasing the mixing ratios of these particulates by factors of 5.7 and 2.6 on average. There was sufficient nss-$SO_4^=$ to take up all of the NH_4^+ present, with enough excess nss-$SO_4^=$ to also react with dust $CaCO_3$. This suggests that the enhanced NO_3^- was not in fine mode NH_4NO_3. Particulate NO_3^- (p-NO_3^-) constituted 54% of the total NO_3^- (t-NO_3^-) on average, reaching a maximum of 72% in the dust sector. In the nondust sector, p-NO_3^- contributed 37% to t-NO_3^-, likely due to the abundance of sea salts there. In two other sectors where the influence of dust and sea salt were minimal, p-NO_3^- accounted for <15% of t-NO_3^-. *INDEX TERMS:* 0305 Atmospheric Composition and Structure: Aerosols and particles (0345, 4801); 0345 Atmospheric Composition and Structure: Pollution—urban and regional (0305); 0365 Atmospheric Composition and Structure: Troposphere—composition and chemistry; 0368 Atmospheric Composition and Structure: Troposphere—constituent transport and chemistry; *KEYWORDS:* heterogeneous uptake of nitrate, Asian dust, TRACE-P

Citation: Jordan, C. E., J. E. Dibb, B. E. Anderson, and H. E. Fuelberg, Uptake of nitrate and sulfate on dust aerosols during TRACE-P, *J. Geophys. Res.*, *108*(D21), 8817, doi:10.1029/2002JD003101, 2003.

1. Introduction

[2] The two primary objectives of NASA's Transport and Chemical Evolution over the Pacific (TRACE-P) mission were to characterize the sources and chemical composition of Asian outflow and to study the evolution of this outflow. As part of this mission, measurements of aerosol chemical and physical properties were made aboard the DC-8 aircraft [see *Jordan et al.*, 2003; *Dibb et al.*, 2003]. Samples clearly influenced by dust were obtained. Recent modeling and laboratory studies [e.g., *Zhang et al.*, 1994; *Dentener et al.*, 1996; *Xiao et al.*, 1997; *Goodman et al.*, 2000; *Phadnis and Carmichael*, 2000; *Song and Carmichael*, 2001a, 2001b; *Underwood et al.*, 2001] have suggested that alkaline dust particles can take up acids resulting in increased coarse mode NO_3^- and $SO_4^=$. In this paper, we report in situ evidence collected regionally aboard the DC-8 that supports prior indications that such uptake occurs in the atmosphere.

[3] Using 40 years of dust storm records, *Sun et al.* [2001] describe how dust is transported out of China. These dust storms occur predominantly in spring [*Liu*, 1985; *Sun et al.*, 2001] and are due to cold air outbreaks which cause frontal systems and the Mongolian cyclonic depression. About 78% of dust storms are associated with the Mongolian cyclone with the remainder associated solely with the passage of cold fronts [*Sun et al.*, 2001]. There are two dominant source regions of dust in East Asia, the gobi deserts in Mongolia and northern China, and the Taklimakan Desert in western China. Owing to the mountains surrounding the Taklimakan, dust can only be exported out of this region when strong easterlies loft dust above 5 km in altitude (the height of the mountains). At these heights, this dust becomes entrained in the jet stream and may then be transported long distances over the Pacific Ocean and to North America. Dust from the gobi deserts of Mongolia and northern China on the other hand, is generally lofted to altitudes <3 km and then transported in a southeasterly direction, depositing dust on the Loess Plateau, eastern Asia, and the western Pacific (Figure 1 [*Sun et al.*, 2001]).

[4] The mineralogy of loess at its source consists primarily of quartz (SiO_2), feldspars, micas, clays, carbonates (primarily $CaCO_3$), and several minor minerals [*Pye*, 1987; *Gao and Anderson*, 2001]. The carbonate content is relatively constant at 12% by weight in loess, dust, and ground surface samples [*Derbyshire et al.*, 1998]. *Nishikawa et al.* [1991] found that weight fractions of $SO_4^=$ in soils of arid regions of China ranged from <0.01% to 0.46%, insufficient to account for the high fraction of $SO_4^=$ in dust downwind

[1]NASA Langley Research Center, Hampton, Virginia, USA.
[2]Climate Change Research Center, Institute for the Study of Earth, Oceans, and Space, University of New Hampshire, Durham, New Hampshire, USA.
[3]Department of Meteorology, Florida State University, Tallahassee, Florida, USA.

0148-0227/03/2002JD003101$09.00

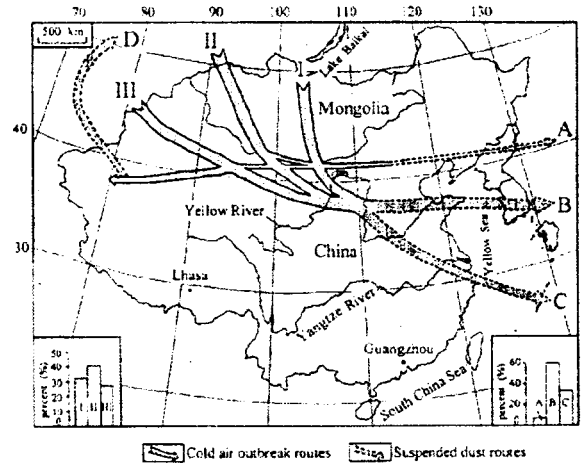

Figure 1. Map of cold air outbreaks and suspended dust routes in East Asia, from *Sun et al.* [2001].

of these regions. Individual dust particles from five dust storms in Beijing examined by *Zhang and Iwasaka* [1999] showed very little water-soluble $SO_4^=$ on the surface of these particles. Only ~15% of the particles had a sulfur peak; even fewer, 11%, showed any NO_3^-. This suggests that little chemical alteration takes place prior to reaching Beijing. Yet, samples collected in Qingdao, 500 km southeast of Beijing, showed 50–80% of the coarse particles (>2 μm diameter) were coated with $SO_4^=$ [*Parungo et al.*, 1995]. This chemical alteration then must occur downstream from Beijing.

[5] The presence of $CaCO_3$ in Asian dust is important because it reacts with acids such as sulfuric and nitric acid. In this way, dust particles may be chemically altered from their original composition at their source. Assuming the dust particles travel along a path where anthropogenic S and N sources are important, the surface area provided by the dust particles may lead to significant alteration of the air mass chemistry as SO_2 and HNO_3 transfer from gas to particulate phase [*Zhang et al.*, 1994; *Xiao et al.*, 1997; *Song and Carmichael*, 2001a, 2001b]. The presence of these acidic ions on dust can change the solubility of the aerosol from hydrophobic to hydrophilic [*Song and Carmichael*, 2001a].

[6] Evidence of $SO_4^=$ and NO_3^- on dust is found in studies of individual particles [e.g., *Wu and Okada*, 1994; *Parungo et al.*, 1995; *Gao and Anderson*, 2001] as well as studies of bulk aerosol composition [e.g., *Choi et al.*, 2001; *Kim and Park*, 2001] and precipitation [e.g., *Minoura et al.*, 1998]. Individual particles show both NO_3^- and $SO_4^=$ inclusions along with $CaCO_3$, as well as particles where all of the $CO_3^=$ has been replaced [*Wu and Okada*, 1994; *Parungo et al.*, 1995; *Gao and Anderson*, 2001]. Bulk aerosols from dust events show that the dominant water-soluble ions are $SO_4^=$, NO_3^-, Ca^{2+}, and Mg^{2+} [*Choi et al.*, 2001; *Kim and Park*, 2001]. Where size-resolved data is available, NO_3^- and $SO_4^=$ are found primarily in the coarse fraction associated with Ca^{2+} during dust events [*Kim and Park*, 2001]. In the absence of dust, $SO_4^=$ is primarily in the fine mode, while NO_3^- can be associated with either NH_4^+ in the fine mode [*Kim and Park*, 2001; *Song and Carmichael*, 2001a] or Na^+ in the coarse mode [*Song and Carmichael*, 2001a]. In precipitation in Japan the highest average concentrations of NO_3^-, $SO_4^=$, and Ca^{2+} are observed during Kosa (dust storm) events [*Minoura et al.*, 1998]. The low pH of precipitation during these dust events is attributed to the large amounts of acidic ions on the Kosa particles scavenged by the precipitation [*Minoura et al.*, 1998]. By the time dust particles reach Korea and Japan, ~75% of the carbonate has been displaced by $SO_4^=$ and NO_3^- [*Nishikawa et al.*, 1991].

[7] Various modeling studies have estimated the degree to which heterogeneous reactions contribute to the production of coarse mode $SO_4^=$ and NO_3^-. *Chameides and Stelson* [1992] estimated >70% of $SO_4^=$ formed by heterogeneous reactions. Using a regional three-dimensional (3-D) model for the period 1–14 March 1994, *Xiao et al.* [1997] estimated chemical conversion of SO_2 in the presence of dust contributed 20–40% to total $SO_4^=$ production in East Asia. *Song and Carmichael* [2001a], also using a regional 3-D model, found heterogeneous reactions account for 10–40% of $SO_4^=$ production in dust plumes and 10–80% in sea-salt-dominant regions. They attribute the greater production of $SO_4^=$ on sea salt versus dust to the dust mass distribution having a larger coarse fraction than sea salt.

[8] *Dentener et al.* [1996] looked at irreversible reactions of HNO_3, N_2O_5, NO_3, HO_2, O_3, and SO_y on dust surfaces. They predicted that a substantial fraction of $SO_4^=$ is associated with mineral aerosol. They also found that an even larger fraction of gas phase HNO_3 may be neutralized by mineral aerosol. *Phadnis and Carmichael* [2000] predict >70% of gas-phase HNO_3 is partitioned onto dust over the gobi deserts, while 10–70% of HNO_3 ends up in particulate phase over the rest of East Asia. *Song and Carmichael* [2001a] predict 10–50% of HNO_3 partitioned into NO_3^- in the boundary layer, with this partitioning exceeding 70% in dust and sea-salt plume centers. In the free troposphere, they predict 10–30% of HNO_3 partitioned into particulate phase, increasing to >50% in dust plume centers. *Song and Carmichael*'s model [2001a] also suggests that while NO_3^- resides primarily in coarse mode, in regions with abundant NH_3 and HNO_3, fine mode NH_4NO_3 may be found. The region where this is most likely to occur is around the lower Huang River, where there is high population density and agricultural activity [*Song and Carmichael*, 2001a].

[9] A laboratory study of the uptake of HNO_3 on $CaCO_3$ particles [*Goodman et al.*, 2000] found the reaction was limited to the particle surface in the absence of water. However, in the presence of water vapor the reaction was not limited to the surface of the particle. *Underwood et al.* [2001] studied the uptake of NO_2 and HNO_3 in the laboratory coupled with model calculations. They found that while uptake of NO_2 does not appear to be significant, uptake of HNO_3 is significant, with mixing ratios reduced by 30%. They note that this fraction is likely to increase under humid in situ conditions versus the dry conditions of their experiment.

[10] A companion paper [*Jordan et al.*, 2003] presents a thorough discussion of the DC-8 aerosol observations during TRACE-P in the context of four source regions based on back trajectories. These four sectors are NNW, Channel, WSW, and SE Asia (moving roughly counterclockwise from north to south). WSW and SE Asia samples were

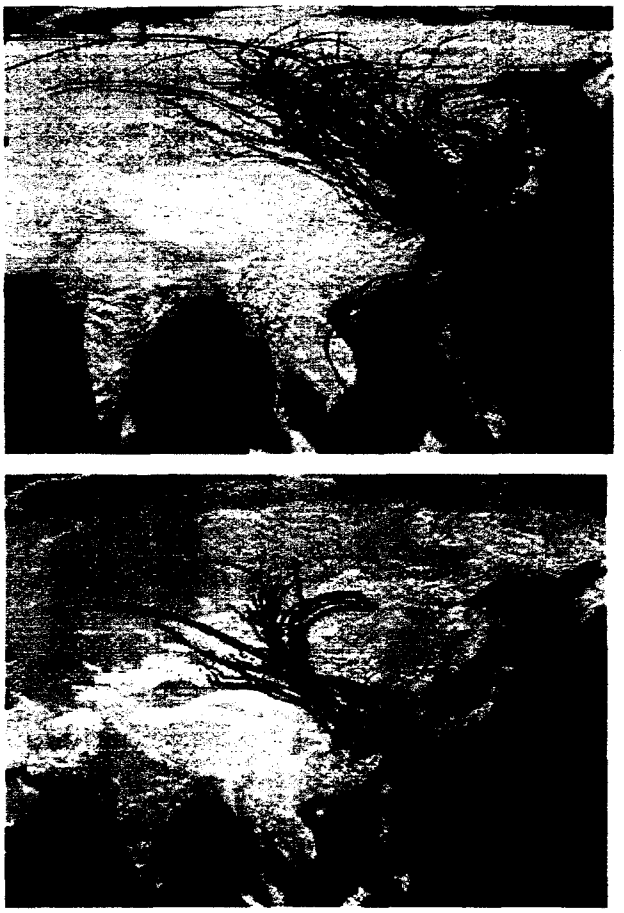

Figure 2. Back trajectories of the dust sector (Channel, green lines) and the nondust sector (NNW, red lines).

generally collected above 2 km altitude and represent relatively long range transport. NNW and Channel included many low altitude samples (<2 km) which were heavily influenced by sea salts (both sectors) and dust (Channel). Here we focus on these latter two sectors to look for evidence of gas to particle transfer of NO_3^- and $SO_4^=$.

2. Approach

[11] Back trajectories coupled with aerosol chemical data were used to classify the DC-8 TRACE-P aerosol data into four groups [*Jordan et al.*, 2003]. The back trajectories were calculated using a kinematic model based on global meteorological analyses from the European Centre for Medium-Range Weather Forecasts (ECMWF) [*Fuelberg et al.*, 2003]. The chemical samples were collected over periods ranging from ~5 to 35 min during level flight legs. The back trajectories were calculated every 5 min during level flight legs. Thus an individual aerosol sample might have anywhere from one to seven back trajectories associated with it. Samples that had multiple trajectories which emanated from more than one of the four sectors were classified as mixed and were not used any further in the analysis. The idea was to obtain a set of samples that represented a given sector with as little interference from other sectors as possible. In this way, 77 samples were obtained for the NNW sector, 38 for Channel, 31 for SE Asia, and 47 for WSW.

[12] NNW and Channel trajectories both emanate from northern Asia, with the Channel trajectories bounding the NNW trajectories to the south and west (Figure 2, top). The Channel trajectories themselves are bounded to the south by the Tibetan Plateau. WSW trajectories (not shown here) typically reflect high altitude, long range transport from the west as far away as Africa. SE Asia trajectories tend to circle over the western Pacific and southeast Asia. Both of these latter sectors have much lower mixing ratios of aerosols in general than the two former sectors, making them less appropriate for a comparison which tries to isolate the dust component. For a more extensive discussion of the sampling method and back trajectory calculations, please refer to the work of *Jordan et al.* [2003]. A complete discussion of the aerosol properties of each sector appears in that paper. Here the intention is to use just the Channel and NNW sectors to examine the influence of dust on aerosol chemistry, particularly, the uptake of NO_3^- and $SO_4^=$ on dust surfaces. Note that mixing ratios (pptv) were converted to moles or mass per unit volume using standard cubic meters rather than volumetric cubic meters (e.g., $\mu g\ m^{-3}$ STP or $\mu mol\ SCM^{-1}$).

3. Discussion

[13] *Sun et al.* [2001] described the pathways of the cold air outbreaks which lead to dust storms, as well as the pathways the suspended dust particles follow once suspended (Figure 1). Pathway I is followed by cold air masses near Lake Baikal which move southward across central Mongolia and China. Pathway II involves cold air masses in the northwest which result in dust storms along the Hexi Corridor (a northwest-southeast trending geographic region which connects the Xinjiang and Gansu provinces) and gobi deserts in northern China. Pathway III results in dust storms both in the Hexi Corridor and Taklimakan Desert. Most of the cold air outbreaks follow pathway II (41%), followed by pathway 3 (37%), and pathway I (32%). *Sun et al.* [2001] then break down the routes the suspended dust travels. Routes A, B, and C (Figure 1) carry dust from the gobi deserts in Mongolia and China depositing it en route to Korea, Japan, and the Pacific Ocean. Route B is most common (60%) followed by C (33%), then A (7%). Route D carries dust out of the Taklimakan Desert to high altitudes where it becomes entrained in the jet stream and is transported long distances downwind [*Sun et al.*, 2001].

[14] During TRACE-P, using aerosol chemistry coupled with back trajectories, we determined the path followed by the majority of the dust observed by the DC-8 [*Jordan et al.*, 2003]. The back trajectories for these dust samples (Figure 2, bottom) closely resemble the C and B routes described by *Sun et al.* [2001] (Figure 1).

[15] In order to investigate the role of dust in heterogeneous uptake of NO_3^- and $SO_4^=$, we compare the dust sector (Channel) to the adjacent sector (NNW). The primary distinction between these sectors is the presence of dust. However, Channel also has higher pollution inputs as well, as evidenced by gas phase species such as HNO_3 and CO (Table 1). This results in all aerosol species showing higher

Table 1. Means, Standard Deviations, Medians, Minima, Maxima, and Number of Samples for Various Aerosol and Gas Phase Species[a]

	NO_3^-, nmol/m^3	nss-$SO_4^=$, nmol/m^3	nss-Ca^{2+}, nmol/m^3	Na^+, nmol/m^3	NH_4^+, nmol/m^3	HNO_3, nmol/m^3	SO_2, nmol/m^3	CO, ppbv	Ethyne/CO, pptv/ppbv
				Channel					
Mean ± st. dev.	74 ± 110	91 ± 91	168 ± 177	64 ± 91	104 ± 115	44 ± 49	147 ± 173	258 ± 138	3.3 ± 1.1
Median (min.-max.)	40 (1–60)	78 (5–491)	115 (2–622)	26 (1–314)	92 (6–639)	33(6–264)	115(1–931)	256 (109–830)	3.2 (1.9–8.0)
No. of samples	38	38	38	38	38	38	33	38	38
				NNW					
Mean ± st. dev.	13 ± 16	35 ± 26	10 ± 12	57 ± 70	38 ± 29	17 ± 13	24 ± 36	176 ± 49	3.0 ± 0.8
Median (min.-max.)	6 (1–90)	31 (3–96)	5 (0–59)	12 (1–255)	26 (1–101)	17(3–61)	8(1–174)	185 (43–266)	3.1 (0.9–4.6)
No. of samples	77	77	77	77	77	76	62	77	75

[a]St. dev., standard deviation; min., minimum; max., maximum; no., number.

means in Channel than NNW except for Na^+. The primary source of Na^+ in the DC-8 measurements is sea salt; hence there is little difference between the mean mixing ratios for these groups.

[16] As discussed by *Keene et al.* [1986], Na^+ and Mg^{2+} are generally considered the best tracers of sea salt. However, this can become complicated when crustal sources add a significant amount to these species in coastal environments. Comparing the measured ratio of Mg^{2+}/Na^+ to the equivalence ratio of 0.227 found in bulk seawater [*Wilson*, 1975; *Keene et al.*, 1986], one can determine which species to use as the reference sea-salt species. A ratio in excess of 0.227 indicates a crustal Mg^{2+} influence, while a ratio less than this suggests a crustal Na^+ component. Here the data closely adheres to the sea-salt ratio for the NNW group (Figure 3). However, Mg^{2+} is clearly enhanced in Channel, altering the slope significantly from what one would expect for sea salt (Figure 3). Thus for this study, Na^+ is used as the reference species for sea salt, since it appears less likely to suffer from major deviations from the marine source. However, it is known that Na^+ is a component of Asian dust [*Song and Carmichael*, 2001b]. Hence in calculating the sea-salt and non-sea-salt components of the aerosol species reported here, the sea-salt component will be somewhat overestimated, leading to an underestimate of non-sea-salt species for the Channel group.

[17] The distribution of NO_3^-, HNO_3, nss-Ca^{2+}, Na^+, nss-$SO_4^=$, and NH_4^+ as a function of altitude show that most species are enhanced at low altitudes (Figure 4). Density ellipses which enclose 90% of the points within each group show Channel mixing ratios enhanced compared to those of NNW. The enhancement of NO_3^- may be due to three possible reaction routes: (1) uptake of HNO_3 by sea salt, (2) uptake of HNO_3 by alkaline dust, primarily by reaction with $CaCO_3$, or (3) formation of fine mode NH_4NO_3. The first pathway may be eliminated since there is little difference in the availability of Na^+ between Channel and NNW (Figure 4). Further, several of the high NO_3^- samples (circles in Figure 4) appear at low concentrations of Na^+. Four of the high NO_3^- samples (blue circles in Figure 4) do have high Na^+ concentrations; however, these samples also have the highest nss-Ca^{2+} measured (Figure 4). This suggests the high Na^+ in these samples is due to crustal dust rather than to sea salt. All of the high NO_3^- samples are also high nss-Ca^{2+} samples. In addition to the high NO_3^- markers (circles), there are many samples with enhanced dust (red squares in Figure 4). These samples do not have enhanced HNO_3, which suggests that both HNO_3 and nss-Ca^{2+} need to be enhanced to yield enhanced NO_3^- via uptake on dust. Another possible explanation for the enhanced NO_3^- may be the formation of fine mode NH_4NO_3 rather than coarse mode uptake of NO_3^-. All of the enhanced NO_3^- samples are observed to have enhanced NH_4^+ as well (Figure 4). Most of the markers also show enhanced nss-$SO_4^=$ (Figure 4). Hence both mechanisms 2 and 3 may be important.

[18] Taking nss-Ca^{2+} values >100 neq/m^3 to indicate enhanced dust, there are clearly two populations of NO_3^- (Figure 5). Samples where NO_3^- is $\gtrsim$ about 100 neq/m^3 (circles in Figure 5) tend to fall near the 1:1 line, although generally there is excess nss-Ca^{2+} compared to NO_3^-. The other population is denoted by red squares. For these samples, although nss-Ca^{2+} indicates an abundance of dust, there is little appreciable increase in NO_3^-. Note that the one green square indicates a sample that is likely to be predominantly sea salt, since it lies on the seawater slope shown in Figure 3. The blue circles in Figure 5 have NO_3^- in excess of 100 neq/m^3, yet they are well away from the 1:1 line. Given their very high amount of nss-Ca^{2+}, it is possible that either the sample was obtained prior to the air mass reaching chemical equilibrium between the dust and HNO_3, or there was insufficient HNO_3 to produce more particulate NO_3^-. The correlation between the black circles and nss-Ca^{2+} is

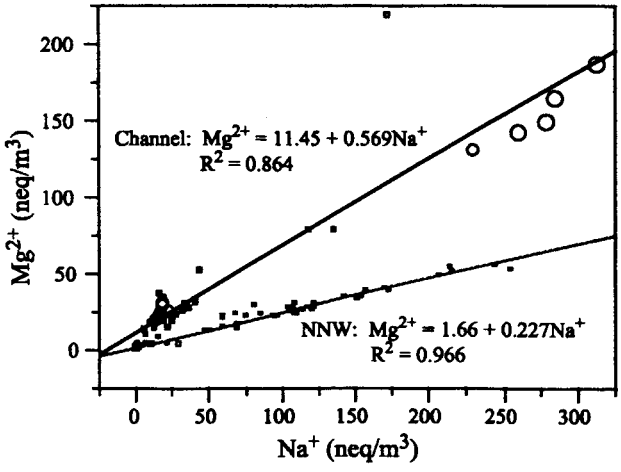

Figure 3. Mg^{2+} versus Na^+. Red linear fit to Channel data points; green fit to NNW data points. Circles indicate dust samples with enhanced NO_3^- and nss-$SO_4^=$. Red squares indicate dust samples without enhanced pollution species.

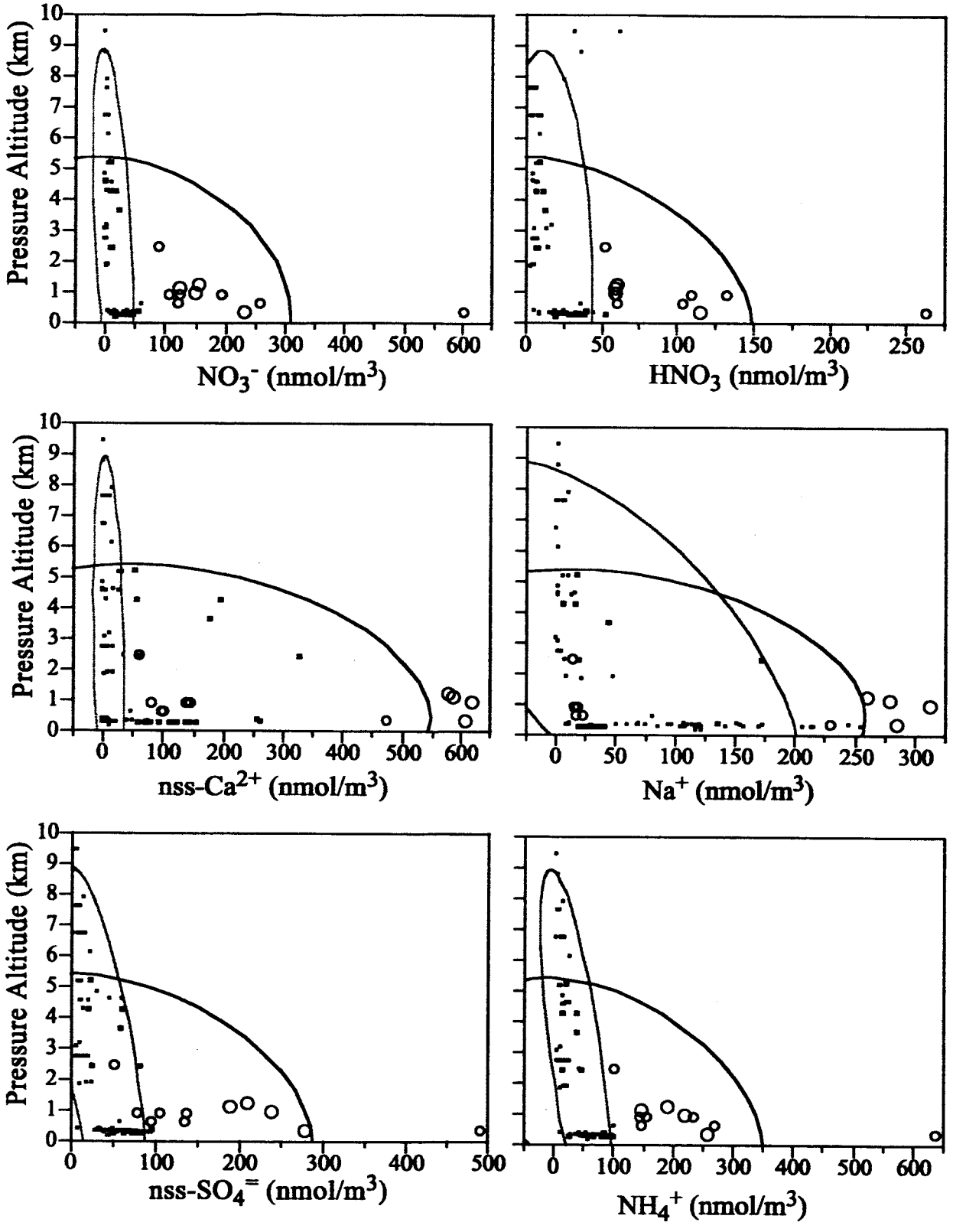

Figure 4. Aerosol and HNO_3 mixing ratios shown as a function of altitude. The density ellipses enclose 90% of the points within their respective groups, Channel (red ellipse) and NNW (green ellipse). Circles indicate dust samples with enhanced NO_3^- and nss-$SO_4^=$. Red squares indicate dust samples without enhanced pollution species.

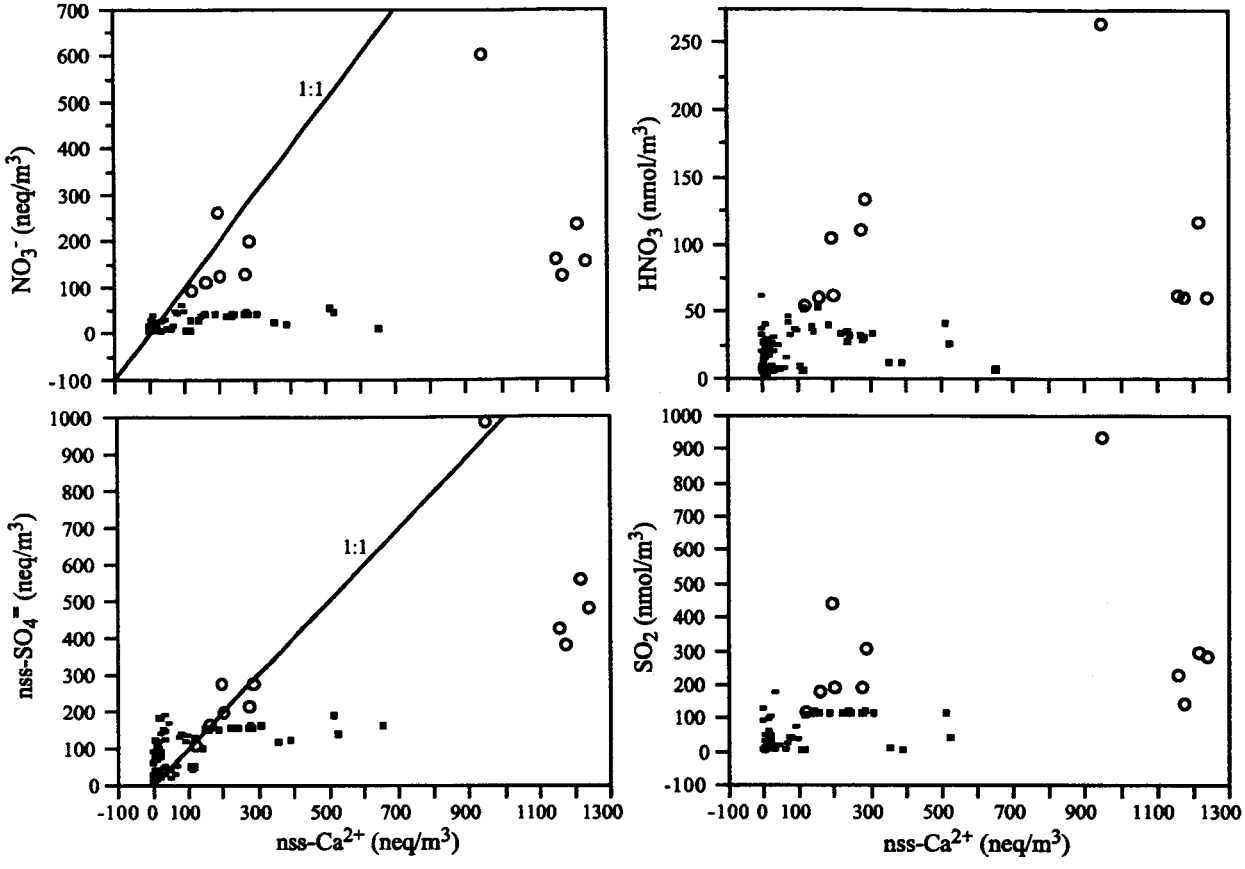

Figure 5. NO_3^-, nss-$SO_4^=$, HNO_3, and SO_2 shown as a function of dust (nss-Ca^{2+}). Circles indicate dust samples with enhanced NO_3^- and nss-$SO_4^=$. Red squares indicate dust samples without enhanced pollution species.

even closer to 1:1 for nss-$SO_4^=$ (Figure 5) than for NO_3^-. Again, there is little increase in nss-$SO_4^=$ with increasing nss-Ca^{2+} for the red square population. The blue circles are still set apart with respect to nss-$SO_4^=$ and nss-Ca^{2+}. HNO_3 and SO_2 (Figure 5), suggest the circles reflect the presence of higher levels of gas phase pollution than is present for the red squares (or the non-dust-enhanced black squares). This suggests that only dust intermingled with a sufficient amount of gas phase pollution will show significant uptake of NO_3^- and $SO_4^=$. Note that where nss-Ca^{2+} is low, there are still appreciable amounts of nss-$SO_4^=$. Presumably, this nss-$SO_4^=$ is due to uptake of nss-$SO_4^=$ on sea salts (coarse mode) or the presence of fine mode NH_4HSO_4 and $(NH_4)_2SO_4$. These results are similar to those reported by *Choi et al.* [2001]. They also reported cases in Seoul where some dust events were enhanced in pollution species, while other events were not.

[19] Next consider the possibility that the observed NO_3^- resides in fine mode NH_4NO_3 particles. There is a stunning correlation between NO_3^- and NH_4^+ (Figure 6), with the data points lying along the 1:1 line indicative of NH_4NO_3. There is some excess NH_4^+ compared to the NO_3^-, but not much. This suggests that particulate NO_3^- is in fine rather than coarse mode. However, the relationship between nss-$SO_4^=$ and NH_4^+ (Figure 6) argues against this scenario. There is clearly more than enough nss-$SO_4^=$ to accommodate all of the NH_4^+. Given the preferential formation of NH_4HSO_4 and $(NH_4)_2SO_4$ to that of the more volatile NH_4NO_3 for typical atmospheric temperatures and pressures, it seems unlikely that the bulk of NH_4^+ is associated with NO_3^- in this region. The correlation observed here may be coincidental. There are very good correlations between NH_4^+ and both HNO_3 and SO_2 (Figure 6) suggesting that NH_4^+ is simply a good tracer for pollutants. Investigating this possibility further, there are excellent correlations between CO and NH_4^+ (R^2 = 0.94) and Ethyne/CO and NH_4^+ (R^2 = 0.92) for the dust sector data (Figure 7). Both of these, CO and Ethyne/CO, are used as tracers for pollution. Neither one plays any role in the formation of NH_4^+, which supports the assertion that the good correlation between NH_4^+ and NO_3^- seen here is coincidental. Although modeling work by *Song and Carmichael* [2001a] suggests that NH_4NO_3 may form along the "lower courses of the Huang River" (which underlies the path of the dust flows), there is evidence suggesting that NO_3^- is associated with the coarse mode. *Wu and Okada* [1994] found coarse NO_3^- in all of their samples collected in Nagoya, Japan, including on the surface of dust particles during a Kosa event. Further, *Kim and Park* [2001] comparing samples during a dust storm and nondust periods in Seoul, Korea, found that the maximum concentration of NH_4^+ was in the fine mode (<2 μm diameter) under both conditions. Meanwhile, both $SO_4^=$ and NO_3^- were enhanced

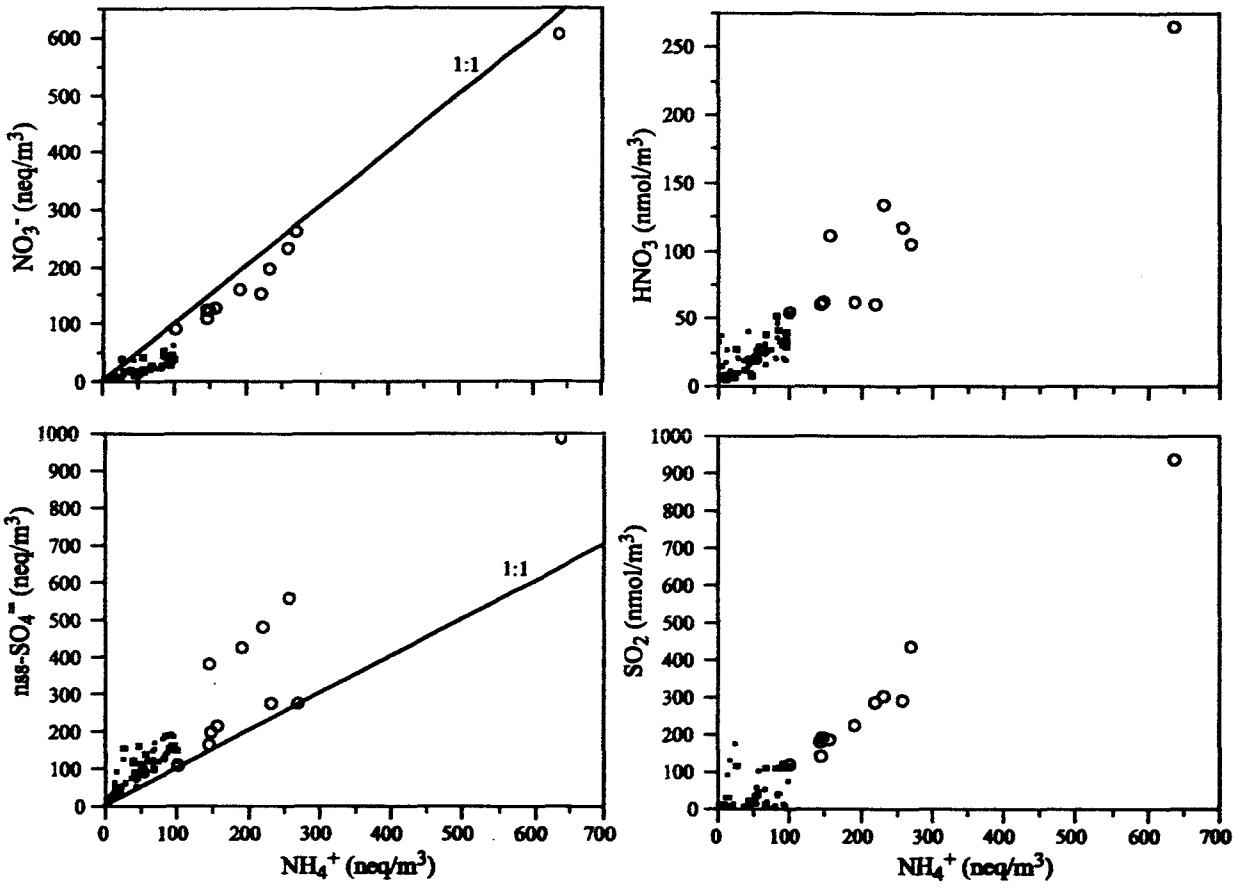

Figure 6. NO_3^-, nss-$SO_4^=$, HNO_3, and SO_2 shown as a function of NH_4^+. Circles indicate dust samples with enhanced NO_3^- and nss-$SO_4^=$. Red squares indicate dust samples without enhanced pollution species.

during the dust storm in the coarse fraction and were well correlated with coarse mode Ca^{2+}. In plots of *Kim and Park*'s [2001] size-resolved data, there is no evidence of a fine mode peak in NO_3^-. In the absence of size-resolved aerosol chemical measurements during TRACE-P, these observations argue against $SO_4^=$ and NO_3^- being primarily associated with NH_4^+ in the presence of dust.

[20] To estimate how much nss-$SO_4^=$ remains available for uptake on nss-Ca^{2+}, assume all particulate NH_4^+ is in the form of $(NH_4)_2SO_4$. Then, measured NH_4^+ equivalence is subtracted from measured nss-$SO_4^=$ equivalence to yield excess nss-$SO_4^=$ (Table 2). Further, NO_3^- is added to this excess nss-$SO_4^=$, and the sum is compared to nss-Ca^{2+} (Table 2). On average, 57% of the available nss-$SO_4^=$ can be taken up by NH_4^+, with the remainder available for uptake on dust and sea-salt surfaces. Even including NO_3^-, there is ample nss-Ca^{2+} to take up the measured NO_3^- and excess nss-$SO_4^=$. Indeed, even if there were no NH_4^+, the available nss-$SO_4^=$ and NO_3^- would only react with 76% of the available nss-Ca^{2+}.

[21] This suggests the uptake of nss-$SO_4^=$ and NO_3^-, in the heavily dust-impacted Channel samples, is limited by the amount of HNO_3 and SO_2 present, not by dust. Although, it is possible that all the available Ca^{2+} on the surface of the particles is associated with NO_3^- and $SO_4^=$, while the remaining Ca^{2+} is in the core of the particles where it cannot react with external gas phase species, this scenario is unlikely given the study by *Goodman et al.* [2000]. They found that in the presence of water vapor, the reaction of HNO_3 can proceed into the bulk of the particles driving off all of the $CO_3^=$. This makes all of the observed Ca^{2+} potentially available for reaction. Given this argument, the uptake observed during TRACE-P was probably limited by the availability of acidic gases, rather than dust.

[22] In comparison, in the NNW sector where dust is not so prevalent, there is insufficient nss-Ca^{2+} available to take up the available excess nss-$SO_4^=$ and NO_3^- (Table 2). Here these species are more likely to be associated with sea salt and are present at much lower levels than observed in the dust sector. To further illustrate this, Figure 8 shows excess nss-$SO_4^=$ versus nss-Ca^{2+}. If there was sufficient nss-$SO_4^=$ to react with all of the nss-Ca^{2+} present, the data would fall along the 1:1 line. In fact, where dust is not enhanced, there is more nss-$SO_4^=$ than can be accounted for by dust (black squares in Figure 8). This suggests this $SO_4^=$ is associated with fine mode NH_4^+ or perhaps with coarse mode sea salt. However, where there is plenty of dust (circles and red squares in Figure 8), excess nss-$SO_4^=$ is well correlated with nss-Ca^{2+} (R^2 = 0.87) with a slope of 0.2. Further, when NO_3^- is included in this analysis, the most polluted samples

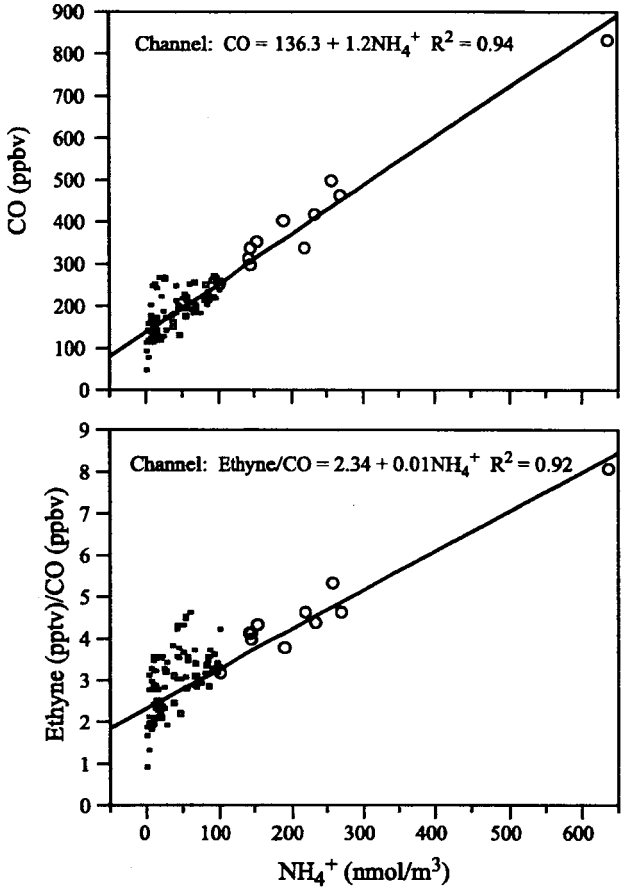

Figure 7. CO and Ethyne/CO versus $NH4^+$. All data from NNW and Channel are plotted, but only those from Channel are used for the linear fits. Circles indicate dust samples with enhanced NO_3^- and nss-$SO_4^=$. Red squares indicate dust samples without enhanced pollution species.

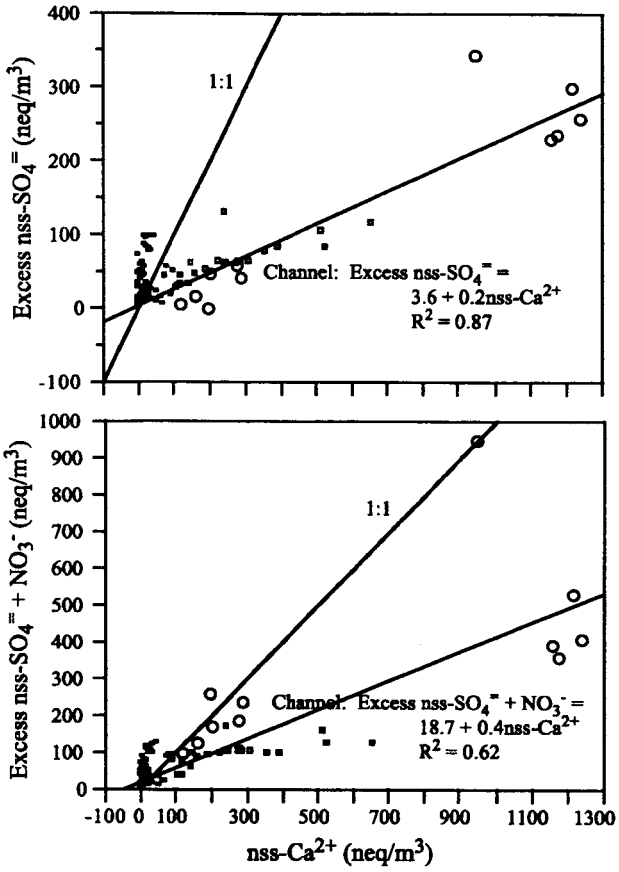

Figure 8. Excess nss-$SO_4^=$ and excess nss-$SO_4^=$ + NO_3^- versus nss-Ca^{2+} show how much of these species are available for uptake by dust after allowing NH_4^+ to take up as much nss-$SO_4^=$ as possible. Circles indicate dust samples with enhanced NO_3^- and nss-$SO_4^=$. Red squares indicate dust samples without enhanced pollution species.

are seen to lie along the 1:1 line (Figure 8), suggesting most of the $CO_3^=$ in the dust has been displaced. For the remainder of the dust enhanced samples, the uptake appears to be limited by the availability of HNO_3 and SO_2.

[23] This exercise probably underestimates the amount of excess nss-$SO_4^=$. As noted earlier, the non-sea-salt fractions have been underestimated, since some component of the Na^+ present is due to dust, even though it is all assumed to be sea salt. Thus the total amount of species in non-sea-salt fractions is somewhat higher than that shown here. Another issue to bear in mind comes from a study of individual particle composition. *Gao and Anderson* [2001] reported that fly ash particles (distinguishable from dust by their spherical rather than irregular shape) also show aggregation with $CaSO_4$. This is attributed to the use of $CaCO_3$ to scrub SO_2 from stack emissions. This can confound the interpre-

Table 2. Means, Standard Deviations, Medians, Minima, Maxima, and Number of Samples for Excess nss-$SO_4^=$ and NO_3^- Compared to Available Dust

	nss-$SO_4^=$, neq/m^3	NH_4^+, neq/m^3	Excess nss-$SO_4^=$, neq/m^3	NO_3^-, neq/m^3	Excess nss-$SO_4^=$ + NO_3^-, neq/m^3	nss-Ca^{2+}, neq/m^3
			Channel			
Mean ± st. dev.	182 ± 183	104 ± 115	78 ± 84	74 ± 110	152 ± 178	335 ± 353
Median (min.-max.)	156 (11–982)	92 (6–639)	58 (0–343)	40 (1–60)	103 (6–945)	229 (4–1245)
No. of samples	38	38	38	38	38	38
			NNW			
Mean ± st. dev.	70 ± 52	38 ± 29	32 ± 28	13 ± 16	45 ± 37	19 ± 24
Median (min.-max.)	62 (6–191)	26 (1–101)	23 (3–98)	6 (1–90)	39 (3–128)	12 (0–119)
No. of samples	77	77	77	77	77	74

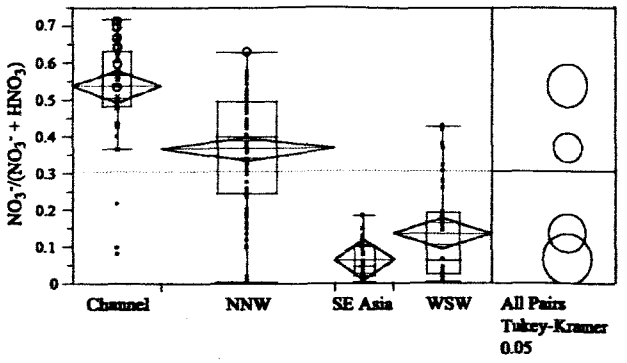

Figure 9. Comparison of NO_3^- partitioning between the dust sector (Channel), a sector with lots of sea salt (NNW), and two sectors where the influence of dust and sea salt are minimal (SE Asia and WSW). Green diamonds show means (center horizontal line) with the 95% confidence interval indicated by the upper and lower points of the diamonds, while the width of the diamond is proportional to the group size. Red rectangles show quantiles, with upper and lower bars indicating the 90th and 10th percentiles, respectively, top and bottom of box are at the 75th and 25th percentiles, respectively, and the red line in the box is the median. Circles on the right indicate whether the means are statistically different. The center of each circle is aligned with the mean of its respective group; the diameter of the circle spans the 95% confidence level. When the circles do not overlap, the means are significantly different. When they do overlap, the means may not be significantly different.

tation of non-size-resolved aerosol chemistry, because there will be a component of the nss-Ca^{2+} in the fine fraction which is not related to dust. However, in the presence of large dust outbreaks it is expected that this contribution to the total nss-Ca^{2+} will be small.

[24] Finally, the partitioning between particulate NO_3^- (p-NO_3^-) and gas phase HNO_3 is shown for dust (Channel) versus nondust (NNW) sectors (Figure 9). For comparison the partitioning is also shown for the other two sectors studied during TRACE-P, SE Asia and WSW. The samples from these sectors have minimal sea salt and dust influences (see *Jordan et al.* [2003] for a complete description of these sectors). Here we see that while the means for SE Asia and WSW may not be significantly different from each other, they are both significantly different from the other two, which are also significantly different from each other (Figure 9). For the groups least affected by the presence of sea salt and dust (SE Asia and WSW), the amount p-NO_3^- accounts for is only 6–13% of the total NO_3^- (t-NO_3^- = p-NO_3^- + HNO_3) present, on average (Table 3). Where dust is not a dominant component of the atmosphere (NNW), p-NO_3^- accounts for 37% of the t-NO_3^- on average, probably due to the influence of sea salts in this sector. For the dust sector, p-NO_3^- makes up 54% of the total on average, with maximum values of 72% observed (Table 3). These numbers agree well with those predicted by *Song and Carmichael* [2001a] where 10–50% of t-NO_3^- would be particulate in the presence of dust and sea salts, with >70% in dust and sea salt plume centers in the boundary layer, while in the free troposphere, 10–30% would be p-NO_3^- on sea salts and >50% in dust plume centers.

4. Summary

[25] Dust storms are prevalent in East Asia, with the dust being carried downwind along well-defined routes [*Sun et al.*, 2001]. This dust starts out with very little NO_3^- or $SO_4^=$ in the dust grains [*Nishikawa et al.*, 1991; and *Zhang and Iwasaka*, 1999]. However, in the presence of pollution, these dust particles can take up NO_3^- and $SO_4^=$, altering both the partitioning between particulate and gas phases of these species, as well as their size distributions in the atmosphere (especially, $SO_4^=$). During the TRACE-P mission, dust was found to be well confined to a particular sector emanating from Asia in good agreement with the routes described by *Sun et al.* [2001].

[26] This dust sector also contained the highest mixing ratios of pollutant species observed, with gas-phase HNO_3 2.7 times higher on average than in the adjacent nondust sector. Similarly, SO_2, CO, and the ratio of Ethyne/CO were 6.2, 1.5, and 1.1 times higher in the dust samples. Sea salt could not account for the enhancements in NO_3^- and $SO_4^=$ (factors of 5.7 and 2.6, respectively), since the mean mixing ratios of Na^+ in the dust and nondust regions were comparable (64 and 57 nmol/m^3, respectively). Although a good correlation between NO_3^- and NH_4^+ was observed, it appears that this was coincidental. As a tracer of anthropogenic species, NH_4^+ also exhibited excellent correlations with CO and the Ethyne/CO ratio (0.94 and 0.92, respectively). These species are not involved in any way with NH_4^+ formation. Prior observations in East Asia where size-resolved data was available did not show fine mode peaks of NO_3^- when dust was present. Further, calculations showed that there is ample nss-$SO_4^=$ to occupy the available NH_4^+ and still have enough left over to react with dust.

[27] During TRACE-P, the uptake of NO_3^- and $SO_4^=$ appeared to be limited by the availability of gas phase species. Where there is ample HNO_3 and SO_2 along with dust particles, the uptake of NO_3^- and $SO_4^=$ can be substantial and in some cases may entirely drive off the $CO_3^=$ in the dust aerosol. The partitioning between particulate and gas-phase NO_3^- shows 54% of the total NO_3^- (t-NO_3^-) in the dust sector is in particulate (p-NO_3^-) phase on average. In some samples, p-NO_3^- exceeded 70%. This is in good agreement with model predictions [*Song and Carmichael*, 2001a]. In the nondust sector, p-NO_3^- constituted 37% of t-NO_3^-, likely due to the heavy influence of sea salt. Two other sectors with little influence of dust or sea salt had p-NO_3^- contributing a small fraction to the total, <15%.

[28] These results provide evidence of in situ uptake of acidic gases on alkaline dust particles in support of model predictions and laboratory studies. This uptake may result in

Table 3. Means, Standard Deviations, Medians, Minima, Maxima, and Number of Samples for Nitrate Partition Comparison $NO_3^-/(NO_3^- + HNO_3)$

NNW	Channel	WSW	SE Asia
0.37 ± 0.16	0.54 ± 0.15	0.13 ± 0.13	0.06 ± 0.05
0.40 (0.00–0.63)	0.57 (0.08–0.72)	0.06 (0.00–0.43)	0.04 (0.00–0.18)
76	38	43	26

enhanced removal of nitrogen from the atmosphere, which may be important on regional scales. The presence of NO_3^- and $SO_4^=$ on coarse particles may lead to enhanced acid deposition along with its detrimental effects to terrestrial ecosystems than would be observed in regions without dust outbreaks. Enhanced deposition of NO_3^- to marine ecosystems may make more of this limiting nutrient available to the coastal biota. These effects may be magnified, if emissions of pollutant N and S increase with further industrialization in East Asia.

[29] **Acknowledgments.** The authors wish to thank the NASA Global Tropospheric Chemistry Program and the National Research Council for their support of this work.

References

Chameides, W. L., and A. W. Stelson, Aqueous phase chemical processes in deliquescent sea-salt aerosols: A mechanism that couples the atmospheric cycles of S and sea salt, *J. Geophys. Res.*, *97*, 20,565–20,580, 1992.

Choi, J. C., M. Lee, Y. Chun, J. Kim, and S. Oh, Chemical composition and source signature of spring aerosol in Seoul, Korea, *J. Geophys. Res.*, *106*, 18,067–18,074, 2001.

Dentener, F. J., G. R. Carmichael, Y. Zhang, J. Lelieveld, and P. J. Crutzen, Role of mineral aerosol as a reactive surface in the global troposphere, *J. Geophys. Res.*, *101*, 22,869–22,889, 1996.

Derbyshire, E., X. Meng, and R. A. Kemp, Provenance, transport and characteristics of modern aeolian dust in western Gansu Province, China, and interpretation of the Quaternary loess record, *J. Arid Environ.*, *39*, 497–516, 1998.

Dibb, J. E., R. W. Talbot, E. Scheuer, G. Seid, M. Avery, and H. Singh, Aerosol chemical composition in Asian continental outflow during Transport and Chemical Evolution over the Pacific, *J. Geophys. Res.*, *108*(D21), 8815, doi:10.1029/2002JD003111, in press, 2003.

Fuelberg, H. E., C. Kiley, J. R. Hannan, D. J. Westberg, M. A. Avery, and R. E. Newell, Meteorological conditions and transport pathways during the transport and chemical evolution over the Pacific experiment, *J. Geophys. Res.*, *108*(D20), 8782, doi:10.1029/2002JD003092, 2003.

Gao, Y., and J. R. Anderson, Characteristics of Chinese aerosols determined by individual particle analysis, *J. Geophys. Res.*, *106*, 18,037–18,045, 2001.

Goodman, A. L., G. M. Underwood, and V. H. Grassian, A laboratory study of the heterogeneous reaction of nitric acid on calcium carbonate particles, *J. Geophys. Res.*, *105*, 29,053–29,064, 2000.

Jordan, C. E., et al., Chemical and physical properties of bulk aerosols within four sectors observed during Transport and Chemical Evolution over the Pacific, *J. Geophys. Res.*, *108*(D21), 8813, doi:10.1029/2002JD003337, in press, 2003.

Keene, W. C., A. A. P. Pszenny, J. N. Galloway, and M. E. Hawley, Sea-salt corrections and interpretation of constituent ratios in marine precipitation, *J. Geophys. Res.*, *91*, 6647–6658, 1986.

Kim, B.-G., and S.-U. Park, Transport and evolution of a winter-time Yellow sand observed in Korea, *Atmos. Environ.*, *35*, 3191–3201, 2001.

Liu, T. S., *Loess and the Environment*, 251 pp., China Ocean, Beijing, 1985.

Minoura, H., S. Mizawa, and Y. Iwasaka, Seasonal changes in the concentrations of major cations and anions in precipitations in urban Nagoya, Japan: Local emission and long-range transport by Asian dust storms (KOSA) and typhoons, *J. Meteorol. Soc. Jpn.*, *76*, 13–27, 1998.

Nishikawa, M., S. Kanamori, N. Kanamori, and T. Misoguchi, Environmental significance of Kosa aerosol (yellow sand dust) collected in Japan, in *Proc. Second IUAPPA Reg. Conf. Air Pollut.*, pp. 35–41, Int. Union of Air Pollut. Prev. and Environ. Protect. Assoc., Brighton, UK, 1991.

Parungo, F., Y. Kim, C.-J. Zhu, J. Harris, R. Schnell, X.-S. Li, D.-Z. Yang, M.-Y. Zhou, Z. Chen, and K. Park, Asian dust storms and their effects on radiation and climate, *STC Rep. 2906*, Sci. and Tech. Corp., Hampton, Va., 1995.

Phadnis, M. J., and G. R. Carmichael, Influence of mineral aerosol on the tropospheric chemistry of East Asia, *J. Atmos. Chem.*, *36*, 285–323, 2000.

Pye, K., *Aeolian Dust and Dust Deposits*, Academic, San Diego, California, 1987.

Song, C. H., and G. R. Carmichael, A three-dimensional modeling investigation of the evolution processes of dust and sea-salt particles in East Asia, *J. Geophys. Res.*, *106*, 18,131–18,154, 2001a.

Song, C. H., and G. R. Carmichael, Gas-particle partitioning of nitric acid modulated by alkaline aerosol, *J. Atmos. Chem.*, *40*, 1–22, 2001b.

Sun, J., M. Zhang, and L. Tungsheng, Spatial and temporal characteristics of dust storms in China and its surrounding regions, 1960–1999: Relations to source area and climate, *J. Geophys. Res.*, *106*, 10,325–10,333, 2001.

Underwood, G. M., C. H. Song, M. Phadnis, G. R. Carmichael, and V. H. Grassian, Heterogeneous reactions of NO_2 and HNO_3 on oxides and mineral dust: A combined laboratory and modeling study, *J. Geophys. Res.*, *106*, 18,055–18,066, 2001.

Wilson, T. R. S., Salinity and the major elements of sea water, in *Chemical Oceanography*, vol. 1, 2nd ed., edited by J. P. Riley and G. Skirrow, pp. 365–413, Academic, San Diego, Calif., 1975.

Wu, P.-M., and K. Okada, Nature of coarse nitrate particles in the atmosphere—A single particle approach, *Atmos. Environ.*, *28*, 2053–2060, 1994.

Xiao, H., G. R. Carmichael, J. Durchenwald, D. Thornton, and A. Bandy, Long-range transport of SO_x and dust in East Asia during the PEM B experiment, *J. Geophys. Res.*, *102*, 28,589–28,612, 1997.

Zhang, D., and Y. Iwasaka, Nitrate and sulfate in individual Asian dust-storm particles in Beijing, China in spring of 1995 and 1996, *Atmos. Environ.*, *33*, 3213–3223, 1999.

Zhang, Y., Y. Sunwoo, V. Kotamarthi, and G. Carmichael, Photochemical oxidant processes in the presence of dust: An evaluation of the impact of dust on particulate nitrate and ozone formation, *J. Appl. Meteorol.*, *33*, 813–824, 1994.

B. E. Anderson and C. E. Jordan, NASA Langley Research Center, MS 483, Hampton, VA 23681, USA. (b.e.anderson@larc.nasa.gov; c.e.jordan@larc.nasa.gov)

J. E. Dibb, Climate Change Research Center, Institute for the Study of Earth, Oceans, and Space, University of New Hampshire, Durham, NH 03824, USA. (jack.dibb@unh.edu)

H. E. Fuelberg, Department of Meteorology, Florida State University, Tallahassee, FL 32306, USA. (Fuelberg@met.fsu.edu)

JOURNAL OF GEOPHYSICAL RESEARCH, VOL. 108, NO. D20, 8804, doi:10.1029/2002JD003184, 2003

Chemical composition of Asian continental outflow over the western Pacific: Results from Transport and Chemical Evolution over the Pacific (TRACE-P)

R. S. Russo,[1] R. W. Talbot,[1] J. E. Dibb,[1] E. Scheuer,[1] G. Seid,[1] C. E. Jordan,[3] H. E. Fuelberg,[2] G. W. Sachse,[3] M. A. Avery,[3] S. A. Vay,[3] D. R. Blake,[4] N. J. Blake,[4] E. Atlas,[5] A. Fried,[5] S. T. Sandholm,[6] D. Tan,[6] H. B. Singh,[7] J. Snow,[8] and B. G. Heikes[8]

Received 18 November 2002; revised 28 April 2003; accepted 13 May 2003; published 23 September 2003.

[1] We characterize the chemical composition of Asian continental outflow observed during the NASA Transport and Chemical Evolution over the Pacific (TRACE-P) mission during February–April 2001 in the western Pacific using data collected on the NASA DC-8 aircraft. A significant anthropogenic impact was present in the free troposphere and as far east as 150°E longitude reflecting rapid uplift and transport of continental emissions. Five-day backward trajectories were utilized to identify five principal Asian source regions of outflow: central, coastal, north-northwest (NNW), southeast (SE), and west-southwest (WSW). The maximum mixing ratios for several species, such as CO, C_2Cl_4, CH_3Cl, and hydrocarbons, were more than a factor of 2 larger in the boundary layer of the central and coastal regions due to industrial activity in East Asia. CO was well correlated with C_2H_2, C_2H_6, C_2Cl_4, and CH_3Cl at low altitudes in these two regions ($r^2 \sim 0.77–0.97$). The NNW, WSW, and SE regions were impacted by anthropogenic sources above the boundary layer presumably due to the longer transport distances of air masses to the western Pacific. Frontal and convective lifting of continental emissions was most likely responsible for the high altitude outflow in these three regions. Photochemical processing was influential in each source region resulting in enhanced mixing ratios of O_3, PAN, HNO_3, H_2O_2, and CH_3OOH. The air masses encountered in all five regions were composed of a complex mixture of photochemically aged air with more recent emissions mixed into the outflow as indicated by enhanced hydrocarbon ratios ($C_2H_2/CO \geq 3$ and $C_3H_8/C_2H_6 \geq 0.2$). Combustion, industrial activities, and the burning of biofuels and biomass all contributed to the chemical composition of air masses from each source region as demonstrated by the use of C_2H_2, C_2Cl_4, and CH_3Cl as atmospheric tracers. Mixing ratios of O_3, CO, C_2H_2, C_2H_6, SO_2, and C_2Cl_4 were compared for the TRACE-P and PEM-West B missions. In the more northern regions, O_3, CO, and SO_2 were higher at low altitudes during TRACE-P. In general, mixing ratios were fairly similar between the two missions in the southern regions. A comparison between CO/CO_2, CO/CH_4, C_2H_6/C_3H_8, NO_x/SO_2, and $NO_y/(SO_2 + nss\text{-}SO_4)$ ratios for the five source regions and for the 2000 Asian emissions summary showed very close agreement indicating that Asian emissions were well represented by the TRACE-P data and the emissions inventory. *INDEX TERMS:* 0365 Atmospheric Composition and Structure: Troposphere—composition and chemistry; 0368 Atmospheric Composition and Structure: Troposphere—constituent transport and chemistry; 0345 Atmospheric Composition and Structure: Pollution—urban and regional (0305)

Citation: Russo, R., et al., Chemical composition of Asian continental outflow over the western Pacific: Results from Transport and Chemical Evolution over the Pacific (TRACE-P), *J. Geophys. Res.*, *108*(D20), 8804, doi:10.1029/2002JD003184, 2003.

[1]University of New Hampshire, Durham, New Hampshire, USA.
[2]Florida State University, Tallahassee, Florida, USA.
[3]NASA Langley Research Center, Hampton, Virginia, USA.
[4]University of California, Irvine, Irvine, California, USA.
[5]National Center for Atmospheric Research, Boulder, Colorado, USA.
[6]Georgia Institute of Technology, Atlanta, Georgia, USA.
[7]NASA Ames Research Center, Moffett Field, California, USA.
[8]University of Rhode Island, Narragansett, Rhode Island, USA.

0148-0227/03/2002JD003184$09.00

1. Introduction

[2] The impact of industrialization and population growth in Asia on the composition of the western Pacific troposphere over the last several decades was not well documented, but it is likely to have been very significant. Recently, Asian anthropogenic emissions have been increasing, and for some species, such as SO_2 and NO_x, they are projected to continue increasing over the next 20 years [*Streets and Waldhoff*, 2000; *van Aardenne et al.*, 1999]. By

2020, China is predicted to be the largest emitter of NO_x in the world [*van Aardenne et al.*, 1999]. However, *Streets et al.* [2003] revealed that the economic downturn in Asia in the late 1990s resulted in lower SO_2 and NO_x emissions than expected. Owing to the potential of Asian emissions to modify the global tropospheric composition, it is crucial to the global community and to the formation of environmental policies to characterize and document these temporal variations in Asian emissions.

[3] It is well documented that Asian anthropogenic emissions and dust are transported over the North Pacific Ocean [e.g., *Duce et al.*, 1980; *Merrill et al.*, 1989; *Jaffe et al.*, 1999]. Several studies have documented the influence of Asian outflow on the western U. S. and the impact of rising Asian emissions on the global troposphere [e.g., *Berntsen et al.*, 1999; *Jacob et al.*, 1999; *Yienger et al.*, 2000]. The magnitude of this impact varies throughout the year due to different meteorological situations in the various seasons. During the summer and fall, the Pacific high is located over the western Pacific and inhibits outflow from the Asian continent. The high causes an easterly flow of aged marine air to the western Pacific. In the spring, this high-pressure system is displaced eastward allowing the rapid and direct transport of continental outflow from Asia to the western Pacific [*Bachmeier et al.*, 1996]. A strong Siberian high-pressure system is also present during winter [*Fuelberg et al.*, 2003]. These two high-pressure systems result in maximum outflow from the Asian continent occurring in the late winter and spring [*Merrill et al.*, 1989, 1997].

[4] Two previous aircraft missions were conducted to document the impact of seasonal variations in Asian outflow on the western Pacific. The Pacific Exploratory Mission (PEM)-West A was conducted in September–October 1991, and PEM-West B occurred in February–March 1994. Asian outflow was found to be the main contributor to the tropospheric composition below 5 km [*Talbot et al.*, 1997; *Gregory et al.*, 1997]. PEM-West B was characterized by two-fold enhancements in anthropogenic species, such as C_2H_2, C_2H_6, and C_3H_8, and decreased photochemical activity compared to PEM-West A. Increased source emissions and the winter/spring time period of PEM-West B were the presumed explanations for these differences. Wet convection was an important mechanism for transporting air to the upper troposphere during both missions [*Talbot et al.*, 1997]. The PEM-West missions provided valuable documentation of the trace gas and aerosol signatures of Asian outflow and information about the impact of Asian emissions on the western Pacific troposphere.

[5] A wide variety of pollution sources contribute emissions to the western Pacific troposphere because of differences in demographic and industrialization patterns. This results in specific sources being more predominant in certain regions of Asia. Fossil fuel combustion (e.g., electrical power generation) is the primary source of energy in Asia leading to emissions of SO_2, CO, CO_2, hydrocarbons, and reactive nitrogen species. China is the largest Asian source of SO_2 because of its use of high sulfur coal as a primary energy source [*Streets et al.*, 2003; *Carmichael et al.*, 2003b; *Kato and Akimoto*, 1992]. Biofuels (e.g., crop residues, fuel wood, animal waste, and charcoal) are estimated to be ~24 % of the total energy use [*Streets and Waldhoff*, 1998]. Biofuels are typically used for cooking and heating and are the dominant energy source in developing countries. Also, biomass burning is widespread in southeast Asia [*Crutzen and Andreae*, 1990]. As a result, emissions of CO, hydrocarbons, CH_3Cl, and nitrogen species are expected from SE Asia. The domestic sector of central China is an important source of both fossil fuel and biofuel emissions [*Carmichael et al.*, 2003b]. Industrial activities (i.e., petroleum refining, solvent usage, fuel evaporation during storage and transport, and natural gas leakage) have a considerable impact on the tropospheric composition of East Asia and result in emissions of C_2Cl_4, CCl_4, CH_3CCl_3, and CFCs [*Blake et al.*, 1996]. Also, biogenic (i.e., vegetation, ocean) emission and uptake processes influence the composition of the western Pacific [e.g., *Talbot et al.*, 1996a, 1997].

[6] The focus of the NASA TRACE-P mission was to provide a comprehensive assessment of the impact of these various pollution sources on the atmospheric composition of the western Pacific and to study the chemical evolution and aging of Asian outflow. A secondary goal of TRACE-P was to determine if increasing Asian emissions over the past decade had a measurable impact on the tropospheric chemistry over the western Pacific and if the emission projections were substantially correct. A variety of methods were used to analyze and study the TRACE-P data, including examining the partitioning of specific species, models, emission inventories, meteorology patterns, transport mechanisms, and air mass trajectories. The results are presented in the many companion papers in this issue. In this paper we characterize and compare the chemical composition of outflow originating from the predominant source regions identified on the Asian continent and its transport to the western Pacific.

2. Experiment

[7] The TRACE-P mission was conducted during February–April 2001. The scientific rationale for the mission, species measurement details, and descriptions of the individual flights are presented in the TRACE-P overview paper [*Jacob et al.*, 2003]. The large-scale meteorology of the region during February–April 2001 and air mass trajectory details are described by *Fuelberg et al.* [2003]. The measurements used in this paper were made on the NASA Dryden DC-8 aircraft. The mission was composed of 17 transit and science intensive flights in the geographic region of 0–50°N latitude and 110–180°E longitude. The aircraft flew at altitudes ranging from 0.3 to 12.5 km. Flight 6 was a transit flight from Guam to Hong Kong, Flights 7–12 were based out of Hong Kong, and Flights 13–17 were based out of Yokota Air Force Base, Japan.

3. Database

[8] The data utilized in this paper was collected during Flights 6–17 within the geographic region of 10–45°N latitude and 110–150°E longitude. Merged data products for specific time intervals were created by NASA Langley Research Center due to the wide range of measurement time resolutions for the various species. The data presented in this paper was averaged to a 1 min time resolution. Measurements reported as below the limit of detection of

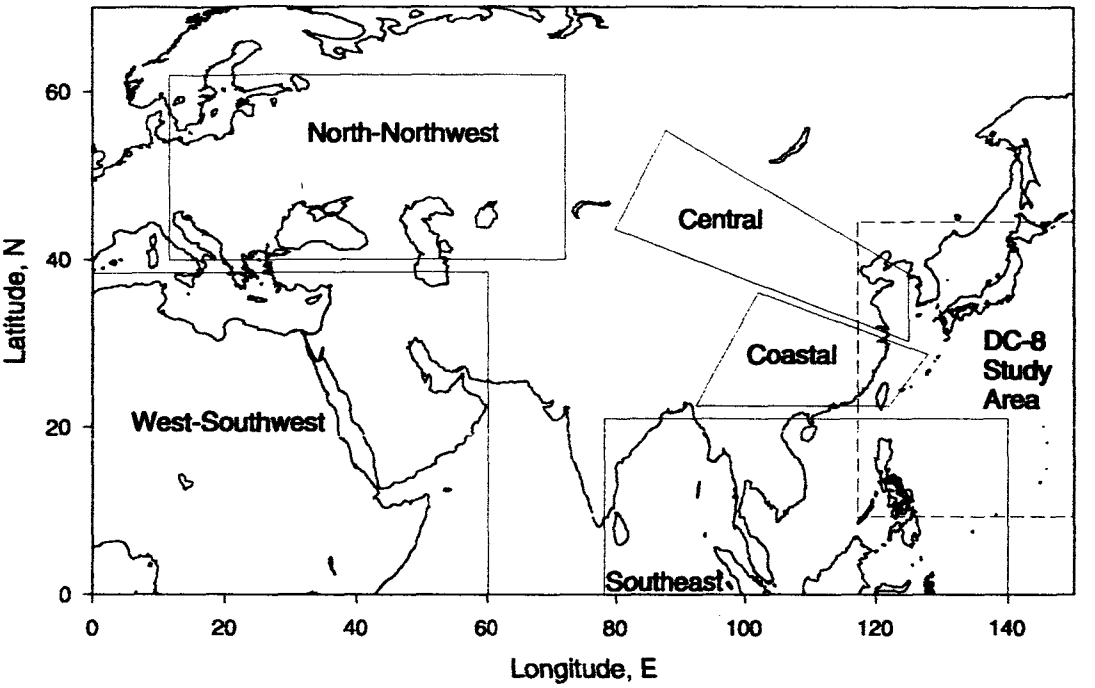

Figure 1. General locations of the five source regions of Asian continental outflow determined from 5-day backward trajectories. Data was collected within the geographic region 10–45°N and 110–150°E indicated by the dashed line box. This region only represents the DC-8 study area for Flights 6–17.

the instrument or that were influenced by stratospheric air were not included in the analysis. Stratospherically influenced air was defined as O_3 above 100 ppbv and CO less than ~70 ppbv (Northern Hemispheric background mixing ratio). When enhancements of both species were observed, the data was not removed from the database and was considered to be a mix of stratospheric and polluted air.

[9] Five-day backward trajectories, calculated by Florida State University [*Fuelberg et al.*, 2003], were used to identify continental source regions of outflow. Only measurements made during constant altitude flight legs were separated into the source region designations while data collected during the spiral ascents and descents was not included due to spatial heterogeneity in the air masses. Transport was dominated by strong westerly flow off of the Asian continent. Trajectories that did not travel over a continent, which was an infrequent occurrence, were not included in any of the source region groups.

[10] Examination of the five-day backward trajectories indicated that there were five general source regions of outflow (Figure 1). The five regions and their approximate latitude and longitude ranges are: central (30–60°N, 80–130°E), coastal (20–40°N, 90–130°E), southeast (SE) (0–25°N, 80–140°E), north-northwest (NNW) (40–65°N, 10–70°E), and west-southwest (WSW) (0–40°N, 0–60°E). These five source regions represent the general positions of the air masses five days prior to when they were encountered by the DC-8 over the western Pacific. Classification of the trajectories was based on their region of origin and the path that they followed to the western Pacific. *Jordan et al.* [2003] used the same source region classification to characterize the aerosol distribution in East Asia and included examples and descriptions of the trajectories in each source region. *Jordan et al.* [2003] refers to the central region as "Channel."

[11] The data was further separated into three altitude ranges, <2 km, 2–7 km, and >7 km, representing the boundary layer, middle troposphere, and upper troposphere. The three bins reflect the aircraft's altitude at the sampling time. The ranges were chosen based on vertical distributions of O_3 and aerosols obtained by the DIAL instrument [*Browell et al.*, 2003]. The data was not evenly distributed across the five source regions during the time period of the measurements due to the altitudes flown by the DC-8. For example, the WSW region did not contain any boundary layer data, and the coastal region does not have data above ~4 km. Also, the trajectories that comprise the central region were constrained by mountains to the north and the Tibetan Plateau to the south. As a result, the central region does not have data >7 km because the high-altitude trajectories are not affected by the topography of this region [*Jordan et al.*, 2003].

4. Characterization of Flights 6–17

[12] This section discusses some general features of the observed trace gas distributions over the western Pacific for Flights 6–17, including measurements made during both constant altitude and spiral flight legs. The term "enhanced" is used to indicate when a species mixing ratio was greater than its Northern Hemisphere background mixing ratio. Measurements obtained during Flight 5, which was a transit flight from Hawaii to Guam, were used to estimate the background mixing ratios. Several

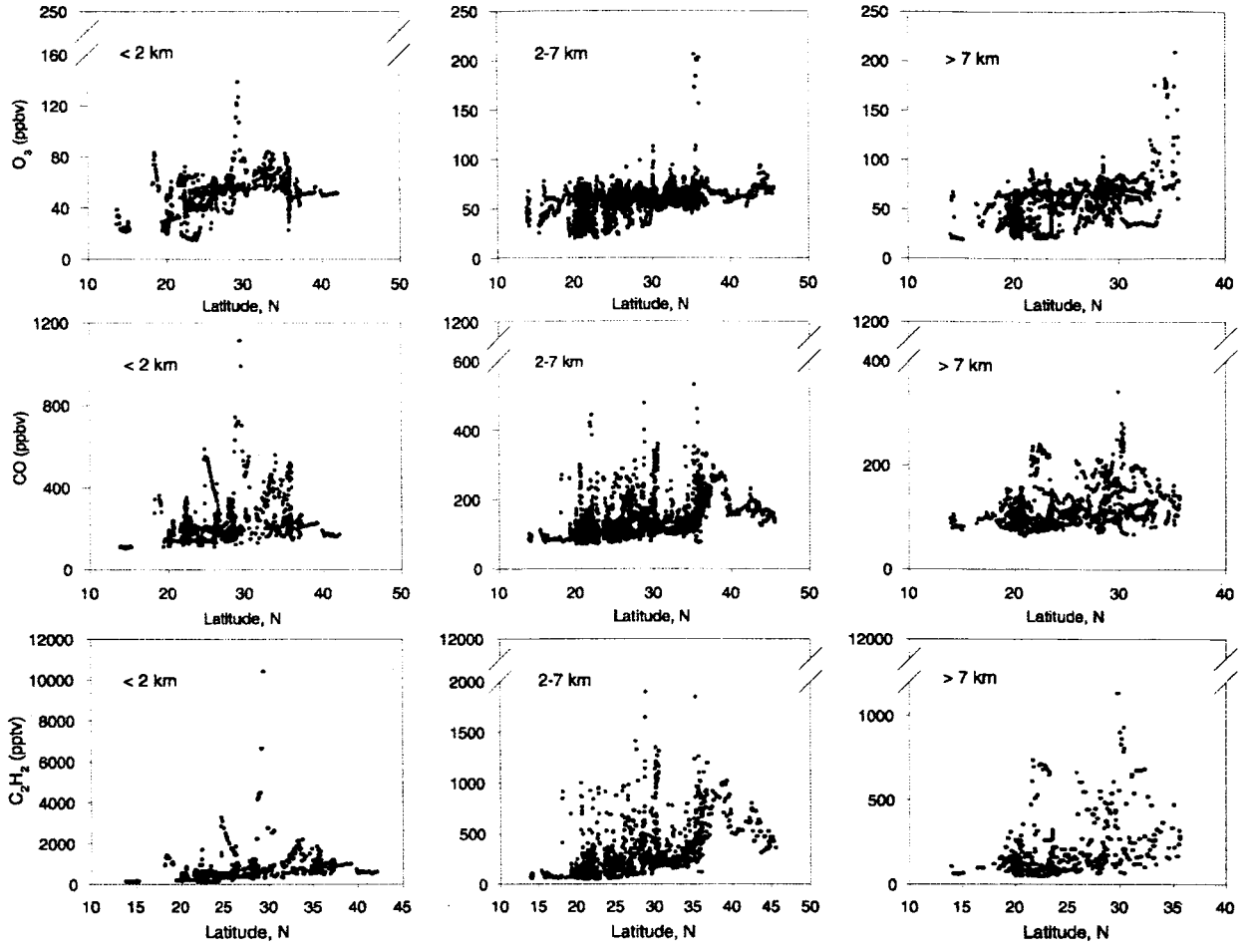

Figure 2. Latitudinal distribution of O_3, CO, and C_2H_2 mixing ratios for Flights 6–17 for three altitude ranges: <2, 2–7, and >7 km.

of the back trajectories from Flight 5 only traveled over the ocean indicating that the air masses were composed of clean, aged marine air, and thus should be fairly representative of springtime, Northern Hemispheric background air. Background was considered to be the lowest one third of measurements in each altitude range. Background mixing ratios for several gases are listed below. The first value corresponds to the background mixing ratio below 2 km, the second corresponds to 2–7 km, and the third number is the background above 7 km: CO = 90, 80, 74 ppbv, O_3 = 15, 20, 15 ppbv, C_2Cl_4 = 3, 2.5, 2 pptv, CH_3Cl = 530, 530, 520 pptv, C_2H_2 = 120, 65, 50 pptv, C_2H_6 = 650, 480, 420 pptv, C_3H_8 = 50, 20, 15 pptv, and SO_2 = 7, 20, 14 pptv.

[13] The latitudinal distribution of O_3 in the three altitude ranges over the western Pacific basin was relatively similar. The mean O_3 mixing ratio at all altitudes was ~50–60 ppbv (Figure 2). The large peaks approaching 200 ppbv in the middle and upper altitudes occurred in air masses with a mix of stratospheric and polluted air. Coincident with the high O_3 were enhanced mixing ratios of CO (80–150 ppbv) indicative of a combustion influence in these air masses. As a result, the stratospheric influence could not be completely removed. The mean CO mixing ratio in the boundary layer was ~200 ppbv, and 100–130 ppbv in the middle and upper troposphere (Figure 2). This suggests that an anthropogenic influence was present at all altitudes over the western Pacific. The abnormally large peak in the boundary layer near 30°N was due to the Shanghai plume which will be discussed in more detail in a later section.

[14] The most significant outflow occurred in the boundary layer between 20 and 40°N latitude, which corresponds to surface outflow directly off of China, Japan and Korea. Several species, such as CO, CO_2, C_2H_2, C_2H_6, C_3H_8, and C_2Cl_4, exhibited enhanced mixing ratios between ~30 and 45°N suggesting a general trend increasing with latitude (Figure 2, only CO and C_2H_2 shown). This feature was particularly noticeable in the middle altitudes. Several companion papers also concluded that the strongest outflow occurred in this midlatitude band [e.g., *Liu et al.*, 2003; *Vay e tal.*, 2003]. During PEM-West B, *Blake et al.* [1997] found a sharp transition at 25°N latitude with stronger outflow and larger mixing ratios for C_2H_6, C_2H_2, and C_2Cl_4 to the north, and this trend was most pronounced in the middle altitudes. Both the location of the major industrial areas and the strong outflow conditions in the late winter and spring at these latitudes were proposed to be responsible for the high mixing ratios.

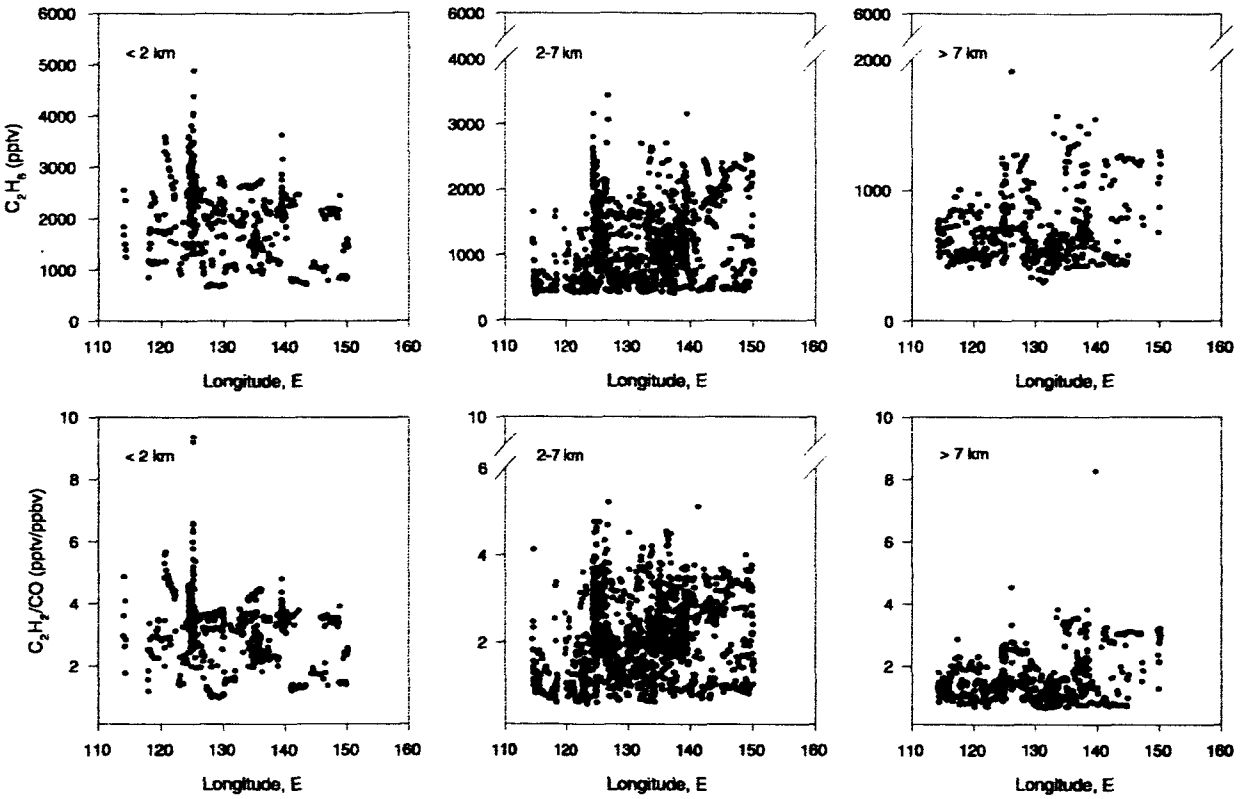

Figure 3. Longitudinal distribution of C_2H_6 mixing ratios and the C_2H_2/CO ratio for Flights 6–17 for <2, 2–7, and >7 km.

[15] An important finding of TRACE-P was that significant outflow was encountered in the middle and upper troposphere and as far east as 150°E longitude (Figure 3). This indicates that anthropogenic influences were not confined to surface regions close to the Asian continent and suggests that emissions were rapidly uplifted and transported over the western Pacific. CO, CO_2, SO_2, C_2Cl_4, CH_3Cl, and non-methane hydrocarbons (NMHCs), such as C_2H_2, C_2H_6, C_3H_8, C_2H_4, had enhanced mixing ratios in the free troposphere. For instance, at 150°E longitude, CO reached over 250 ppbv in the middle altitudes and ~200 ppbv at higher altitudes. SO_2 mixing ratios peaked at approximately 6000 pptv in the middle altitude range. Also, C_2H_6 reached ~3000 pptv and ~1500 pptv in the middle and upper troposphere, respectively (Figure 3). In addition, *Vay et al.* [2003] found that the most efficient continental outflow and that nearly 80% of the CO_2 flux from the Asian continent occurred in the middle troposphere between 35 and 40°N.

[16] The relative age of an air mass resulting from atmospheric processing (mixing and photochemistry) can be estimated because of the different reactivities of chemical species emitted during combustion. NMHCs with short lifetimes will be removed from an air mass before longer-lived species; thus the mixing ratio of the short-lived species will decrease more quickly and alter the ratio value [e.g., *McKeen and Liu*, 1993; *Smyth et al.*, 1996]. The C_2H_2/CO and C_3H_8/C_2H_6 ratios are used in this paper to indicate air mass processing. A higher ratio (i.e., C_2H_2/CO > 3, C_3H_8/C_2H_6 > 0.3) suggests that an air mass contains recent emissions (less than a few days old) while a lower ratio (i.e. C_2H_2/CO < 1, C_3H_8/C_2H_6 < 0.1) is indicative of an aged air mass (~1 week old) [e.g., *Gregory et al.*, 1997].

[17] During TRACE-P, both recent and aged emissions reached the free troposphere and were transported into the central Pacific as indicated by the longitudinal distribution of the C_2H_2/CO (Figure 3) and C_3H_8/C_2H_6 ratios. At 150°E longitude, the C_2H_2/CO ratio had values as large as 4, and this was particularly noticeable in the middle altitude range. These results indicate that the combustion emissions were only 2 or 3 days old, implying rapid uplifting from the Asian continent and transport to these remote oceanic areas. The C_3H_8/C_2H_6 ratio demonstrated similar behavior and trends in its values. In each altitude range and at 150°E longitude, the C_3H_8/C_2H_6 ratio reached values of approximately 0.2 and higher.

5. Characterization of Air Mass Source Regions

[18] This section discusses and compares the characteristics of the five principal Asian source regions identified by analysis of backward trajectories. Atmospheric tracer species were used to determine which pollution sources contributed emissions to regional outflow. Elevated mixing ratios of CO and C_2H_2 are indicative of combustion sources [*Singh and Zimmerman*, 1992]. C_2Cl_4 is an industrial/urban tracer since its only known source is through anthropogenic activities [*Blake et al.*, 1996; *Wang et al.*, 1995]. In addition, CH_3Cl and HCN are good tracers of biomass burning [*Blake et al.*, 1996; *Singh et al.*, 2003; *Li et al.*, 2003]. Tables 1–5 present summary statistical information describing the chemical

Table 1. Mixing Ratios for Selected Species From the Central Source Region[a]

	<2 km						2–7 km					
Species	Mean	Median	Std. Dev.	Max	Min	N	Mean	Median	Std.Dev.	Max	Min	N
O_3	64	64	13	138	41	229	60	61	6	76	47	129
CO	303	264	153	1113	135	215	140	135	25	219	104	128
NO	73	48	77	399	0	211	14	11	11	64	2	82
NO_2	530	477	421	2926	8	184	55	51	38	177	0	71
NO_y	2430	1726	2249	13487	222	228	297	276	150	938	65	129
HNO_3	1323	833	1293	7412	222	229	202	169	110	938	106	120
PAN	1225	888	1014	4264	2	102	194	175	69	364	118	41
SO_2	4172	2621	4428	30736	353	205	80	65	64	284	10	91
CO_2	378	377	3	392	374	199	374	374	1	376	372	118
H_2O_2	567	446	441	2137	20	122	741	535	552	1725	134	49
CH_3OOH	98	88	50	293	36	107	228	225	108	482	104	35
CH_2O	2640	1690	2884	9824	208	35	85	82	19	122	61	17
C_2H_6	2695	2540	662	4888	1396	110	1415	1334	221	1968	1125	44
C_2H_4	396	106	681	3052	4	108	27	19	22	93	3	44
C_2H_2	1465	860	1639	10403	308	110	339	313	107	645	209	44
C_3H_8	1010	822	586	3774	271	110	308	279	96	540	184	44
C_6H_6	431	240	549	3101	61	110	64	62	25	147	28	44
i-C_4H_{10}	205	125	231	1345	31	110	40	39	16	83	15	44
n-C_4H_{10}	290	209	229	1384	46	110	67	58	30	151	27	44
CH_4	1856	1855	33	1983	1788	208	1797	1794	13	1837	1767	118
C_2Cl_4	18	12	19	123	8	110	6	6	2	10	4	44
CCl_4	104	100	11	162	98	110	99	99	1	102	97	44
CH_3CCl_3	43	41	5	66	40	110	40	40	0	41	39	44
CH_3Cl	654	559	239	1677	530	110	568	563	23	643	542	44
CH_3Br	10	9	4	29	8	110	9	9	0.27	9	8	44
CFC-11	264	262	7	293	259	110	259	259	2	262	255	44
CFC-12	543	540	12	615	534	110	535	535	3	543	528	44
CFC-113	81	80	5	113	77	110	79	79	1	80	78	44
C_2H_2/CO	3.87	3.37	1.34	9.35	2.24	102	2.40	2.35	0.40	3.82	1.91	43
C_3H_8/C_2H_6	0.35	0.33	0.09	0.77	0.19	110	0.21	0.21	0.04	0.31	0.15	44

[a]Mixing ratios are given in parts per trillion by volume except for O_3, CO, and CH_4 which are in parts per billion by volume and for CO_2 which is in parts per million by volume. The C_2H_2/CO ratio is in parts per trillion by volume/parts per billion by volume.

composition of the five source regions. This information is used in our discussion of each of the five source regions.

5.1. Central

[19] The most striking feature of the central region was the Shanghai plume which was sampled in the boundary layer (~0.3 km) during Flight 13 over the Yellow Sea (Figure 4). Several species had their highest mixing ratios measured during the entire mission in this plume (Table 1), including CO, SO_2, C_2H_2, C_2H_6, C_2H_4, C_3H_8, CH_2O, C_2Cl_4, CCl_4, CH_3CCl_3, CH_3Cl, HNO_3, PAN, and NO_y (NO_y = NO + NO_2 + HNO_3 + PAN + PPN + C_1-C_5 alkyl nitrates). For example, CO mixing ratios peaked at ~1100 ppbv, C_2H_2 at ~10,000 pptv, SO_2 at ~31,000 pptv, C_2Cl_4 at 123 pptv, and CH_3Cl at ~1700 pptv. Aerosol Ca^{+2} and NO_3^- were also significantly enhanced in the boundary layer indicating a strong dust and anthropogenic influence [*Jordan et al.*, 2003]. The Shanghai plume was largely composed of recent combustion emissions that were less than 1 day old (maximum C_2H_2/CO = 9.4, C_3H_8/C_2H_6 = 0.77). The observed composition of the plume was most likely quite similar to its original composition. Photochemical species, such as O_3, PAN, HNO_3, CH_3OOH, and H_2O_2, were also enhanced. For example, O_3 reached ~140 ppbv while PAN peaked near 4300 pptv. These high levels indicate significant photochemical activity even at this time of the year. Correlations of O_3 and CO (r^2 = 0.82) and O_3 and PAN (r^2 = 0.69) were fairly robust and suggested that O_3 and PAN were photochemically produced from combustion derived precursor gases in the outflow. The strong correlation between O_3 and CO reflects the recent emission inputs into the Shanghai plume where dilution and mixing processes had not acted to significantly alter the overall composition of the plume. O_3 and CO were poorly correlated in the other four source regions, where the emissions were clearly more than 1 day old. *Simpson et al.* [2003] discuss the chemistry and production of C_2-C_5 alkyl nitrates in Asian outflow and concluded that the Shanghai plume contained very fresh emissions of these species and that dilution was not a significant factor affecting the observed plume composition.

[20] Pollution plumes from other urban regions around the world show enhancements in many of the same anthropogenic species, specifically CO, NMHCs, and halocarbons. However, these enhancements occur in varying degrees compared to the Shanghai plume. For example, NMHC mixing ratios in the southeast U.S. and Houston, Texas have been found to be substantially higher than in the Shanghai plume [e.g., *Kang et al.*, 2001]. The mixing ratios of several hydrocarbons (e.g., C_2H_6, C_3H_8, C_2H_2, C_6H_6) have been found to be factors of ~2–50 higher in Mexico City [*Blake and Rowland*, 1995]. Also, C_2H_6, C_2H_2, C_3H_8, C_6H_6, and CO were observed to be approximately a factor of 2 larger in London in the winter than the maximum values of these species observed in the Shanghai plume [*Derwent et al.*, 1995]. A notable difference between the Shanghai plume and other urban regions is the large influence from biofuel emissions most likely reflecting their use for cooking and heating in East Asia. C_3H_8, C_2H_2, C_2H_6, C_6H_6, i-C_4H_{10}, and n-C_4H_{10} mixing ratios observed in South Korea were fairly comparable with the Shanghai

Table 2. Mixing Ratios of Selected Species From the Coastal Source Region[a]

	<2 km						2–4 km					
Species	Mean	Median	Std. Dev.	Max	Min	N	Mean	Median	Std. Dev.	Max	Min	N
O_3	41	43	14	83	15	290	58	60	6	69	43	111
CO	201	166	107	586	124	264	151	132	47	272	107	83
NO	7	2	15	79	0	221	23	17	20	110	5	94
NO_2	41	13	89	503	0	195	35	33	22	137	6	65
NO_y	541	386	525	3267	56	283	431	475	260	1096	24	110
HNO_3	439	322	365	2120	128	267	368	326	169	876	135	95
PAN	207	19	336	1065	1	104	142	115	126	412	15	51
SO_2	207	48	377	1554	4	105	27	21	19	120	10	38
CO_2	376	375	3.5	389	373	233	374	374	1.1	376	372	84
H_2O_2	1243	1176	611	3179	339	108	1404	1553	591	3093	416	58
CH_3OOH	470	351	359	1535	53	100	269	280	117	531	84	55
CH_2O	763	461	797	3553	92	90	265	245	128	488	55	32
C_2H_6	1498	1353	716	3598	669	105	1085	929	336	1974	793	39
C_2H_4	208	9	452	1794	3	93	30	22	25	87	3	23
C_2H_2	665	384	749	3264	125	105	376	255	222	908	181	39
C_3H_8	375	211	448	2069	27	105	171	131	89	375	65	39
C_6H_6	189	79	272	1207	30	105	77	42	55	185	27	39
$i\text{-}C_4H_{10}$	94	32	160	738	9	89	23	12	20	65	4	39
$n\text{-}C_4H_{10}$	121	38	211	1030	4	93	36	16	30	100	7	39
CH_4	1816	1808	34	1915	1735	241	1779	1776	11	1831	1761	72
C_2Cl_4	9	8	6	32	3	105	5	5	2	11	3	39
CCl_4	102	100	6	127	97	105	100	100	1	102	99	39
CH_3CCl_3	41	41	3	54	39	105	40	40	1	41	39	39
CH_3Cl	638	580	176	1333	522	105	589	575	32	662	549	39
CH_3Br	10	9	2	18	8	105	9	9	0.43	10	8	39
CFC-11	262	261	4	277	256	105	261	261	1	264	259	39
CFC-12	540	538	6	559	532	105	539	538	3	544	534	39
CFC-113	80	80	1	85	77	105	80	80	1	81	79	39
C_2H_2/CO	2.46	2.28	1.19	5.66	0.94	94	2.27	1.91	0.71	3.94	1.66	31
C_3H_8/C_2H_6	0.19	0.16	0.12	0.58	0.04	105	0.15	0.13	0.05	0.24	0.08	39

[a]Mixing ratios are given in parts per trillion by volume except for O_3, CO, and CH_4 which are in parts per billion by volume and for CO_2 which is in parts per million by volume. The C_2H_2/CO ratio is in parts per trillion by volume/parts per billion by volume.

Table 3. Mixing Ratios of Selected Species From the SE Source Region[a]

	<2 km						2–7 km						>7 km					
Species	Mean	Median	Std. Dev.	Max	Min	N	Mean	Median	Std. Dev.	Max	Min	N	Mean	Median	Std. Dev.	Max	Min	N
O_3	39	40	3	43	27	25	52	57	13	72	27	244	39	32	17	70	18	620
CO	208	205	18	254	157	25	123	88	69	331	74	231	98	88	27	223	67	557
NO							16	15	12	130	1	171	92	47	157	805	9	377
NO_2							31	26	16	65	5	89	14	11	11	48	0	240
NO_y	795	796	43	884	730	25	369	301	325	1439	5	219	172	125	177	1158	6	589
HNO_3	784	783	47	884	713	25	336	238	230	1352	100	174	86	66	66	320	3	502
PAN	17	17	8	27	3	9	159	86	186	660	8	98	62	54	56	238	6	287
SO_2	23	20	11	45	7	16	32	23	56	415	6	102	38	21	51	284	10	93
CO_2	376	376	0.65	377	374	23	372	371	2	379	370	222	372	371	1	374	370	279
H_2O_2	5660	5699	508	6199	4857	9	739	266	1019	5391	48	96	164	109	154	686	15	210
CH_3OOH	1351	1331	223	1791	1121	10	257	216	195	1083	30	71	114	103	65	340	29	125
CH_2O	346	300	114	516	268	4	162	127	108	406	53	36	248	143	286	1138	56	50
C_2H_6	1182	1155	104	1412	1105	7	737	528	405	1775	422	88	594	514	194	1270	370	279
C_2H_4	6	6	1	8	5	5	31	14	38	132	2	43	16	5	31	160	3	84
C_2H_2	459	456	82	627	369	7	252	93	321	1210	48	88	129	89	105	609	47	279
C_3H_8	123	112	18	156	109	7	81	35	108	430	15	88	54	33	49	257	11	279
C_6H_6	88	86	16	118	70	7	53	13	84	328	3	86	18	11	21	124	3	259
$i\text{-}C_4H_{10}$	14	17	5	19	7	7	28	11	32	103	3	35	12	7	10	44	3	122
$n\text{-}C_4H_{10}$	18	19	6	24	8	7	28	6	41	144	3	53	14	8	15	66	3	163
CH_4	1800	1799	5	1809	1786	25	1762	1754	28	1836	1690	194	1757	1755	13	1799	1713	456
C_2Cl_4	5	5	0	5	4	7	4	2	3	15	1	88	2	2	1	6	1	279
CCl_4	99	100	1	100	98	7	99	99	1	103	97	88	98	98	1	101	95	279
CH_3CCl_3	39	40	1	40	38	7	40	39	2	45	37	88	39	39	1	41	38	279
CH_3Cl	620	624	23	654	588	7	582	567	41	709	536	88	569	561	32	641	525	279
CH_3Br	9	9	0	9	8	7	8	8	1	11	8	88	8	8	0	9	7	279
CFC-11	260	260	1	261	259	7	260	260	2	268	256	88	258	258	2	263	254	279
CFC-12	536	536	1	537	534	7	536	537	4	552	528	88	534	534	4	543	525	266
CFC-113	79	79	1	80	78	7	79	79	1	82	77	88	79	79	1	81	77	279
C_2H_2/CO	2.26	2.24	0.23	2.51	1.82	7	1.50	1.01	0.98	4.13	0.63	83	1.15	1.01	0.47	2.74	0.63	250
C_3H_8/C_2H_6	0.10	0.10	0.01	0.12	0.09	7	0.08	0.06	0.05	0.24	0.03	88	0.08	0.06	0.04	0.20	0.02	279

[a]Mixing ratios are given in parts per trillion by volume except for O_3, CO, and CH_4 which are in parts per billion by volume and for CO_2 which is in parts per million by volume. The C_2H_2/CO ratio is in parts per trillion by volume/parts per billion by volume.

Table 4. Mixing Ratios of Selected Species From the NNW Source Region[a]

	<2 km						2–7 km						>7 km					
Species	Mean	Median	Std. Dev.	Max	Min	N	Mean	Median	Std. Dev.	Max	Min	N	Mean	Median	Std. Dev.	Max	Min	N
O_3	55	54	7	67	36	399	62	60	17	206	48	491	131	151	53	208	59	25
CO	204	207	25	266	136	368	145	126	46	420	74	443	103	105	9	118	88	25
NO	61	18	136	1450	0	297	33	10	78	465	0	402	56	55	28	97	22	17
NO_2	463	72	766	3349	0	190	51	27	63	664	1	402	23	23	13	40	5	17
NO_y	940	597	881	5115	12	391	397	260	397	3341	10	492	585	782	390	1230	88	24
HNO_3	447	436	195	1198	63	375	189	120	229	2028	49	452	456	543	349	1099	41	25
PAN	505	514	326	1422	1	160	293	193	229	998	89	229	116	124	28	151	80	16
SO_2	517	272	559	2821	4	328	403	42	1038	6989	7	398	31	24	17	70	12	18
CO_2	377	376	2	387	374	389	374	374	1.6	380	370	466	372	372	0.9	373	371	19
H_2O_2	543	425	442	2276	22	158	440	397	308	1058	30	210	96	90	59	201	22	10
CH_3OOH	169	111	172	1091	25	124	208	138	139	597	28	180	76	75	26	109	45	4
CH_2O	723	739	395	1935	83	113	292	138	400	1877	50	44	160	176	42	188	99	4
C_2H_6	2356	2353	407	3607	1276	135	1670	1646	411	2813	641	216	882	916	175	1076	597	14
C_2H_4	150	101	180	1228	19	134	38	15	59	318	3	179	5	5	2	8	3	8
C_2H_2	756	757	166	1205	268	135	398	304	211	1098	117	216	179	164	34	238	138	14
C_3H_8	859	804	310	1907	194	135	446	413	199	1115	96	216	149	133	60	232	71	14
C_6H_6	182	175	50	326	68	135	76	52	61	308	3	216	19	21	7	25	7	8
$i\text{-}C_4H_{10}$	144	130	71	386	20	135	60	52	35	189	8	216	7	6	3	12	4	14
$n\text{-}C_4H_{10}$	247	213	130	681	21	135	107	95	62	344	14	214	14	12	4	23	7	14
CH_4	1843	1841	17	1897	1803	318	1806	1802	22	1875	1750	438	1761	1760	11	1779	1744	25
C_2Cl_4	12	12	2	21	6	135	8	7	3	18	2	216	2	2	1	4	1	14
CCl_4	100	100	1	102	98	135	99	99	1	103	90	216	95	96	2	97	92	14
CH_3CCl_3	42	42	1	45	40	135	40	40	1	43	38	216	38	38	1	39	36	14
CH_3Cl	552	553	17	589	518	135	552	547	21	618	514	216	544	545	12	559	523	14
CH_3Br	9	9	1	18	9	135	9	9	1	11	8	216	9	9	0	9	8	14
CFC-11	262	262	2	269	257	135	260	260	3	266	245	216	253	255	5	258	244	14
CFC-12	540	540	3	549	530	135	537	538	4	550	518	216	530	532	8	537	517	14
CFC-113	80	80	1	82	78	135	79	79	1	82	75	216	78	77	1	79	76	14
C_2H_2/CO	3.60	3.56	0.47	4.61	2.80	117	2.54	2.37	0.56	4.02	1.00	172	1.72	1.62	0.25	2.19	1.44	14
C_3H_8/C_2H_6	0.35	0.36	0.07	0.53	0.15	135	0.26	0.25	0.07	0.49	0.12	217	0.16	0.15	0.04	0.22	0.12	14

[a]Mixing ratios are given in parts per trillion by volume except for O_3, CO, and CH_4 which are in parts per billion by volume and for CO_2 which is in parts per million by volume. The C_2H_2/CO ratio is in parts per trillion by volume/parts per billion by volume.

Table 5. Mixing Ratios of Selected Species From the WSW Source Region[a]

	2–7 km						>7 km					
Species	Mean	Median	Std. Dev.	Max	Min	N	Mean	Median	Std. Dev.	Max	Min	N
O_3	64	65	10	91	29	145	62	66	15	120	26	625
CO	110	108	17	175	78	136	134	121	48	281	70	556
NO	44	51	31	119	7	60	93	82	55	285	9	445
NO_2	45	43	19	83	10	52	29	24	21	149	2	358
NO_y	322	235	349	2257	5	140	297	245	211	1138	3	619
HNO_3	210	131	312	1987	33	128	121	100	83	762	25	518
PAN	187	187	63	341	78	67	268	181	186	699	44	246
SO_2	72	26	88	298	10	26	51	28	100	569	7	151
CO_2	372	372	1	373	371	131	372	372	2	376	369	521
H_2O_2	415	255	314	1091	94	60	205	193	125	589	22	215
CH_3OOH	170	195	70	286	25	47	120	98	91	540	25	141
CH_2O	262	189	272	1166	56	16	266	218	188	729	54	59
C_2H_6	824	893	191	1242	451	56	801	731	294	1569	295	260
C_2H_4	17	14	11	50	3	33	41	26	38	129	3	140
C_2H_2	211	190	108	602	81	56	291	208	219	930	47	260
C_3H_8	110	120	54	202	19	56	93	77	63	259	12	260
C_6H_6	31	24	23	107	7	56	46	30	43	179	3	223
$i\text{-}C_4H_{10}$	11	11	5	23	3	49	16	13	11	41	3	166
$n\text{-}C_4H_{10}$	19	20	9	36	3	51	21	14	18	65	3	203
CH_4	1767	1771	13	1794	1726	136	1771	1772	19	1831	1694	482
C_2Cl_4	3	3	1	6	2	56	3	2	2	12	0	260
CCl_4	98	98	1	101	96	56	98	98	2	101	87	260
CH_3CCl_3	39	39	1	41	37	56	39	39	2	41	31	260
CH_3Cl	568	566	19	621	538	56	595	588	29	668	543	260
CH_3Br	8	8	0	9	8	55	8	8	0.45	10	8	260
CFC-11	259	259	2	263	255	56	258	257	2	264	253	260
CFC-12	535	535	4	543	527	56	534	534	3	544	527	258
CFC-113	79	79	1	87	77	56	79	79	1	81	73	260
C_2H_2/CO	1.88	1.82	0.63	4.49	0.98	52	1.95	1.59	0.80	3.81	0.67	229
C_3H_8/C_2H_6	0.13	0.13	0.04	0.21	0.04	56	0.10	0.10	0.04	0.21	0.03	260

[a]Mixing ratios are given in parts per trillion by volume except for O_3, CO, and CH_4 which are in parts per billion by volume and for CO_2 which is in parts per million by volume. The C_2H_2/CO ratio is in parts per trillion by volume/parts per billion by volume.

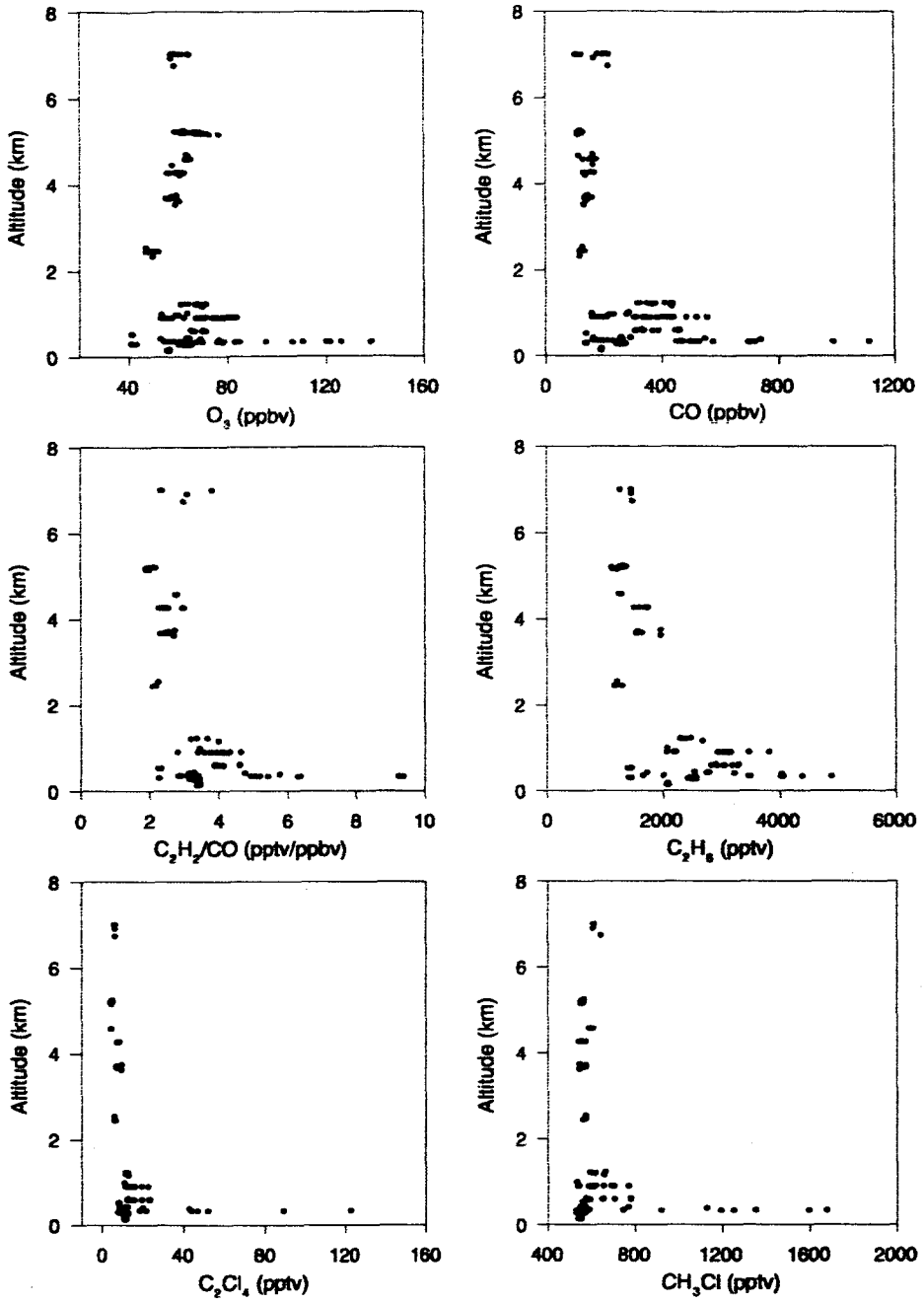

Figure 4. Vertical distributions of selected species in air masses originating in the Central source region.

plume [*Na et al.*, 2003]. These comparisons for polluted regions around the world suggest that the Shanghai plume is fairly representative of the magnitude of pollutants being transported from these large population centers.

[21] In the boundary layer outflow of the central region, CO was strongly correlated with C_2H_2, C_2H_4, and C_2H_6 ($r^2 \geq 0.86$). CO and C_2H_2 were also correlated with C_2Cl_4 ($r^2 = 0.77$ and 0.96, respectively) and with CH_3Cl ($r^2 = 0.81$ and 0.90, respectively). These results indicate that the outflow contained a complex mixture of fresh and processed emissions from combustion, industrial activities, and biomass/biofuel burning. This makes it difficult to distinguish between fossil fuel and biofuel emissions. The strong correlations, particularly with C_2H_2, were dominated by the emissions sampled directly from the Shanghai plume. Additional tracers have been identified which can specifically distinguish between Chinese (halon-1211) and Japanese/Korean (CH_3Br) emissions [*Blake et al.*, 2003]. Correlations between CO, C_2H_2, and C_3H_8 with H-1211 ($r^2 = 0.72-0.93$) were stronger than the correlations with CH_3Br ($r^2 = 0.67-0.76$). As expected, these results suggest a stronger influence from Chinese sources in the boundary layer.

[22] Above the boundary layer, mixing ratios of most species were decreased significantly. The median CO and

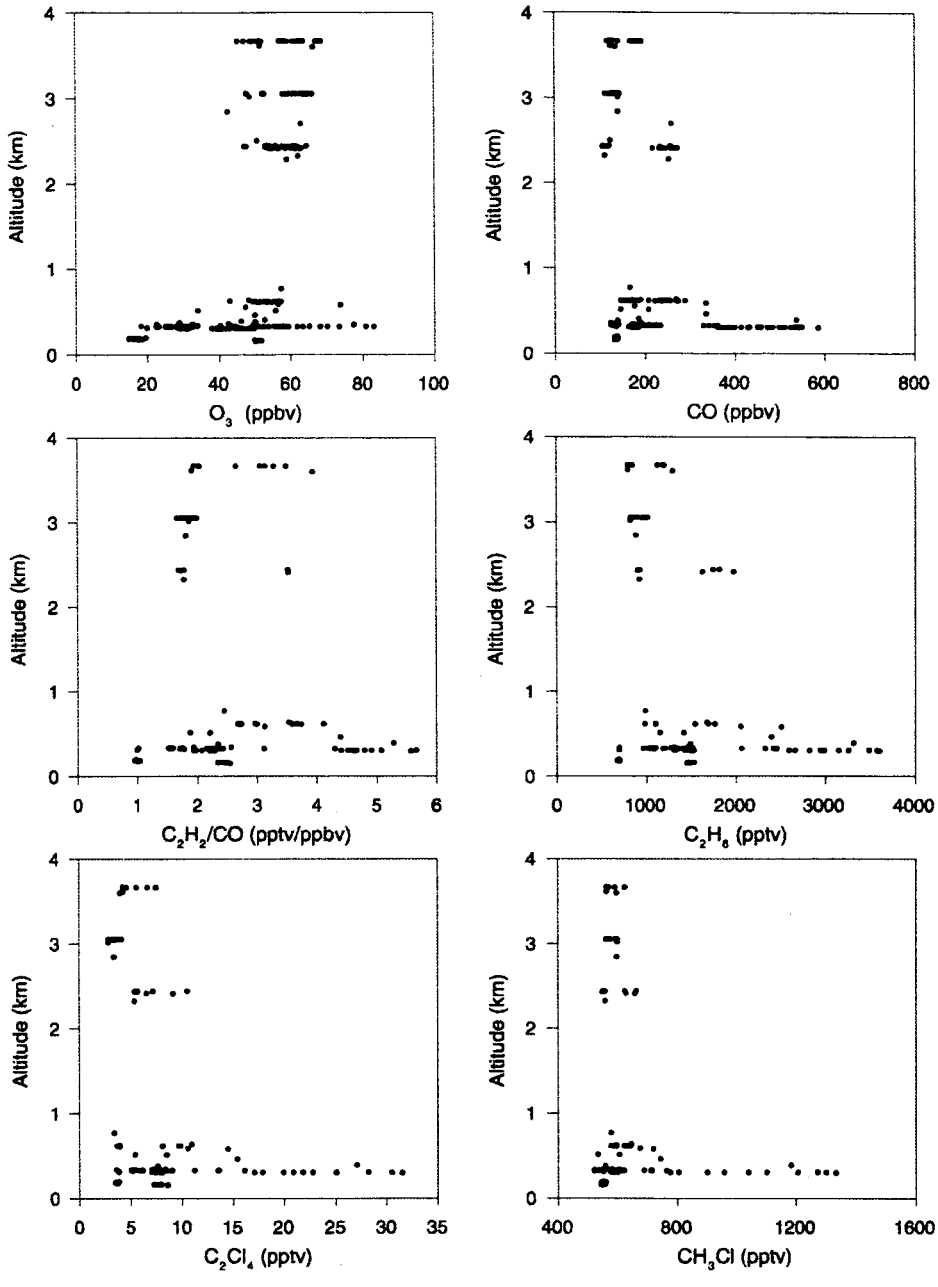

Figure 5. Vertical distributions of selected species in air masses originating in the Coastal source region.

NMHC mixing ratios were at least a factor of 2–3 lower in the middle altitudes compared to the boundary layer but they were still enhanced substantially above background levels. The hydrocarbon ratios were lower due to a lack of recent emission inputs and additional air mass processing and dilution. Correlations of CO and C_2H_2 with CH_3Cl (r^2 = 0.83 and 0.58, respectively) indicate an influence from combustion and, in particular, biomass/biofuel burning emissions in the middle altitudes.

5.2. Coastal

[23] The middle altitudes of the coastal region only reflect data collected at 2–4 km while observations were available for the other four regions from 2 to 7 km. Air masses in the coastal region had short transport distances to the western Pacific and apparently underwent minimal vertical uplifting. Aside from the differences in the air mass transport patterns and the strong dust influence in the central region [*Jordan et al.*, 2003], the chemistry of the central and coastal regions was essentially the same. The composition of the boundary layer in these two regions was directly influenced by recent emissions from anthropogenic activities in East Asia. Mixing ratios of CO, NMHCs, C_2Cl_4, and CH_3Cl were at least a factor of 3 higher than background (Figure 5, Table 2). Furthermore, O_3, PAN, NO_x, HNO_3, H_2O_2, and CH_3OOH were enhanced, suggestive of relatively recent photochem-

ical processing. This is supported by the strong correlation of CO and C_2H_2 with PAN ($r^2 \sim 0.85$). Recent (~1 day old) combustion inputs were present in the boundary layer outflow ($C_2H_2/CO \sim 5$ and $C_3H_8/C_2H_6 \sim 0.5$) along with extensively processed air. CO_2 and CH_4 were also enhanced in the boundary layer, and they were correlated with CO and C_2H_2 ($r^2 > 0.8$) suggesting an anthropogenic rather than biogenic source. In addition, CO_2 and CH_4 were correlated with combustion species ($r^2 > 0.6$) in the altitude ranges where outflow occurred in the other four source regions. *Vay et al.* [2003] analyzed eleven pollution plumes with $CO_2 > 380$ ppmv and CO > 250 ppbv and concluded that anthropogenic sources were responsible for the enhancements followed by frontal lifting associated with mid-latitude cyclones.

[24] In the middle altitudes, species mixing ratios decreased substantially, similar to those from the central region. Species, such as CO, C_2H_6, C_2H_4, C_2Cl_4, and CH_3Cl, were a factor of 2 or 3 lower compared to their maximum mixing ratios in the boundary layer. O_3, PAN, and H_2O_2 exhibited enhancements again showing significant photochemical processing. CO and C_2H_2 were well correlated with industrial tracer species, such as C_2Cl_4 ($r^2 > 0.91$ below 2 km and $r^2 \sim 0.7$ above 2 km). As found in the central region, CO and C_2H_2 were strongly correlated with CH_3Cl ($r^2 \geq 0.87$) in both altitude ranges. O_3 levels are often high in air masses containing aged biomass emissions [*Tang et al.*, 2003]. Biomass/biofuel burning may therefore explain the enhanced O_3 (~80 ppbv) observed in the boundary layer. Also, a combination of emissions from both Chinese and Japanese/Korean sources appear to be important as indicated by the strong correlations of CO, C_2H_2, C_2H_6, and C_3H_8 with both H-1211 and CH_3Br ($r^2 > 0.78$) in the boundary layer.

5.3. Southeast

[25] The SE region was characterized by two principal outflow regions, ~3 and 10 km (Figure 6). The outflow plume at 10 km altitude was especially impressive, with mixing ratios of CO exceeding 200 ppbv, C_2H_6 above 1000 pptv, and enhanced hydrocarbon ratios ($C_2H_2/CO \sim 3$ and $C_3H_8/C_2H_6 \sim 0.2$) (Table 3). Both outflow plumes had enhancements in CO, SO_2, NO_y, NMHCs, CH_3Cl, C_2Cl_4, CH_3CCl_3, and CCl_4. In the high-altitude outflow, water-soluble species, such as HNO_3, H_2O_2, and CH_3OOH, were not enhanced. In air masses that have recently been influenced by wet convection, the CH_3OOH/H_2O_2 ratio is usually >1 due to the greater solubility of H_2O_2 which is preferentially scavenged by precipitation [*Heikes*, 1992]. At high altitude, the CH_3OOH/H_2O_2 ratio was >1, suggesting that wet convection lifted the emis-sions from the surface. This is consistent with the results from *Liu et al.* [2003] who suggested that the La Nina conditions during spring 2001 resulted in more frequent and stronger convection in SE Asia. This could be responsible for outflow of biomass burning emissions at high altitude. *Fuelberg et al.* [2003] also discuss the La Nina conditions during spring 2001 and its impact on transport patterns. O_3 had a wide range of mixing ratios varying from 20 to 70 ppbv at all altitudes. The enhanced O_3 mixing ratios at high altitude may be attributed to photochemical production from the uplifted biomass burning emissions. Extensively processed air masses containing background air with low hydrocarbon ratios were also encountered above 2 km.

[26] The highest mixing ratios of H_2O_2 and CH_3OOH originated from the SE source region at altitudes of up to ~3 km. The median mixing ratios of H_2O_2 and CH_3OOH in the boundary layer were a factor of 4–15 larger than the medians in the other three source regions that had boundary layer data (i.e., central, coastal, NNW). Areas affected by significant biomass burning outflow, such as over the South Atlantic, have been found to contain considerably enhanced mixing ratios of H_2O_2 and CH_3OOH due to efficient photochemical production [*Talbot et al.*, 1996b; *Heikes et al.*, 1996]. Mixing ratios of NO_2, PAN, and HNO_3 were enhanced in the 3 km outflow, but NO was not enhanced presumably due to conversion to other reactive nitrogen species. This indicates that combustion was a significant source of reactive nitrogen in the Asian outflow.

[27] An anthropogenic influence was apparent in all three altitude ranges, with the strongest correlations found in the middle altitudes where CO was highly correlated with C_2H_2, C_2H_6, C_2Cl_4, and CH_3Cl ($r^2 \geq 0.89$). CH_3Cl has also been found to have an oceanic source [*Khalil et al.*, 1999] which may have made a minor contribution to the enhancements observed in the SE, central, and coastal regions. However, the correlations with the combustion species in these regions argue strongly for an anthropogenic source of CH_3Cl. Furthermore, biomass burning has been found to be a larger source of CH_3Cl than the ocean [*Lobert et al.*, 1999; *Khalil et al.*, 1999]. HCN has also been proposed to be a good tracer of biomass burning [*Singh et al.*, 2003; *Li et al.*, 2003]. Correlations of CH_3Cl, CO, C_2H_6, and C_2H_2 with HCN ($r^2 \geq 0.7$) are relatively strong providing further evidence of a significant impact from biomass burning in the SE region. Furthermore, it is likely that biomass burning made a large contribution because spring is the dry season in Asia and extensive biomass burning occurs at this time of year in India and SE Asia [e.g., *Bey et al.*, 2001; *Blake et al.*, 1997]. Several companion papers have also found evidence of substantial biomass burning emissions being transported from SE Asia. For instance, *Heald et al.* [2003] concluded that biomass burning was responsible for approximately 30% of the CO emissions south of 30°N. *Carmichael et al.* [2003a] also found that biomass burning emissions were transported from SE Asia above 2 km and below 30°N.

5.4. North-Northwest

[28] The vertical distributions for the NNW region show that outflow occurred at several altitudes between 2 and 8 km with several species exhibiting a general decreasing trend with altitude (Figure 7). Mixing ratios of CO, C_2Cl_4, and NMHCs decreased by factors of 3–4 from the boundary layer to the upper troposphere (Table 4). NO was enhanced (465 pptv) at ~7.5 km with coincident enhancements in several species, such as CO, C_2H_6, C_2H_2, CH_3Cl, and C_2Cl_4, suggesting that recent surface emissions were lifted to this altitude. The composition of the upper troposphere of the NNW region was influenced by a mixture of stratospheric and surface level air. O_3 and CO were both enhanced with mixing ratios of ~100 ppbv and higher. Also, the air masses were freshest at low altitude,

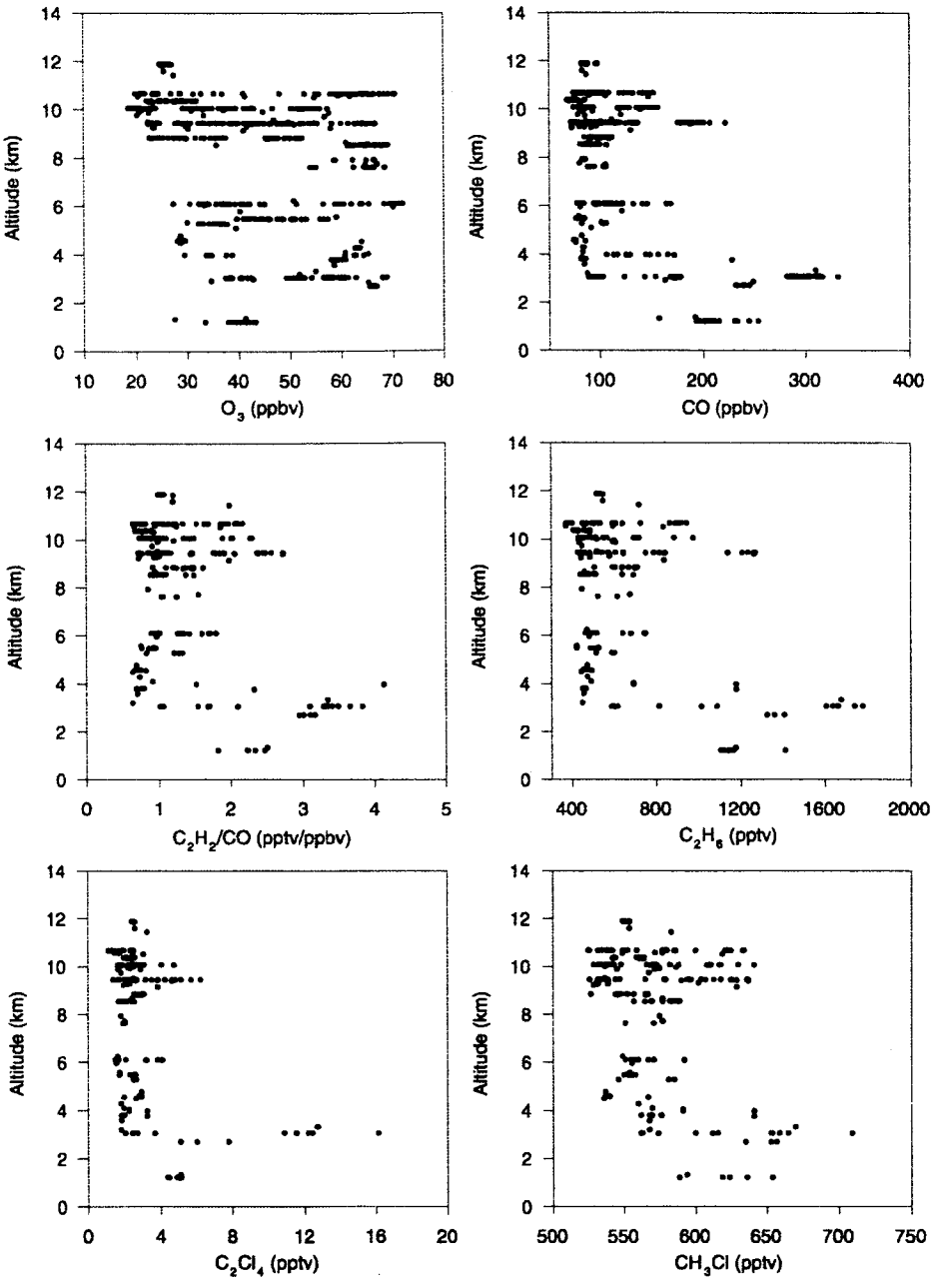

Figure 6. Vertical distributions of selected species in air masses originating in the Southeast source region.

and the relative age generally increased with altitude reflecting both stratospheric and aged surface emissions at the highest altitudes.

[29] Aged and diluted industrial and biomass/biofuel burning emissions were mixed with recent combustion emissions in the boundary layer. CO was weakly correlated with C_2Cl_4 and CH_3Cl ($r^2 < 0.3$) below 2 km, however, correlations of CO and C_2H_6 with C_2H_2 ranged from r^2 = 0.74 to 0.92 at low and middle altitudes. Emissions from industrial activity impacted the middle altitudes where CO and C_2H_2 were fairly well correlated with C_2Cl_4 (r^2 = 0.68 and 0.84, respectively).

[30] The presence of middle and high altitude outflow in the NNW, SE, and WSW regions undoubtedly reflects the longer transport distance for air masses which allows uplift and entrainment of continental emissions. Furthermore, these air masses may contain more processed and diluted emissions because of the long distance from source inputs. The relatively strong anthropogenic influence in and above the boundary layer of the NNW region may be from the uplift of emissions from the central region as the air masses passed over it on route to the western Pacific. Since the DC-8 did not sample over the Asian continent, there is really no way to separate these potential confounding influences

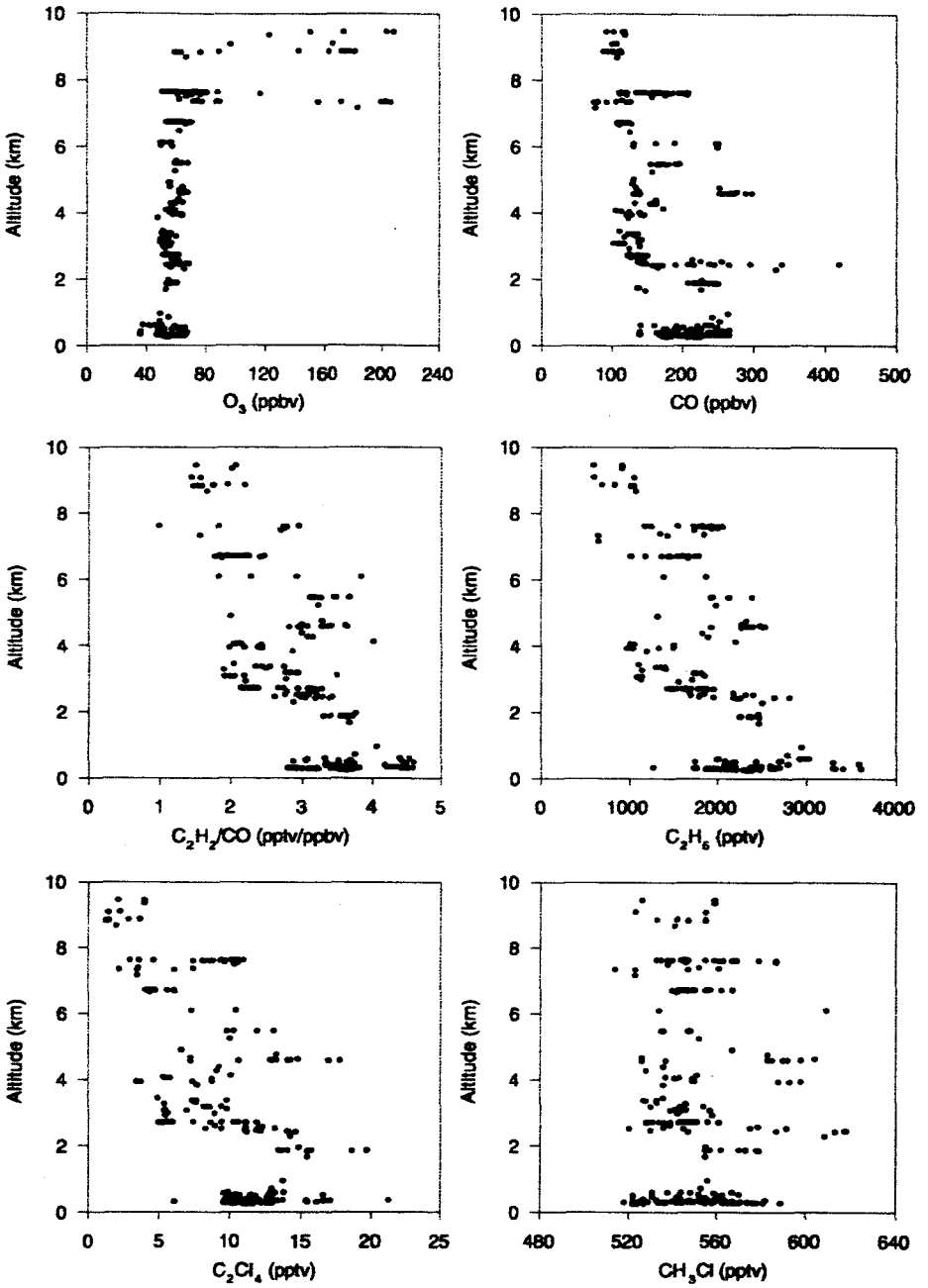

Figure 7. Vertical distributions of selected species in air masses originating in the North-Northwest source region.

from the two source regions. However, these two regions are kept separate because the NNW region trajectories originated at a much greater distance from the western Pacific. In addition, *Jordan et al.* [2003] demonstrated that the aerosol composition of the central region contained significantly more Ca^{+2} which separates it uniquely from the NNW region. Another possible explanation is transport of pollution from Europe or western Asia. However, only a small amount of the back trajectories in the NNW region originated over Europe [*Fuelberg et al.*, 2003]. This suggests that the long-range transport of European emissions was not significant but nevertheless may have contributed to the air mass composition. Surface data has found evidence of a large CO plume from European fossil fuel combustion that is advected eastward over Siberia in the spring [*Rockmann et al.*, 1999]. Also, surface level data from the NOAA/CMDL sites in eastern Europe have found maximum CO mixing ratios to occur in the late winter/spring [e.g., *Novelli et al.*, 1998]. Previous work in the western Pacific has found evidence of a European pollution signal in Asian continental outflow. For example, the transport of European emissions to the western Pacific was a possible cause of high-altitude

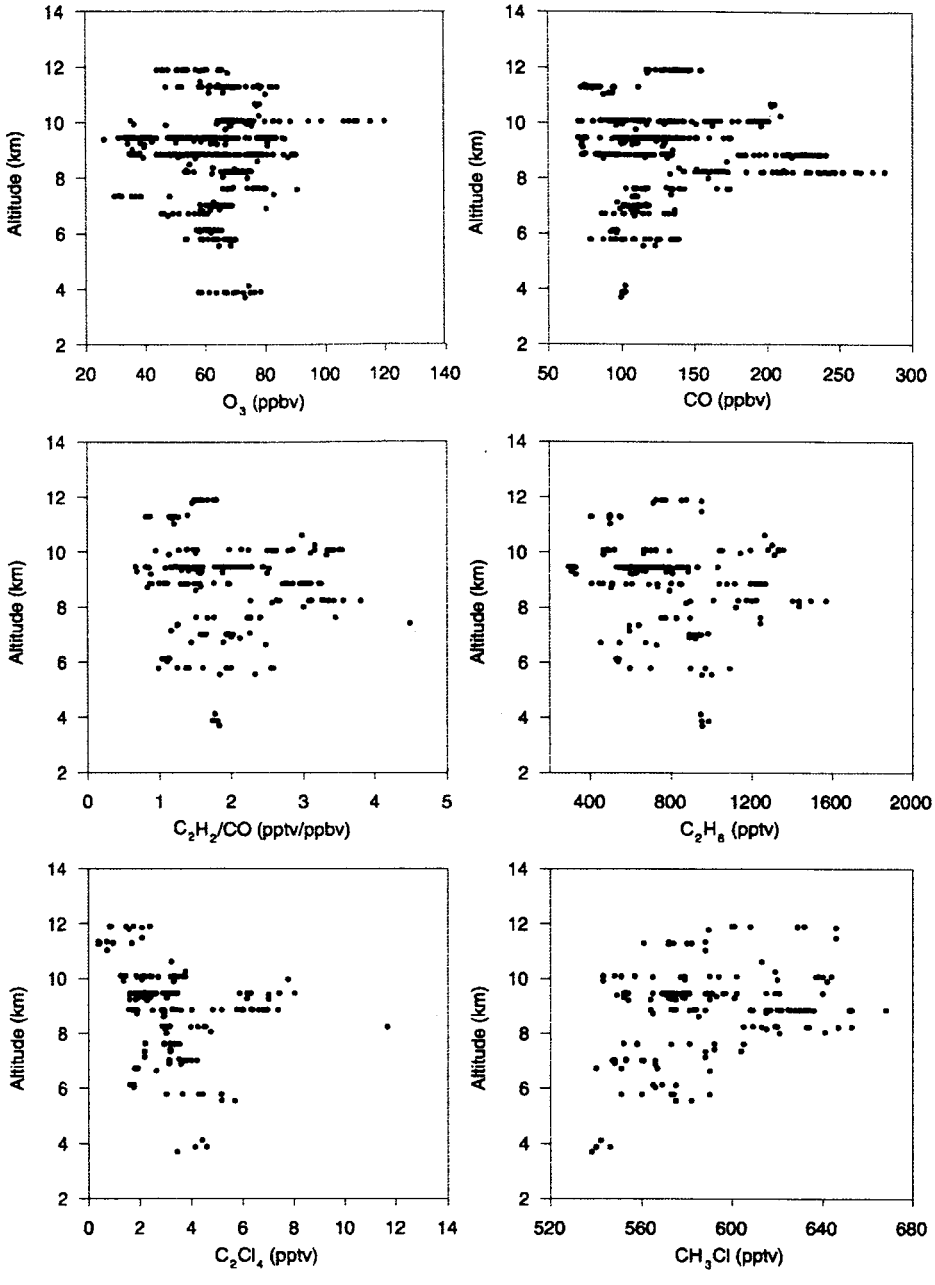

Figure 8. Vertical distributions of selected species in air masses originating in the West-Southwest source region.

species enhancements in the continental north group during PEM-West B [*Talbot et al.*, 1997]. In addition, anthropogenic emissions from Europe have been found to contribute significantly to Asian outflow at latitudes north of 40°N [*Bey et al.*, 2001]. However, any European influence south of 40°N indicated by 3-D simulations of CO mixing ratios was undetectable due to the strong Asian pollution signal [*Liu et al.*, 2003].

5.5. West-Southwest

[31] The WSW region only exhibited continental outflow in the middle and upper altitudes. The vertical distributions in the WSW and SE regions were similar in that significant outflow was present at high altitude (Figure 8, Table 5). Outflow from the WSW region occurred between 8 and 10 km. The CH_3OOH/H_2O_2 ratio was occasionally >1 in the outflow suggesting that some of the surface emissions may have been lifted by wet convection. Also, the lifting of emissions by midlatitude cyclones and their associated fronts appears to have been important for exporting emissions from the WSW region. This was the dominant transport pathway during TRACE-P [*Liu et al.*, 2003]. Furthermore, the C_2H_2/CO (>3) and C_3H_8/C_2H_6 (~0.2) ratios were enhanced above 7 km indicating that the outflow

contained relatively recent combustion inputs. As found in the SE region, background mixing ratios of several species, such as CO, O_3, C_2H_6, C_2H_2, C_3H_8, C_2Cl_4, and CH_3Cl, were also present intermittently in both the middle and upper troposphere indicating that substantial atmospheric processing had occurred. The similarities between the air mass composition in the WSW and SE regions may be a result of convective uplift of emissions from the SE region where they became entrained in the WSW region outflow.

[32] A striking feature of the WSW region is that both NO and CH_3Cl mixing ratios increased with altitude. The highest mixing ratios of NO were observed between 11 and 12 km, possibly from stratospheric inputs, lightning, or aircraft exhaust. Mixing ratios of O_3 (120 ppbv) and CO (~200 ppbv) were also enhanced around 10 km implying that these high-altitude air parcels contained a mixture of stratospheric and polluted air. *Talbot et al.* [2003] found that relationships between NO_x, O_3, and HNO_3 suggest a stratospheric source was responsible for enhanced NO_x in the upper troposphere. These results are consistent with data collected during the CARIBIC aircraft campaign that studied air masses at 10–11 km between Germany and the Indian Ocean [*Zahn et al.*, 2002]. This study area includes a portion of the WSW region. The CARIBIC study found that stratospheric inputs and photochemical production contributed equally to O_3 levels in the spring at middle latitudes. In contrast, photochemical production was responsible for the majority of the high-altitude O_3, with stratospheric inputs having a minimal influence, in the tropics [*Zahn et al.*, 2002]. This supports that both stratospheric and continental air was present in the upper troposphere of the WSW region and provides evidence that there are differences in the chemistry of the WSW and SE regions.

[33] NO and CH_3Cl were poorly correlated ($r^2 < 0.1$) above 7 km suggesting that biomass burning emissions were not responsible for the enhanced NO. *Liu et al.* [2003] concluded that CO emissions from African biomass burning were not detectable in air masses from the WSW region because any signal would be masked by the significant Asian pollution sources. Vertical lifting of emissions from the SE region is the most likely explanation for the enhanced CH_3Cl in the upper troposphere. However, an African contribution cannot be completely ruled out because a significant amount of the 5-day back trajectories in the WSW region originated over Africa. Also, biomass burning emissions from Africa have been shown to make a major contribution to Asian outflow at low latitudes and in the middle and upper troposphere [*Bey et al.*, 2001], and sources in the Middle East may have contributed to high-altitude outflow during PEM-West B [*Talbot et al.*, 1997].

[34] Recently injected anthropogenic emissions had a minimal influence on the composition of the middle troposphere in the WSW region. These air masses were aged several days and lacked strong correlations between key tracer species. C_2Cl_4 mixing ratios were enhanced ~9 km (~12 pptv), however, it was poorly correlated with CO and C_2H_2 ($r^2 < 0.4$ at middle and high altitudes) which is indicative of aged industrial emissions. Similar to the SE region, the high altitude outflow contained combustion and biomass/biofuel burning emissions as indicated by correlations of CO, C_2H_2, and C_2H_6 with CH_3Cl ($r^2 \sim 0.62-0.71$). Furthermore, C_2H_2 and C_2H_6 were moderately correlated with the biomass burning tracer, HCN ($r^2 = 0.78$ and 0.74, respectively). Among the high altitudes of the WSW, NNW, and SE regions, the highest mean and median mixing ratios of CO, C_2H_4, C_2H_2, C_6H_6, CH_3Cl, SO_2, PAN, and H_2O_2 were in air masses from the WSW region. Except for SO_2, these species are all characteristic of biomass burning. According to *Streets et al.* [2003], India is the second largest Asian source of SO_2, with power generation and industry being the largest sectors, and thus is a possible source of the enhanced SO_2. Similar results were found by the INDOEX campaign in 1999. Examination of air masses from India and SE Asia also found a minor contribution from industrial sources (low C_2Cl_4 and CH_3CCl_3) and an important influence in the free troposphere from biomass burning sources [*Scheeren et al.*, 2002].

6. Comparison With PEM-West B

[35] The TRACE-P and PEM-West B missions both occurred in late winter and spring but were conducted seven years apart. *Fuelberg et al.* [2003] concluded that the meteorological scenarios during the two missions were fairly similar; therefore meteorology most likely had a minimal influence on any variations in the tropospheric chemistry. Differences in the timing and design of the missions must also be considered. TRACE-P began later in February and lasted for a longer period of time than PEM-West B. As a result, the chemical composition may be influenced more by the characteristics of the springtime troposphere [*Fuelberg et al.*, 2003]. Furthermore, *Dibb et al.* [2003] suggest that the direct sampling of continental outflow, specifically near the Yellow Sea and the coast of China, during TRACE-P is a significant factor explaining different chemical and aerosol distributions between the two missions. This area was not probed during PEM-West B, and it clearly is a region heavily polluted by continental outflow.

[36] The three altitude ranges used in this paper are the same ranges used to characterize outflow during PEM-West B, thus allowing the vertical distributions to be compared. *Talbot et al.* [1997] separated the data at 20°N latitude into continental north and continental south groups. The NNW, central, coastal, and WSW regions are located at more northern latitudes and can thus be compared with the continental north group, and the SE and continental south regions can also be compared more or less directly. The median, maximum, and minimum mixing ratios of selected species are compared for the two missions in Tables 6–8. The "All" column represents all data from Flights 6–17 of TRACE-P, including data collected during spiral maneuvers. The WSW region is not included in the <2 km table (Table 6) because no boundary layer outflow was sampled. The central and coastal regions are not included in the >7 km table (Table 8) because they did not have high-altitude outflow due to their proximity to the flight paths.

6.1. Northern Regions

[37] The most striking difference between the two missions is that in all three altitude ranges the median O_3 mixing ratios were generally ~10–20 ppbv higher during TRACE-P. Although the seasonal timing of the two missions was fairly similar, TRACE-P did extend two weeks

Table 6. Comparison of Mixing Ratios for Selected Species From the TRACE-P and PEM-West B Missions for Data <2 km[a]

		All	Central	Coastal	NNW	PEM West B-North	SE	PEM West B-South
O_3	Median	53	64	43	54	42	40	41
	Max	138	138	83	67	144	43	76
	Min	15	41	15	36	34	27	16
CO	Median	201	264	166	207	186	205	187
	Max	1113	1113	586	266	623	254	260
	Min	99	135	124	136	145	157	125
C_2H_2	Median	643	860	384	757	792	456	464
	Max	10403	10403	3264	1205	3356	627	835
	Min	122	308	125	268	463	369	176
C_2H_6	Median	2079	2540	1353	2353	2294	1155	1053
	Max	4888	4888	3598	3607	4323	1412	1528
	Min	661	1396	669	1276	1582	1105	655
SO_2	Median	348	2621	48	272	104	20	68
	Max	30736	30736	1554	2821	29770	45	2290
	Min	4	353	4	4	26	7	52
C_2Cl_4	Median	11	12	8	12	20	5	7.6
	Max	123	123	32	21	50	5	13
	Min	3	8	3	6	9	4	5.4

[a]The All column refers to all data from Flights 6–17. Units are in pptv except for O_3 and CO which are in ppbv.

Table 7. Comparison of Mixing Ratios for Selected Species From the TRACE-P and PEM-West B Missions for Data Between 2 and 7 km[a]

		All	Central	Coastal	NNW	WSW	PEM West B-North	SE	PEM West B-South
O_3	Median	59	61	60	60	65	45	57	56
	Max	206	76	69	206	91	69	72	66
	Min	19	47	43	48	29	23	27	16
CO	Median	122	135	132	126	108	138	88	88
	Max	530	219	272	420	175	300	331	203
	Min	70	104	107	74	78	72	74	81
C_2H_2	Median	252	313	255	304	190	471	93	65
	Max	2233	645	908	1098	602	1481	1210	847
	Min	46	209	181	117	81	28	48	50
C_2H_6	Median	1078	1334	929	1646	893	1614	528	555
	Max	3441	1968	1974	2813	1242	3771	1775	1601
	Min	401	1125	793	641	451	469	422	468
SO_2	Median	38	65	21	42	26	22	23	12
	Max	6989	284	120	6989	298	1432	415	26
	Min	5	10	10	7	10	5	6	12
C_2Cl_4	Median	4	6	5	7	3	13	2	5
	Max	115	10	11	18	6	27	16	8
	Min	1	4	3	2	2	3.4	1	4

[a]The All column refers to all data from Flights 6–17. Units are in pptv except for O_3 and CO which are in ppbv.

more into the springtime than PEM-West B which may result in increased O_3 production. Several companion papers found that this seasonal difference could be an important factor explaining the observed trace gas distributions during TRACE-P compared with PEM-West B [e.g., *Blake et al.*, 2003; D. D. Davis et al., Trends western North-Pacific ozone photochemistry as defined by observations from NASA's PEM-West B [1994] and TRACE-P [2001] field studies, submitted to *Journal of Geophysical Research*, 2003].

[38] Another noticeable difference between the two missions was the approximate factor of 2 lower mixing ratios of C_2Cl_4 during TRACE-P. This is likely a reflection of reduced emissions of industrial species, such as C_2Cl_4, CH_3CCl_3, and CCl_4, in Asia [*Blake et al.*, 2003]. CO mixing ratios were somewhat higher during TRACE-P at both low and high altitude. In the middle troposphere, CO mixing ratios were fairly similar particularly when comparing the heavily polluted central and coastal regions with the continental north group. At low and middle altitudes, C_2H_2 and C_2H_6 were generally lower during TRACE-P than they were during PEM-West B possibly because of increased OH oxidation in the spring or better emission controls in East Asia [*Streets et al.*, 2003]. The only exception is the central group in which C_2H_2 and C_2H_6 had higher median and maximum mixing ratios in the boundary layer due to the Shanghai plume. The median SO_2 mixing ratios were significantly larger in the low and middle altitudes of the "All," central, and NNW groups during TRACE-P. This result is unexpected given that *Streets et al.* [2003] estimated a 17.2% reduction in SO_2 emissions during 1994–2001 in East Asia. The fact that the higher median SO_2 mixing ratios were in the central and NNW regions may be evidence of the importance of the extensive sampling over the Yellow Sea during TRACE-P as explained by *Dibb et al.* [2003]. Also, China still dominates Asian sulfur emissions [*Streets et al.*, 2003] which may be a factor. Furthermore, ground based data from the south China coast found similar results with higher O_3 and SO_2 during TRACE-P [*Wang et al.*, 2003].

6.2. Southern Regions

[39] A similarity between both missions is that mixing ratios for the six species used in this comparison were generally lower in the SE and continental south groups than in the northern TRACE-P regions and the continental north group. This is likely a result of the industrial cities and strong westerly outflow north of 20°N. In contrast to the northern groups, the median O_3 mixing ratios in the SE and continental south groups were remarkably similar in all altitude ranges. CO demonstrated the same trend as in the northern groups, with larger mixing ratios at low and high altitude during TRACE-P and with similar mixing ratios at middle altitudes.

Table 8. Comparison of Mixing Ratios for Selected Species From the TRACE-P and PEM-West B Missions for Data >7 km[a]

		All	NNW	WSW	PEM West B-North	SE	PEM West B-South
O_3	Median	53	151	66	51	32	35
	Max	208	208	120	119	70	69
	Min	18	59	26	25	18	21
CO	Median	102	105	121	94	88	81
	Max	341	118	281	316	223	111
	Min	63	88	70	62	67	57
C_2H_2	Median	146	164	208	131	89	67
	Max	1132	238	930	1513	609	274
	Min	47	138	47	35	47	16
C_2H_6	Median	631	916	731	672	514	543
	Max	1911	1076	1569	2463	1270	912
	Min	295	597	295	439	370	280
SO_2	Median	24	24	28	22	21	23
	Max	569	70	569	62	284	57
	Min	7	12	7	5	10	5
C_2Cl_4	Median	2	2	2	22	2	4.1
	Max	12	4	12	62	6	7.9
	Min	0	1	0	5	1	1.4

[a]The All column refers to all data from Flights 6–17. Units are in pptv except for O_3 and CO which are in ppbv.

Table 9. Comparison of Species Ratios for the Five TRACE-P Source Regions and the 2000 Asian Emissions Summary

Location	CO/CO_2	CO/CH_4	NO_x/SO_2	C_2H_6/C_3H_8
		Emissions Summary		
China	0.048	1.8	0.8	2.1
Other East Asia	0.014	2.2	2.7	1.3
Japan	0.009	3.7	3.8	1.1
Rep. of Korea	0.011	1.1	2.2	1.1
SE Asia	0.061	1.9	1.7	3.8
South Asia	0.054	1.1	1.1	2.7
India	0.053	1.1	1.2	2.6
	$\Delta CO/\Delta CO_2$	$\Delta CO/\Delta CH_4$	$\Delta NO_y/\Delta$ (SO_2 + nss SO_4)	$\Delta C_2H_6/\Delta C_3H_8$
		TRACE-P		
Central	0.022	1.6	0.3	2.6
Coastal	0.017	1.4	0.7	4.2
SE	0.013	3.4	4.8	5.2
NNW	1.017	1.4	0.5	2.8
WSW	0.020	2.1	3.6	5.2

In the middle troposphere, both the SE and continental south groups had a median CO value of 88 ppbv. C_2H_2, C_2H_6, and SO_2 did not exhibit any definite trends between the two missions. At low altitudes, C_2H_2 was fairly similar during the two missions while it appears higher in the SE group at middle and high altitudes. At low altitudes, SO_2 was significantly lower in the SE region compared to the continental south group. At high altitude in the WSW and SE regions, instances of significantly enhanced SO_2 were encountered as indicated by high maximum mixing ratios, but this did not occur in the upper troposphere during PEM-West B. C_2Cl_4 was also lower in the SE region than in the PEM-West B continental south group presumably reflecting reduced emissions of industrial species.

7. Comparison of Source Regions With Emissions Summary

[40] In order to gain insight on how well the 2000 Asian anthropogenic emissions summary developed by *Streets et al.* [2003] represented the Asian continent and how representatively the DC-8 sampled Asian outflow, emission ratios were compared with species ratios from each of the five source regions identified and characterized in this paper. The $\Delta CO/\Delta CO_2$, $\Delta CO/\Delta CH_4$, $\Delta C_2H_6/\Delta C_3H_8$, and $\Delta NO_y/\Delta(SO_2 + nss\text{-}SO_4)$ ratios for each of the five source regions were compared with the ratios from the emissions summary. The Δ refers to the difference between the measured and background mixing ratios and represents the impact from Asian emissions. The emissions summary provides data for NO_x and SO_2, so the NO_x/SO_2 ratio was compared with the observed $\Delta NO_y/\Delta(SO_2 + nss\text{-}SO_4)$ ratio. This latter ratio accounts for conversion of primary nitrogen and sulfur species present in the atmosphere after emission from various sources. Here nss-SO_4 represents non-sea-salt sulfate as presented by *Dibb et al.* [2003].

[41] The total anthropogenic emissions data was used from the emissions inventory. The median mixing ratios of all the data for each species in the five TRACE-P source regions were used in the calculations. Background mixing ratios were determined from Flight 5 as discussed previously in this paper. The background mixing ratios used were: CO = 70 ppbv, CO_2 = 370 ppmv, CH_4 = 1750 ppbv, C_2H_6 = 420 pptv, C_3H_8 = 15 pptv, SO_2 + nss-SO_4 = 50 pptv, and NO_y = 60 pptv. These ratios only provide a rough comparison of the emissions summary and the TRACE-P data. The TRACE-P measurements were collected from several altitudes while the emission summary ratios may be more representative of surface measurements. TRACE-P ratios using only <2 km data were calculated and compared with the ratios using all the data from the three altitude ranges. There was very little difference between the ratios so we used the larger data set composed of the data from all three altitude bins. Also, the five source regions identified in this paper and the regions used in the emissions inventory are not exactly the same. Furthermore, the emission summary represents an entire year, but the TRACE-P source regions are only representative of 6 weeks of data. However, *Streets et al.* [2003] concluded that emissions during the TRACE-P period were near their average values.

[42] In general, there was remarkably good agreement and correspondence between the ratios for our five source regions and the emissions summary (Table 9). All calculated TRACE-P ratios were generally within the same order of magnitude as the emission summary ratios. The $\Delta CO/\Delta CO_2$ ratio for TRACE-P was ~0.02 in all five source regions which is within the estimated range of emission ratios, ~0.01–0.06. Both the CO/CH_4 and $\Delta CO/\Delta CH_4$ ratios were between 1 and 4, and both the C_2H_6/C_3H_8 and $\Delta C_2H_6/\Delta C_3H_8$ ratios were between ~1 and 5.2 for all regions compared. *Carmichael et al.* [2003b] examined numerous chemical species ratios using both observed and modeled results and found that high values of the C_2H_6/C_3H_8 ratio (~8) are representative of biomass burning in SE Asia while a lower ratio value (~2) reflects biofuel combustion. The $\Delta C_2H_6/\Delta C_3H_8$ values are highest in the SE and WSW source regions (~5.2), and the highest C_2H_6/C_3H_8 values from the emissions inventory are in the SE and South Asia groups, which is somewhat consistent with the *Carmichael et al.* [2003b] results. The $\Delta C_2H_6/\Delta C_3H_8$ ratio value in the central and NNW regions is ~2.7 which is near the expected value due to the higher use of fossil fuels and biofuels in central China.

[43] The $\Delta CO/\Delta CO_2$, $\Delta CO/\Delta CH_4$, $\Delta C_2H_6/\Delta C_3H_8$, and $\Delta NO_y/\Delta(SO_2 + nss\text{-}SO_4)$ ratios in the central and coastal regions were similar and comparable to the respective ratios

from the China region. For example, the NO_x/SO_2 ratio value of 0.77 for China is very comparable with the $\Delta NO_y/\Delta(SO_2 + nss\text{-}SO_4)$ ratios of 0.30 and 0.73 for the central and coastal regions, respectively. These ratio values are consistent with the observed NO_y/SO_x values ($\sim$0.2–0.5) for Chinese cities from *Carmichael et al.* [2003b]. The values are also fairly similar with the NO_x/SO_2 ratio ($\sim$0.31) based on emission estimates of *Kato and Akimoto* [1992]. The consistency of these four ratios suggests that the Asian emission inventory and DC-8 sampling during TRACE-P were fairly representative of Asian anthropogenic sources.

8. Conclusions

[44] In this paper we present the chemical composition of Asian outflow during the NASA TRACE-P mission in spring 2001. Outflow from the Asian continent had a significant influence on the tropospheric chemical composition over the western Pacific, and this impact extended into the central Pacific. The strongest outflow occurred between 20 and 40°N latitude and at low altitudes. Recent combustion emissions ($C_2H_2/CO \sim 4$) and enhanced species mixing ratios were encountered in the free troposphere and as far east as 150°E longitude reflecting rapid uplift and transport of continental emissions.

[45] Using 5-day backward trajectories, five source regions of continental outflow were identified. These regions were central, coastal, southeast, north-northwest, and west-southwest Asia. Outflow from all five regions was composed of a complex mixture of recent and photochemically aged combustion, industrial, and biomass/biofuel burning emissions. The outflow in each source region contained enhancements in many of the same anthropogenic species. A single pollution source did not dominate any of the air masses sampled from a specific source region. The distance of air mass origin from the western Pacific and the degree of processing in air masses influenced the vertical distribution and magnitude of the species enhancements. These results provide valuable documentation of species mixing ratios and the complexity of Asian continental outflow.

[46] The outflow in each source region contained CO that was at least 3 times larger than background ($\sim$70 ppbv) and relatively recent emissions as indicated by enhanced hydrocarbon ratios ($C_2H_2/CO \geq 3$ and $C_3H_8/C_2H_6 \geq 0.2$). As expected, the anthropogenic activity in East Asia had a direct impact on the chemical composition of air masses in the central and coastal regions. The highest mixing ratios for many species and most recent combustion emissions were found in the boundary layer of these two regions. CO, C_2H_2, CH_3Cl, and C_2Cl_4 were strongly correlated ($r^2 \sim 0.6$ to 0.98) in the central, coastal, and SE regions. Biomass burning was a large source of emissions in SE Asia; however, combustion and industrial sources were also significant. Recent combustion emissions were mixed with processed industrial and biomass/biofuel burning emissions in the NNW region. Aged industrial emissions were also found in the WSW region and were mixed with combustion and biomass burning emissions in the upper troposphere. Convection or lifting associated with mid-latitude cyclones was most likely responsible for the high altitude enhancements observed in the SE and WSW regions. Based on the backward trajectories, the long-range transport of emissions from Africa, the Middle East, or Europe may have also made a minor contribution to the composition of air masses in the middle and upper troposphere of the NNW and WSW regions.

[47] A comparison between the TRACE-P and PEM-West B missions revealed some important differences. At northern latitudes, O_3 mixing ratios were higher during TRACE-P but were relatively unchanged in southern regions. At low and high altitude, CO was higher during TRACE-P, but it was quite similar in the middle troposphere. C_2H_2, C_2H_6, and SO_2 did not exhibit a definite trend between the two missions. C_2Cl_4 was lower at all altitudes during TRACE-P. The $\Delta CO/\Delta CO_2$, $\Delta CO/\Delta CH_4$, $\Delta C_2H_6/\Delta C_3H_8$, and $\Delta NO_y/\Delta(SO_2 + nss\text{-}SO_4)$ ratios for each source region were compared with the CO/CO_2, CO/CH_4, C_2H_6/C_3H_8, and NO_x/SO_2 ratios using data from the 2000 Asian emissions summary. The ratios agreed remarkably well indicating that the measurements obtained during TRACE-P and the emissions inventory were both representative of Asian emissions.

[48] **Acknowledgments.** We would like to thank the NASA Dryden Research Center flight and ground crews for their support during TRACE-P. This research was supported by the NASA Global Tropospheric Chemistry program.

References

Bachmeier, M A. S., R. E. Newell, M. C. Shipham, Y. Zhu, D. R. Blake, and E. V. Browell, PEM-West A: Meteorological overview, *J. Geophys. Res.*, *101*, 1655–1677, 1996.

Berntsen, T. K., S. Karlsdottir, and D. A. Jaffe, Influence of Asian emission on the composition of air reaching the northwestern United States, *Geophys. Res. Lett.*, *26*, 2171–2174, 1999.

Bey, I., D. J. Jacob, J. A. Logan, and R. M. Yantosca, Asian chemical outflow to the Pacific in spring: Origins, pathways and budgets, *J. Geophys. Res.*, *106*, 23,097–23,113, 2001.

Blake, D. R., and F. S. Rowland, Urban leakage of liquefied petroleum gas and its impact on Mexico City air quality, *Science*, *269*, 953–956, 1995.

Blake, D. R., T.-Y. Chen, T. W. Smith Jr., J.-L. C.Wang, O. W. Wingenter, N. J. Blake, and F. S. Rowland, Three-dimensional distribution of nonmethane hydrocarbons and halocarbons over the northwestern Pacific during the 1991 Pacific Exploratory Mission (PEM-West A), *J. Geophys. Res.*, *101*, 1763–1778, 1996.

Blake, N. J., D. R. Blake, T.-Y. Chen, J. E. Collins Jr., G. W. Sachse, B. E. Anderson, and F. S. Rowland, Distribution and seasonality of selected hydrocarbons and halocarbons over the western Pacific basin during PEM-West A and PEM-West B, *J. Geophys. Res.*, *102*, 28,315–28,331, 1997.

Blake, N. J., et al., NMHCs and halocarbons in Asian continental outflow during TRACE P: Comparison to PEM-West B, *J. Geophys. Res.*, *108*(D20), 8806, doi:10.1029/2002JD003367, in press, 2003.

Browell, E. V., et al., Large-scale ozone and aerosol distributions, air mass characteristics, and ozone fluxes over the western Pacific Ocean in late-winter/early-spring, *J. Geophys. Res.*, *108*(D20), 8805, doi:10.1029/2002JD003290, in press, 2003.

Carmichael, G. R., et al., Regional-scale chemical transport modeling in support of intensive field experiments: Overview and analysis of the TRACE-P observations, *J. Geophys. Res.*, *108*(D21), 8823, doi:10.1029/2002JD003117, in press, 2003a.

Carmichael, G. R., et al., Evaluating regional emission estimates using the TRACE-P observations, *J. Geophys. Res.*, *108*(D21), 8810, doi:10.1029/2002JD003116, in press, 2003b.

Crutzen, P. J., and M. O. Andreae, Biomass burning in the tropics: Impact on atmospheric chemistry and biogeochemical cycles, *Science*, *250*, 1669–1678, 1990.

Derwent, R. G., D. R. Middleton, R. A. Field, M. E. Goldstone, J. N. Lester, and R. Perry, Analysis and interpretation of air quality data from an urban roadside location in central London over the period from July 1991 to July 1992, *Atmos. Environ.*, *29*, 923–946, 1995.

Dibb, J. E., R. W. Talbot, E. Scheuer, G. Seid, M. Avery, and H. Singh, Aerosol chemical composition in Asian continental outflow during TRACE-P: Comparison to PEM-West B, *J. Geophys. Res.*, *108*(D21), 8815, doi:10.1029/2002JD003111, in press, 2003.

Duce, R. A., C. K. Unni, B. J. Ray, J. M. Prospero, and J. T. Merrill, Long-range atmospheric transport of soil dust from Asia to the tropical North Pacific: Temporal variability, *Science*, *209*, 1522–1524, 1980.

Fuelberg, H., C. M. Kiley, J. R. Hannan, D. J. Westberg, M. A. Avery, and R. E. Newell, Atmospheric transport during the Transport and Chemical Evolution over the Pacific (TRACE-P) experiment, *J. Geophys. Res.*, *108*(D20), 8782, doi:10.1029/2002JD003092, in press, 2003.

Gregory, G. L., J. T. Merrill, M. C. Shipham, D. R. Blake, G. W. Sachse, and H. B. Singh, Chemical characteristics of tropospheric air over the Pacific Ocean as measured during PEM-West B: Relationship to Asian outflow and trajectory history, *J. Geophys. Res.*, *102*, 28,275–28,285, 1997.

Heald, C. L., D. J. Jacob, P. I. Palmer, M. J. Evans, G. W. Sachse, H. Singh, and D. Blake, Biomass burning emission inventory with daily resolution: Application to aircraft observations of Asian outflow, *J. Geophys. Res.*, *108*(D21), 8811, doi:10.1029/2002JD003082, in press, 2003.

Heikes, B. G., Formaldehyde and hydroperoxides at Mauna Loa Observatory, *J. Geophys. Res.*, *97*, 18,001–18,013, 1992.

Heikes, B., M. Lee, D. Jacob, R. Talbot, J. Bradshaw, H. Singh, D. Blake, B. Anderson, H. Fuelberg, and A. M. Thompson, Ozone, hydroperoxides, oxides of nitrogen, and hydrocarbon budgets in the marine boundary layer over the South Atlantic, *J. Geophys. Res.*, *101*, 24,221–24,234, 1996.

Jacob, D. J., J. A. Logan, and P. P. Murti, Effect of Asian emissions on surface ozone in the United States, *Geophys. Res. Lett.*, *26*, 2175–2178, 1999.

Jacob, D. J., J. H. Crawford, M. M. Kleb, V. E. Connors, R. J. Bendura, J. L. Raper, G. W. Sachse, J. C. Gille, and L. Emmons, The Transport and Chemical Evolution over the Pacific (TRACE-P) mission: Design, execution, and overview of first results, *J. Geophys. Res.*, *108*(D20), 8781, doi:10.1029/2002JD003276, in press, 2003.

Jaffe, D. A., et al., Transport of Asian air pollution to North America, *Geophys. Res. Lett.*, *26*, 711–714, 1999.

Jordan, C. E., B. Anderson, R. W. Talbot, J. E. Dibb, H. E. Fuelberg, C. H. Hudgins, C. M. Kiley, R. Russo, E. Scheuer, G. Seid, K. L. Thornhill, and E. Winstead, Chemical and physical properties of bulk aerosols within four sectors observed during TRACE-P, *J. Geophys. Res.*, *108*(D21), 8813, doi:10.1029/2002JD003337, in press, 2003.

Kang, D., V. P. Aneja, R. G. Zika, C. Farmer, and J. D. Ray, Nonmethane hydrocarbons in the rural southeast United States national parks, *J. Geophys. Res.*, *106*, 3133–3155, 2001.

Kato, N., and H. Akimoto, Anthropogenic emissions of SO_2 and NO_x in Asia: Emission inventories, *Atmos. Environ.*, *26A*, 2997–3017, 1992.

Khalil, M. A. K., R. M. Moore, D. B. Harper, J. M. Lobert, D. J. Erickson, V. Koropalov, W. T. Sturges, and W. C. Keene, Natural emissions of chlorine-containing gases: Reactive Chlorine Emissions Inventory, *J. Geophys. Res.*, *104*, 8333–8346, 1999.

Li, Q., D. J. Jacob, R. M. Yantosca, C. L. Heald, H. Singh, M. Koike, Y. Zhao, G. W. Sachse, and D. G. Streets, A global 3-D model evaluation of the atmospheric budgets of HCN and CH_3CN: Constraints from aircraft measurements over the western Pacific, *J. Geophys. Res.*, *108*(D21), 8827, doi:10.1029/2002JD003075, in press, 2003.

Liu, H., D. J. Jacob, I. Bey, R. M. Yantosca, B. N. Duncan, and G. W. Sachse, Transport pathways for Asian combustion outflow over the Pacific: Interannual and seasonal variations, *J. Geophys. Res.*, *108*(D20), 8786, doi:10.1029/2002JD003102, in press, 2003.

Lobert, J. M., W. C. Keene, J. A. Logan, and R. Yevich, Global chlorine emissions from biomass burning: Reactive Chlorine Emissions Inventory, *J. Geophys. Res.*, *104*, 8373–8389, 1999.

McKeen, S. A., and S. C. Liu, Hydrocarbon ratios and photochemical history of air masses, *Geophys. Res. Lett.*, *20*, 2363–2366, 1993.

Merrill, J. T., M. Uematsu, and R. Black, Meteorological analysis of long range transport of mineral aerosols over the North Pacific, *J. Geophys. Res.*, *94*, 8584–8598, 1989.

Merrill, J. T., R. E. Newell, and A. S. Bachmeier, A meteorological overview for the Pacific Exploratory Mission-West Phase B, *J. Geophys. Res.*, *102*, 28,241–28,253, 1997.

Na, K., Y. P. Kim, and K. C. Moon, Diurnal characteristics of volatile organic compounds in the Seoul atmosphere, *Atmos. Environ.*, *37*, 733–742, 2003.

Novelli, P. C., K. A. Masarie, and P. M. Lang, Distributions and recent changes of carbon monoxide in the lower troposphere, *J. Geophys. Res.*, *103*, 19,015–19,033, 1998.

Rockmann, T., C. A. M. Brenninkmeijer, M. Hahn, and N. F. Elansky, CO mixing and isotope ratios across Russia: Trans-Siberian railroad expedition TROICA 3, April 1997, *Chemosphere Global Change Sci.*, *1*, 219–231, 1999.

Scheeren, H. A., J. Lelieveld, J. A. de Gouw, C. van der Veen, and H. Fischer, Methyl chloride and other chlorocarbons in polluted air during INDOEX, *J. Geophys. Res.*, *107*(D19), 8015, doi:10.1029/2001JD001121, 2002.

Simpson, I. J., N. J. Blake, E. Atlas, F. Flocke, J. H. Crawford, H. E. Fuelberg, C. M. Kiley, F. S. Rowland, and D. R. Blake, Photochemical production and evolution of selected C_2-C_5 alkyl nitrates in tropospheric air influenced by Asian outflow, *J. Geophys. Res.*, *108*(D20), 8808, doi:10.1029/2002JD002830, in press, 2003.

Singh, H. B., and P. B. Zimmerman, Atmospheric distribution and sources of nonmethane hydrocarbons, in *Gaseous Pollutants: Characterization and Cycling*, John Wiley, New York, 1992.

Singh, H. B., et al., In situ measurements of HCN and CH_3CN in the Pacific troposphere: Sources, sinks, and comparisons with spectroscopic observations, *J. Geophys. Res.*, *108*(D20), 8795, doi:10.1029/2002JD003006, in press, 2003.

Smyth, S., et al., Comparison of free tropospheric western Pacific air mass classification schemes for the PEM-West A experiment, *J. Geophys. Res.*, *101*, 1743–1762, 1996.

Streets, D. G., and S. T. Waldhoff, Biofuel use in Asia and acidifying emissions, *Energy*, *23*, 1029–1042, 1998.

Streets, D. G., and S. T. Waldhoff, Present and future emissions of air pollutants in China: SO_2, NO_x and CO, *Atmos. Environ.*, *34*, 363–374, 2000.

Streets, D. G., et al., An inventory of gaseous and primary aerosol emissions in Asia in the year 2000, *J. Geophys. Res.*, *108*(D21), 8809, doi:10.1029/2002JD003093, in press, 2003.

Talbot, R. W., et al., Chemical characteristics of continental outflow from Asia to the troposphere over the western Pacific Ocean during September–October 1991: Results from PEM-West A, *J. Geophys. Res.*, *101*, 1713–1725, 1996a.

Talbot, R. W., et al., Chemical characteristics of continental outflow over the tropical South Atlantic Ocean from Brazil and Africa., *J. Geophys. Res.*, *101*, 24,202–24,287, 1996b.

Talbot, R. W., et al., Chemical characteristics of continental outflow from Asia to the troposphere over the western Pacific Ocean during February–March 1994: Results from PEM-West B, *J. Geophys. Res.*, *102*, 28,255–28,274, 1997.

Talbot, R., J. Dibb, E. Scheuer, G. Seid, R. Russo, S. Sandholm, D. Tan, H. Singh, D. Blake, N. Blake, E. Atlas, G. Sachse, and M. Avery, Reactive nitrogen in Asian continental outflow over the western Pacific: Results from the NASA TRACE-P airborne mission, *J. Geophys. Res.*, *108*(D20), 8803, doi:10.1029/2002JD003129, in press, 2003.

Tang, Y., et al., The influences of biomass burning during TRACE-P experiment identified by the regional chemical transport model, *J. Geophys. Res.*, *108*(D21), 8824, doi:10.1029/2002JD003110, in press, 2003.

van Aardenne, J. A., G. R. Carmichael, H. Levy II, D. Streets, and L. Hordijk, Anthropogenic NO_x emissions in Asia in the period 1990–2020, *Atmos. Environ.*, *33*, 633–646, 1999.

Vay, S. A., et al., The influence of regional-scale anthropogenic emissions on CO_2 distributions over the western North Pacific, *J. Geophys. Res.*, *108*(D20), 8801, doi:10.1029/2002JD003094, in press, 2003.

Wang, C. J.-L., D. R. Blake, and F. S. Rowland, Seasonal variations in the atmospheric distribution of a reactive chlorine compound, tetrachloroethene ($CCl_2 = CCl_2$), *Geophys. Res. Lett.*, *22*, 1097–1100, 1995.

Wang, T., A. J. Ding, D. R. Blake, W. Zahorowski, C. N. Poon, and Y. S. Li, Chemical characterization of the boundary layer outflow of air pollution to Hong Kong during February–April 2001, *J. Geophys. Res.*, 2003.

Yienger, J. J., M. Galanter, T. A. Holloway, M. J. Phadnis, S. K. Guttikunda, G. R. Carmichael, W. J. Moxim, and H. Levy II, The episodic nature of air pollution transport from Asia to North America, *J. Geophys. Res.*, *105*, 26,931–26,945, 2000.

Zahn, A., C. A. M. Brenninkmeijer, W. A. H. Asman, P. J. Crutzen, G. Heinrich, H. Fischer, J. W. M. Cuijpers, and P. F. J. van Velthoven, Budgets of O_3 and CO in the upper troposphere: CARIBIC passenger aircraft results 1997–2001, *J. Geophys. Res.*, *107*(D17), 4337, doi:10.1029/2001JD001529, 2002.

E. Atlas and A. Fried, National Center for Atmospheric Research, Boulder, CO 80307, USA. (atlas@ucar.edu; fried@ucar.edu)

M. A. Avery, C. E. Jordan, G. W. Sachse, and S. A. Vay, NASA Langley Research Center, Hampton, VA 23665, USA. (m.a.avery@larc.nasa.gov; c.e.jordan@larc.nasa.gov; g.w.sachse@larc.nasa.gov; s.a.vay@larc.nasa.gov)

D. R. Blake and N. J. Blake, University of California, Irvine, Irvine, CA 92716, USA. (drblake@uci.edu; nblake@uci.edu)

J. E. Dibb, R. S. Russo, E. Scheuer, G. Seid, and R. W. Talbot, University of New Hampshire, Durham, NH 03820, USA. (jack.dibb@unh.edu; rrusso@resolution.sr.unh.edu; eric.scheuer@unh.edu; garry.seid@unh.edu; robert.talbot@unh.edu)

H. E. Fuelberg, Florida State University, Tallahassee, FL 32306, USA. (fuelberg@met.fsu.edu)

B. G. Heikes and J. Snow, University of Rhode Island, Narragansett, RI 02882, USA. (zagar@notos.gso.uri.edu; snow@gso.uri.edu)

S. T. Sandholm and D. Tan, Georgia Institute of Technology, Atlanta, GA 30332, USA. (scott.sandholm@eas.gatech.edu; tan@easlidar.gtri.gatech.edu)

H. B. Singh, NASA Ames Research Center, Moffett Field, CA 94035, USA. (hsingh@mail.arc.nasa.gov)

JOURNAL OF GEOPHYSICAL RESEARCH, VOL. 108, NO. D20, 8803, doi:10.1029/2002JD003129, 2003

Reactive nitrogen in Asian continental outflow over the western Pacific: Results from the NASA Transport and Chemical Evolution over the Pacific (TRACE-P) airborne mission

R. Talbot,[1] J. Dibb,[1] E. Scheuer,[1] G. Seid,[1] R. Russo,[1] S. Sandholm,[2] D. Tan,[2] H. Singh,[3] D. Blake,[4] N. Blake,[4] E. Atlas,[5] G. Sachse,[6] C. Jordan,[6] and M. Avery[6]

Received 1 November 2002; revised 22 April 2003; accepted 2 May 2003; published 31 October 2003.

[1] We present here results for reactive nitrogen species measured aboard the NASA DC-8 aircraft during the Transport and Chemical Evolution over the Pacific (TRACE-P) mission. The large-scale distributions total reactive nitrogen ($NO_{y,sum}$ = NO + NO_2 + HNO_3 + PAN + C_1–C_5 alkyl nitrates) and O_3 and CO were better defined in the boundary layer with significant degradation of the relationships as altitude increased. Typically, $NO_{y,sum}$ was enhanced over background levels of ~260 pptv by 20-to-30-fold. The ratio C_2H_2/CO had values of 1–4 at altitudes up to 10 km and as far eastward as 150°E, implying significant vertical mixing of air parcels followed by rapid advection across the Pacific. Analysis air parcels originating from five principal Asian source regions showed that HNO_3 and PAN dominated $NO_{y,sum}$. Correlations of $NO_{y,sum}$ with C_2Cl_4 (urban tracer) were not well defined in any of the source regions, and they were only slightly better with CH_3Cl (biomass tracer). Air parcels over the western Pacific contained a complex mixture of emission sources that are not easily resolvable as shown by analysis of the Shanghai mega-city plume. It contained an intricate mixture of pollution emissions and exhibited the highest mixing ratios of $NO_{y,sum}$ species observed during TRACE-P. Comparison of tropospheric chemistry between the earlier PEM-West B mission and the recent TRACE-P data showed that in the boundary layer significant increases in the mixing ratios of $NO_{y,sum}$ species have occurred, but the middle and upper troposphere seems to have been affected minimally by increasing emissions on the Asian continent over the last 7 years. *INDEX TERMS:* 0365 Atmospheric Composition and Structure: Troposphere—composition and chemistry; 0368 Atmospheric Composition and Structure: Troposphere—constituent transport and chemistry; 0322 Atmospheric Composition and Structure: Constituent sources and sinks

Citation: Talbot, R., et al., Reactive nitrogen in Asian continental outflow over the western Pacific: Results from the NASA Transport and Chemical Evolution over the Pacific (TRACE-P) airborne mission, *J. Geophys. Res.*, *108*(D20), 8803, doi:10.1029/2002JD003129, 2003.

1. Introduction

[2] The Transport and Chemical Evolution over the Pacific (TRACE-P) airborne mission was conducted by the National Aeronautics and Space Administration to better understand how outflow of anthropogenic emissions and crustal dust from the Asian continent affects the composition of the global atmosphere. The TRACE-P flights were designed to determine the pathways and chemical evolution of trace gases and aerosols transported to and across the north Pacific troposphere. TRACE-P built upon the results and experience from previous NASA missions conducted in this region in 1991 and 1994, the Pacific Exploratory Missions-West A and B, respectively [*Hoell et al.*, 1996, 1997]. Owing to the rapid industrialization on the Asian continent during the 1990s [*Streets et al.*, 2003], TRACE-P was conducted to quantify the corresponding increase in emissions and their impact on tropospheric chemistry over the Pacific basin. The airborne mission was conducted in February–April 2001, the time period of the year characterized by the most significant outflow of pollutants and crustal dust from the Asian continent [*Jacob et al.*, 2003]. The timing of this expedition compared to PEM-West presented an ideal situation to assess decadal changes in Asian inter-continental transport.

[3] PEM-West A was conducted in the September–October 1991 time frame and demonstrated the complex nature of emissions over the western Pacific. For example, in the lower troposphere continental outflow was enhanced in numerous combustion and industrial tracers but at higher

[1]Institute for the Study of Earth, Oceans, and Space, Climate Change Research Center, University of New Hampshire, Durham, New Hampshire, USA.
[2]Georgia Institute of Technology, Atlanta, Georgia, USA.
[3]NASA Ames Research Center, Moffett Field, California, USA.
[4]University of California, Irvine, Irvine, California, USA.
[5]National Center for Atmospheric Research, Boulder, Colorado, USA.
[6]NASA Langley Research Center, Hampton, Virginia, USA.

0148-0227/03/2002JD003129$09.00

altitudes the ratio C_2H_2/CO was <1.5 indicating much older inputs, possibly from European origin [*Talbot et al.*, 1996]. In the upper troposphere air parcels were enhanced in CH_4 but depleted in CO_2 and COS, indicating potential biogenic emissions of CH_4 and vegetative uptake of CO_2 and COS.

[4] A much more comprehensive sampling and analysis of Asian outflow was conducted during PEM-West B (1994) which revealed important subtle details. Backward 5-day isentropic trajectories and atmospheric chemistry together indicated that there was extensive rapid outflow from Asian continental areas below 5 km altitude [*Talbot et al.*, 1997a, 1997b]. Aged marine air was rarely encountered over the western Pacific due to the strong late winter/springtime continental outflow, and then it was only sampled at latitudes <20°N. The outflow at low altitude had significant enhancements of industrial tracers such as C_2Cl_4, CH_3CCl_3, and C_6H_6 intermixed with the combustion products C_2H_2, C_2H_6, CO, and NO. In the middle-to-upper troposphere, Middle Eastern and European source regions were implicated as possible contributors to the outflow. The importance of vertical convective transport was apparent, with subsequent removal of water-soluble species like HNO_3, SO_2, and H_2O_2. The long-range transport of PAN in the midtroposphere with subsequent downward mixing and conversion to NO_x was postulated to be an important source of reactive nitrogen to the remote Pacific boundary layer [*Dibb et al.*, 1997].

[5] The rapid industrialization on the Asian continent is of compelling interest to atmospheric chemistry and climate change. Energy use in eastern Asia has increased by 5% yr^{-1} over the past decade and is expected to continue at this rate for several more decades [*U.S. Department of Energy*, 1997]. Combustion of fossil fuels is the main source of energy, with emissions of NO_x predicted to increase nearly five-fold by 2020 [*Van Aardenne et al.*, 1999].

[6] The suite of NASA western Pacific missions has observed the time-dependent impact on the Northern Hemispheric tropospheric chemistry of a major industrial revolution on the Asian continent. Long-term observations from ground sites provide a continuous framework, but aircraft and satellite observations significantly augment our understanding of dynamical and chemical processes affecting atmospheric composition over a large remote geographic region like the Pacific basin. TRACE-P is the most recent NASA mission in the Pacific Rim region, and it provided a detailed chemical characterization of Asian continental outflow and emissions. In this paper we focus specifically on the suite of reactive nitrogen species, which are critical in determining the overall photochemical mixture of chemical species in continental outflow over the north Pacific. This outflow is expected to begin to influence atmospheric chemistry over North America within the current decadal time frame [*Bernsten and Karlsdottir*, 1999; *Jacob et al.*, 1999].

2. Airborne Mission

[7] The airborne component discussed in this paper was conducted aboard the NASA Dryden DC-8 research aircraft. Transit and intensive science missions comprised 20 flights, with each one averaging ~8 hours in duration and covering an altitude range of 0.3–12.5 km. The flights over the western Pacific, from which the data for this paper are drawn, were centered in the region west of 150°E longitude. The base of operations for these flights was from Hong Kong (seven missions) and Yokota, Japan (five missions).

[8] The overall scientific rationale and description of the individual aircraft missions are described in the TRACE-P overview paper [*Jacob et al.*, 2003]. The features of the large-scale meteorological regime and associated air parcel backward trajectory analyses for the February–March 2001 time frame are presented by *Fuelberg et al.* [2003]. A general description of the chemical composition of the Asian continental outflow is in a companion paper [*Russo et al.*, 2003]. The focus of that paper is primarily CO, O_3, and hydrocarbons, with minimal discussion of the NO_y family. The purpose of this paper is to fill that gap and provide more detail that can be addressed in a general discussion of continental outflow.

[9] We present here a broad description of the outflow chemistry focused on the reactive nitrogen family and refer to the overview paper [*Jacob et al.*, 2003] and companion papers for descriptions of the various measurements. Additionally, more specific information is included below for measurement details of the reactive nitrogen species. Since total reactive nitrogen (NO_y) was not measured on the DC-8, we use the sum of NO, NO_2, PAN, HNO_3, and C_1–C_5 alkyl nitrates to represent NO_y ($NO_{y,sum}$). Aerosol nitrate and PPN were not included in $NO_{y,sum}$ since their contribution to $NO_{y,sum}$ rarely exceeded 5% and 1%, respectively, and because in the case of nitrate its measurement time base (~10 min) was substantially longer than that for gas phase species. In general, the agreement between $NO_{y,sum}$ and NO_y measured with a gold catalytic converter is ~20% for the suite of TRACE-P instruments and NO_y mixing ratios in the range 100–3000 pptv [*Talbot et al.*, 1999].

[10] NO and NO_2 were measured by the Georgia Institute of Technology using photofragmentation two-photon laser-induced fluorescence (TP-LIF) [*Sandholm et al.*, 1990]. The method spectroscopically detects NO, with UV laser photolysis of NO_2 and subsequent detection of NO. The optical detection scheme involves sequentially exciting rotationally resolved transitions in the $X^2\Pi - A^2\Sigma$ and the $A^2\Sigma - D^2\Sigma$ bands of NO using laser wavelengths centered at 226 nm and 1.1 μm, respectively. The resulting blue shift in fluorescence is monitored near 190 nm. Calibration utilized a NIST certified NO standard (±1–2%). The overall uncertainty of the measurements is estimated to be on the order of 20–30% [*Eisele et al.*, 2003]. The sampling inlet was comprised of a 10 cm ID glass-coated (vapor-deposited) intake flowing by ram force at ~6×10^3 cm s^{-1}, giving a residence time of 40 ms. The details of the entire system are described by *Bradshaw et al.* [1999].

[11] PAN was measured by NASA Ames Research Center using cryogenic preconcentration of ambient air and analysis of it using gas chromatography with electron capture detection. PAN was measured every 5 min aboard the DC-8 by an electron-capture gas-chromatographic technique [*Singh et al.*, 2001]. Typically, 160 ml of ambient air was preconcentrated at −140°C over a 2-min period. PAN calibrations were performed by using a 2-ml diffusion tube filled with pure liquid PAN in an *n*-tridecane matrix. A dynamic dilution system was used to generate low-pptv mixing ratios of PAN. The technique has a measurement

sensitivity of better than 1 pptv PAN. Instrument precision and accuracy are estimated to be ±10% and ±25%, respectively. Intercomparison studies performed during TRACE-P further confirmed that the reliability of the PAN measurements was within these specifications [*Eisele et al.*, 2003].

[12] Nitric acid was measured by the University of New Hampshire using the mist chamber/ion chromatography technique [*Talbot et al.*, 2000]. Sampling was conducted using a high-flow manifold (3000 liters per min) that was glass-coated (vapor-deposited) and heated to 50°C. The manifold was 8 cm ID and had a diffuser configuration over the entrance to boost the flow/pressure and facilitate sampling at the high velocities (Mach 0.88) of the DC-8. The inlet design was nearly identical to that used for NO/NO_2 [*Bradshaw et al.*, 1999] and OH/HO_2 [*Brune et al.*, 1998]. The inlet was equipped with the capability to conduct standard additions of HNO_3 into the manifold and quantify its passing efficiency frequently during flight. A permeation source was used for HNO_3 from which the output was tracked using Nylon filters and a NO_x chemiluminescence instrument equipped with a molybdenum NO_y converter heated to 350°C. The output of the permeation source was about 200 ppbv of HNO_3 that could be readily diluted to pptv levels and quantified in our manifold. Thus standard additions were conducted at approximately twice ambient HNO_3 mixing ratios. The precision and accuracy of the HNO_3 measurements are both in the range of 10–20% depending on the ambient mixing ratio. The time resolution of the ambient measurements was two minutes. Inter-comparisons with a chemical ionization mass spectrometer instrument aboard the NASA P-3 aircraft during TRACE-P showed good agreement (±20%) under most atmospheric conditions [*Eisele et al.*, 2003].

[13] Alkyl nitrate species were measured by the University of California, Irvine and the National Center for Atmospheric Research (NCAR) after collection of ambient air samples in 2-liter electropolished stainless steel canisters. A two-stage metal bellows pump was used to pressurize the canisters to 3.8 hPa. Samples were obtained every 3–7 min during horizontal flight legs with a collection interval of 8 s at 150 m to 90 s at 12 km. The following alkyl nitrates were measured in each sample: methyl nitrate (CH_3ONO_2), ethyl nitrate ($C_2H_5ONO_2$), n-propyl nitrate (n-$C_3H_7ONO_2$), i-propyl nitrate (i-$C_3H_7ONO_2$), 2-butyl nitrate (2-$C_4H_9ONO_2$), 2-pentyl nitrate (2-$C_5H_{11}NO_3$), and 3-pentyl nitrate (3-$C_5H_{11}NO_3$). The analytical procedures are detailed by *Colman et al.* [2001]. The C_1–C_5 alkyl nitrates were separated using three of the five column-detector combinations in the UC-Irvine laboratory. The limit of detection for alkyl nitrates was typically 0.02 pptv with a precision of ±5% at mixing ratio >5 pptv and ±10% below 5 pptv. Calibration for alkyl nitrates used regular analysis of whole air standards which were intercalibrated with synthetic air standards prepared at NCAR. Analysis of duplicate samples and standards by both laboratories agreed within ±2%.

3. General Trends Over the Western Pacific

[14] To present the overall distribution of reactive nitrogen over the western Pacific, the entire 1 min data set for flights 6–17 was utilized. For species with a time response greater than 1 min, duplicated values generated by the merging process were removed from the database. Data collected above 7 km altitude was filtered additionally to remove stratospheric air influences using O_3 (>120 ppbv), CO (<70 ppbv), and dew point temperature (<−50°C) values indicative of stratospheric influence. However, the air parcels in this region often had both combustion and stratospheric influences superimposed, so it was impossible to completely remove the stratospheric component. The data set we used has some higher values of O_3 while the mixing ratios of other species such as CO were quite elevated. We only removed the most strongly influenced stratospheric cases.

[15] The latitudinal distributions of $NO_{y,sum}$ and CO are presented in Figure 1, and they illustrate the widespread influence of combustion emissions on atmospheric chemistry over the western Pacific. The close correspondence in the distribution of mixing ratios of CO and $NO_{y,sum}$ in the heavily polluted plumes suggests a direct source relationship between combustion and reactive nitrogen species. Indeed, at all altitudes in the latitudinal band of 20–40 °N well-defined plumes contained $NO_{y,sum}$ in excess of 1000 pptv. However, as shown later in this paper, outside the few large plumes the general correspondence between CO and $NO_{y,sum}$ is not readily apparent (they are largely uncorrelated).

[16] The relationship between $NO_{y,sum}$ and CO is shown in Figure 2. The correspondence in $NO_{y,sum}$ and CO was most apparent in the boundary layer and was not well defined at altitudes above it. Presumably this reflects sampling of less processed air parcels down low and the close proximity of major emission sources on the Asian continent. Even in the boundary layer the relationship between $NO_{y,sum}$ and CO was strongly driven by sampling of heavily polluted plumes advected over the Pacific Rim region from concentrated urban centers such as Shanghai. At higher altitudes the air parcels had undergone more processing, and they are also likely impacted by both Asian and other more distant sources. For example, a European influence was hypothesized for altitudes >7 km over the western Pacific during the PEM-West B time frame [*Talbot et al.*, 1997a]. However, for TRACE-P the European influence above 7 km appears to have been minimal based on three-dimensional (3-D) model results [*Liu et al.*, 2003].

[17] Photochemical processing of air parcels that have NO_x-rich hydrocarbon mixtures leads to production of a suite of reactive nitrogen compounds and O_3. Thus the correspondence between $NO_{y,sum}$ and O_3 is of interest. In general, the correlations between $NO_{y,sum}$ and O_3 were poorly defined in the Asian outflow over the western Pacific (Figure 2). As in the case of CO, the tightest relationship was found in the boundary layer, where it was again determined largely by the most heavily polluted plumes. In the midtroposphere the values were centered on an O_3 mixing ratio of 60 ppbv, with $NO_{y,sum}$ being as high as 2500 pptv. Observations very similar to these reported here were obtained during PEM-West B, except that it was centered on O_3 mixing ratios in the 40–50 ppbv range [*Koike et al.*, 1997]. Above 7 km altitude there was a weak linear trend in $NO_{y,sum}$ and O_3 that may be related to the strong linear correspondence between these species (i.e., HNO_3 and O_3) in stratospheric air [e.g., *Talbot et al.*, 1997b]. As stated earlier, air parcels in this region were

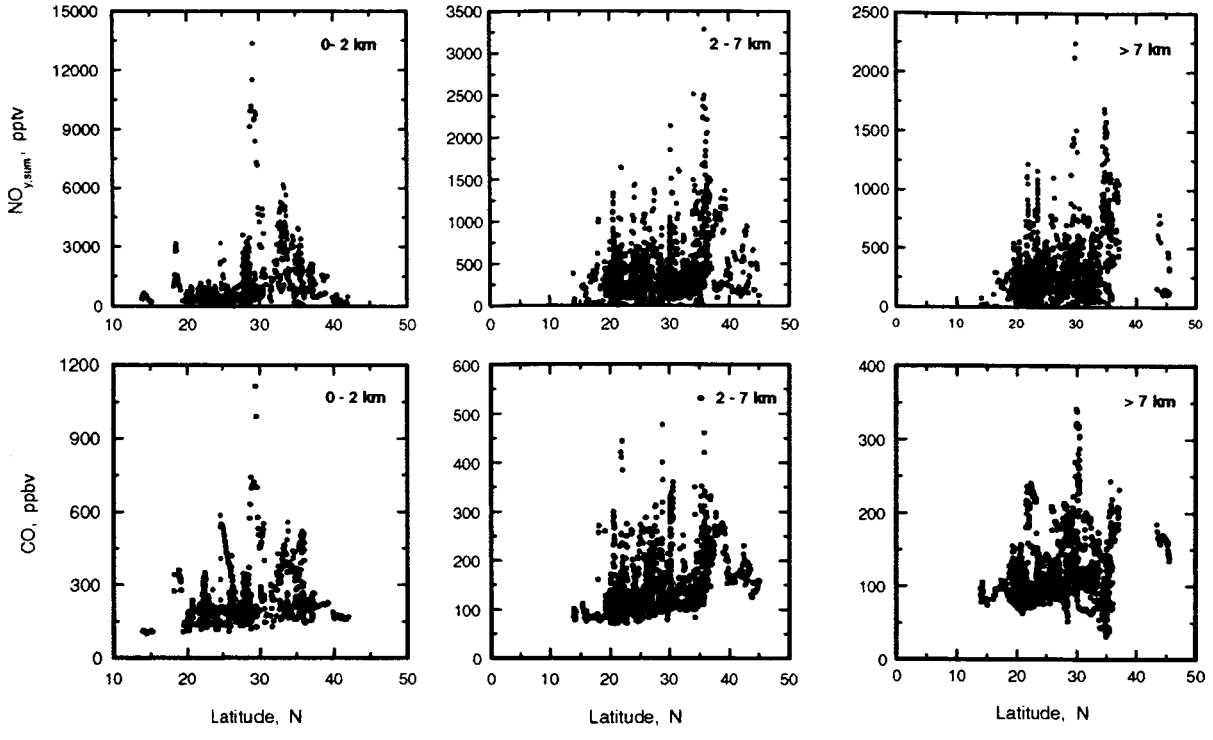

Figure 1. Latitudinal distribution of mixing ratios of NO_y and CO over the western Pacific west of 150°E longitude. Data is shown for three altitude bins of 0–2, 2–7, and >7 km.

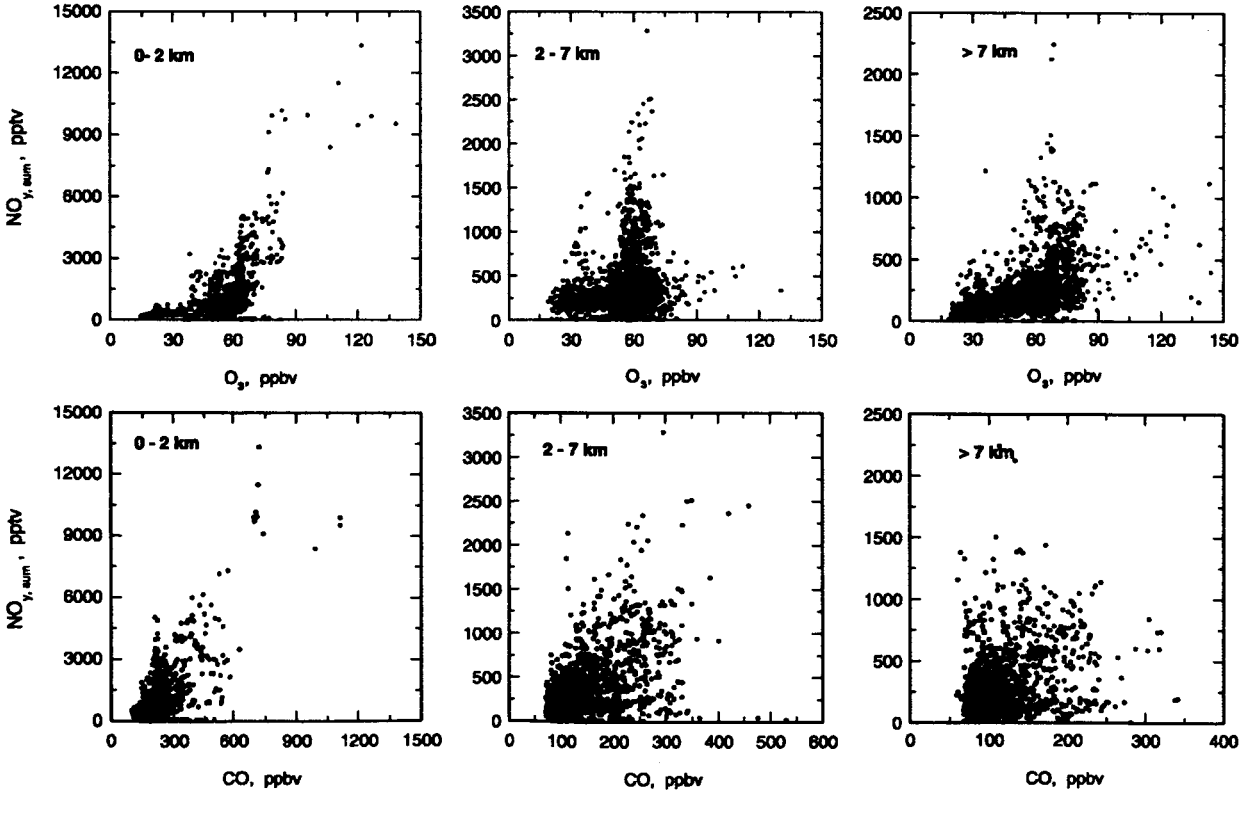

Figure 2. Relationships between mixing ratios of NO_y and CO or O_3 in three altitude bins of 0–2, 2–7, and >7 km.

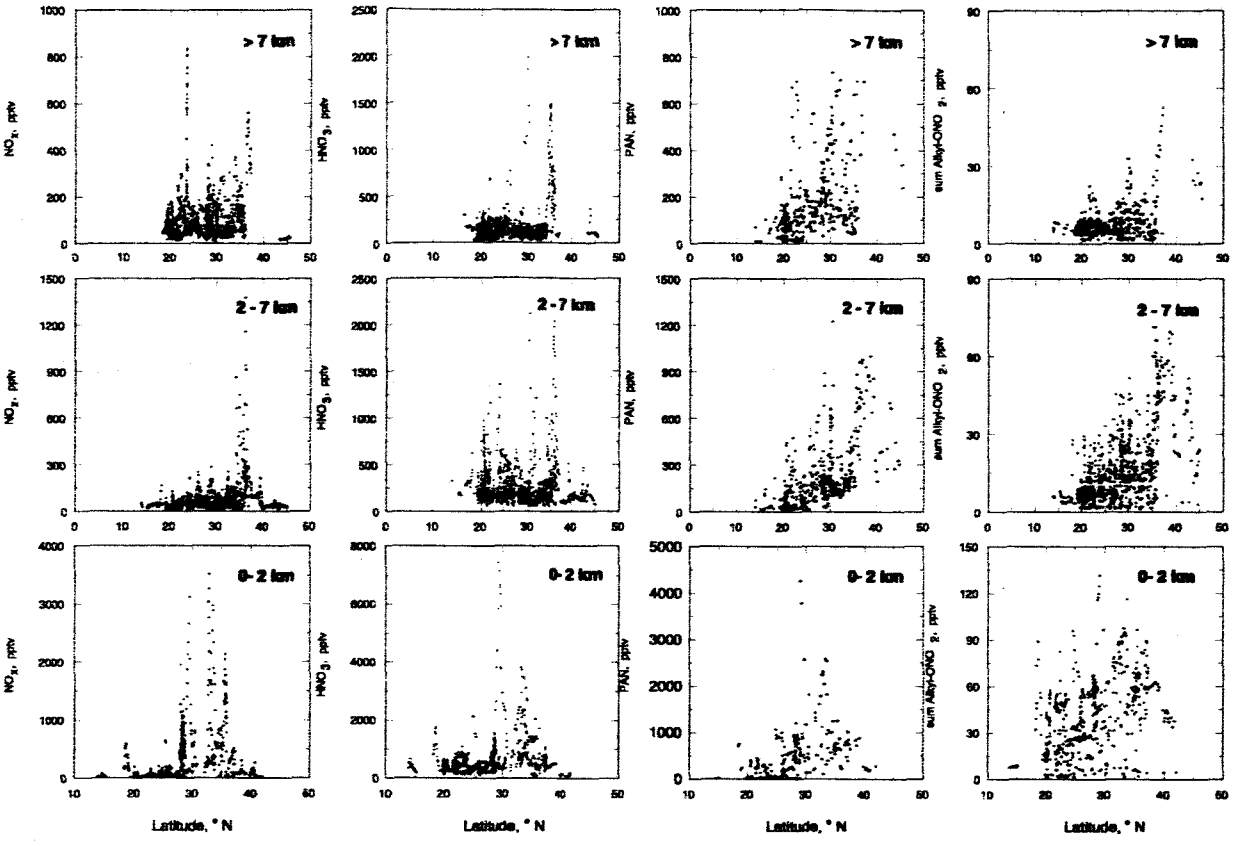

Figure 3. Latitudinal distribution of individual NOy species in three altitude bins of 0–2, 2–7, and >7 km.

influenced coincidently by combustion and stratospheric sources which could not be separated adequately. Alternatively, the positive correlation could have been the result of biomass burning emissions occurring in southeastern Asia. This point is addressed further in this paper when we examine specific characteristics of various Asian source regions based on analysis of air parcel backward trajectories.

[18] The latitudinal pattern of individual reactive nitrogen species over the western Pacific is presented in Figure 3. For the most part, mixing ratios of NO_x were <100 pptv, suggesting that the sampled air parcels were aged at least 1–2 days which allowed for transformations of it to HNO_3, PAN, and other $NO_{y,sum}$ species. The largest enhancements in all species occurred at 30°N when the DC-8 sampled the Shanghai mega-city urban plume during a boundary layer leg over the Yellow Sea. This plume contained mixing ratios of NO_x, HNO_3, PAN, and alkyl nitrates of up to 3,000, 8,000, 4,300, and 225 pptv, respectively. In a later section of this paper we discuss the chemical composition of this plume in detail.

[19] The vertical distribution of reactive nitrogen species provides insight to the nature of their sources, and in particular the association of origin either on the Asian continent or from long-range transport into the western Pacific region. These distributions are summarized in Figure 4, where the alkyl nitrate species are represented as the sum of the individual species (i.e., sum Alkyl-ONO_2). Shown also is aerosol nitrate based on Teflon filter measurements with approximately 10 min time resolution as described by *Dibb et al.* [2003].

[20] All the gas phase reactive nitrogen species showed significant deviations and enhancements well above their background values, defined as the median of the lowest 15% of the observed mixing ratios at a given altitude. The background mixing ratios exhibited little altitude dependence, and representative values were as follows: NO_x (25 pptv), HNO_3 (125 pptv), PAN (100 pptv), alkyl nitrates (7 pptv), aerosol nitrate (25 pptv), and $NO_{y,sum}$ (257 pptv). The enhancements occurred at all altitudes up to the 12 km ceiling of the DC-8 aircraft. It was not uncommon for the enhanced mixing ratios to be 10-to-20-fold larger than their corresponding background value. The greatest enhancement generally occurred in the boundary layer indicating the predominance of surface sources in Asia on regional tropospheric chemistry. Particularly noteworthy were the alkyl nitrate species which exhibited combined increases of up to 50 pptv at altitudes up to 8 km. The alkyl nitrate distribution was dominated by 2-butyl nitrate which comprised on average 30% of the sum depicted in Figure 4. In general, the vertical distributions indicate a strong surface source for $NO_{y,sum}$ species with a strong influence up to 10 km altitude. We argue later in this paper that based on C_2H_2/CO ratios of 1–4 these enhancements reflect fairly recent Asian emissions rather than influence from long-range transport.

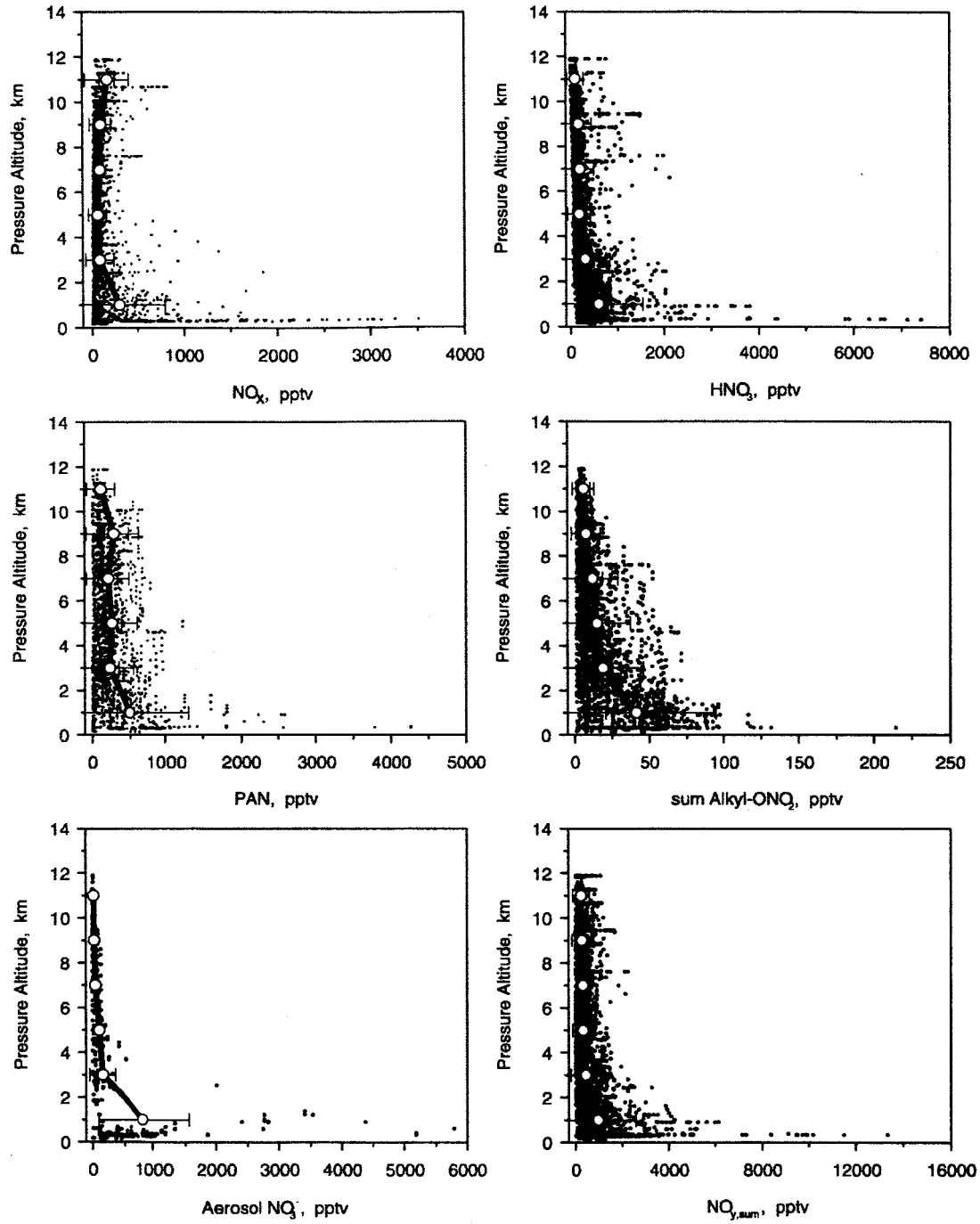

Figure 4. Vertical distribution of individual NO_y species over the western Pacific west of 150°E longitude. The open circles represent the mean value with one standard deviation indicated by the horizontal bar for two km thick altitude bins.

[21] The largest mixing ratios of aerosol nitrate were observed in the Asian coastal marine boundary layer. On some occasions ppbv values of aerosol nitrate were measured that far exceeded attendant mixing ratios of HNO_3. Undoubtedly, the high levels of nitrate reflected uptake of HNO_3 by sea salt aerosols, as evidenced by coincidently large mixing ratios of sodium and chloride [*Dibb et al.*, 2003; *Jordan et al.*, 2003].

[22] An important consideration for interpretation of the TRACE-P observations is the relative processing of air parcels over various spatial and temporal scales. Here we use the ratio C_2H_2/CO as a scaling factor in this regard since it is unaffected by physical removal processes. The ratio is decreased over time by chemical attack by OH (i.e., C_2H_2 lifetime about 2 weeks compared with CO of several months) and physical mixing processes. The distribution

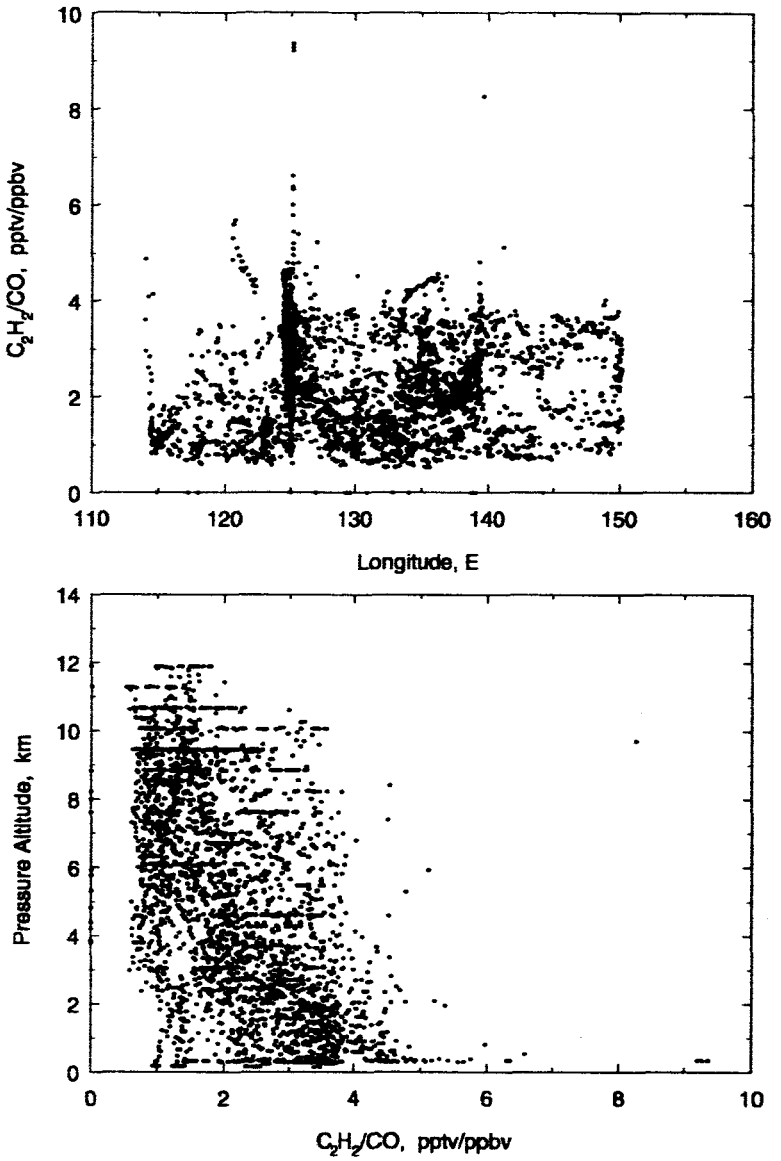

Figure 5. Vertical and longitudinal distributions of the C_2H_2/CO ratio over the western Pacific west of 150°E longitude.

of the values of this ratio over the western Pacific provides key insight into transport and mixing processes on various time scales. Values >1 indicate fairly recent emissions (<5 days) while ratios <1 indicate extensively processed air by mixing and chemical decomposition.

[23] The vertical altitudinal ensemble of values in C_2H_2/CO is presented in Figure 5 along with the longitudinal variation. The distributions are striking; ratio values in the middle-to-upper troposphere mimic the boundary layer and also indicate transport of continent emissions across the Pacific. Further, the data suggest that frontal uplifting and vertical transport must be rapid and operating continuously over the Asian continent in combination with extensive westerly transport of pollutants at all altitudes. The travel distances and timing implied by the backward trajectories suggest the uplifting and vertical transport must be occurring on the time scale of hours. A more detailed analysis is needed to better constrain these various transport rates. These results explain the blurred correlations between $NO_{y,sum}$ and CO or O_3. The continuous intermixing of air parcels of various ages and processing would lead directly to very complex distributions and relationships of $NO_{y,sum}$, CO, and O_3 over the western Pacific, which is exactly what we observed. This same picture was captured by the observation-based climatologies developed by *Emmons et al.* [2000]. For the western Pacific the model simulations for the PEM-West field campaigns showed the same vertical patterns and mixing ratios observed during TRACE-P for O_3, CO, and NO_x, but deviations were up to two-fold for HNO_3 and PAN. The model predicted ratios of PAN/NO_x and HNO_3/NO_x were 2–3 times higher than observations in the 2–8 km altitude range, indicating the difficulty in

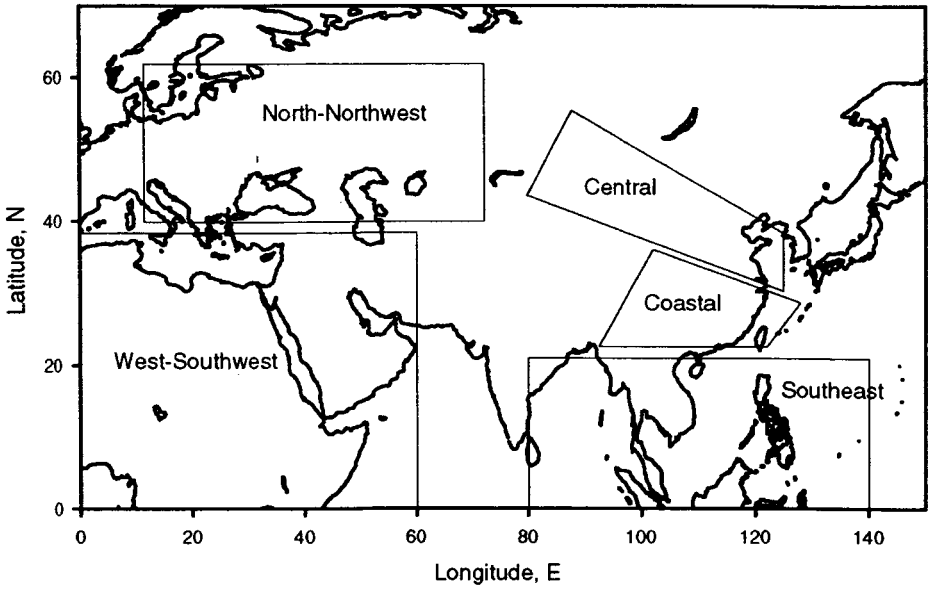

Figure 6. Geographic representation of the five principal source regions on the Asian continent determined from analysis of air parcel isentropic backward trajectories.

estimating the degree of air mass processing and interconversion of NO_y species.

[24] An important transport pattern over Asia during winter is bifurcation of westerly flow when it passes over the Tibetan Plateau. Here the northern branch forms many blocked anticyclones while the southern one forms many troughs or cut-off lows, such as the Bangladesh trough and other troughs in southern China. The two branches merge at the eastern edge of the Plateau, resulting in strong winds over the southern Sea of Japan, where the maximum wind speed can reach over 70 m s^{-1} at 500 mb [*Zhang*, 1992]. Such a dynamic system is conducive to the occurrence of unstable weather systems in southern China in winter. The associated dynamical processes help explain why the TRACE-P data show pollutants mixed to high altitudes and transported eastward rapidly to 150°E.

4. Relationships Based on Source Region Apportionments

[25] To examine the detailed relationships of $NO_{y,sum}$ species with source tracer species and their spatial variability, air parcel backward trajectories were used to establish the principal source region locations on the Asian continent. Isentropic backward trajectories were provided by Florida State University for TRACE-P, and a description of the method is provided in *Fuelberg et al.* [2003]. For consistency with other TRACE-P analyses, we adopted the source region designations in this paper determined by *Russo et al.* [2003] and *Jordan et al.* [2003]. Five regions were identified in their analyses as depicted in Figure 6. These were classified as follows: (1) north-northwest (NNW), (2) west-southwest (WSW), (3) southeast Asia (SE Asia), (4) coastal and, (5) central. The major urban/industrial centers in China are located within the coastal and central source regions.

[26] Since we have introduced the general latitudinal and vertical distributions of reactive nitrogen species for the western Pacific region, more specific source region relationships are presented here. We begin with the altitudinal budget of $NO_{y,sum}$ species in air masses with backward trajectories from the various source regions (Figure 7). In the southeast and coastal groups, HNO_3 dominated $NO_{y,sum}$ in the boundary layer and midtroposphere. This was especially true for the coastal group where HNO_3 comprised nearly 80% of $NO_{y,sum}$. There were nearly equal contributions from HNO_3 and PAN in the other three source regions, with PAN favored in the NNW and WSW groups at all altitudes. These distributions are consistent with expectations of less PAN in warmer locations due to its thermal instability and more PAN at higher altitudes where it is more stable. The predominance of HNO_3 and PAN in the $NO_{y,sum}$ budget indicates that the majority of sampled air parcels were aged several days with significant photochemical processing over that time interval. It is not clear why NO_x comprised 20–25% of $NO_{y,sum}$ in the middle to upper troposphere in the WSW group. This finding was quite different than in the other four groups where its contribution was <10%. Possibilities include recent inputs from sources such as biomass burning, lightning, and stratospheric inputs or decreased photochemical activity (i.e., less efficient conversion to other $NO_{y,sum}$ species).

[27] Together these data indicate that significant outflow of reactive nitrogen occurs at all altitudes from the Asian continent with much of it residing in the reservoir species PAN. Owing to its long lifetime in the middle and upper troposphere, it can subsequently carry reactive nitrogen over long distances and be a source of NO_x to various areas of the Northern Hemisphere troposphere. During PEM-West B strong outflow in the mid-troposphere contained high levels of PAN, and *Dibb et al.* [1997] hypothesized that it was a significant source of NO_x and subsequently aerosol nitrate to the remote marine boundary layer over the central Pacific.

[28] To assess the regional combustion influence on the $NO_{y,sum}$ distribution over the western Pacific, correlations

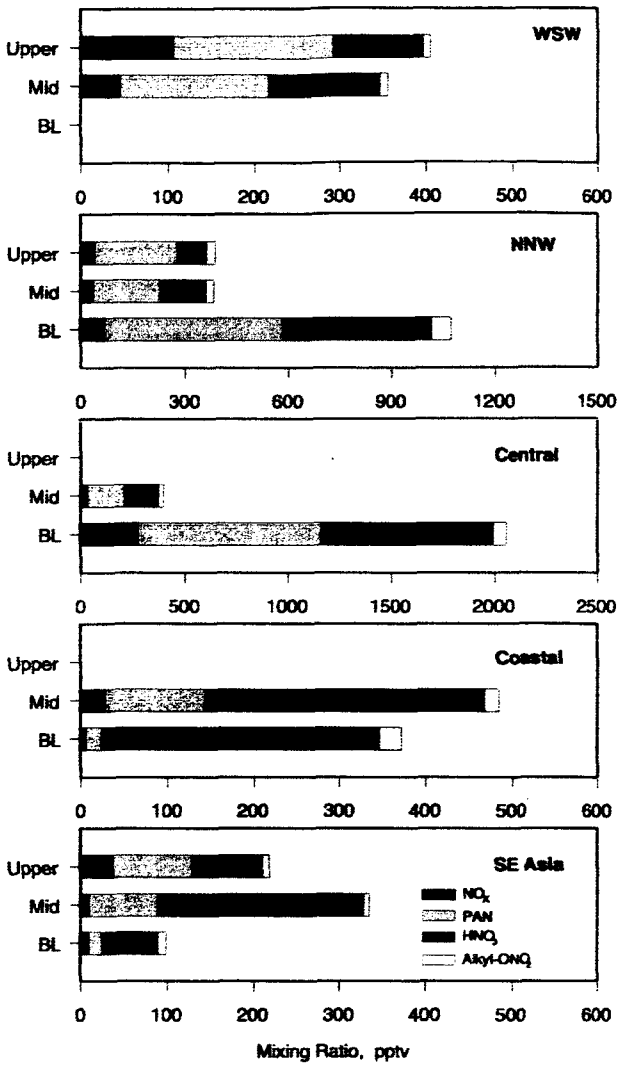

Figure 7. NO_y budget comparison for the five Asian source regions as a function of altitude (0–2, 2–7, and >7 km). Median values were used for to construct these budgets.

between C_2H_2 and $NO_{y,sum}$ were examined for the five primary Asian source areas defined in Figure 6. These relationships are illustrated in Figure 8. To the best of our understanding, the only source of C_2H_2 to the atmosphere is combustion [*Singh and Zimmerman*, 1992]. $NO_{y,sum}$ and C_2H_2 were highly correlated in the SE Asia region, and to a lesser extent in the central and coastal groups. The central group exhibited the best correspondence between $NO_{y,sum}$ and C_2H_2, but this was largely driven by the highly polluted nature of the Shanghai plume. There was little or no correlation between these species in the NNW and WSW regions. These two regions are the farthest from the western Pacific, and as such have likely undergone more atmospheric processing than the other groups. The source relationships are consequently more blurred in these datasets. As presented previously, the WSW group also showed the largest mixing ratios of NO_x above 7 km of all five source regions. The apparent low correlation with combustion suggests that the NO_x may be related to stratospheric inputs or be from recycled reactive nitrogen in the upper troposphere. However, why these NO_x sources would affect only this region is unclear.

[29] To check for stratospheric inputs, correlations were examined between NO_x and H_2O vapor, dew point, O_3, CO, and HNO_3 in upper troposphere for the WSW group. There was a trend of higher mixing ratios of NO_x occurring coincidently with low mixing ratios of H_2O vapor, dew point temperature, and CO (Figure 9). The highest mixing ratios of NO occurred simultaneously with the lowest dew point temperature and CO values near 50 ppbv, clearly indicative of stratospheric air. Mixing ratios of HNO_3 sporadically reached 300–800 pptv in these same air parcels (not shown). Although these trends lean toward a stratospheric source for the enhanced upper tropospheric NO_x in the WSW group, other sources such as lightning and combustion cannot be ruled out. Furthermore, it is clear that the air parcels in this upper tropospheric region were influenced by multiple sources, as the relative proportions of HNO_3 and PAN to $NO_{y,sum}$ are not consistent with a purely stratospheric source and the intermittent presence of CO mixing ratios in the 100–300 ppbv range.

[30] C_2Cl_4 is released exclusively by urban/industrial processes [*Blake et al.*, 1996], and as such is a good tracer of air parcels influenced by metropolitan areas. In the central and coastal groups there were very general linear relationships between $NO_{y,sum}$ and C_2Cl_4, but they were uncorrelated in the other groups (Figure 10). We examined correlations between individual $NO_{y,sum}$ component species and they too showed no clear correspondence with C_2Cl_4. However, it appears that the use or release of C_2Cl_4 has decreased since the PEM-West B mission. *Russo et al.* [2003] found that median values of C_2Cl_4 were about two-fold less than those observed in the PEM-West B study. This reduced urban/industrial signal probably contributed to the weak correlations between $NO_{y,sum}$ and C_2Cl_4 during TRACE-P. As indicated by the central group, concentrated urban sources of C_2Cl_4 still do exist on the Asian continent. Mixing ratios of C_2Cl_4 peaked near 125 pptv when the Shanghai urban plume was sampled over the Yellow Sea.

[31] Biomass burning on the Asian continent is expected to be a large source of $NO_{y,sum}$ [*Streets et al.*, 2003]. These emissions originate from fossil fuel combustion, bio-fuels for space heating and cooking, and agricultural practices. Good tracers of biomass burning emissions include soot carbon, fine aerosol potassium and ammonium, HCN, and CH_3Cl [*Crutzen et al.*, 1979; *Crutzen and Andreae*, 1990]. Here we have chosen to use CH_3Cl due to its availability on a 1-min time basis. The $NO_{y,sum}$ correlations with CH_3Cl over the western Pacific are depicted in Figure 11. The tightest correspondence was observed for the central source region, but it is entirely driven by sampling of the Shanghai plume. There were weak linear correlations in the SE Asia and coastal groups, and none in the NNW and WSW areas. Correlations very similar to those shown in Figure 11 were found using HCN instead of CH_3Cl (not shown). This is a bit unexpected, especially for the SE Asian region where extensive biomass burning was indicated by satellite surveying during the TRACE-P time period (available at http://www.people.fas.harvard.edu/~heald/fires.html). Both the

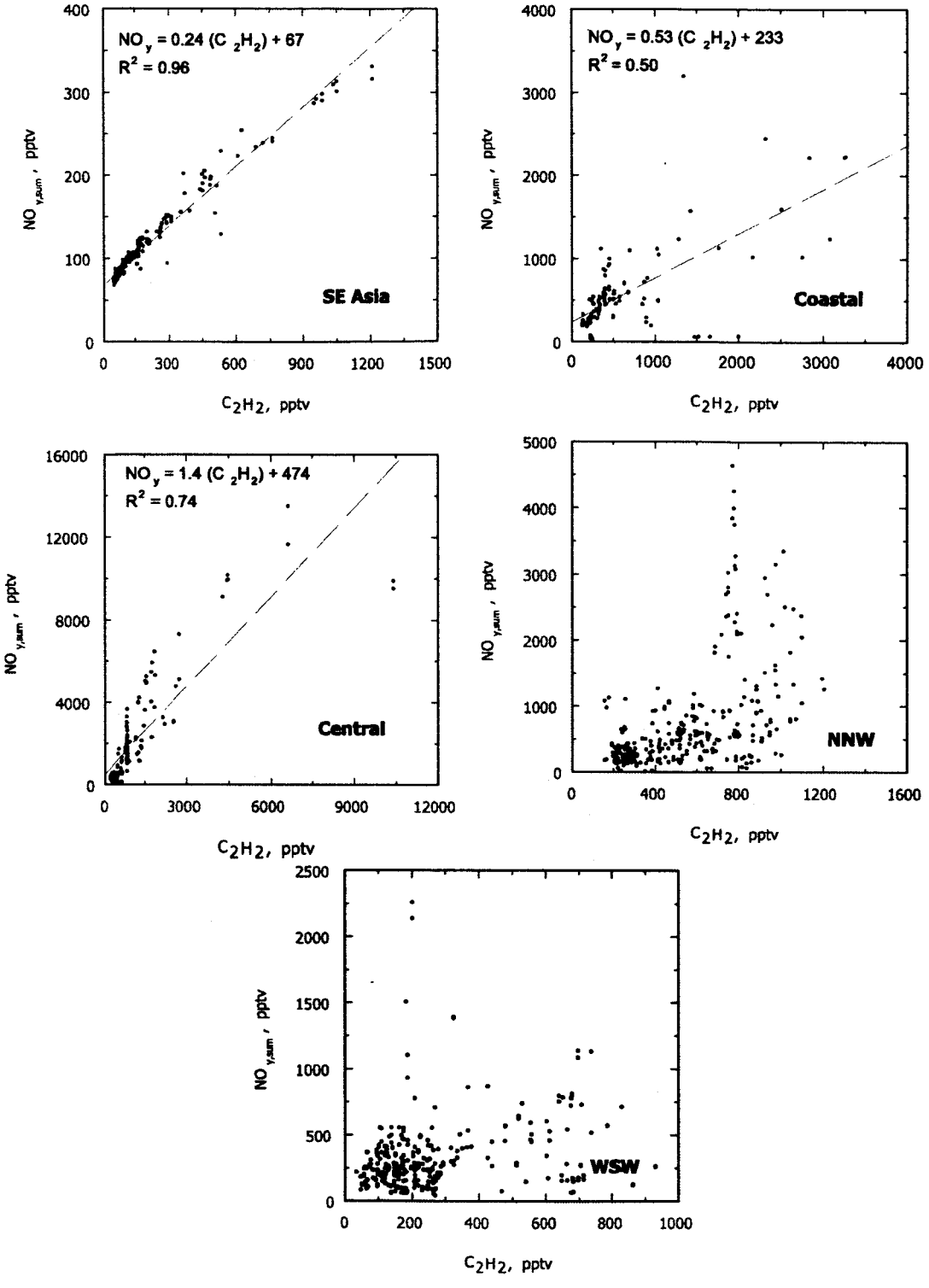

Figure 8. Relationships between NO_y and C_2H_2 for each of the five Asian source regions. C_2H_2 is a unique indicator of combustion emissions.

Heald et al. [2003] and *Singh et al.* [2003] companion papers indicate that HCN is a better tracer of biomass burning than CH_3Cl in the free troposphere, but this does not appear to hold up for clearly identifying a biomass burning source for $NO_{y,sum}$. For species with simpler chemical transformations such as CO or C_2H_2, good correlations were found with HCN in a few limited cases [*Russo et al.*, 2003].

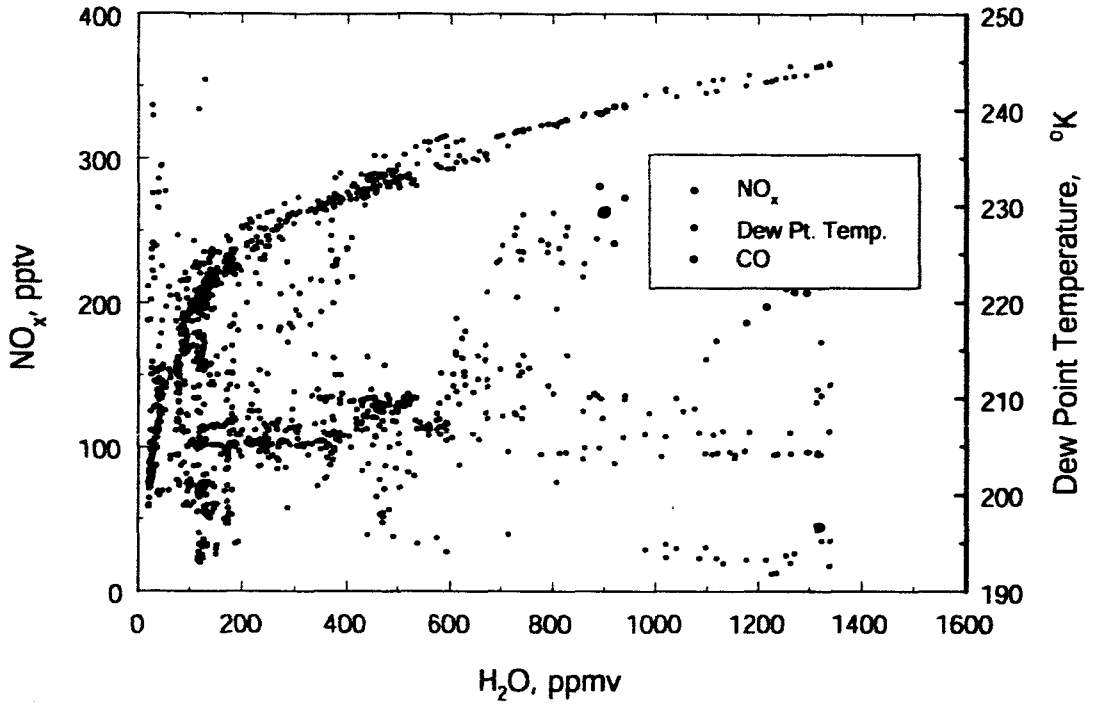

Figure 9. Relationship between NO_x and H_2O vapor (red) and dew point temperature (blue) in upper tropospheric air parcels originating over the WSW source region.

[32] Overall, it appears that a unique source signal rarely remained in air parcels advected from over the Asian continent to the western Pacific after extensive processing during transport at the spatial resolution of the present analysis. Both C_2Cl_4 and CH_3Cl, which are fairly specific tracers of urban and biomass burning emissions respectively, provided minimal insight to the relative importance of these sources. This may be related to removal of NO_y during transport eroding the original source signatures and correlations. For urban/industrial tracers we expanded our efforts to include CH_3CCl, Halon-1211, and CH_3Br (enhanced greatly in Japanese urban areas). None of these improved the source recognition issues. Most distributions were centered commonly around the median mixing ratio of the tracer species employed in the analysis. This result implies that we must rely more than ever on mesoscale modeling results and associated emission inventories to facilitate our understanding of continental scale atmospheric chemistry and intercontinental transport.

5. Characterization of the Shanghai Plume

[33] The Shanghai urban plume was sampled during flight 13 at 0.34 km altitude over the Yellow Sea. The plume was encountered ~100 km north of Shanghai and sampled along a 300 km transect over a 38-min period around midday. The wind speed in the plume averaged 7 m s^{-1}, yielding a travel time of 4 hours at the south end to 16 hours at the northernmost point sampled. Thus the plume seemingly sampled air originating in the Shanghai urban center in the late night hours (northern point) and midmorning at the southern end of the transect. Thus it is possible that the peak mixing ratios represent the morning rush hour time period. However, this is pure speculation and we do not know the three-dimensional positioning of the plume and how the DC-8 transected it. This plume contained the largest mixing ratios of most species, with O_3 being one exception, observed during the TRACE-P mission. The plume was a combination of various age air parcels, with the freshest components exhibiting a C_2H_2/CO ratio of 9.3 and the rest in the 4–6 range (Figure 5). These values suggest a well-defined plume with emissions less than 1 day old.

[34] The large mixing ratios of highly reactive species such as C_2H_4 are evidence of the very recent emissions associated with the Shanghai plume (Figure 12). The combustion nature of the plume was captured by the very high levels (~10,000 pptv) of C_2H_2. Mixing ratios of CO peaked at 1100 ppbv and 392 ppmv for CO_2 (not shown). The urban/industrial signature of the plume contained a large ensemble of enhanced volatile organic compounds, including C_2Cl_4 and CH_3Br (Figure 12). Mixing ratios of CH_3Cl and HCN exceeded 1600 pptv (3 times background levels), indicating that a strong biomass burning/biofuel component also influenced the chemical composition of the plume (not shown). *Li et al.* [2003] hypothesized a possible source from residential coal combustion for both CH_3Cl and for HCN in this plume.

[35] Since the Shanghai plume appears to represent a large source of reactive nitrogen to the marine boundary layer over the Yellow Sea, we examined its $NO_{y,sum}$ budget in detail. This included examination of the distribution of individual $NO_{y,sum}$ species, plus a breakdown of the seven alkyl nitrate compounds measured by the UCI-NCAR

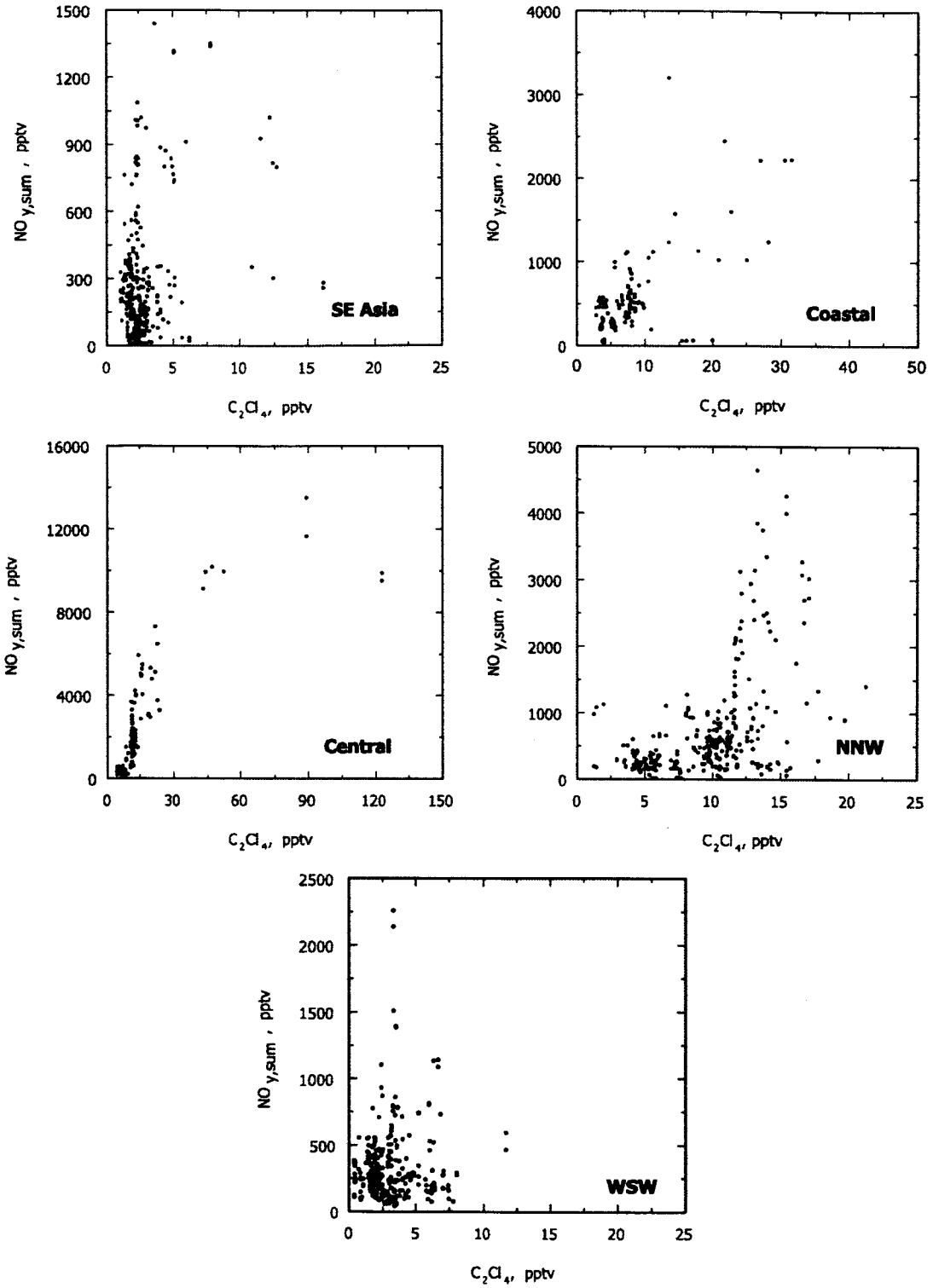

Figure 10. Relationships between NO_y and C_2Cl_4 for each of the five Asian source regions. C_2Cl_4 is an indicator of urban/industrial emissions.

groups. These data show that i-propyl and 2-butyl nitrate were the most abundant alkyl nitrate species in this urban/industrial plume. Their peak mixing ratios were ~70 pptv, followed by the pentyl nitrates at 20–25 pptv. Methyl and ethyl nitrate were among the least abundant, opposite to their distribution over the tropical Pacific where they appear to be released from the surface ocean contributing to the 30–50 pptv levels typical of the remote marine boundary

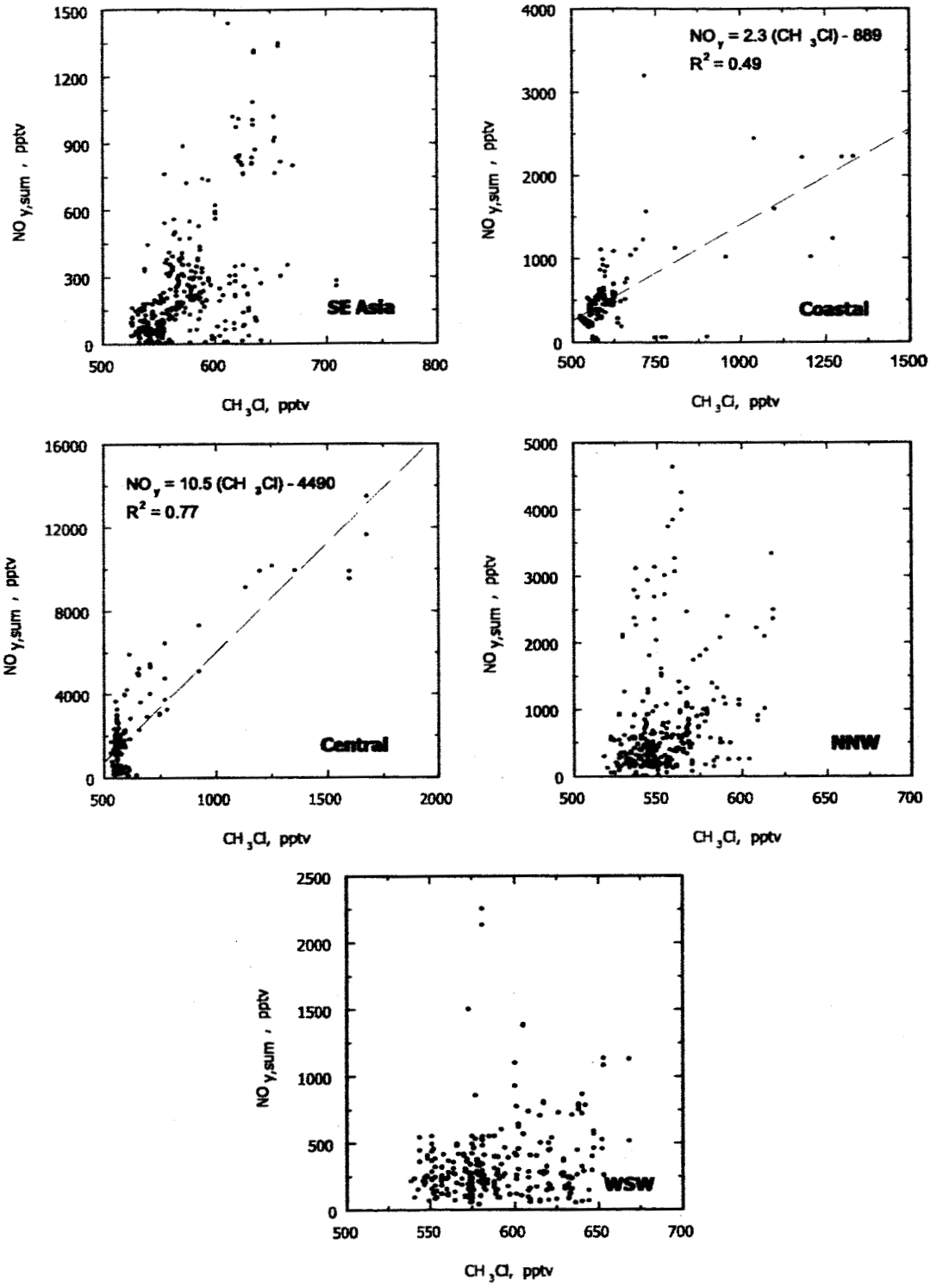

Figure 11. Relationships between NO_y and CH_3Cl for each of the five Asian source regions. CH_3Cl is an indicator of biomass burning emissions.

layer [*Talbot et al.*, 2000; *Blake et al.*, 2003]. Together the alkyl nitrate sum exceeded 200 pptv in the heart of the plume, a very significant amount but still less than 2% of total $NO_{y,sum}$.

[36] The distribution of individual $NO_{y,sum}$ species showed the following approximate contributions: NO_x (15%), HNO_3 (53%), PAN (30%), and alkyl-ONO_2 (2%). At one point in the marine boundary layer aerosol nitrate

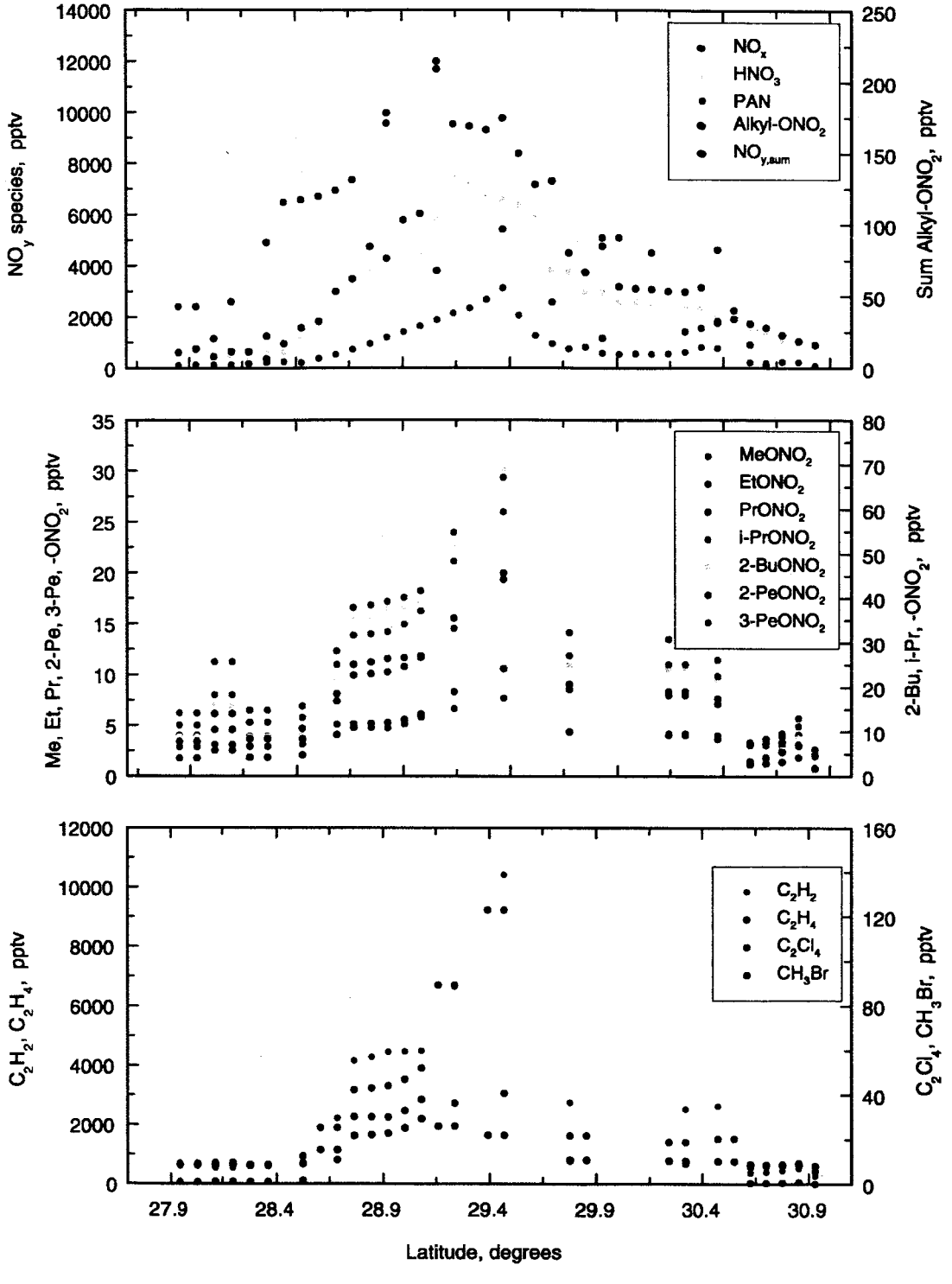

Figure 12. Chemical relationships and breakdown of individual NO_y species in the Shanghai mega-city plume. The DC-8 flight track was located along a 300 km north-south longitudinal transect at 125°E.

reached 13,500 pptv in the plume [*Dibb et al.*, 2003]. Thus it was equal to or greater than total gas phase $NO_{y,sum}$. This finding suggests that the Shanghai plume contains very large mixing ratios of HNO_3 over the Asian continent, but that it is rapidly lost to sea salt aerosols over the ocean. Together the HNO_3 and aerosol nitrate must exceed 20,000 pptv over the Asian continent, with HNO_3 likely dominating the phase partitioning. These data indicate that OH levels in the plume are probably controlled to a large extent by reaction with NO_2 to form HNO_3. However, detailed measurements are

required over the Asian continent to confirm such speculations concerning this mega-city urban/industrial plume.

6. Comparison of TRACE-P With PEM-West B Results

[37] Owing to rapid industrialization on the Asian continent, it is of great interest to examine changes in tropospheric chemistry over the western Pacific during the past decade. Since PEM-West B was conducted during the same monthly time frame in 1994 that TRACE-P covered in 2001, direct meaningful comparisons are possible. In addition, many of the species were measured by the same investigator groups during both missions, minimizing measurement biases.

[38] *Russo et al.* [2003] found few changes in the distributions and mixing ratios of a large suite of trace gases. One exception to this was O_3, which appears to have increased by 10–20 ppbv throughout the western Pacific. There was a very significant increase in the mixing ratios of water-soluble aerosol species during TRACE-P compared to PEM-West B [*Dibb et al.*, 2003]. It is difficult to access how much of the 2–5 fold increases were due to emissions compared to other confounding factors such as variations in the degree of precipitation scavenging.

[39] For the comparisons we used summary statistics for the PEM-West B period reported by *Talbot et al.* [1997a]. The PEM-West B data were broken into two groups, continental north and south, divided by a geographic separation at 20°N. We thus compared the continental north group with the TRACE-P coastal, central, and NNW groups and the continental south region with the SE Asia group. The WSW group was not used in these comparisons since it overlaps significantly with both PEM-West B source regions. The values of $NO_{y,sum}$ for PEM-West B were taken from *Talbot et al.* [1997a, 1997b].

[40] Tables 1 and 2 contain a summary of $NO_{y,sum}$ species comparisons for the two western Pacific missions. In the boundary layer for the northern groupings median mixing ratios of HNO_3 and PAN were 2–5 times higher during TRACE-P compared to PEM-West B. An exception was for PAN in the coastal group. Although most of the differences in mean values are statistically significant (t-test, $P = 0.05$), the maximum values are relatively similar. The comparisons for $NO_{y,sum}$ are not significantly different except for the central group at 0–2 km altitude where they were much greater than the PEM-West B results ($P = 0.05$). Comparisons for the middle and upper troposphere revealed a remarkable similarity over the 7 year period between the missions. The only significant difference was for HNO_3 in the coastal group where the mean values for TRACE-P were a factor of 2 higher than in PEM-West B ($P = 0.05$).

[41] Comparisons of the continental south group with the TRACE-P SE Asia group showed that differences existed but they did not vary in a systematic manner. In the boundary layer median mixing ratios of HNO_3 and $NO_{y,sum}$ were eight-fold and six-fold lower during TRACE-P, respectively. This may be due to the fact that during PEM-West B relatively few data were obtained in the continental south region [*Talbot et al.*, 1997b]. We clearly did not get a good statistical sampling of air parcels in 1994, so the results are

Table 1. TRACE-P Nitrogen Budget Summary Statistics

Source Region		NO_x	PAN	HNO_3	ΣAlkyl-ONO_2	$NO_{y,sum}$[a]
			NNW			
0–2 km	mean	351	505	447	56	940
	stdev.	695	326	195	12	881
	median	69	514	436	54	597
	min	0.79	1.3	63	26	12
	max	3507	1422	1198	89	5115
2–7 km	mean	68	292	197	25	388
	stdev.	79	244	243	15	413
	median	38	189	133	21	255
	min	5.1	89	49	7.1	59
	max	688	998	2028	71	3341
>7 km	mean	132	282	152	21	416
	stdev.	172	157	191	15	327
	median	41	236	86	23	295
	min	8.3	80	41	3.6	60
	max	557	550	1030	50	1123
			Central			
0–2 km	mean	395	1225	1323	69	2422
	stdev.	437	1014	1293	33	2248
	median	276	888	833	58	1723
	min	25	2.4	222	25	222
	max	3111	4264	7412	214	13487
2–7 km	mean	48	194	202	20	297
	stdev.	44	69	110	5.1	150
	median	33	175	169	19	276
	min	1.1	118	106	9.1	65
	max	205	364	938	30	938
			Coastal			
0–2 km	mean	34	207	439	11	541
	stdev.	89	336	365	20	525
	median	6.5	19	322	25	386
	min	0.52	1.3	128	10	56
	max	581	1065	2120	104	3267
2–7 km	mean	40	142	439	17	431
	stdev.	42	126	365	7.9	260
	median	29	115	326	13	475
	min	6.3	15	135	10	24
	max	247	412	876	33	1096
			SE Asia			
0–2 km	mean	81	46	139	3.7	218
	stdev.	187	51	217	4.3	273
	median	9.4	16	65	8.1	91
	min	9.0	2.7	12	3.2	6.4
	max	836	237	884	19	1158
2.7 km	mean	81	157	338	10	384
	stdev.	187	190	233	11	330
	median	9.4	80	240	5.4	306
	min	1.1	8.4	100	3.1	5.0
	max	836	660	1352	45	1439
7–12.5 km	mean	39	81	102	3.2	174
	stdev.	32	58	78	4.2	108
	median	38	91	83	6.2	162
	min	1.3	6.2	3.0	2.3	5.8
	max	139	238	320	20	495
			WSW			
2–7 km	mean	70	172	137	8.8	240
	stdev.	46	62	47	2.8	118
	median	45	172	130	8.3	211
	min	7.8	78	81	5.0	81
	max	154	311	306	14	569
7–12.5 km	mean	112	258	138	8.5	309
	stdev.	66	182	170	5.1	249
	median	106	186	106	7.1	247
	min	12	30	25	1.8	3.5
	max	354	699	1987	23	2257

[a]Sum of the individual species (see text).

Table 2. PEM-WEST B Nitrogen Budget Summary Statistics

Source Region		NO	PAN	HNO_3	ΣAlkyl-ONO_2	$NO_{y,sum}$[a]
		Continental North				
0–2 km	mean	31	559	617	NA	1084
	stdev.	67	434	1263	NA	1587
	median	18	134	229	NA	624
	min	3.1	54	30	NA	123
	max	937	2187	6596	NA	10243
2–7 km	mean	16	289	168	NA	449
	stdev.	18	190	166	NA	305
	median	13	108	126	NA	406
	min	2.6	1.7	37	NA	64
	max	568	885	1115	NA	1923
>7 km	mean	49	177	166	NA	473
	stdev.	68	164	69	NA	208
	median	39	98	146	NA	449
	min	7.4	20	62	NA	153
	max	833	965	389	NA	1033
		Continental South				
0–2 km	mean	13	78	615	NA	941
	stdev.	7.8	82	316	NA	1114
	median	6.8	6.4	548	NA	721
	min	4.6	6.4	219	NA	159
	max	40	247	1275	NA	7029
2–7 km	mean	15	35	455	NA	279
	stdev.	7.8	22	344	NA	206
	median	17	13	421	NA	257
	min	4.5	5.4	55	NA	75
	max	30	68	1225	NA	868
>7 km	mean	57	57	124	NA	234
	stdev.	34	28	47	NA	132
	median	56	38	122	NA	243
	min	7.9	8.8	55	NA	68
	max	339	149	279	NA	540

[a]Sum of the individual species [*Talbot et al.*, 1997a, 1997b].

unlikely to be representative of that region. It may be fortuitous for the previous reason that the middle and upper tropospheric data are similar for both missions. Nevertheless, it appears that in general the $NO_{y,sum}$ loading above the boundary layer has been affected minimally by increasing emissions on the Asian continent over the last 7 years. The data show that the biggest changes and influences were in the boundary layer. *Liu et al.* [2003] hypothesize that the higher mixing ratios of water-soluble aerosol in TRACE-P relative to PEM-West B [*Dibb et al.*, 2003] together with higher $NO_{y,sum}$ in the boundary layer, may reflect stronger boundary layer outflow during TRACE-P because of more frequent frontal passages. Such interannual variability in the western Pacific region requires careful documentation to distinguish it from response to changes in emission sources.

7. Summary

[42] We presented the general distributions of $NO_{y,sum}$ and individual $NO_{y,sum}$ species over the western Pacific during the TRACE-P study period of February–March 2001. In general, $NO_{y,sum}$ was dominated by HNO_3 and PAN, while NO_x mixing ratios were commonly <100 pptv except in plumes where they exceeded 1000 pptv on a few occasions. There was a significant combustion influence over the western Pacific, as evidenced by the distributions of CO and C_2H_2. Correlations of $NO_{y,sum}$ with an urban tracer such as C_2Cl_4 and CH_3Cl for biomass burning were not well defined in most cases.

[43] The distribution of the ratio C_2H_2/CO was striking, showing values in the middle to upper troposphere that mimicked the boundary layer and ones that support a scenario of rapid advective transport of continent emissions across the Pacific to at least 150°E. These findings suggest that extensive and rapid frontal uplifting and vertical transport is operating continuously over the Asian continent combined with extensive westerly transport of pollutants at all altitudes. This result helps explain the blurred correlations observed between $NO_{y,sum}$ and CO or O_3. Such continuous intermixing of air parcels of various ages and processing would lead directly to the very complex distributions and relationships that we observed for $NO_{y,sum}$, CO, and O_3. In addition, removal of NO_y during transport would further distort source signatures and species intercorrelations.

[44] On one occasion the Shanghai mega-city plume was characterized during a flight over the Yellow Sea. The plume was intercepted at 0.34 km altitude and exhibited peak mixing ratios of more than 10,000 pptv C_2H_2, 3,000 pptv C_2H_4, 12,000 $NO_{y,sum}$, 8,000 pptv HNO_3, and 30 pptv CH_3Br. C_1–C_5 alkyl nitrates totaled 100–200 pptv, being dominated by 2-BuONO_2 and i-PrONO_2. Our results suggest that the Shanghai plume represents a large source of reactive nitrogen to the marine boundary layer over the Yellow Sea.

[45] Comparison of results between the earlier PEM-West B mission and the recent TRACE-P campaign show remarkable similarities in tropospheric chemistry. This was most evident in the middle and upper troposphere where $NO_{y,sum}$ loadings appear to have been affected minimally by increasing emissions on the Asian continent over the last 7 years. However, significant increases in the mixing ratios of $NO_{y,sum}$ species were readily apparent in the boundary layer.

[46] **Acknowledgments.** We appreciate the support provided by the DC-8 flight and ground crews at the NASA Dryden Flight Research Center. This research was supported by the NASA Global Tropospheric Chemistry program in the Office of Earth Science.

References

Bernsten, T. K., and S. Karlsdottir, Influence of Asian emissions on the composition of air reaching the North Western United States, *Geophys. Res. Lett.*, *26*, 2171–2174, 1999.

Blake, D. R., T.-Y. Chen, T. W. Smith Jr., C. J.-L Wang, O. W. Wingenter, F. S. Rowland, and E. W. Mayer, Three dimensional distribution of NMHCs and halocarbons over the northwestern Pacific during the 1991 Pacific Exploratory Mission (PEM-West A), *J. Geophys. Res.*, *101*, 1763–1778, 1996.

Blake, N. J., D. R. Blake, A. L. Swanson, E. Atlas, F. Flocke, and F. S. Rowland, Latitudinal, vertical, and seasonal variations in C_1–C_4 alkyl nitrates in the troposphere over the Pacific Ocean during PEM-Tropics A and B: Oceanic and continental sources, *J. Geophys. Res.*, *108*(D2), 8242, doi:10.1029/2001JD001444, 2003.

Bradshaw, J., et al., Photofragmentation two-photon laser-induced detection of NO_2 and NO: Comparison of measurements with model results based on airborne observations during PEM-Tropics A, *Geophys. Res., Lett.*, *26*, 471–474, 1999.

Brune, W. H., I. C. Faloona, D. Tan, A. J. Weinheimer, T. Campos, B. A. Ridley, S. A. Vay, J. E. Collins, G. W. Sachse, L. Jaegle, and D. J. Jacob, Airborne in-situ OH and HO_2 observations in the cloud-free troposphere and lower stratosphere during SUCCESS, *Geophys. Res. Lett.*, *25*, 1701–1704, 1998.

Colman, J. J., A. L. Swanson, S. Meinarde, and D. R. Blake, Description of the analysis of a wide range of volatile organic compounds in whole air samples collected during PEM-Tropics A and B, *Anal. Chem.*, *73*, 3723–3731, 2001.

Crutzen, P. J., and M. O. Andreae, Biomass burning in the tropics: Impact on atmospheric chemistry and biogeochemical cycles, *Science*, *250*, 1669–1678, 1990.

Crutzen, P. J., L. E. Heidt, J. P. Krasnec, W. H. Pollock, and W. Seiler, Biomass burning as a source of atmospheric gases CO, H_2, N_2O, NO, CH_3Cl, and COS, *Nature*, *282*, 253–256, 1979.

Dibb, J. E., R. W. Talbot, B. L. Lefer, and E. Scheuer, Distributions of beryllium-7 and lead-210 over the western Pacific: PEM-West B, February–March 1994, *J. Geophys. Res.*, *102*, 28,287–28,302, 1997.

Dibb, J. E., R. W. Talbot, E. Scheuer, G. Seid, M. Avery, and H. Singh, Aerosol chemical composition in Asian continental outflow during TRACE-P: Comparison to PEM-West B, *J. Geophys. Res.*, *108*(D21), 8815, doi:10.1029/2002JD003111, in press, 2003.

Eisele, F. L., et al., Informal instrument intercomparison summary of selected atmospheric species on the NASA DC-8 and P-3 during TRACE-P, *J. Geophys. Res.*, *108*(D20), 8791, doi:10.1029/2002JD003167, in press, 2003.

Emmons, L. K., D. A. Hauglustaine, J.-F. Muller, M. A. Carroll, G. P. Brasseur, D. Brunner, J. Staehelin, V. Thouret, and A. Marenco, Data composites of airborne observations of tropospheric ozone and its precursors, *J. Geophys. Res.*, *105*, 20,497–20,538, 2000.

Fuelberg, H., C. M. Kiley, J. R. Hannan, D. J. Westberg, M. A. Avery, and R. E. Newell, Atmospheric transport during the Transport and Chemical Evolution over the Pacific (TRACE-P) experiment, *J. Geophys. Res.*, *108*(D20), 8782, doi:10.1029/2002JD003092, in press, 2003.

Heald, C. L., D. J. Jacob, P. I. Palmer, M. J. Evans, G. W. Sachse, H. B. Singh, and D. R. Blake, Biomass burning emission inventory with daily resolution: Application to aircraft observations of Asian outflow, *J. Geophys. Res.*, *108*(D21), 8811, doi:10.1029/2002JD003082, in press, 2003.

Hoell, J. M., D. D. Davis, S. C. Liu, R. Newell, M. Shipman, H. Akimoto, R. J. McNeal, R. J. Bendura, and J. W. Drewery, Pacific Exploratory Mission-West A (PEM-West A): September–October 1991, *J. Geophys. Res.*, *101*, 1641–1653, 1996.

Hoell, J. M., D. D. Davis, S. C. Liu, R. E. Newell, H. Akimoto, R. J. McNeal, and R. J. Bendura, The Pacific Exploratory Mission-West Phase B: February–March, 1994, *J. Geophys. Res.*, *102*, 28,233–28,239, 1997.

Jacob, D. J., J. A. Logan, and P. P. Murti, Effect of rising Asian emissions on surface ozone in the United States, *Geophys. Res. Lett.*, *26*, 2175–2178, 1999.

Jacob, D. J., J. H. Crawford, M. M. Kleb, V. E. Connors, R. J. Bendura, J. L. Raper, G. W. Sachse, J. C. Gille, L. Emmons, and C. L. Heald, The Transport and Chemical Evolution over the Pacific (TRACE-P) aircraft mission: Design, execution, and first results, *J. Geophys. Res.*, *108*(D20), 8781, doi:10.1029/2002JD003276, in press, 2003.

Jordan, C. E., et al., Chemical and physical properties of bulk aerosols within four sectors observed during TRACE-P, *J. Geophys. Res.*, *108*(D21), 8813, doi:10.1029/2002JD003337, in press, 2003.

Koike, M., Y. Kondo, S. Kawakami, H. Nakajima, G. L Gregory, G. W. Sachse, H. B. Singh, E. V. Browell, J. T. Merrill, and R. E. Newell, Reactive nitrogen and its correlation with O_3 and CO over the Pacific in winter and early spring, *J. Geophys. Res.*, *102*, 28,385–28,404, 1997.

Li, Q., D. J. Jacob, R. M. Yantosca, C. L. Heald, H. B. Singh, M. Koike, Y. Zhao, G. W. Sachse, and D. G. Streets, A global 3-D model evaluation of the atmospheric budgets of HCN and CH_3CN: Constraints from aircraft measurements over the western Pacific, *J. Geophys. Res.*, *108*(D21), 8827, doi:10.1029/2002JD003075, in press, 2003.

Liu, H., D. J. Jacob, I. Bey, M. Yantosca, B. N. Duncan, and G. W. Sachse, Transport pathways for Asian combustion outflow over the Pacific: Interannual and seasonal variations, *J. Geophys. Res.*, *108*(D20), 8786, doi:10.1029/2002JD003102, in press, 2003.

Russo, R., et al., Chemical composition of Asian continental outflow over the western Pacific: Results from TRACE-P, *J. Geophys. Res.*, *108*(D20), 8804, doi:10.1029/2002JD003184, in press, 2003.

Sandholm, S., J. D. Bradshaw, K. S. Dorris, M. O. Rogers, and D. D. Davis, An airborne-compatible photofragmentation two-photon laser-induced fluorescence instrument for measuring background tropospheric NO, NO_x, and NO_2, *J. Geophys. Res.*, *95*, 10,155–10,161, 1990.

Singh, H. B., and P. B. Zimmerman, Atmospheric distribution and sources of nonmethane hydrocarbons, in *Gaseous Pollutants: Characterization and Cycling*, John Wiley, New York, 1992.

Singh, H., Y. Chen, A Staudt, D. Jacob, D. Blake, B. Heikes, and J. Snow, Evidence from the Pacific troposphere for large global sources of oxygenated organic compounds, *Nature*, *410*, 1078–1081, 2001.

Singh, H. B., et al., In situ measurements of HCN and CH_3CN in the Pacific troposphere: Sources, sinks, and comparisions with spectroscopic observations, *J. Geophys. Res.*, *108*(D20), 8789, doi:10.1029/2002JD003006, in press, 2003.

Streets, D. G., et al., A year-2000 inventory of gaseous and primary aerosol emissions in Asia to support TRACE-P modeling and analysis, *J. Geophys. Res.*, *108*(D21), 8809, doi:10.1029/2002JD003093, in press, 2003.

Talbot, R. W., et al., Chemical characteristics of continental outflow from Asia to the troposphere over the western Pacific Ocean during September–October 1991: Results from PEM-West A, *J. Geophys. Res.*, *101*, 1713–1725, 1996.

Talbot, R. W., et al., Chemical characteristics of continental outflow from Asia to the troposphere over the western Pacific Ocean during February–March 1994: Results from PEM-West B, *J. Geophys. Res.*, *102*, 28,255–28,274, 1997a.

Talbot, R. W., et al., Large-scale distributions of tropospheric nitric, formic, and acetic acids over the western Pacific basin during wintertime, *J. Geophys. Res.*, *102*, 28,303–28,313, 1997b.

Talbot, R. W., et al., Reactive nitrogen budget during the NASA SONEX mission, *Geophys. Res. Lett.*, *26*, 3057–3060, 1999.

Talbot, R. W., J. E. Dibb, E. M. Scheuer, J. D. Bradshaw, S. T. Sandholm, H. B. Singh, D. R. Blake, N. J. Blake, E. Atlas, and F. Flocke, Tropospheric reactive odd nitrogen over the South Pacific in austral springtime, *J. Geophys. Res.*, *105*, 6681–6694, 2000.

U.S. Department of Energy, *International Energy Outlook (IEO)*, Energy Inf. Admin., Washington, D. C., 1997.(Available at http://www.eia.doe.gov/oiaf/ieo97).

Van Aardenne, J. A., G. A. Carmichael, H. Levy II, D. Streets, and L. Hordijk, Anthropogenic NO_x emissions in Asia in the period 1990–2020, *Atmos. Environ.*, *33*, 633–646, 1999.

Zhang, Y., *Synoptic Meteorology and Climate*, pp. 600–601, Meteorology Press, Beijing, China, 1992.

E. Atlas, National Center for Atmospheric Research, Boulder, CO 80305, USA. (atlas@acd.ucar.edu)

M. Avery, C. Jordan, and G. Sachse, NASA Langley Research Center, Hampton, VA 23665, USA. (m.a.avery@larc.nasa.gov; c.e.jordan@larc.nasa.gov; g.w.sachse@larc.nasa.gov)

D. Blake and N. Blake, University of California, Irvine, Irvine, CA 92716, USA. (drblake@uci.edu; nblake@uci.edu)

J. Dibb, R. Russo, E. Scheuer, G. Seid, and R. Talbot, University of New Hampshire, Durham, NH 03820, USA. (jack.dibb@unh.edu; rsrusso@cisunix.unh.edu; eric.scheuer@unh.edu; gseid@mail.kgi.edu; robert.talbot@unh.edu)

S. Sandholm, H. Singh, and D. Tan, Georgia Institute of Technology, Atlanta, GA 30332, USA. (sts@minitower.eas.gatech.edu; hanwat.b.singh@nasa.gov; dtan@eas.gatech.edu)